PROGRAMA OFICIAL DE POSGRADO

INGENIERÍA Y PRODUCCIÓN INDUSTRIAL

DOCTORAL THESIS

Study of the transport of heavy metal ions through cation-exchange membranes applied to the treatment of industrial effluents

Manuel César Martí Calatayud

Directed by:

Dr. D. Valentín Pérez Herranz

Dra. Dª Montserrat García Gabaldón

València, November 2014

Acknowledgements / Agradecimientos / Agraïments

En primer lugar quisiera agradecer a Valentín y a Montse por haberme dado la oportunidad de investigar con ellos, por introducirme en un mundo que me ha fascinado, por haberme dirigido, por haberme ayudado en momentos de desasosiego; porque, en definitiva, creo que hemos formado un gran equipo.

Quisiera agradecer a la Universitat Politècnica de València la financiación recibida para realizar la tesis. En general, he de agradecer al sistema de educación pública que ha permitido que un hijo de trabajadores como yo haya podido llegar hasta aquí. Además, quiero aprovechar para exigir un sistema de educación público, de calidad, e igualitario, que forme a personas con espíritu crítico y libre; puesto que sólo así se conseguirá que progresemos como sociedad.

I would also like to thank to all the people from the group of Chemical Process Engineering of the RWTH Aachen University, especially to Matthias Wessling and Said Abdu, for accepting me in their research group. They have been very kind to me and I have learnt a lot from them and from this fruitful and unforgettable experience in Aachen.

También quisiera agradecer a Daniella Buzzi por haberme dejado ser su "chefinho", por tantos momentos buenos y algún que otro momento crítico vividos juntos, porque es bonito saber que tengo una gran amiga al otro lado del charco.

Gracias al Grupo IEC, en especial a mis compañeros, con los que he pasado más momentos juntos. Ellos han sido mi familia investigadora. Gracias a Isaac y Carlos, porque han sido para mí un referente, a Jordi y Ramón, porque han estado desde el principio, han sido como mis hermanos, y a Vir y Tepe, ellas han contribuido a que haya un ambiente de trabajo inmejorable! Quiero también dar las gracias al resto de componentes del grupo por su ayuda, en especial a Emma Ortega, a José Luis Guiñón por su ayuda con los equilibrios, y a Anna Igual porque con su energía consigue contagiar su pasión por la investigación.

El fruto del trabajo de todos estos años tampoco sería posible sin los momentos vividos junto a mis amigos, el "Kanchy". Ellos son "los de toda la vida", los que siempre han estado, están y estarán ahí. Quisiera hacer mención especial a Lidia por su ayuda con la Tesis, y cómo no, a Sergio, porque juntos hemos arreglado el mundo un millón de veces... ¡para volverlo a destrozar otras tantas!

No quiero olvidarme de ninguna de las personas con las que he coincidido y he pasado buenos momentos tanto en Valencia, como en Berlín o en Aachen... Maite, Laura,

Guillaume... es imposible nombrarlos a todos... pero quiero agradecer en especial a Tania, porque con ella no existe el tiempo ni la distancia, sé que siempre está ahí a mi lado.

Ha arribat el moment d'agrair a les quimixiques els grans moments viscuts. Amb elles hem format una gran família. Em sent molt afortunat d'haver caigut en un grup tan de "puça mare": gràcies a les Silvies, Elena, Gabriel·la, Angeleta, Rosa de Xeraco, Alicia, i en especial a Susana, la meua companya de batalles, i a Ingrid, una gran amiga.

Per últim voldria donar-li les gràcies a "Enrique Barsello" de Llanera de Ranes i "Tere la Pacaleta" de l'Alcúdia de Crespins, mon pare i ma mare, perquè ells sempre m'han recolzat, i han tingut que suportar els meus moments d'estrès. Sempre recordaré amb un somriure quan vaig sentir a mon pare dir-li a algú: "El millor llegat que li puc deixar als meus fills, és una bona educació". També vull agrair-li a Maria José "la retruc", per eixes vesprades d'evasió jugant al truc. Ella em va ensenyar això de "si jugar i perdre és bonico, què serà jugar i guanyar?". Per últim, em queda agrair-li a la meua germana Maite, per tot el seu amor i per ser un pilar fonamental en la meua vida, i a Mario i a Marc, el meu gamberret! A tots vosaltres, VOS VULL MOLT, MOLTÍSSIMES GRÀCIES!

"I woke up with a loved one's eyes upon me
loved one's arms around me
Oh...she's my one and only

I grew up in the bosom of my family
eight strong arms around me
Oh...from the seed they've grown me

And I thank those,
those who kept me company.
They are a wall of arms around me
Oh...it is they who are my army
Oh... it is they who are my army

Through these eyes
there's no god above me
no devil below me
no purgatory, no pearly gates.
The worms are what await me
It's only me that can forgive me and
I have faith, oh...I have faith
I have faith, oh...I have faith
In those who put up with me"

Wall of arms, The Maccabees.

ABSTRACT

The development of sustainable technologies applied to the valorization of waste effluents deserves an increasing attention due to the growing demand of the Earth's resources. In this context, electromembrane processes are an emerging alternative for the treatment of metal containing effluents, since they allow the recovery of valuable metals and clean water for reuse, hence implying important benefits for the environment. Industrial effluents that contain multivalent metals can be very diverse and complex, and usually form weak electrolytes. Consequently, the energy consumption and the efficiency of the mass transfer in electromembrane processes are strongly affected by the type of ions that cross the membranes. For this reason, it is important to achieve a better understanding of the mass transfer phenomena involved in these processes in order to make them economically competitive with other less sustainable processes.

Ion sorption properties, chronopotentiometric and current-voltage curves have been obtained in order to characterize the ion uptake equilibrium and the ion transport taking place in systems formed by a Nafion 117 cation-exchange membrane and various metallic solutions. The results obtained with systems of single salt solutions of Na(I), Ni(II), Cr(III) and Fe(III) have proven that the type of species transported through the membranes strongly depends on the initial electrolyte concentration and the applied current density. In systems with trivalent metals, apart from free cations (Cr^{3+} and Fe^{3+}), other charged complex species can cross the membrane ($CrSO_4^+$, $FeSO_4^+$...). In systems of multivalent metals and under the application of high current densities, the initial equilibrium conditions at the depleting diffusion boundary layer can be altered, thus inducing the formation of hydroxilated complexes and the formation of precipitates ($Ni(OH)_2$ and $Fe(OH)_3$) at the depleting membrane surface, which increase the electrical resistance of the membrane systems.

The competitive ion transport through the membranes has been investigated using two different mixtures that resemble the composition of industrial wastewaters. In systems of $NiSO_4$ and CrO_3 (spent rinse waters of the metal finishing industry), a decrease in the $[Ni^{2+}]/[H^+]$ ratio in the equilibrating solution reduced significantly the transport of Ni^{2+} ions through the membranes, but increased the limiting current density and decreased the electrical resistance of the membrane system. In mixtures of $Fe_2(SO_4)_3$ and Na_2SO_4 (acid mine drainage), the transport of Na^+ ions occurs preferentially at low current densities and the transport of Fe^{3+} ions at high underlimiting currents. Moreover, the dissociation of $FeSO_4^+$ ions into Fe^{3+} and SO_4^{2-} ions at high underlimiting currents

promotes a reduction in the electrical resistance of the membrane systems due to the higher conductivity of the free ions with respect to that of complex ionic species.

The overlimiting mechanisms of ion transport have been also investigated. An increase in the concentration of multivalent metals can promote the development of coupled convection (gravitational convection and electroconvection) for lower membrane voltage drops, thus reducing the energy cost of using overlimiting current densities. On the contrary, high concentrations of H^+ ions hamper coupled convection phenomena and increase the membrane voltage drops necessary to reach the overlimiting range of current densities. These results were also corroborated in long-term galvanostatic tests.

RESUMEN

El desarrollo de tecnologías sostenibles aplicadas a la valorización de residuos está recibiendo una atención creciente debido a la demanda intensiva de los recursos del planeta. En este contexto, los procesos electroquímicos de membrana se sitúan como una alternativa emergente para el tratamiento de efluentes industriales que contienen metales, puesto que permiten la recuperación de metales valiosos y de agua limpia para su reutilización, implicando con ello importantes beneficios para el medio ambiente. Los efluentes industriales que contienen metales multivalentes pueden ser muy diversos y complejos, y normalmente se encuentran formando electrolitos débiles. En consecuencia, el consumo energético y la eficiencia en la transferencia de materia en los procesos electroquímicos de membrana dependen de forma significativa del tipo de iones transportados a través de las membranas. Por este motivo, es importante lograr un mayor conocimiento acerca de los fenómenos de transporte implicados en dichos procesos, con el fin de situarlos como una alternativa económicamente competitiva frente a otras tecnologías menos sostenibles.

En la presente Tesis Doctoral se han estudiado los fenómenos de polarización por concentración en sistemas formados por una membrana de intercambio catiónico Nafion 117 y varias disoluciones metálicas mediante la obtención de las propiedades de intercambio iónico y de las curvas cronopotenciométricas y de polarización. Los resultados obtenidos con sistemas unicomponentes de sales de Na(I), Ni(II), Cr(III) y Fe(III) indican que el tipo de especies transportadas a través de las membranas depende de la concentración inicial del electrolito y de la densidad de corriente aplicada. En sistemas con metales trivalentes, además del los iones libres (Cr^{3+} y Fe^{3+}), diferentes especies complejas cargadas también pasan a través de la membrana ($CrSO_4^+$, $FeSO_4^+$,...). En disoluciones con metales multivalentes y bajo la aplicación de elevadas densidades de corriente, las condiciones de equilibrio iniciales pueden cambiar, implicando con ello la formación de complejos hidroxilados y de precipitados metálicos en la superficie de la membrana en el compartimento diluido ($Ni(OH)_2$ y $Fe(OH)_3$), lo cual conlleva un aumento de la resistencia eléctrica del sistema de membrana.

El transporte competitivo de iones a través de las membranas se ha investigado utilizando dos mezclas multicomponentes diferentes que simulan la composición de aguas industriales. En mezclas de $NiSO_4$ y CrO_3 (baños de lavado agotados de la industria de recubrimiento de superficies metálicas), un descenso del ratio $[Ni^{2+}]/[H^+]$ en la disolución conlleva una importante disminución del transporte de iones Ni^{2+} a través de la

membrana, pero también implica un incremento de la densidad de corriente límite y un descenso en la resistencia eléctrica del sistema membrana/electrolito. En mezclas de $Fe_2(SO_4)_3$ y Na_2SO_4 (drenaje ácido de minas), el transporte de iones Na^+ tiene lugar preferentemente a bajas densidades de corriente, mientras que el transporte de iones Fe^{3+} es más importante a densidades de corriente elevadas pero inferiores a la límite. Además, la disociación de los iones $FeSO_4^+$ en Fe^{3+} y SO_4^{2-} implica una reducción en la resistencia eléctrica del sistema de membrana debido a la mayor conductividad de los iones libres con respecto a la de especies iónicas complejas.

Los mecanismos de transporte iónico a densidades de corriente superiores a la límite también se han investigado. Un incremento en la concentración de metales multivalentes conlleva el desarrollo de fenómenos convectivos (convección gravitacional y electroconvección) para caídas de voltaje a través de la membrana reducidas, disminuyendo con ello el coste energético asociado con el uso de densidades de corriente superiores a la límite. Por el contrario, elevadas concentraciones de iones H^+ dificultan los fenómenos convectivos y aumentan la caída de voltaje transmembranal que es necesario superar para alcanzar el rango de densidades de corriente superiores a la límite. Estos resultados también se corroboraron mediante ensayos galvanostáticos de larga duración.

RESUM

El desenvolupament de tecnologies sostenibles aplicades a la valorització de residus està rebent una atenció creixent degut a la demanda intensiva dels recursos del planeta. En aquest context, els processos electroquímics de membrana es posicionen com una alternativa emergent per al tractament d'efluents industrials que contenen metalls, atès que permeten la recuperació de metalls valuosos i d'aigua neta per a la seua reutilització, implicant així importants beneficis per al medi ambient. Els efluents industrials que contenen metalls multivalents poden ser molt diversos i complexes, i normalment es troben en forma d'electròlits febles. En conseqüència, el consum energètic i l'eficiència en la transferència de matèria en els processos electroquímics de membrana depenen en gran mesura del tipus d'ions transportats a través de les membranes. Per aquest motiu, és important abastir un major coneixement dels fenòmens de transport implicats en dits processos, amb la finalitat de situar-los com una alternativa econòmicament competitiva amb altres tecnologies menys sostenibles.

En la present Tesi Doctoral s'han estudiat els fenòmens de polarització per concentració en sistemes formats per una membrana d'intercanvi catiònic Nafion 117 i diverses dissolucions metàl·liques mitjançant l'obtenció de les propietats d'intercanvi iònic i de les corbes cronopotenciomètriques i de polarització. Els resultats obtinguts amb sistemes unicomponents de sals de Na(I), Ni(II), Cr(III) i Fe(III) indiquen que el tipus d'espècies transportades a través de les membranes depèn de la concentració inicial de l'electròlit i de la densitat de corrent aplicada. En sistemes amb metalls trivalents, a més dels ions lliures (Cr^{3+} i Fe^{3+}), també passen a través de la membrana espècies complexes carregades ($CrSO_4^+$, $FeSO_4^+$,...). En dissolucions amb metalls multivalents sotmesos a l'aplicació d'elevades densitats de corrent, les condicions d'equilibri inicials poden canviar, implicant amb això la formació de complexos hidroxilats i de precipitats metàl·lics en la superfície de la membrana situada en el compartiment de dilució ($Ni(OH)_2$ i $Fe(OH)_3$), augmentant així la resistència elèctrica del sistema de membrana.

El transport competitiu d'ions a través de les membranes s'ha investigat utilitzant dos mescles multicomponent diferents que simulen la composició d'aigües industrials. En mescles de $NiSO_4$ i CrO_3 (banys de llavat esgotats de la indústria de recobriment de peces metàl·liques), un descens del ràtio $[Ni^{2+}]/[H^+]$ en la dissolució comporta una important disminució del transport d'ions Ni^{2+} a través de la membrana, però també implica un increment de la densitat de corrent límit i un descens de la resistència elèctrica del

sistema membrana/electròlit. En mescles de $Fe_2(SO_4)_3$ i Na_2SO_4 (drenatge àcid de mines), el transport d'ions Na^+ ocorre preferentment a baixes densitats de corrent, mentre que el transport d'ions Fe^{3+} és més important a densitats de corrent elevades però inferiors a la límit. A més a més, la dissociació dels ions $FeSO_4^+$ en Fe^{3+} i SO_4^{2-} implica una reducció de la resistència elèctrica del sistema de membrana degut a la major conductivitat dels ions lliures, comparada amb la d'espècies iòniques complexes.

En la present Tesi Doctoral també s'han investigat els mecanismes de transport iònic a densitats de corrent superiors a la límit. Un increment en la concentració de metalls multivalents comporta el desenvolupament de fenòmens convectius (convecció gravitacional i electroconvecció) per a caigudes de voltatge a través de la membrana reduïdes, disminuint tanmateix el cost energètic associat a l'ús de densitats de corrent superiors a la límit. Pel contrari, elevades concentracions d'ions H^+ dificulten els fenòmens convectius i augmenten la caiguda de voltatge transmembranal que és necessari superar per a abastar el rang de densitats de corrent superiors a la límit. Aquests resultats també es van corroborar mitjançant assaigs galvanostàtics de llarga duració.

PUBLICATIONS RELATED TO THE DOCTORAL THESIS

ARTICLES IN INTERNATIONAL JOURNALS

- *Determination of transport properties of Ni(II) through a Nafion cation-exchange membrane in chromic acid solutions.*
  M.C. Martí-Calatayud, M. García-Gabaldón, V. Pérez-Herranz, E. Ortega.
  Journal of Membrane Science, 379 (2011) 449-458.

- *Study of the effects of the applied current regime and the concentration of chromic acid on the transport of Ni^{2+} ions through Nafion 117 membranes.*
  M.C. Martí-Calatayud, M. García-Gabaldón, V. Pérez-Herranz.
  Journal of Membrane Science, 392-393 (2012) 137-149.

- *Effect of the equilibria of multivalent metal sulfates on the transport through cation-exchange membranes at different current regimes.*
  M.C. Martí-Calatayud, M. García-Gabaldón, V. Pérez-Herranz
  Journal of Membrane Science, 443 (2013) 181-192.

- *Ion transport through homogeneous and heterogeneous ion-exchange membranes in single salt and multicomponent electrolyte solutions.*
  M.C. Martí-Calatayud, D.C. Buzzi, M. García-Gabaldón, A.M. Bernardes, J.A.S. Tenório, V. Pérez-Herranz
  Journal of Membrane Science, 466 (2014) 45-57.

PREDOCTORAL RESEARCH STAY IN A FOREIGN INSTITUTE

A predoctoral research stay was carried out from October 2012 to March 2013 at the Chemical Process Engineering Department of the RWTH-Aachen University (Aachen, Nordrhein-Westfalen, Germany). The work was supervised by Prof. Dr.-Eng. Matthias Wessling, head of the Institute of Membrane Technology, and was conducted in close cooperation with Said Abdu. The main topic of this research stay was to modify the surface of cation-exchange membranes in order to induce properties of monovalent ion selectivity. As a result of this research stay, the following article was published:

- *Layer-by-layer modification of cation exchange membranes controls ion selectivity and water splitting*.
  S. Abdu, M.C. Martí-Calatayud, J.E. Wong, M. García-Gabaldón, M. Wessling
  ACS Applied Materials & Interfaces, 6 (2014) 1843-1854.

RESEARCH COLLABORATIONS WITH OTHER RESEARCH INSTITUTES

In addition to the research stay, we have conducted other collaborative research studies with the Instituto de Tecnología Cerámica de la Universitat Jaume I de Castelló (Spain). These studies consisted on the development of ion-exchange membranes from ceramic materials. The innovative aspect of this research was to synthesize durable membranes that could resist oxidizing and radioactive conditions of industrial effluents, thus making feasible their treatment by means of electromembrane processes. These studies have been materialized in the publication of the following articles:

- *Synthesis and electrochemical behaviour of ceramic cation-exchange membranes based on zirconium phosphate.*
  M.C. Martí-Calatayud, M. García-Gabaldón, V. Pérez-Herranz, S. Sales, S. Mestre.
  Ceramics International, 39 (2013) 4045-4054.

- *Chronopotentiometric study of ceramic cation-exchange membranes base don zirconium phosphate in contact with nickel sulfate solutions.*
  M.C. Martí-Calatayud, M. García-Gabaldón, V. Pérez-Herranz, S. Sales, S. Mestre.
  Desalination and Water Treatment, 51 (2013) 597-605.

We carried out a research study in cooperation with Andrea Moura Bernardes and Daniella Cardoso Buzzi, from the Department of Materials Engineering of the Universidade Federal do Rio Grande do Sul (UFGRS) (Porto Alegre, Rio Grande do Sul, Brazil). The main purpose of this study was to evaluate the treatment of acid mine drainage solutions by means of electrodialysis. The following article was published as a result of this work:

- *Sulfuric acid recovery from acid mine drainage by means of electrodialysis.*
  M.C. Martí-Calatayud, D.C. Buzzi, M. García-Gabaldón, E. Ortega, A.M. Bernardes, J.A.S. Tenório, V. Pérez-Herranz
  Desalination, 343 (2014) 120-127.

CONGRESS PRESENTATIONS

- *Development of electrodialysis membranes from ceramic materials for environmental applications*, M.C. Martí-Calatayud, M. García-Gabaldón, V. Pérez-Herranz, S. Sales, S. Mestre, **10th European Symposium on Electrochemical Engineering**, Sardinia (Italy), September 2014.

- *Role of electrolytes on the overlimiting ion conductance of cation-exchange membranes*, M.C. Martí-Calatayud, M. García-Gabaldón, E. Ortega, V. Pérez-Herranz, **65th Annual Meeting of the International Society of Electrochemistry**, Lausanne (Switzerland), September 2014.

- *Synthesis of ceramic ion-exchange membranes with bipolar behaviour for electrodialytic water splitting*, M.C. Martí-Calatayud, M. García-Gabaldón, V. Pérez-Herranz, S. Sales, S. Mestre, **IX Ibero-american Congress on Membrane Science and Technology**, Santander (Spain), May 2014.

- *Layer-by-layer assembly of polyelectrolytes applied to obtain cation exchange membranes with monovalent ion selectivity*, M.C. Martí-Calatayud, S. Abdu, J.E. Wong, M. García-Gabaldón, V. Pérez-Herranz, M. Wessling, **IX Ibero-American Congress on Membrane Science and Technology**, Santander (Spain), May 2014.

- *Treatment of industrial wastewaters containing multivalent metals by means of electrodialytic techniques*. M.C. Martí-Calatayud, M. García-Gabaldón, E. Ortega, V. Pérez-Herranz, **13th International Conference on Environmental Science and Technology**, Athens (Greece), September 2013.

- *Evaluation of two cation-exchange membranes for the separation of Fe(III) from acid mine drainage solutions*, M.C. Martí-Calatayud, M. García-Gabaldón, V. Pérez-Herranz, D.C. Buzzi, A.M. Bernardes, J.A.S. Tenório, **XXXIV Reunión Bienal de la Sociedad Española de Química**, Santander (Spain), September 2013.

- *Enhancement of the monovalent ion selectivity of cation-exchange membranes modified with the layer-by-layer deposition of polyelectrolyte multilayers thin film*, M.C. Martí-Calatayud, S. Abdu, J.E. Wong, M. García-Gabaldón, E. Ortega, V. Pérez-Herranz, M. Wessling, **XXXIV Reunión de Electroquímica de la Real Sociedad Española de Química**, Valencia (Spain), July 2013.

- *Novel ceramic anion-exchange membranes based on hydrous zirconium oxide for the treatment of industrial wastewaters*, M.C. Martí-Calatayud, M. García-Gabaldón, V. Pérez-Herranz, S. Sales, S. Mestre, **Membrane Processes for Industrial Pollution Control with Water and Products Recovery**, Lisboa (Portugal), July 2013.

- *Sulfuric acid recovery from acid mine drainage by means of electrodialysis*, M.C. Martí-Calatayud, M. García-Gabaldón, V. Pérez-Herranz, D.C. Buzzi, A.M. Bernardes, J.A.S. Tenório, **1st International Conference on Desalination using Membrane Technology**, Sitges (Spain), April 2013.

- *Transport of Fe^{3+} ions through homogeneous and heterogeneous cation-exchange membranes*, M.C. Martí-Calatayud, M. García-Gabaldón, E. Ortega, V. Pérez-Herranz, D.C. Buzzi, A.M. Bernardes, J.A.S. Tenório, **63rd Annual Meeting of the International Society of Electrochemistry**, Prague (Czech Republic), August 2012.

- *Chronopotentiometric study of ion-exchange membranes with sodium and iron(III) sulfate solutions*, D.C. Buzzi, M.C. Martí-Calatayud, M. García-Gabaldón, A.M. Bernardes, J.A.S. Tenório, V. Pérez-Herranz, **VIII Simposio Internacional de Qualidade Ambiental**, Porto Alegre (Brazil), June 2012.

- *Chronopotentiometric study of ceramic cation-exchange membranes based on zirconium phosphate with nickel sulfate solutions*, M.C. Martí-Calatayud, M. García-Gabaldón, V. Pérez-Herranz, S. Sales, S. Mestre, **Conference on Desalination for the Environment, Clean Water and Energy**, Barcelona (Spain), April 2012.

- *Evaluation of the transport of Cr^{3+} ions present in chromium plating solutions through a cation-exchange membrane*, M.C. Martí-Calatayud, M. García-Gabaldón, V. Pérez-Herranz, **13 Network of Young Membrains**, Enschede (The Netherlands), July 2011.

- *Influence of the initial $NiSO_4$ and CrO_3 concentration on the transport number of Ni^{2+} ions through a cation-exchange membrane*, M.C. Martí-Calatayud, M. García-Gabaldón, E. Ortega, V. Pérez-Herranz, **9th European Symposium on Electrochemical Engineering**, Chania (Greece), June 2011.

- *Chronopotentiometric study of the transport of Fe^{3+} through cation-exchange membranes for the regeneration of chromium plating baths*, M.C. Martí-Calatayud, M. García-Gabaldón, E. Ortega-Navarro, V. Pérez-Herranz, **2nd Regional Symposium on Electrochemistry**, Belgrade (Serbia), July 2011.

TABLE OF CONTENTS

Chapter 1. Introduction

Chapter 2. Objectives and scope

Chapter 3. Experimental techniques

Chapter 4. Results and discussion

Chapter 5. Conclusions

Chapter 1
INTRODUCTION

1.1 Current socioeconomic situation

1.1.1 Resources of metals in the world

In the recent years the concerns of modern societies for protecting the environment has increased notoriously, which has coincided with the industrial development of southern countries and the steady increase of the Earth's population. In addition, inhabitants of developing countries are having a greater access to technology, such as electronic devices or automobiles. As a result, the demand for natural resources such as fossil fuels, metals, biomass, water and the like provided by the Earth is rapidly increasing and, consequently, they are being intensively exploited.

Fig. 1.1 shows the evolution of the global resources extraction classified by major groups of resources. This plot includes model previsions until 2020 foreseen by the "MOSUS" project (Modelling opportunities and limits for restructuring Europe towards sustainability), which is funded by the European Commission [1]. The figure shows that

metal ores and minerals are the categories with the highest growth rates, which indicates the importance of metals for industrial development. The basis for this important growth is related to the increasing contribution of the world emerging economies, such as the BRIC countries (Brazil, Russia, India, and China), to resource extraction [2].

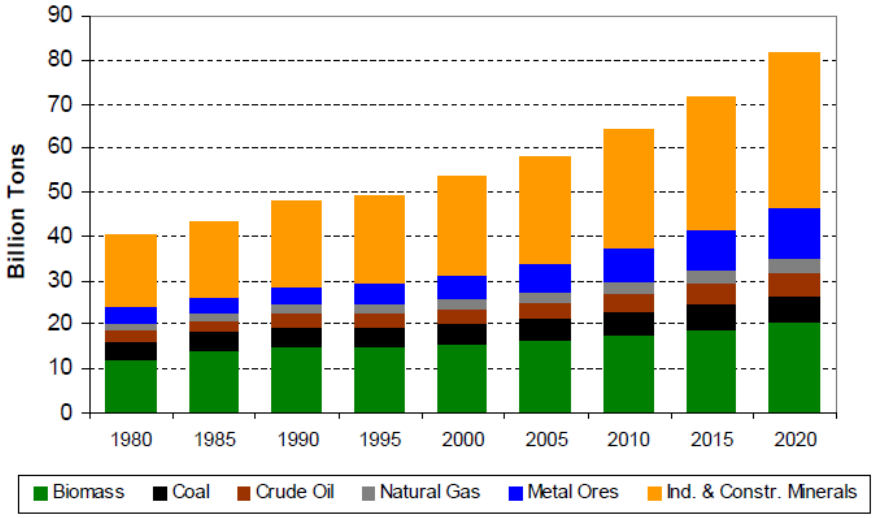

Figure 1.1. Worldwide used materials extraction, classified by groups of resources. (Reproduced from [1]).

Traditionally, metals have been intensively used as engineering materials in buildings and infrastructures, as well as in the automotive industry. However, the rapid growth of technology in the 20th century has led to an increasing use of metals in the field of electronics and energy. Today, a wide variety of metals is used to produce electronic devices such as mobile phones or computers. For example, rare earth metals (Nd, Pr, Dy, Tb, Eu...) are indispensable for the manufacture of hard disk drives, flat panel display screens or portable electronics. They are also very important in the health and medical applications sector. Moreover, the use of metals is becoming more relevant in the energy industry. Metals are used as energy carriers (redox flow batteries), in energy storage systems (lithium, cadmium and nickel based batteries) or as a direct source of energy (uranium and thorium in nuclear energy).

As a consequence of this rapid increase in the demand of metal resources, the exhaustion of metal reserves has been pointed out as a great concern as it could limit the future economic growth [2]. To provide an indication of the relative risk to the supply of elements, the British Geological Survey (BGS) published a list of elements needed to

support modern economies and lifestyle and classified them according to their risk of supply shortage. The relative supply index (ranging from 1 (no risk) to 10) is determined by a number of factors which might affect availability. These include the abundance of elements in the Earth's crust, the location of current production and reserves, the political stability of those locations and the recycling rate and substitutability of these elements. Most of the elements in the risk list are given in Table 1.1. The risk list highlights a group of elements which might be subject to supply disruption, such as the rare earth elements or the platinum group elements, for which global production is concentrated in very few countries and have low rates of recycling and limited substitutes.

Table 1.1. Supply risk index for chemical elements or element groups which are of economic value (Source: NERC 2012 [3]).

Element or element group	Symbol	Relative supply risk index
Rare earth elements	REE	9.5
Tungsten	W	9.5
Antimony	Sb	9.0
Molybdenum	Mo	8.6
Strontium	Sr	8.6
Mercury	Hg	8.6
Barium	Ba	8.1
Beryllium	Be	8.1
Germanium	Ge	8.1
Niobium	Nb	7.6
Platinum group elements	PGE	7.6
Cobalt	Co	7.6
Indium	In	7.6
Gallium	Ga	7.6
Tantalum	Mg	7.1
Selenium	Se	7.1
Cadmium	Cd	6.7
Lithium	Li	6.7
Vanadium	V	6.7
Tin	Sn	6.7
Silver	Ag	6.2
Chromium	Cr	6.2
Nickel	Ni	6.2
Lead	Pb	6.2
Manganese	Mn	5.7
Gold	Au	5.7
Uranium	U	5.7
Zirconium	Zr	5.7
Iron	Fe	5.2
Titanium	Ti	4.8
Aluminium	Al	4.8
Zinc	Zn	4.8
Copper	Cu	4.3

In order to make compatible the current levels of growth with sustainability and reduce the risk of supply shortages, it is crucial to develop new technologies that make feasible the recycling and reuse of metals. For example, in the risk list presented in Table 1.1, copper has a low supply risk index, which is closely related to the feasibility of its recycling. In 2008, copper consumption was about 24 million tones, 8 million of which came from recycling operations, and the remaining 16 million from primary production [4]. However, to be economically competitive with the direct extraction and processing from the earth crust, metal recycling technologies need to be significantly improved.

Along with the constant technologic progress, the increasing prices of mineral raw materials will undoubtedly stimulate the introduction and development of recycling processes in the industry. In this regard, it is important to note that the majority of metals are not mined for themselves but as recovered by-products in parent ores. Fig. 1.2 shows a scheme of the typical host-companion relationships in ore deposits. As the richest mines become exhausted, more low-quality ores are mined, leading to an overall decrease in ore grades [5]. The mining of lower-grade ore causes an increase in energy use, even with improved extraction methods [6]. The extraction of metals would also require more complicated purifying operations, thus increasing water use, pollution and the cost of extraction, which would contribute to increase the interest in recycling the metals present in wastes.

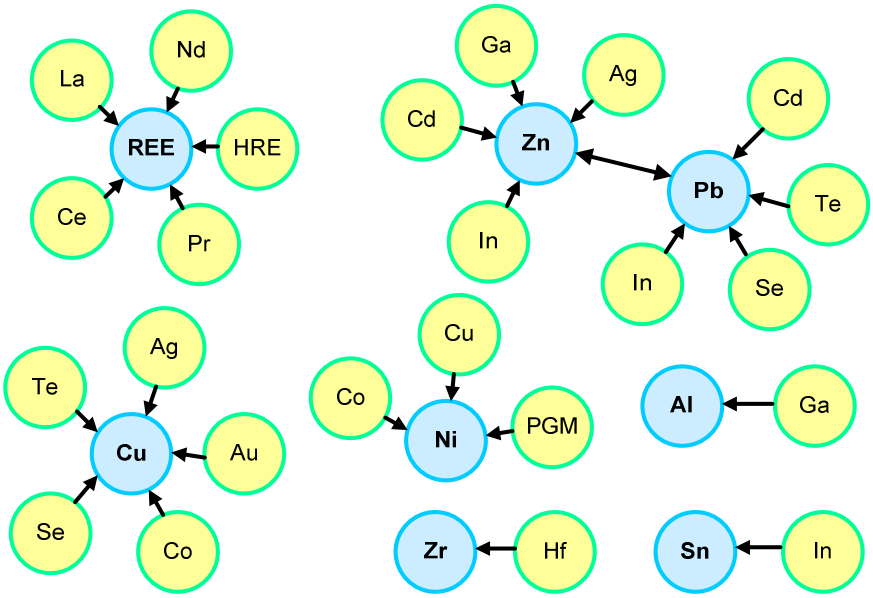

Figure 1.2. Typical occurrences of companion metals within host metal ore bodies. REE: rare earth elements; HRE: heavy rare earths; PGM: platinum group metals. (Reproduced from [7]).

By way of example, the historical evolution of prices and consumption of three different metals are illustrated in Fig. 1.3 [8]. We selected the data corresponding to iron, chromium and nickel due to different reasons. Iron is important due to its high volume of production, chromium due to its harmful effects on the environment, and nickel due to its comparatively high price. Moreover, as it will be discussed below, all of them are used in different industries and can be found as components of industrial aqueous effluents, which is the focus of the present Thesis. In general, Fig. 1.3 illustrates an increasing trend in the world production of the three metals. As mentioned previously, this trend is associated with global industrial growth. With regard to the prices, a general increase is also observed. However, prices are more volatile and highly susceptible to changes in supply and demand. For example, nickel has been considered as a "strategic" metal, as corroborated by the sharp price increases occurred in the late 1960's and in 2007. The former price increase was due to prolonged strikes at the Sudbury Mine (one of the largest global producers), whereas the latter was apparently caused by the increased demand for nickel in the production of stainless steel [9]. Therefore, the unstable and oscillating prices are an additional incentive for boosting the recovery and recycling of metals in industrial processes, as well as from waste effluents.

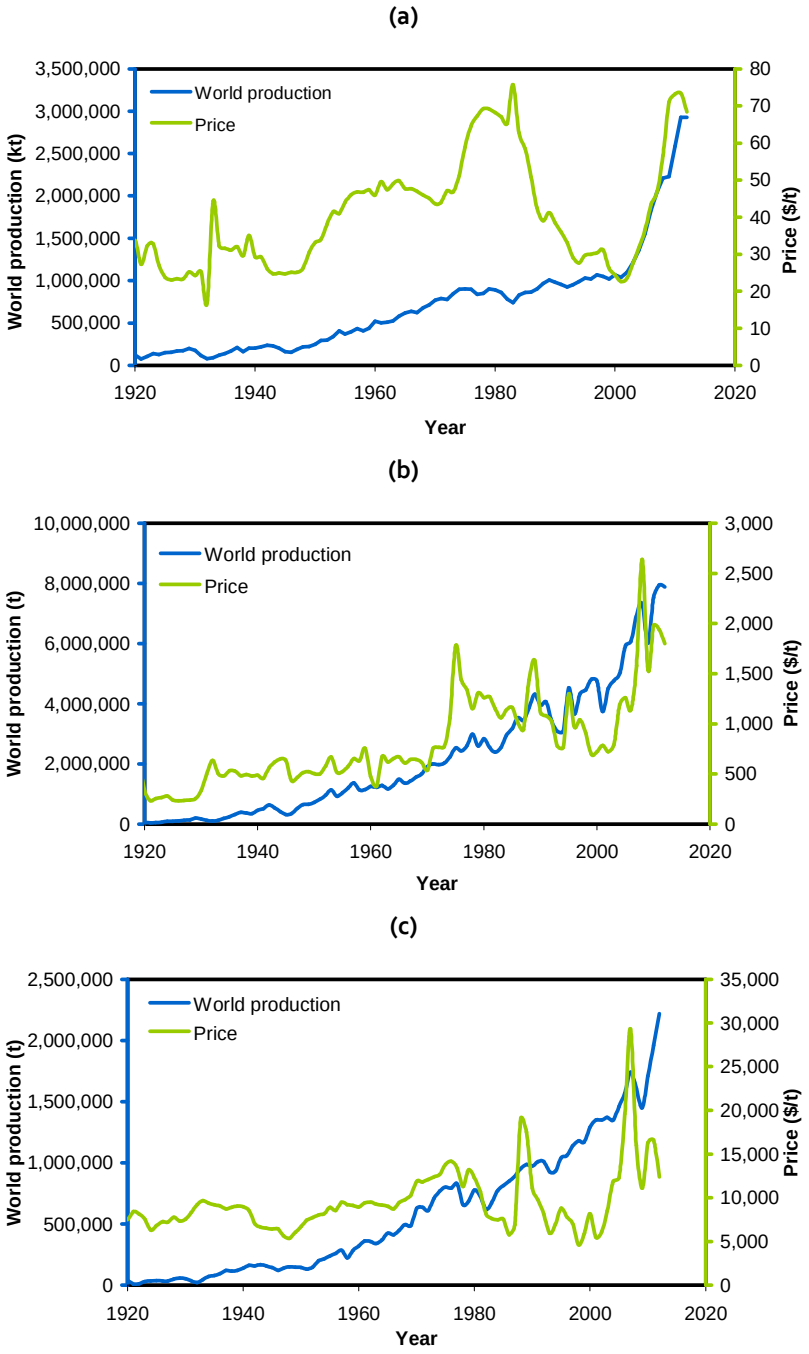

Figure 1.3. Evolution of the global production and price of (a) iron ores, (b) chromium ores and (c) nickel ores (Source: US geological survey [8]).

In addition to the economic, geopolitical and sustainability-related arguments the environmental and health hazards associated with the discharge of metals into natural watercourses also justifies the development of clean technologies for the recovery and recycling of metals. Accordingly, the importance of treating metal-containing effluents will be discussed in the following section from a perspective based on environmental aspects.

1.1.2 Environmental and health effects of heavy metals

Although metals have multitude of important applications and some of them are essential for human life (in trace amounts); they can also imply important environmental and health hazards. Specially, heavy metals are of greater concern because they are persistent and toxic even at low concentrations. Heavy metals are elements with relatively high atomic weights and a specific gravity greater than 5.0 [10]. Some examples of heavy metals are the following: antimony, arsenic, bismuth, calcium, chromium, cobalt, copper, iron, lead, mercury, nickel, tin, uranium and zinc.

Heavy metals may be incorporated into the human body through food, water, air or absorption through the skin. However, the major concern is focused on the intake of heavy metals through the food chain, which is mainly caused by their discharge into natural watercourses and aquatic ecosystems. They get into fresh and salt water when industrial wastes are added to the water bodies. Once discharged, heavy metals can bind to the surface of microorganisms, which are then eaten by bigger fish. Heavy metals are difficult to be excreted and are accumulated in the fatty tissues of animals. Consequently, as bigger organisms eat the smaller ones, the heavy metals build-up in concentration in the larger living beings. This increase in concentration of substances over time and in bigger living organisms is classified into two different phenomena, which are schematically represented in Fig. 1.4. The term bioaccumulation refers to the gradual accumulation of contaminants by an organism which has been eating contaminated food during its life. This phenomenon is caused by an absorption of contaminants faster than its rate of removal [11,12]. The term biomagnification refers to the accumulation of contaminants as you move up the food chain. In this case, the pollutants are transferred up the food chain faster than they are excreted. Because of this, animals that are higher in the food chain have larger levels of contaminants than they would have through regular exposure, i.e. the levels of contaminant are magnified [13,14].

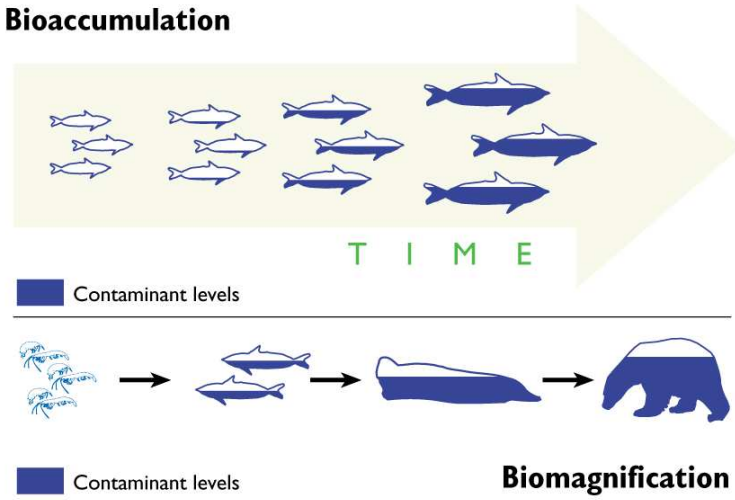

Figure 1.4. Schematic representation of the phenomena of bioaccumulation and biomagnification of persistent contaminants through the food chain.

The effects of the accumulation of heavy metals on the human body have been largely studied. In general, most of them cause skin irritation and problems in the digestive system. However, the toxic dose and the resulting effects can vary for different heavy metals. Toxic heavy metals of particular concern in the treatment of industrial wastewaters include zinc, nickel, mercury, cadmium, lead and chromium [10]. Particularly, nickel exceeding critical levels might result in serious lung and kidney problems. Moreover nickel and hexavalent chromium have been classified as carcinogenic to humans by the International Agency for Research on Cancer (IARC) [15,16]. Mercury and lead are also of great concern because they are neurotoxins and can cause damage to the central nervous system [17].

As mentioned above, the main problem associated with heavy metals is their persistence in the environment. Therefore, it is important to avoid their discharge into natural watercourses or remediate it before it becoming dispersed and accumulated through the food chain. The release of heavy metals into rivers starts during their extraction and transformation in mining sites. Moreover, it is usually accompanied by the generation of acidic effluents as a consequence of the increased exposed area of sulfur-bearing rocks during mining. This phenomenon allows for an excess of acid generation beyond the natural buffering capabilities found in host rock and water resources, thus aggravating the impacts of mining on aquatic ecosystems [18]. Among those impacts are included the

mortality of fauna and flora and the subsequent decrease of biodiversity in important natural reserves, hence also affecting the related human activities. Fig. 1.5 shows a picture of a wetland contaminated as a consequence of the mining activities carried out in the surrounding areas. The treatment of acid mine drainage in the exploitation sites before it could contaminate rivers and lakes could be a solution in order to remediate the impacts of mining on the human health and the environment.

Figure 1.5. Wetlands close to a coal extracting site contaminated by acid mine drainage (Criciúma/SC, Brazil).

Apart from the impacts of mining, there are also many industries which generate metal-containing effluents, such as metal finishing industries, petroleum refining industries, textile industries or leather tanneries. In order to diminish the consequences of these industrial activities on the human health and the environment, the law restrictions are becoming more severe. This favors the introduction of clean alternative techniques in industrial processes that allow a better use of the metal resources, diminish the discharge of metals into the environment and allow the reclamation of large volumes of water. Among them, the use of electromembrane processes stands out because they offer several advantages with respect to other techniques. They have the potential to recover valuable metals for reuse in industrial processes without the addition of reagents, and minimize the amount of residual waste destined to disposal. Electrodialysis is classified among the "Best Available Techniques" recommended by the European Commission for various industrial activities [19,20]. Moreover, it is considered as a clean and sustainable technique that has the potential to aid in the development of zero discharge processes in the industry [21-24]. However, in order to be competitive with cheaper, simpler but less

sustainable techniques, it is crucial to make some efforts to improve electromembrane processes and optimize their operating conditions. To this end, it is important to achieve a better understanding of the different mass transfer phenomena involved in electromembrane processes.

1.2 The potential of electrodialysis for the recovery of heavy metals

1.2.1 Principle of electrodialysis

Electrodialysis is an electromembrane separation process which is applied to remove ionic contaminants from aqueous solutions. Normally, the feed stream in electrodialysis units is a saline solution that is converted into two product streams: a desalted and a concentrated solution. The driving force for the ion transfer is a difference in the electric potential and the mass transfer takes place through ion-exchange membranes, which have two different functions: to separate the different aqueous streams and to facilitate the transport of ions from the diluate compartments toward the concentrated ones.

Ion-exchange membranes consist of polymeric films with ionic groups attached to their structure, which make them permeable to ions of the opposite charge sign. More specifically, anion-exchange membranes bear positive fixed charges (e.g. $-N^{+}(CH_3)_3$) and allow the passage of anions, whereas cation-exchange membranes bear negative fixed charges (e.g. $-SO_3^{-}$) and allow the passage of cations. The basic principle of an electrodialysis unit is shown in Fig. 1.6. When an electric field is applied between the cathode and anode, the electrolyte ions are driven by the potential difference toward different compartments. Cations (M^{+n}) are transported through cation-exchange membranes attracted by the cathode, and anions (X^{-y}) are transported through anion-exchange membranes attracted by the anode. However, when the ions face the surface of a membrane with the same polarity, they are rejected and retained in the feed compartments. Consequently, when anion- and cation-exchange membranes are arranged sequentially, the electrolyte concentration increases in alternate compartments (concentrate) while the other solutions become depleted of ions (diluate).

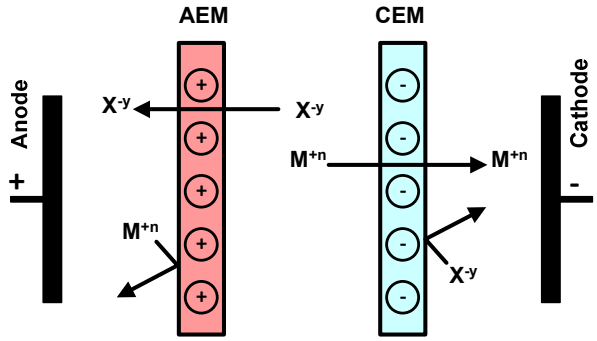

Figure 1.6. Schematic illustration of the principle of electrodialysis systems.

The most basic part of an electrodialysis system consists of a single unit cell or cell pair. A cell pair consists of an anion- and a cation-exchange membrane, which separate different electrolyte compartments, as shown schematically in Fig. 1.6. Moreover, an electrodialysis unit has two electrodes, the cathode and the anode. An electrodialysis unit can be operated at constant current (galvanostatic) or at constant voltage difference between cathode and anode, and the flux of ions through the membranes can be incremented by increasing the strength of the applied electric field. However, the flux of ions is usually limited by the increase in the electrical resistance of the system, especially due to the decrease of conductivity in the depleting compartments. In order to obtain a more efficient use of the current, the number of cell pairs installed between the two electrodes can be increased, as shown in Fig. 1.7. These configurations are called stacks and can be composed of more than one hundred cell pairs. The feed solution is divided into different desalted and concentrated solutions which flow through alternating compartments and are then collected separately.

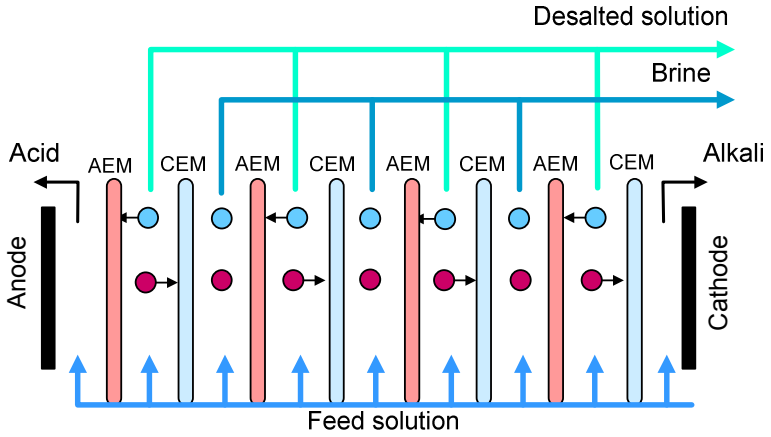

Figure 1.7. Schematic diagram of the arrangement of an electrodialysis stack with several cell pairs. (AEM: anion-exchange membrane, CEM: cation-exchange membrane, ●: cation, ●: anion).

The progress in electrodialysis has been associated with the development of ion-exchange membranes with improved mechanical and chemical properties. The advances in polymer chemistry during the 1950's allowed the production of ion-exchange membranes with enhanced selectivity and positioned electrodialysis as a practical process [25]. The first successful electrodialysis plant to desalinate water was installed in 1952 by Ionics [26]. So far, significant advances have been performed in terms of stack design, optimization of operating parameters and ion-exchange membranes; to such an extent that today electrodialysis is considered a mature technology. Some of the most established applications of electrodialysis are summarized as follows:

- Desalination of brackish water. There are several plants operating in the world. Despite that electrodialysis is competing directly with reverse osmosis, in a certain range of feed water concentrations electrodialysis has an economic advantage over other desalination processes. Moreover, for certain locations where high water recoveries are desired electrodialysis is preferred [26].

- Concentration of seawater to produce table salt. This is a very important technology confined to Japan, which has no domestic salt sources [25].

- Removal of specific contaminants. Certain ionic contaminants cannot be effectively removed in reverse osmosis (RO) plants. In such cases the installation of electrodialysis reversal (EDR) plants allows the production of high quality

drinking water with minimum presence of contaminants. An example of this is the EDR plant installed in the area of Barcelona to provide drinking water with low risk of trihalomethane formation [27].

- Membrane chlor-alkali industry. The development of perfluorosulfonic Nafion membranes by DuPont® allowed the use of ion-exchange membranes to produce NaOH and Cl_2 in chlor-alkali processes. These membranes are characterized by having high ionic conductivities and excellent chemical stability. Moreover, these membranes have found multitude of applications in fuel cells.

- Several applications in the food industry. Electrodialysis is applied to remove salt from cheese whey so that the other components of whey can be used as food for humans and animals; and also to concentrate salts of organic acids produced by fermentation [28].

The above mentioned processes are used on large industrial scale and can be considered as state-of-the-art technology [29]. However, electromembrane processes are growing rapidly again as a number of new applications related to energy and industrial processes have been identified [29]. These new applications are raising the interest in basic fundamental research on the mass transport phenomena through ion-exchange membranes as well as in the development of new types of membranes. Some of the most emerging applications of electromembrane processes are summarized as follows:

- Bipolar electrodialysis. These processes are applied to obtain acids and bases from concentrated salts. They have found application in the valorization of effluents such as reverse osmosis brines, as well as in the recovery of organic acids from fermentation processes [28].

- Microbial fuel cells. This technology makes possible to degrade organic matter and generate electricity simultaneously [30].

- Reverse electrodialysis. This process is based on the mixing of sea water with river water through ion-exchange membranes to produce electricity. The electrochemical potential gradient associated to the process of mixture generates an electrical current between the cathode and anode [31].

- Electrodeionization. This process is applied to remove contaminants to the ppb level from diluted streams. The principle is the same as in electrodialysis, but in this case the diluted compartments are filled with ion exchange beds in order to reduce the electrical resistance of the cell [25].

In addition to the listed processes, one of the most promising applications of electrodialysis is the **treatment of metal containing wastewaters**. In this sense, electrodialysis can be considered as an environmentally friendly technology, since it not only allows for the removal of heavy metals from industrial effluents, but also facilitates their recovery and reuse as added value resources. Compared to other existing technologies, which are focused on the removal of heavy metals from aqueous streams but imply the generation of sludge or wastes destined to disposal, electrodialysis is a more sustainable technology. However, the industrial processes in which metal containing effluents are produced can vary significantly, thus complicating the electrodialysis operations. Therefore, it is important to identify the main challenges of electromembrane processes applied to the treatment of solutions containing heavy metals in order to make them more economically competitive. The advantages and challenges of electrodialysis are indicated in more detail in the following section.

1.2.2 Advantages and challenges of electrodialysis applied to the treatment of metal containing effluents

The best available technologies used to treat industrial effluents containing heavy metals include reverse osmosis, the chemical precipitation of metals by means of adding hydroxides, the use of ion exchange resins and evaporative techniques [19]. Electrodialytic techniques imply some advantages in relation to these technologies, which are summarized as follows:

- Electrodialysis does not involve changes of phase to promote the chemical separation. Consequently the energetic costs are significantly lower than those of evaporative techniques.

- In contrast to pressure-driven membrane processes, electrodialysis implies the separation of species in different compartments based on their ionic charge. This type of separation allows the conversion of the wastewaters in profitable streams. For example, the metallic impurities built-up in the chromium plating baths (Ni^{2+}, Fe^{3+}, Zn^{2+}, etc.) and the Cr(VI) present in the form of anions ($Cr_2O_7^{2-}$, CrO_4^{2-}, $HCrO_4^-$) can be concentrated in different compartments, so that the regenerated chromium can be reused in the plating process. On the contrary, in reverse osmosis the separation of anions and cations is not possible and the presence of impurities in the concentrates makes unviable their reuse in the industry.

- Electrodialysis can be operated in continuous mode, hence making feasible its integration as a part of industrial processes. The adaptability and flexibility of electrodialysis is relatively high due to the modularity and easy monitoring of the operating parameters. In this regard, other technologies such as the use of ion exchange beds or the chemical precipitation are batch processes, which imply the frequent replacement of the ion exchange resins and additional steps for the removal of sludge.

- In contrast with the chemical precipitation or the use of ion exchange beds, in electrodialysis, the electric current is used as reagent and the addition of chemicals is in principle not required. Moreover, the use of photovoltaic energy to power electrodialysis systems could increase the sustainability of electrodialysis and extend its applicability to developing countries [32]. In reverse osmosis, chemicals are also added in order to clean the fouled membranes. However, in the case of electrodialysis membranes, the fouling can be easily prevented by changing periodically the polarity of the electrodes together with the concentrated and diluted streams by using automatic switchable valves. This type of electrodialysis is known as electrodialysis reversal and does not require the addition of reagents to clean the membranes.

- The generation of wastes is minimized in electrodialysis. The desalted streams can be reused as a source of clean water, whereas the concentrated streams can be usually used in industrial processes as valuable resources. This advantage increases the sustainability of electromembrane processes.

In spite of the advantages of electrodialysis to treat metal containing effluents, the complexity of industrial effluents can be very diverse, so that the control of electrodialysis systems could be complex and imply certain limitations. The main focus of this Thesis is to study the mass transfer mechanisms taking place in electromembrane processes in order to minimize these limitations and optimize the function of ion-exchange membranes. Among the most relevant challenges of electrodialysis we highlight the following ones:

- The flux of ions through ion-exchange membranes is not unlimited. Due to the facilitated ion transport occurring through the membranes, concentration gradients develop near the membrane/solution interfaces. When a certain current density known as the limiting current density (i_{lim}) is reached, the concentration of ions near the membrane depleting surface drops practically to zero and the supply of ions to the membrane becomes limited by diffusion.

- The energy consumption of electrodialysis systems varies during the treatment process. This is caused by the gradual depletion of ions in the diluting compartments and the concomitant decrease of conductivity. The dissipation of energy in the membrane/solution interfaces accounts for an important part of the energy losses. Therefore it is important to operate at optimum current densities that minimize these energetic losses. Other approaches such as the design of electrodialysis stacks with improved hydrodynamic conditions are also beneficial in order to decrease the energy losses.

- Ion-exchange membranes are not completely semipermeable and some leakage of electrolyte ions of the same charge as the membrane can occur, especially at high electrolyte concentrations. This can significantly reduce the quality of the recovered products.

- Membrane fouling could occur and decrease the performance of electrodialysis processes. In the case of solutions containing heavy metals, the formation of precipitates can be very problematic since it can completely block the ion transport through the membranes and increase the energy consumption. In this regard, it is important to determine the best operating conditions in order to avoid the membrane fouling. The selection of underlimiting currents or the use of specific modes of operation, such as electrodialysis reversal or pulsed electric currents, could contribute to avoid these problems.

- Metal containing wastewaters could be composed of mixtures of several ions. Therefore, the competitive transport of ions with the same charge through the membranes could diminish the purity and the added value of the recovered solutions. To avoid such problems, operating conditions that favor the transport of specific ions could be applied. Moreover, the development of membranes with selectivity for certain ions (i.e. monovalent-ion-selective membranes) can imply a significant advance in this respect.

- Industrial effluents are usually characterized by having extreme pH values and high oxidizing strengths. These conditions imply the requirement for membranes with higher chemical stabilities. Nafion is a reference for such applications, however, they are expensive and so far they have not found competitive alternative membranes.

The transport phenomena and the energy consumption in electromembrane processes depend strongly upon the characteristics of the ion-exchange membranes. Accordingly, the mass transfer processes occurring in systems of ion-exchange membranes are explained below in more detail.

1.3 Ion-exchange membranes

1.3.1 Structure and properties of ion-exchange membranes

Ion-exchange membranes are the key components of electrodialysis cells. They are polymers bearing fixed charges in their structure. These charges show electrostatic affinity toward ions with opposite charge (electrolyte counterions) and repulsive forces against those ions having the same charge sign (electrolyte coions). Ion-exchange membranes can be divided into two types: cation-exchange membranes and anion-exchange membranes. Cation-exchange membranes possess negative fixed ionic groups (e.g.: $-SO_3^-$, $-COO^-$, $-PO_3^{2-}$, $-PO_3H^-$, $-C_6H_4O^-$, etc.) and are selective for cations; whereas anion-exchange membranes possess positive fixed ionic groups (e.g.: $-NH_3^+$, $-NRH_2^+$, $-NR_2H^+$, $-NR_3^+$, $-PR_3^+$, $-SR_2^+$, etc.) and are selective for anions [33]. The principle of the selectivity of ion-exchange membranes is shown schematically in Fig. 1.8. The applied

electric field determines the direction of ion movement, whereas the charge of the membranes determines if a specific ion can be transferred from one compartment to another: i.e. only the membrane counterions are able to cross the membranes, whereas coions are rejected and retained in the feed compartments.

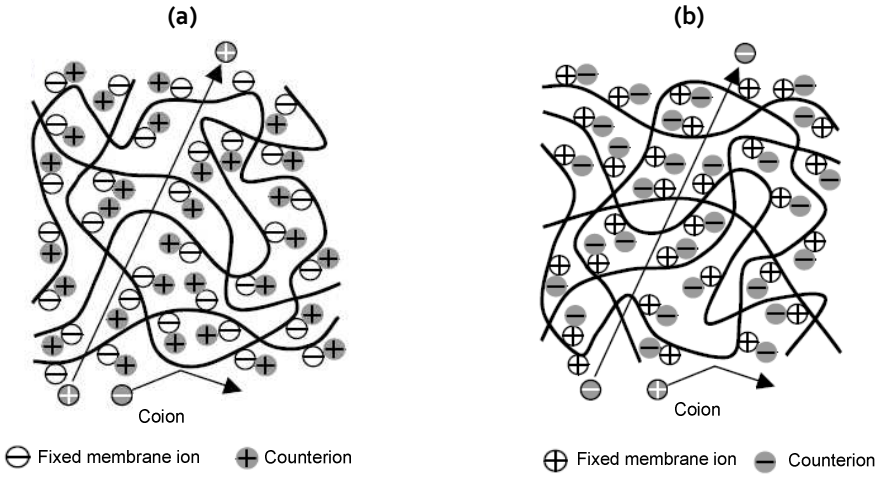

Figure 1.8. Structure of ion-exchange membranes and principle of counterion attraction and coion repulsion for (a) cation-exchange membranes and (b) anion-exchange membranes.

The ability of ion-exchange membranes to discriminate between oppositely charged ions was put on a mathematical basis by Donnan [34]. The term Donnan potential (φ_{Don}), which is used to refer to the potential difference between a membrane (φ^m) and a solution (φ^s), is given by Eq. (1.1) [35]:

$$\varphi_{Don} = \varphi^m - \varphi^s = \frac{RT}{z_j F} \ln \frac{a_j^s}{a_j^m} \tag{1.1}$$

Here, R is the universal gas constant, T is the absolute temperature, F is the Faraday's constant; and z_j, a_j^s and a_j^m are the electrochemical valence, the activity in the solution and in the membrane of the component j, respectively. The Donnan potential is equal for all components in the solution. Therefore, if a univalent salt completely dissociated in its forming ions is considered, the subscript j can be replaced by + and – to refer to the salt cation and anion, respectively. Moreover, in the case of a dilute solution the activities can

be replaced by concentrations. Accordingly, Eq. (1.1) can be transformed into the following expression:

$$\varphi_{Don} = \frac{RT}{F}\ln\frac{c_+^s}{c_+^m} = -\frac{RT}{F}\ln\frac{c_-^s}{c_-^m} \tag{1.2}$$

Which can be simplified to obtain Eq. (1.3):

$$\frac{c_+^s}{c_+^m} = \frac{c_-^m}{c_-^s} \tag{1.3}$$

If it is assumed that the electroneutrality is accomplished in the cation-exchange membrane, the concentration of counterions in the membrane (c_+^m) is equal to the sum of the concentration of coions in the membrane (c_-^m) and the density of fixed charges of the membrane (X):

$$c_+^m = c_-^m + X \tag{1.4}$$

Whereas in the solution the concentration of counterions and coions is the same as the electrolyte concentration (c_0) for a univalent salt:

$$c_+^s = c_-^s = c_0 \tag{1.5}$$

Therefore, the concentration of coions in the membrane phase can be obtained by substituting Eqs. (1.5) and (1.4) into (1.3), which results in the following expression:

$$c_-^m = \frac{{c_0}^2}{X + c_-^m} \tag{1.6}$$

If it is assumed that the concentration of coions in the membrane phase is much lower than the fixed charge density ($c_-^m <<< X$), Eq. (1.6) can be simplified according to Eq. (1.7):

$$c_{-}^{m} = \frac{{c_0}^2}{X} \tag{1.7}$$

It can be deduced from Eq. (1.7) that the Donnan exclusion, i.e. the exclusion of coions, is most effective when the membrane contains a high concentration of fixed charges and the electrolyte concentration is low. Since commercial cation-exchange membranes have a high concentration of fixed charges, when salt concentrations are lower than the membrane ion exchange capacity, anions are almost completely excluded. This range of concentrations is commonly referred as the Donnan coion exclusion domain. However, at higher salt concentrations, the cation-exchange membranes become measurably permeable to anions [25].

The fraction of current carried by the anions and cations is usually known as the transport number. In the case of a 1:1 strong electrolyte composed of a single salt solution (i.e.: NaCl), the transport number in the membrane phase for the cations is T_+ and the transport number for the anions is T_-. Since the current is transported through an ion-exchange membrane either by anions or cations, it is assumed that:

$$T_+ + T_- = 1 \tag{1.8}$$

For a multicomponent electrolyte, where several cations and anions could pass through the membrane, Eq. (1.8) is converted into:

$$\sum_j T_+ + \sum_j T_- = 1 \tag{1.9}$$

Where the subscript j accounts for the different cations and anions present in the solution. In single salt solutions and concentrations lower than the concentration of fixed charges in the membrane (i.e.: in the Donnan coion exclusion domain) the coions are mainly excluded from the membrane and their transport number is very small, normally between 0 and 0.05. On the contrary, the membrane counterions carry almost all the current, having transport numbers between 0.95 and 1.0.

In addition to the high selectivity for membrane counterions, membranes should posses other important features. The main characteristics that ion-exchange membranes should have can be summarized as follows [36]:

- High permselectivity. Membranes should allow the transport of a high fraction of counterions and avoid the permeation of coions.
- Low electrical resistance. The low electrical resistances in membrane systems are required in order to achieve the desired desalination rates with lower energy consumptions.
- Good mechanical strength and dimensional stability.
- Good chemical and radiation stability, durability.
- Reasonable cost.

The membrane properties determine to a great extent the efficiency of the separation process through the electrodialysis cells, i.e. the rate of removal of contaminants and the electrical consumption of the treatment process. In addition, the preparation of durable membranes also affects the economic viability of electromembrane processes, since the frequent replacement of damaged ion-exchange membranes raises the investment costs.

1.3.2 Ion transport and concentration polarization

The transport of ions in electrodialysis cells is significantly affected by the selectivity of the ion-exchange membranes. Due to the membrane selectivity the electric current is carried through the membranes predominantly by counterions (cations in a cation-exchange membrane and anions in an anion-exchange membrane), which have transport numbers close to 1. On the contrary, in the bulk solution the current is transported by both counterions and coions, which have similar transport numbers (~0.5). This difference in the transport numbers implies that the transport of counterions occurs faster in the membrane than in the bulk solution and, as a result, concentration changes take place in the solution close to the membrane surface. According to the IUPAC nomenclature, these concentration gradients are called concentration polarization [37].

Fig. 1.9 shows a schematic representation of the concentration and potential gradients formed in an electrodialysis cell. As can be seen, the gradients in the electrical potential between each compartment due to the applied electric field act as a driving force for the movement of ions through the membranes, which act as a selective barrier only allowing the transport of counterions. The effects of concentration polarization are also schematically depicted in each membrane/electrolyte interface. At the surface of the membranes facing the diluted compartments the concentration decreases. On the other hand, there is an accumulation of counterions at the surface of the membranes in the concentrated compartments. The solution layers where the concentration gradients are formed are denominated diffusion boundary layers. The diffusion boundary layers in the concentrated compartments do not affect significantly the performance of the cell. However, the decrease in concentration at the depleting diffusion boundary layers implies a limitation in the ion transport as well as a reduction in the ionic conductance of these layers, which leads to an increased electrical resistance of the entire cell.

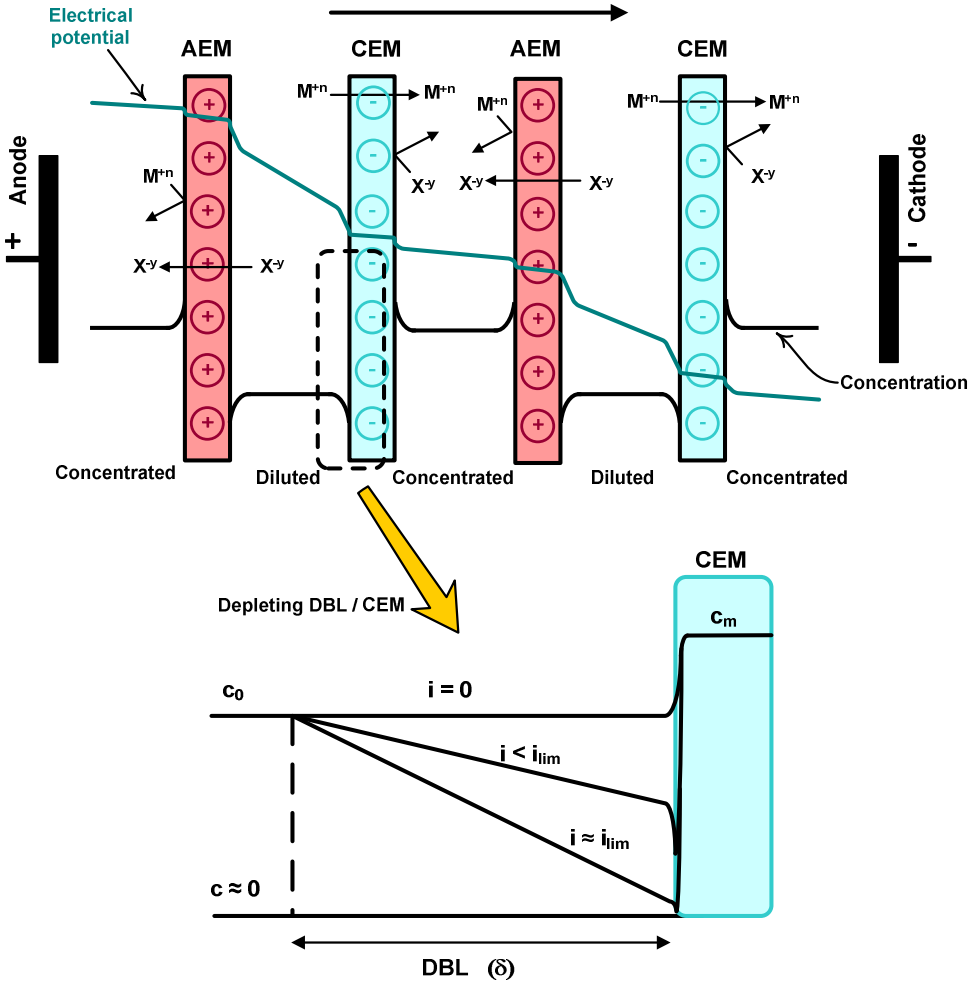

Figure 1.9. Schematic representation of the concentration and potential profiles in the different compartments of an electrodialysis cell. Counterion concentration profiles in the depleting diffusion boundary layer formed next to a cation-exchange membrane (AEM: anion-exchange membrane, CEM: cation-exchange membrane, DBL: diffusion boundary layer).

Since the target of the present Thesis is the study of the transport of metal ions through cation-exchange membranes, we will focus on the transport phenomena occurring in the depleting diffusion boundary layer formed next to a cation-exchange membrane. The counterion concentration profiles in this solution layer at different current densities are plotted in more detail in Fig. 1.9. When the system is in equilibrium without the application of current, the diffusion boundary layer is not formed and the concentration is equal to the initial one (c_0) within the entire diluted compartment (including the solution

layer next to the membrane). The concentration of counterions in the membrane phase (c_m) may be higher, close to the ion exchange capacity of the membrane.

However, when a current is applied, the ions tend to move due to the influence of the electric field. In the membrane phase we can assume that the transport of counterions takes place predominantly by migration (i.e. movement caused by an electric field), and the flux of counterions through the membrane (J_+^m) can be expressed by means of Eq. (1.10) [38]:

$$J_+^m = \frac{iT_+}{z_+F} \tag{1.10}$$

Where i is the applied current density and z_+ is the valence of the membrane counterion. In the solution layer next to the membrane the flux of counterions (J_+^s) is due to migration and diffusion (i.e. driven by differences of concentration), and can be thus described by Eq. (1.11) [38]:

$$J_+^s = \frac{it_+}{z_+F} + D\left(\frac{\partial c_+}{\partial x}\right)_x \tag{1.11}$$

Where D is the diffusion coefficient of the salt, x is the coordinate in the direction perpendicular to the membrane surface, t_+ is the transport number of the cation in the solution and c_+ is the concentration of the cation. Therefore, when a current is imposed to an ion-exchange membrane system, the material balance at the membrane/solution interface ($x = 0$) may be expressed through the equality of ingoing and outgoing ion flux densities:

$$\frac{it_+}{z_+F} + D\left(\frac{\partial c_+}{\partial x}\right)_{x=0} = \frac{iT_+}{z_+F} \tag{1.12}$$

The difference in transport numbers ($T_+ > t_+$) implies that the migration flux of counterions from the bulk solution to the membrane surface is lower than the migration flux from the surface toward the membrane bulk. This difference leads to a decrease of the electrolyte concentration in the solution layer next to the membrane surface and to

the formation of the diffusion boundary layer, as indicated in the detailed profiles of Fig. 1.9. When the magnitude of the current is not too high ($i<i_{lim}$), the diffusion and convection contribution into the ionic flux in the solution compensate for the difference in the migration fluxes in the solution and the membrane [39]. However, as the current is increased, the equilibrium concentration at the membrane surface becomes lower. When the current is increased up to the extent that the concentration at the membrane surface approaches zero; the supply of ions to the membrane becomes limited by diffusion. This current density is usually known as the limiting current density, i_{lim}, and can be calculated by using the following expression, known as the Peers' equation [40]:

$$i_{\lim} = \frac{z_+ D c_0 F}{\delta(T_+ - t_+)} \tag{1.13}$$

In Eq. (1.13) δ refers to the thickness of the diffusion boundary layer and c_0 to the initial salt concentration. When the i_{lim} is reached, the current density becomes saturated and the voltage drop measured through the membrane increases considerably. Therefore, the excess in current density beyond the i_{lim} is consumed in parasitic processes and contributes to increase the electrical resistance of the membrane region (membrane and adjacent solution layers).

In an electrodialysis system, the increase in resistance associated with the attainment of the i_{lim} is usually detected by representing the Cowan-Brown plot [41,42]. In such graphics, the electrical resistance across the membrane stack is represented against the reciprocal of the electric current. Fig. 1.10 shows an example of a Cowan-Brown plot of an electrodialysis unit. At current densities lower than the i_{lim} the electrical resistance of the system is very low. However, when the i_{lim} is surpassed, the current is not used to transport counterions and the resistance increases abruptly.

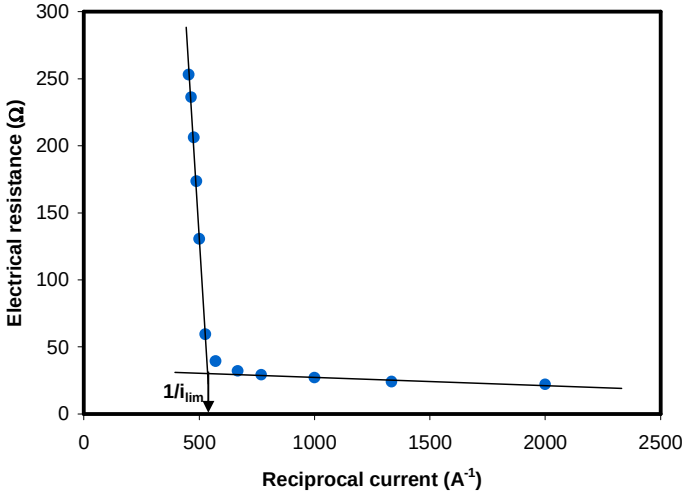

Fig. 1.10. Cowan-Brown plot of an electrodialysis system.

One of the most important contributions to the increase in the resistance of the electrodialysis system is associated with the processes occurring in the membrane regions, especially in the depleting diffusion boundary layers. Since the electrodialysis units are composed of several ion-exchange membrane systems of similar characteristics, it is more precise to study the phenomena occurring in a system formed by a single ion-exchange membrane and the adjoining solution layers. The behavior of the ion-exchange membranes is usually evaluated by analyzing their current-voltage curves, which are plots representing the relationship between the voltage drop across the membrane system (U_m) and the applied current densities. Fig. 1.11 shows a typical current-voltage curve obtained for a cation-exchange membrane. The relationship between current and membrane voltage is linear at low current densities ($i<i_{lim}$). On the contrary, when the i_{lim} is reached, the membrane voltage drop increases very sharply, hence contributing to the increased electrical resistance detected for the entire electrodialysis cell. Nevertheless, the so-called limiting current density can be further exceeded if a certain threshold in the membrane voltage drop is surpassed. The region of currents higher than the i_{lim} ($i>i_{lim}$) is conventionally called the overlimiting region, as indicated in Fig. 1.11. This region is not predicted by the concentration polarization theory, and is not observed in pressure driven membranes.

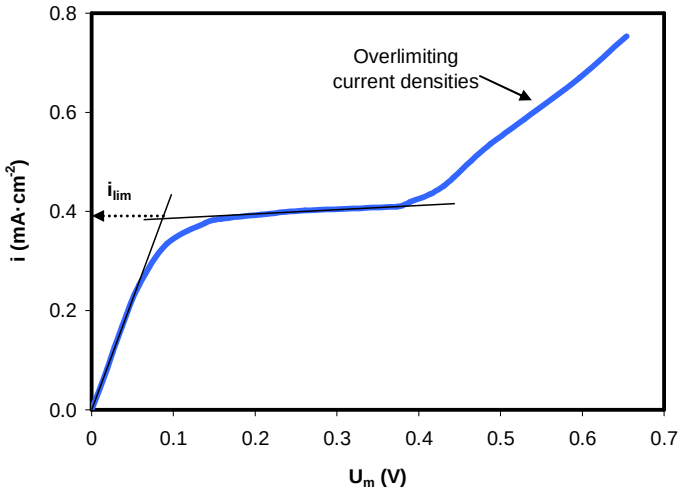

Figure 1.11. Current-voltage curve obtained for a cation-exchange membrane.

Traditionally the overlimiting region has been attributed to the dissociation of water and the subsequent transport of H^+ and OH^- ions through the membranes, which could imply additional effects in an electrodialysis cell. For example, if water splitting takes place, important pH changes may occur near the membranes and metallic precipitates could be formed at the surface of cation-exchange membranes in the diluting compartments, thus blocking the membrane pores [43-45]. In the case of alkaline metals, the formation of scaling in the concentrated compartments has been also reported to cause important operational problems [45,46]. In addition, the intense decrease of the conductivity in the desalting compartments increases the electrical resistance of the cells. Due to these undesired effects, overlimiting currents have been typically avoided. However, there has been proven evidence that also other processes different from water splitting can contribute to the increased ionic flux beyond the i_{lim}. These processes are mainly related to an increased convective mixing in the depleting boundary layers, which could imply an improved transport of counterions through the membranes. For example, it was reported that stable cation removal efficiency rates through a cation-exchange membrane could be maintained at overlimiting currents, even with the formation of precipitates at its surface [47]. Bukhovets et al. also found out that overlimiting current conditions had a positive effect on the transport of aminoacids through cation-exchange membranes, which was caused by the washing out of a fouling layer of the membranes [48]. This has increased the possibilities of the use of electrodialysis systems for new exciting

applications in industrial processes. The potential of the application of electromembrane processes at overlimiting currents is discussed in more detail in the following section.

1.3.3 The potential of the overlimiting current regimes

In general, in electrodialysis systems it is desired to achieve fast desalination rates (high current densities) with the lowest energy consumption (operating costs) and membrane area (investment costs). However, the current density is usually selected according to criteria of energy efficiency. This implies that, in practice, the use of underlimiting currents was traditionally prescribed because the overlimiting currents were attributed to the generation of unwanted species (dissociation of water into H^+ and OH^- ions), to the counterion current exaltation due to the dissociation of water, and to a loss of permselectivity of the membranes. Nevertheless, this conception has changed today as the origin of the overlimiting membrane conductance has been more precisely investigated, and the use of overlimiting current regimes is being considered for some applications.

A variety of investigations have evidenced that the water splitting is a phenomenon more likely to occur in anion-exchange membranes due to the catalytic activity of tertiary amines present in their structures, whereas it was nearly absent in cation-exchange membranes [49-52]. Moreover, it has been proven that overlimiting currents can also be related to an increased transport of electrolyte counterions [53,54]. This increased supply of electrolyte counterions from the bulk solution to the membrane depleting surface is mainly caused by convective phenomena that are induced at an advanced stage of concentration polarization and under the effect of strong electric fields. Gravitational convection and electroconvection are the most important mechanisms of current-induced convection.

Therefore, the proper utilization of overlimiting current modes can signify an important improvement of electromembrane processes, since it may permit obtaining fast desalination rates, thus implying a reduction in the necessary area of ion-exchange membranes. For this reason, several works have been conducted in order to promote the overlimiting currents. For example, it has been proven that the presence of surface and electrical inhomogeneities in the membranes could enhance electroconvection, and according to this, the surface modification of ion-exchange membranes has been widely studied [53,55-57]. With regard to the modes of operation of electrodialysis units, also

some advances have been achieved, such as the application of overlimiting current pulses to the electrodialytic removal of metal ions [58,59]. Nevertheless, most of the research conducted in order to understand the effect of the overlimiting currents on the performance of electrodialysis processes has been done with solutions of NaCl or KCl. Given the diverse applications of electrodialysis for the treatment of metal containing effluents, it is also important to note that the electrolyte properties could also have some influence on the type of overlimiting mechanism and its tendency to occur, which is also studied in the present Thesis.

1.3.4 Transport of heavy metal ions

The transport of metal ions through cation-exchange membranes has been widely studied with solutions of monovalent alkali metal ions, such as Na^+ or K^+. However, as explained in previous sections, the use of electrodialysis to remove heavy metal ions from industrial wastewaters has multitude of potential applications, which could bring about advantages from both environmental and economical points of view. To our knowledge, there are fewer studies focusing on the phenomena related to the transport of heavy metal ions through cation-exchange membranes. Therefore, in order to increase the utilization of electromembrane processes as a sustainable alternative to treat industrial effluents containing heavy metals it is fundamental to gain a better knowledge on the mechanisms of ion transport in these systems.

Among heavy metals, transition metals are of special significance due to their occurrence in several industrial processes, because of their high prices and due to their environmental hazards. The transition metals are those corresponding to the groups 3-12 of the periodic table, which are framed in red in Fig. 1.12. This group of metals is generally defined as elements whose atoms have partially filled d sub-shells, or which can give rise to cations with an incomplete d sub-shell [60]. These are called transition elements since they represent a transition from the metallic character of s-block elements (which mainly form ionic compounds) to the non-metallic character of p-block elements (which show high degree of covalent bonding).

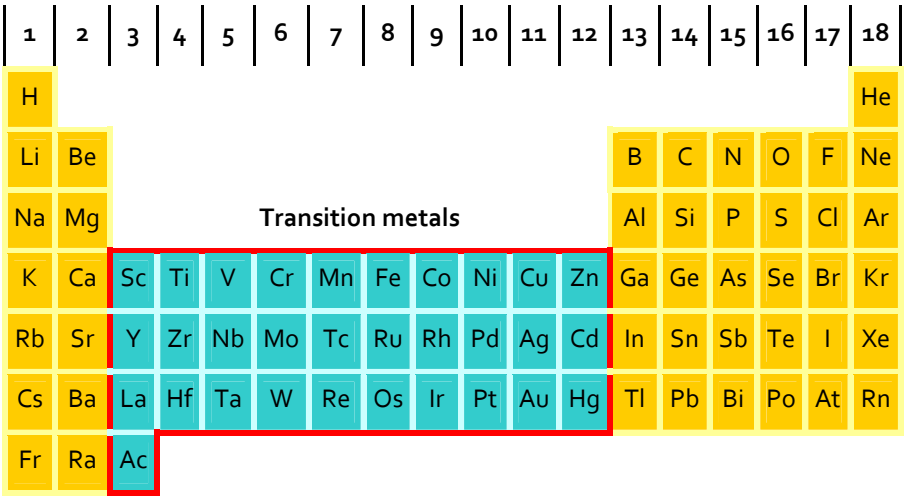

Fig. 1.12. Position of the transition metals in the periodic table of the elements.

One of the main characteristics of transition metal ions is the wide range of oxidation states in which they could occur. Transition metals have 5 d-orbitals and most of them have multiple oxidation states, since it is relatively easy to lose electrons for transition metals compared to the alkali and alkaline earth metals. Table 1.2 shows the common oxidation states of the first-row of transition metals. They can be stable in various multivalent ionic forms, showing all of them (except Sc) oxidation state +2 due to the loss of two 4s electrons. Their metal ions in oxidation state +2 and +3 are quite stable, but many of them can also form multivalent ions of higher oxidation state, such as Mn or Cr.

Table 1.2. Common oxidation states of the first-row transition metals (●: common oxidation states, ○: possible but unlikely oxidation states).

		Sc	Ti	V	Cr	Mn	Fe	Co	Ni	Cu	Zn
		$s^2 d^1$	$s^2 d^2$	$s^2 d^3$	$s^1 d^5$	$s^2 d^5$	$s^2 d^6$	$s^2 d^7$	$s^1 d^8$	$s^1 d^{10}$	$s^2 d^{10}$
Oxidation state	7					●					
	6				●	●	○				
	5			●	○	●	●				
	4		●	●		●	○	○			
	3	●	●	●	●	●	●	●	●		
	2		●	●	●	●	●	●	●	●	●
	1									●	
	0										
		21	22	23	24	25	26	27	28	29	30
		Atomic number									

The different oxidation states and the relatively low reactivity of the unpaired d electrons impart specific properties to transition metals. These metals have the ability to form several charged compounds in many oxidation states, which are commonly known as complex ions. A complex ion has a metal ion at its centre with a number of other ligands surrounding it, which can be attached to the central ion by coordination bonds. Some of the ligands include water molecules, hydroxyl ions, chloride ions or sulfate ions. This characteristic feature makes transition heavy metals especially different from alkali and alkaline earth metals, since they can form several ions of different shapes and characteristics and, thus, of different conductive and transport properties. For example, the structure of the hexaaquo complex formed by Fe^{3+} ions with water is shown in Fig. 1.13. As a consequence of the bigger size of the complex ions with respect to the free ions, the ionic mobilities of the complex species should be lower in relation to the free metal ion.

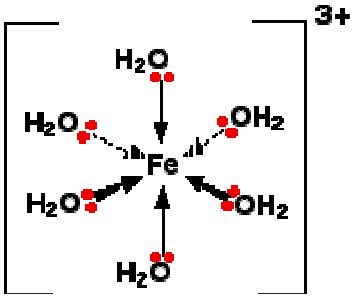

Figure 1.13. Structure of the hexaaquo complex of Fe^{3+} ions, $[Fe(H_2O)_6]^{3+}$.

In addition to the size effects, the different combination possibilities of concentration and pH in heavy metal containing solutions could lead to the formation of several complex ions with different ligands, variable coordination numbers and ionic charge. For example, the ions resulting from dissolving $Fe_2(SO_4)_3$ salts in water could give rise to the coexistence of the following species: Fe^{3+}, $FeSO_4^+$, $Fe(SO_4)_2^-$, $FeOH^{2+}$, $Fe(OH)_2^+$, $Fe(OH)_3$ or $Fe(OH)_4^-$. The salts which give rise to this type of speciation are usually termed as weak electrolytes, because they are forming several complex species instead of staying as free ions in solution (i.e. Fe^{3+} and SO_4^{2-} ions). This characteristic makes solutions of heavy metal ions different from solutions of alkali ions such as NaCl, which are fully dissociated in their forming ions (Na^+ and Cl^-). Moreover, the changes of pH and concentration taking place in the diffusion boundary layers and in the membrane phase could alter the speciation of weak electrolytes, thus implying changes in the species that are transported through the membranes.

The formation of the diffusion boundary layers may also be altered by the presence of ionic species with different properties. In addition to this, the transport through the membrane and the membrane conductivity can also change due to the uptake of different types of ions inside the membrane phase. Some authors reported different affinities of the membrane fixed charges for ions of varying valence. Okada et al. observed that cation-exchange membranes had a higher affinity for trivalent cations than for divalent ones [61]. These characteristics are especially important in the case of industrial wastewaters, which are usually composed of mixtures of several ions. For example, in those cases where the recovery of the most valuable ions is preferred over that of other ions, the different mobilities in the solution and the different affinities for the membrane fixed charges would determine the quality of the recovered product and, therefore, would affect the economic viability of electrodialysis systems. Other important aspects related to the transport of heavy metal ions through ion-exchange membranes

include the possibility of fouling of the membranes due to the formation of precipitates or the role that heavy metal ions could have on the overlimiting current mechanisms [62].

1.4 References

[1] S. Giljum, A. Behrens, F. Hinterberger, C. Lutz, B. Meyer, Modelling scenarios towards a sustainable use of natural resources in Europe, Environmental Science & Policy, 11 (2008) 204-216.

[2] K. Halada, M. Shimada, K. Ijima, Forecasting of the consumption of metals up to 2050, Materials Transactions, 49 (2008) 402-410.

[3] Risk list 2012. British Geological Survey (BGS), 2012.

[4] T. J. Brown, N. E. Idoine, E. R. Raycraft, R. A. Shaw, E. A. Deady, J. Rippingale, T. Bide, C. E. Wrighton, H. Holbrook, World mineral production 2008-2012, British Geological Survey (BGS), Keyworth, Nottingham, 2014.

[5] T. E. Norgate, W. J. Rankin, The role of metals in sustainable development, Green Processing, 1 (2002) 49-55.

[6] M.A. Reuter, C. Hudson, A. van Schaik, K. Heiskanen, C. Meskers, C. Hagelüken, Metal recycling: opportunities, limits, infrastructure. A report of the working group on the global metal flows to the international resource panel, United Nations Environment Programme, 2013.

[7] T. E. Gradel, R. Barr, D. Cordier, M. Enriquez, C. Hagelüken, N. Q. Hammond, S. Kesler, G. Mudd, N. Nassar, J. Peacey, B. K. Reck, L. Robb, B. Skinner, I. Turnbull, R. Ventura Santos, F. Wall, D. Wittmer, Estimating long-run geological stocks of metals., UNEP International Panel on Sustainable Resource Management, Working Group on Geological Stocks of Metals, 2011.

[8] T.D. Kelly, G.R. Matos, Historical statistics for mineral and material commodities in the United States, 2014.

[9] Mineral profile: Nickel, Natural Environment Research Council, British Geological Survey (BGS), 2008.

[10] F. Fu, Q. Wang, Removal of heavy metal ions from wastewaters: A review, Journal of Environmental Management, 92 (2011) 407-418.

[11] A. Maceda-Veiga, M. Monroy, A. de Sostoa, Metal bioaccumulation in the Mediterranean barbel (Barbus meridionalis) in a Mediterranean river receiving effluents from urban and industrial wastewater treatment plants, Ecotoxicology and Environmental Safety, 76 (2012) 93-101.

[12] I. Riba, J. Blasco, N. Jiménez-Tenorio, M.L. González de Canales, T. Ángel DelValls, Heavy metal bioavailability and effects: II. Histopathology-bioaccumulation relationships caused by mining activities in the Gulf of Cádiz (SW, Spain), Chemosphere, 58 (2005) 671-682.

[13] B. Cui, Q. Zhang, K. Zhang, X. Liu, H. Zhang, Analyzing trophic transfer of heavy metals for food webs in the newly-formed wetlands of the Yellow River Delta, China, Environmental Pollution, 159 (2011) 1297-1306.

[14] M. Barwick, W. Maher, Biotransference and biomagnification of selenium copper, cadmium, zinc, arsenic and lead in a temperate seagrass ecosystem from Lake Macquarie Estuary, NSW, Australia, Marine Environmental Research, 56 (2003) 471-502.

[15] International Agency for research on cancer. Nickel and nickel compounds. IARC monographs on the evaluation of carcinogenic risks to humans, 169, 1990.

[16] International Agency for research on cancer. Chromium(VI) compounds. IARC monographs on the evaluation of carcinogenic risks to humans, 147, 1990.

[17] Heavy metals in waste. Final report of the European Commission, 2002.

[18] S.R. Jennings, D.R. Neuman, P.S. Blicker, Acid mine drainage and effects on fish health and ecology: a review, Reclamation Research Group Publication, Bozeman, MT, 2008.

[19] Reference document on best available techniques for the surface treatment of metals and plastics. Integrated Pollution Prevention and Control, European Commission, 2006.

[20] Reference document on best available techniques in the food, drink and milk industries. Integrated Pollution Prevention and Control, European Commission, 2006.

[21] Y. Oren, E. Korngold, N. Daltrophe, R. Messalem, Y. Volkman, L. Aronov, M. Weismann, N. Bouriakov, P. Glueckstern, J. Gilron, Pilot studies on high recovery BWRO-EDR for near zero liquid discharge approach, Desalination, 261 (2010) 321-330.

[22] S. Casas, C. Aladjem, J. L. Cortina, E. Larrotcha, F. Valero, C. Miguel, Concentration of Seawater Reverse Osmosis Brines using Electrodialysis for a Zero Discharge System, Procedia Engineering, 44 (2012) 1749-1750.

[23] J. Shen, J. Huang, L. Liu, W. Ye, J. Lin, B. Van der Bruggen, The use of BMED for glyphosate recovery from glyphosate neutralization liquor in view of zero discharge, Journal of Hazardous Materials, 260 (2013) 660-667.

[24] J.X. Zhuang, Q. Chen, S. Wang, W.M. Zhang, W.G. Song, L.J. Wan, K.S. Ma, C.N. Zhang, Zero discharge process for foil industry waste acid reclamation: Coupling of diffusion dialysis and electrodialysis with bipolar membranes, Journal of Membrane Science, 432 (2013) 90-96.

[25] R. Baker, Membrane technology and applications, John Wiley & Sons, Ltd., Menlo Park, California, 2004.

[26] E.R. Reahl, Half a century of desalination with electrodialysis. GE Water & Process Technologies, 2006.

[27] F. Valero, R. Arbós, Desalination of brackish river water using Electrodialysis Reversal (EDR): Control of the THMs formation in the Barcelona (NE Spain) area, Desalination, 253 (2010) 170-174.

[28] Membrane Technology in the Chemical Industry, Wiley-VCH, 2001.

[29] H. Strathmann, Electrodialysis, a mature technology with a multitude of new applications, Desalination, 264 (2010) 268-288.

[30] B.E. Logan, K. Rabaey, Conversion of wastes into bioelectricity and chemicals by using microbial electrochemical technologies, Science, 337 (2012) 686-690.

[31] S. Pawlowski, J.G. Crespo, S. Velizarov, Pressure drop in reverse electrodialysis: Experimental and modeling studies for stacks with variable number of cell pairs, Journal of Membrane Science, 462 (2014) 96-111.

[32] J.M. Ortiz, E. Expósito, F. Gallud, V. García-García, V. Montiel, A. Aldaz, Desalination of underground brackish waters using an electrodialysis system powered directly by photovoltaic energy, Solar Energy Materials and Solar Cells, 92 (2008) 1677-1688.

[33] T. Xu, Ion exchange membranes: State of their development and perspective, Journal of Membrane Science, 263 (2005) 1-29.

[34] F.G. Donnan, Theory of membrane equilibria and membrane potentials in the presence of non-dialysing electrolytes. A contribution to physical-chemical physiology, Journal of Membrane Science, 100 (1995) 45-55.

[35] J.J. Krol, Doctoral thesis: Monopolar and bipolar ion exchange membranes. Mass transport limitations, University of Twente, Enschede, The Netherlands, 1997.

[36] Y. Mizutani, Structure of ion exchange membranes, Journal of Membrane Science, 49 (1990) 121-144.

[37] Terminology for membranes and membrane processes (IUPAC Recommendation 1996), Journal of Membrane Science, 120 (1996) 149-159.

[38] R. Audinos, G. Pichelin, Characterization of electrodialysis membranes by chronopotentiometry, Desalination, 68 (1988) 251-263.

[39] V.V. Nikonenko, N.D. Pismenskaya, E.I. Belova, P. Sistat, P. Huguet, G. Pourcelly, C. Larchet, Intensive current transfer in membrane systems: Modelling, mechanisms and application in electrodialysis, Advances in Colloid and Interface Science, 160 (2010) 101-123.

[40] A.M. Peers, Membrane phenomena, Discussions of the Faraday Society, 24 (1956) 124-125.

[41] D.A. Cowan, J.H. Brown, Effect of turbulence on limiting current in electrodialysis cells, Industrial & Engineering Chemistry, 51 (1959) 1445-1448.

[42] A. Alcaraz, F.G. Wilhelm, M. Wessling, P. Ramírez, The role of the salt electrolyte on the electrical conductive properties of a polymeric bipolar membrane, Journal of Electroanalytical Chemistry, 513 (2001) 36-44.

[43] M.S. Kang, Y.J. Choi, H.J. Lee, S.H. Moon, Effects of inorganic substances on water splitting in ion-exchange membranes: I. Electrochemical characteristics of ion-exchange membranes coated with iron hydroxide/oxide and silica sol, Journal of Colloid and Interface Science, 273 (2004) 523-532.

[44] Y. Tanaka, M. Seno, Concentration polarization and water dissociation in ion-exchange membrane electrodialysis. Mechanism of water dissociation, Journal of the Chemical Society, Faraday Transactions 1, 82 (1986) 2065-2077.

[45] J. Balster, O. Krupenko, I. Pünt, D.F. Stamatialis, M. Wessling, Preparation and characterisation of monovalent ion selective cation exchange membranes based on sulphonated poly(ether ether ketone), Journal of Membrane Science, 263 (2005) 137-145.

[46] G. Saracco, Transport properties of monovalent-ion-permselective membranes, Chemical Engineering Science, 52 (1997) 3019-3031.

[47] J.H. Chang, A.V. Ellis, C.H. Tung, W.C. Huang, Copper cation transport and scaling of ionic exchange membranes using electrodialysis under electroconvection conditions, Journal of Membrane Science, 361 (2010) 56-62.

[48] A. Bukhovets, T. Eliseeva, N. Dalthrope, Y. Oren, The influence of current density on the electrochemical properties of anion-exchange membranes in electrodialysis of phenylalanine solution, Electrochimica Acta, 56 (2011) 10283-10287.

[49] I. Rubinstein, B. Zaltzman, O. Kedem, Electric fields in and around ion-exchange membranes, Journal of Membrane Science, 125 (1997) 17-21.

[50] Y. Tanaka, Water dissociation in ion-exchange membrane electrodialysis, Journal of Membrane Science, 203 (2002) 227-244.

[51] I. Rubinstein, L. Shtilman, Voltage against current curves of cation exchange membranes, Journal of the Chemical Society , Faraday Transactions 2, 75 (1979) 231-246.

[52] V.I. Vasil'eva, A.V. Zhil'tsova, M.D. Malykhin, V.I. Zabolotskii, K.A. Lebedev, R.K. Chermit, M.V. Sharafan, Effect of the chemical nature of the ionogenic groups of ion-exchange membranes on the size of the electroconvective instability region in high-current modes, Russian Journal of Electrochemistry, 50 (2014) 120-128.

[53] J. Balster, M.H. Yildirim, D.F. Stamatialis, R. Ibanez, R.G.H. Lammertink, V. Jordan, M. Wessling, Morphology and microtopology of cation-exchange polymers and the origin of the overlimiting current, Journal of Physical Chemistry B, 111 (2007) 2152-2165.

[54] I. Rubinstein, B. Zaltzman, Electro-osmotically induced convection at a permselective membrane, Physical Review E, 62 (2000) 2238-2251.

[55] M. Wessling, L.G. Morcillo, S. Abdu, Nanometer-thick lateral polyelectrolyte micropatterns induce macrosopic electro-osmotic chaotic fluid instabilities, Scientific Reports, 4 (2014).

[56] E.D. Belashova, N.A. Melnik, N.D. Pismenskaya, K.A. Shevtsova, A.V. Nebavsky, K.A. Lebedev, V.V. Nikonenko, Overlimiting mass transfer through cation-exchange membranes modified by Nafion film and carbon nanotubes, Electrochimica Acta, 59 (2012) 412-423.

[57] N.P. Berezina, N.A. Kononenko, A.A.R. Sytcheva, N.V. Loza, S.A. Shkirskaya, N. Hegman, A. Pungor, Perfluorinated nanocomposite membranes modified by polyaniline: Electrotransport phenomena and morphology, Electrochimica Acta, 54 (2009) 2342-2352.

[58] T.R. Sun, L.M. Ottosen, P.E. Jensen, G.M. Kirkelund, Effect of pulse current on acidification and removal of Cu, Cd, and As during suspended electrodialytic soil remediation, Electrochimica Acta, 107 (2013) 187-193.

[59] N. Cifuentes-Araya, G. Pourcelly, L. Bazinet, Multistep mineral fouling growth on a cation-exchange membrane ruled by gradual sieving effects of magnesium and carbonate ions and its delay by pulsed modes of electrodialysis, Journal of Colloid and Interface Science, 372 (2012) 217-230.

[60] IUPAC, Compendium of Chemical Terminology. Gold book, 2014.

[61] T. Okada, Y. Ayato, M. Yuasa, I. Sekine, The effect of impurity cations on the transport characteristics of perfluorosulfonated ionomer membranes, Journal of Physical Chemistry B, 103 (1999) 3315-3322.

[62] L. Marder, E.M. Ortega Navarro, V. Pérez-Herranz, A.M. Bernardes, J.Z. Ferreira, Evaluation of transition metals transport properties through a cation-exchange membrane by chronopotentiometry, Journal of Membrane Science, 284 (2006) 267-275.

Chapter 2

OBJECTIVES AND SCOPE

2.1 Objectives and scope

The concerns about the harmful effects of heavy metals on the environment and the human health, as well as the need for a more sustainable management of the Earth's natural resources, have promoted the introduction of clean technologies in industrial processes. Among them, electrodialyis is in a good position because it can be easily coupled into productive processes to reclaim large volumes of water and recover valuable by-products.

Nevertheless, electrodialysis presents certain limitations when it is used to treat solutions containing heavy metal ions. These limitations are related to complex mass transfer processes occurring when multivalent ions cross ion-exchange membranes. Therefore, identifying and understanding these processes would be the first step in order to improve electrodialysis and transform it into a competitive technology for the treatment of metal containing effluents. Accordingly, the principal aim of the present Thesis is:

"**To identify and investigate the main mass transfer phenomena implied in electrodialysis processes in order to optimize the treatment of industrial effluents containing heavy metals**".

The main goal of the Thesis will be accomplished by means of completing several experimental studies, which are planned in order to achieve more specific objectives. These are as follows:

- To identify the main limitations related to the transport of heavy metal ions through cation-exchange membranes and their effects on the performance of electrodialysis units.

- To determine the effects of the electrolyte concentration and composition on the limiting current densities (i_{lim}) and electrical resistances of membrane systems (R_1).

- To evaluate the influence of the speciation of metal containing solutions on the transport of ions and ion complexes through cation-exchange membranes.

- To evaluate the influence of the ion sorption, the development of concentration polarization, and the current regime on the membrane selectivity for ions of different valence present in mixture solutions.

- To identify the predominant mechanisms of overlimiting membrane conductance and evaluate the role of heavy metals on the overlimiting current mechanisms.

- To assess the effect of applying overlimiting currents on the membrane performance during long-term galvanostatic experiments.

2.2 Structure of this Thesis

This Thesis is divided into five different chapters. The structure is schematically presented in Fig. 2.1. The content of each chapter is explained as follows:

Chapter 1 introduces the problematic of the discharge of heavy metals into the environment and the interest in developing clean techniques in order to allow a sustainable use of the Earth's resources. Then, electrodialysis is presented as a sustainable treatment technique and their basic principles are explained. Once the main challenges of electrodialysis applied to the treatment of effluents containing heavy metals are identified, the main objectives of the Thesis are presented in **Chapter 2.**

Chapter 3 describes the procedures and techniques employed to carry out the experimental part of the Thesis and to achieve the proposed objectives.

The experimental results are presented and discussed in **Chapter 4,** which is divided in four different subchapters. **Chapter 4.1** is focused on the study of the transport of heavy metals through cation-exchange membranes in systems of single salt solutions. Different parameters such as the sorption of ions, the electrical resistance of the membranes and the limiting currents are obtained for single salt solutions of monovalent (Na^+) and multivalent ions (Ni^{2+}, Cr^{3+} and Fe^{3+}). The speciation of the different solutions is used in order to compare the behavior of the membranes with solutions of multivalent ions in relation to their behavior with monovalent ones.

Chapter 4.2 is focused on the investigation of the membrane behavior in systems of multicomponent mixture solutions. For this study, two different cases have been considered: the competitive ion transport between multivalent metals and protons (Ni^{2+} vs. H^+); and the competitive ion transport between monovalent and multivalent metals (Na^+ vs. Fe(III) species). As in Chapter 4.1, the ion sorption, the electrical resistance and the limiting current densities are evaluated for the different systems. The behavior of the membranes in multicomponent mixtures is also compared with the results obtained in Chapter 4.1 for single salt solutions.

Chapter 4.3 aims to evaluate the predominance of the mechanisms of overlimiting mass transfer for different electrolyte compositions. Both the dynamic response (chronopotentiometry) and the steady state behavior of the membranes (current-voltage curves) obtained in Chapter 4.1 and 4.2 are evaluated in order to identify the main mechanisms of overlimiting mass transfer. The role of the electrolyte composition on the overlimiting mechanisms is also investigated.

In **Chapter 4.4** the main results obtained from Chapter 4.2 and 4.3 are contrasted and corroborated by means of performing galvanostatic experiments of longer duration (6h). These would allow us to evaluate the effect of the CrO_3 concentration on the transport of Ni^{2+} ions through the membrane, and to assess the viability of applying overlimiting currents by taking into account the influence of other processes occurring in electrodialysis cells. The effects of the electrolyte composition and the current regime on the current efficiency and the energy consumption of each experiment are also investigated.

Finally, **Chapter 5** summarizes the main conclusions of the present Thesis.

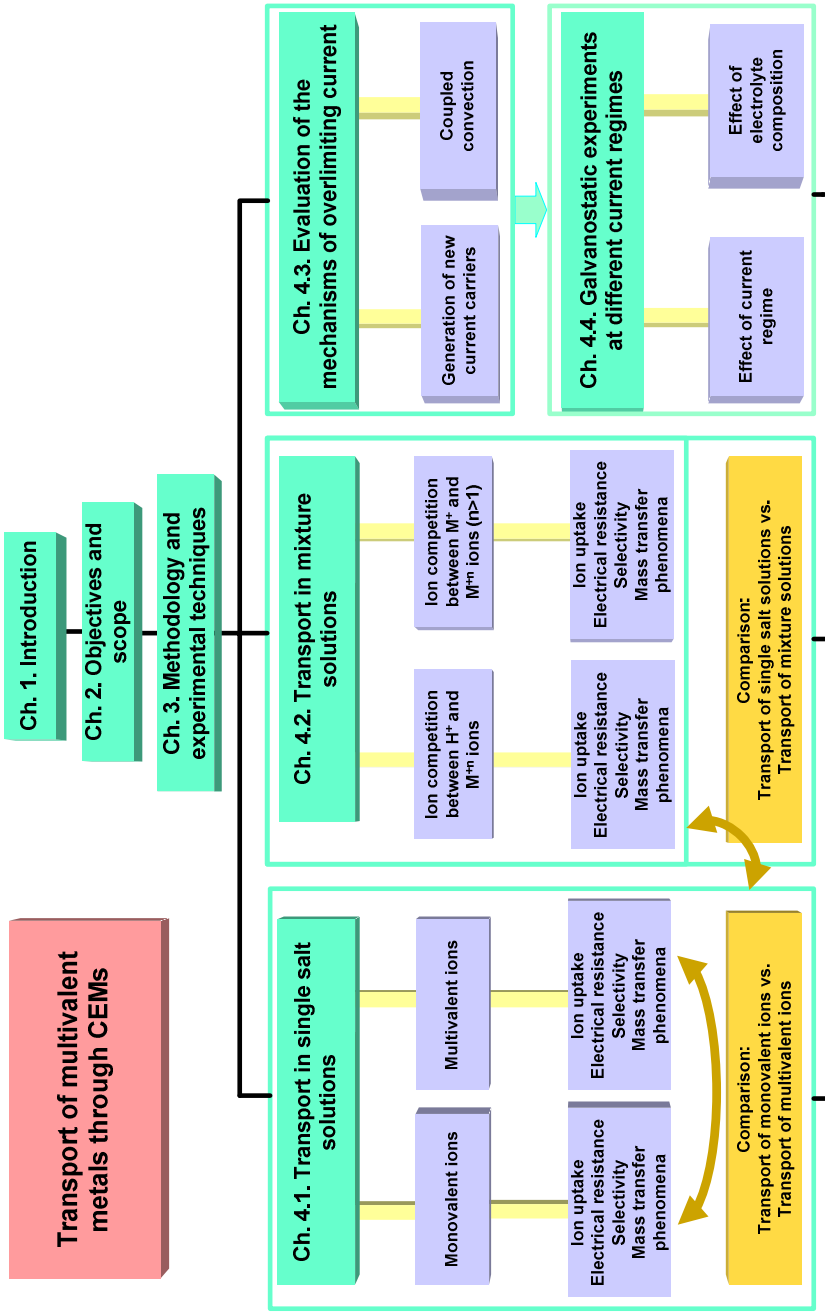

Figure 2.1. Scheme showing the structure of the Doctoral Thesis divided in different chapters.

Chapter 3
EXPERIMENTAL TECHNIQUES

3.1 Introduction

The different experimental techniques employed in the present Thesis are explained in this Chapter. The principles, the materials and the experimental setup used in the experiments are described with the aim to show how these experimental techniques can provide useful information about the properties of the cation-exchange membranes and the mass transfer phenomena taking place in electrodialysis cells.

This Chapter has been divided in different sections according to the purpose for which each technique is employed. First, the membranes used to study the transport of metal ions are described and the surface analysis techniques used to characterize their structure and visualize their morphology are explained. Second, the experiments carried out to determine the membrane affinity for the solution counterions in equilibrium conditions (without the application of an external electric field) are described. Subsequently, a description of the principles of chronopotentiometry, which is applied to characterize the dynamic response of the membranes under the application of an electric field, is

provided. The chronopotentiometric results are also useful to obtain the current-voltage curves of the membrane systems and calculate the transport number of counterions through the membranes. Finally, the conditions of the galvanostatic electrodialysis experiments used to evaluate the performance of electromembrane reactors are also described.

3.2 Ion-exchange membranes used in the Thesis

As it has been emphasized in Chapter 1, the treatment of industrial effluents by means of electromembrane processes requires the utilization of ion-exchange membranes with good properties in terms of chemical resistance and durability. Industrial wastewaters are typically characterized by having extreme pH values (very acidic or very basic) which accelerate the degradation of polymeric membranes. Moreover, many industrial effluents are composed of chemicals with high oxidizing strength, thus limiting the lifetime of the membranes. Therefore, for practical applications it is important to characterize the ion transport through commercial membranes which have good properties in terms of chemical resistance.

Nafion 117 (Du Pont®) was selected as the cation-exchange membrane to carry out the experimental part of this Thesis, since it is considered as a reference due to its high conductivity and excellent chemical resistance. Nafion is a perfluorosulfonic homogeneous membrane, i.e.: it is composed of a hydrophobic fluorinated polymer backbone to which short side chains terminated in sulfonate groups ($-SO_3^-$) are attached. The chemical structure of the Nafion membranes is shown in Fig. 3.1. The high conductivity of Nafion has been attributed to the conformation of the membrane in wet conditions [1,2]. When the membrane is hydrated, it swells and the fixed sulfonate groups form ionic aggregates, which are called ionic clusters. These clusters are connected by short and narrow channels through which the counterions are transported. The morphology of hydrated Nafion is also shown in Fig. 3.1, where the ionic clusters of about 40 Å connected by channels of 10 Å are indicated. Note that the fixed charges of the membranes are balanced with the solution counterions (H^+ in the case of membranes equilibrated in water).

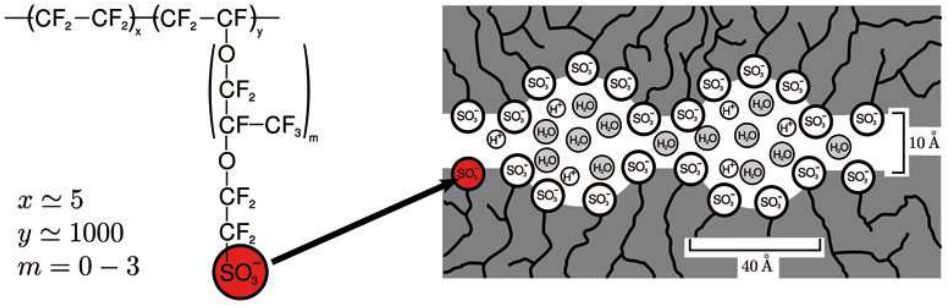

Fig. 3.1. Chemical structure of Nafion membranes and schematic diagram of the conformation of the swollen membrane immersed in an aqueous electrolyte.

The first two digits and the third digit in the nomenclature of Nafion indicate the equivalent weight and the thickness of the membrane, respectively. The equivalent weight of Nafion is defined as the number of grams of dry polymer per mole of SO_3^- groups, which is equal to the inverse of the ion exchange capacity. Therefore, in the case of the Nafion 117 membrane the term 117 indicates that the equivalent weight of the membrane is 1100 g and the thickness is 0.007 inch (~ 0.018 cm). Table 3.1 summarizes some of the properties of the Nafion 117 membrane provided by the manufacturers.

Table 3.1. Properties of the membrane provided by the manufacturers. (Source: DuPont®)

Membrane property	Typical value
Thickness (μm)	183
Basis weight (g/m^2)	360
Conductivity (S/cm)	0.10
Ion exchange capacity (meq/g)	0.90

As it will be explained in more detail below, an anion-exchange membrane was used as auxiliary membrane to conduct chronopotentiometric and electrodialysis experiments. The membrane Ionics AR 204-SZRA-412 (Ionics Inc.), which has a heterogeneous structure with reinforcing fabrics and $-N^+(CH_3)_3$ groups as fixed charges [3], was used as anion-exchange membrane.

3.3 Visualization and characterization of the structure of ion-exchange membranes

The visualization and characterization of the surface and structure of ion-exchange membranes is important because the membrane morphology is strongly correlated with their properties, such as the electrical resistance or the selectivity.

3.3.1 Scanning Electron Microscopy

The scanning electron microscope (SEM) is an instrument used to characterize the surface and structure of organic and inorganic materials. Its working principle is based on the scanning of the surface of a sample with a beam of accelerated electrons. The electrons-sample interactions derive in other signals, which are collected in different sensors in order to generate an image that reveals the surface topology and the morphology of the samples. More specifically, SEM is used in the field of ion-exchange membranes to detect the presence of different components in the membrane structure, such as ion exchange resins, polymer binder or reinforcing fibers. It is also useful to observe the topology of the surfaces and detect geometrical surface heterogeneities which are reported to affect the development of concentration polarization phenomena near ion-exchange membranes.

SEM techniques are considered non-invasive; however, organic samples, such as ion-exchange membranes, must be submitted to a specific pretreatment which could imply a loss of their properties. In the present study, samples of Nafion 117 were prepared by sputtering their surface with an ultrathin layer of conducting material (i.e.: gold) under vacuum conditions. Both surface and cross sections of the membranes were obtained. The samples used to obtain an image of the membrane cross section were frozen in liquid nitrogen and then broken in order to produce a natural cross section. The SEM equipment used to visualize the membrane morphology was a JEOL JSM-3600 and 15 kV were applied to generate the electron beam.

3.3.2 Raman spectroscopy

Raman spectroscopy is a fundamental form of molecular spectroscopy which is used to obtain information about the structure of molecules from their vibrational transitions. Raman scattering is a two-photon event, where the property involved is the change in the

polarizability of the molecule with respect to its vibrational motion. The interaction of the polarizability with the incoming radiation creates an induced dipole moment in the molecule, and the radiation emitted by this induced dipole moment contains the observed Raman scattering [4]. In the field of ion-exchange membranes, Raman spectroscopy is very useful because it is a non-invasive and non-destructive technique that can be employed to obtain the ionic composition of the membrane material immersed in aqueous solutions and to detect the nature and stoichiometry of membrane poisoning ions [5,6].

Raman spectroscopy requires minimal sample preparation. In the present case, membrane samples immersed in water were kept flat between two optical glass plates. Then, Raman spectra were excited with a 632.75 nm radiation from a He-Ne ion laser operated at about 25 mW. For the registration of the Raman spectra we used a Witec 300R$^+$ Raman microscope.

3.4 Ion uptake experiments

The static properties of ion-exchange membranes provide information about the interactions existing under no-current conditions between the fixed sites of the membranes and the electrolyte ions. These properties depend on thermodynamic concepts and attracting/repulsing forces acting between the mobile ionic species present in the electrolyte solution and the membrane fixed charges.

Ion-exchange experiments were performed in order to determine the affinity of the membrane fixed charges toward the counterions present in the different electrolyte solutions. The ion uptake of ion-exchange membranes can be determined by means of successive equilibration steps in which the ions balancing the membrane fixed charges are replaced by other ions present in an equilibrating solution. The procedure followed is schematically represented in Fig. 3.2 and detailed below:

1. Membrane stripes of 3x3 cm^2 were cut and equilibrated in 250 ml of the desired salt solution for 24 h at room temperature (25ºC) and under stirring conditions to reach the equilibrium.

2. The membranes were removed from the electrolyte solution and the electrolyte present at their surface was wiped off using filter paper. Then, the membranes were weighed and measured with a Vernier caliper.

3. The membranes were soaked several times with abundant water during 24 h in order to remove the traces of metals that are not associated with the fixed charges of the membrane. This method is usually known as the many-stage desorption method [7]. The resulting soak solutions were collected and the concentration of metals was measured by means of Atomic Absorption Spectrometry (AAS).

4. The membranes were soaked in 1M H_2SO_4 for 24 h to replace the metallic ions bound to the membrane fixed charges with H^+ ions [8]. The soak solution was then measured for metals by means of AAS. The measurements conducted by AAS are explained in more detail in section 3.6.2.

5. Finally, the membrane samples were dried first with a filter paper and then in an oven at 50ºC during 24 h in order to remove any trace of water and humidity in the membranes. The membranes were weighed to obtain the dry weight of each membrane sample, w_{dry} .

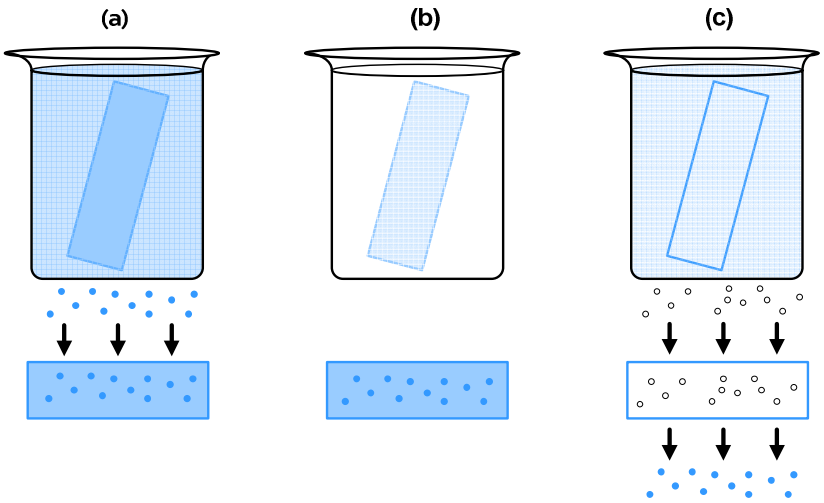

Fig. 3.2. Scheme of the steps conducted during the ion exchange experiment used to determine the membrane counterion concentration. (a) Equilibration of membrane in metal solution, (b) rinse in deionized water, (c) ion-exchange in H_2SO_4 solution. Adapted from [9].

From the determination of the concentration of metals in each soak solution, different membrane properties can be obtained. The concentration of metal counterions exchanged per gram of dry membrane (c_m) is given by Eq. (3.1):

$$c_m = \frac{c_{soak} \cdot V_{soak}}{w_{dry}} \tag{3.1}$$

Where c_{soak} and V_{soak} represent the metal ion concentration and the volume of the sulfuric acid desorbing solution, respectively. The concentration of counterions present in the membrane phase ($\overline{c_m}$, expressed in mmol per volume of membrane) can be determined by using Eq. (3.2):

$$\overline{c_m} = \frac{c_{soak} \cdot V_{soak}}{V_m} \tag{3.2}$$

Where V_m is the volume of the membrane measured in wet conditions. Finally, the partition coefficient of counterions in the membrane phase (K) can be calculated from the ratio between the concentration of counterions in the membrane phase and the concentration of counterions in the equilibrating solution (c_e) with Eq. (3.3):

$$K = \frac{\overline{c_m}}{c_e} \tag{3.3}$$

Solutions of different salts of metal sulfates; Na_2SO_4, $NiSO_4$, $Cr_2(SO_4)_3$ and $Fe_2(SO_4)_3$ (Panreac®, analytical grade); were used to carry out the ion sorption experiments. The range of metal concentrations used for the single salt experiments (corresponding to Chapter 4.1) varied from 10^{-3}M to $2 \cdot 10^{-2}$M, as summarized in Table 3.2.

Table 3.2. Electrolyte concentrations used for the ion sorption experiments conducted with single salt solutions of different metals.

$[M^{+n}]$	Na_2SO_4	$NiSO_4$	$Cr_2(SO_4)_3$	$Fe_2(SO_4)_3$
10^{-3}M	$5{\cdot}10^{-4}$M	10^{-3}M	$5{\cdot}10^{-4}$M	$5{\cdot}10^{-4}$M
$5{\cdot}10^{-3}$M	$2.5{\cdot}10^{-3}$M	$5{\cdot}10^{-3}$M	$2.5{\cdot}10^{-3}$M	$2.5{\cdot}10^{-3}$M
10^{-2}M	$5{\cdot}10^{-3}$M	10^{-2}M	$5{\cdot}10^{-3}$M	$5{\cdot}10^{-3}$M
$2{\cdot}10^{-2}$M	10^{-2}M	$2{\cdot}10^{-2}$M	10^{-2}M	10^{-2}M

Additional experiments were also conducted with mixture solutions of various metals, which correspond to the results shown in section 4.2. In this case, two different mixture solutions were considered taking into account possible applications of electromembrane processes for the treatment of industrial wastewaters: mixtures of $NiSO_4$ and CrO_3, and mixtures of Na_2SO_4 and $Fe_2(SO_4)_3$. The combination of concentrations of each compound used to prepare the mixture solutions of $NiSO_4$ and CrO_3 are summarized in Table 3.3, whereas the concentrations used to prepare the mixtures of Na_2SO_4 and $Fe_2(SO_4)_3$ are shown in Table 3.4. CrO_3 was also of analytical grade (Panreac®).

Table 3.3. Electrolyte concentrations used for the ion sorption experiments conducted with mixture solutions of CrO_3 and $NiSO_4$.

CrO_3	$NiSO_4$
0M	$5{\cdot}10^{-4}$M
	10^{-3}M
	$5{\cdot}10^{-3}$M
	10^{-2}M
10^{-3}M	$5{\cdot}10^{-4}$M
	10^{-3}M
	$5{\cdot}10^{-3}$M
	10^{-2}M
10^{-2}M	$5{\cdot}10^{-4}$M
	10^{-3}M
	$5{\cdot}10^{-3}$M
	10^{-2}M

Table 3.4. Electrolyte concentrations used for the ion sorption experiments conducted with mixture solutions of $Fe_2(SO_4)_3$ and Na_2SO_4.

$Fe_2(SO_4)_3$	Na_2SO_4
$2 \cdot 10^{-2}$M	0M
	10^{-2}M
	$2 \cdot 10^{-2}$M

3.5 Electrochemical characterization of the ion transport through the membranes

The dynamic characterization of ion-exchange membranes is useful to elucidate different transport mechanisms taking place when ions cross the membranes under the influence of an electric field. The characterization of the membranes under the imposition of current is important in order to understand the real behavior of the membranes in electrodialysis systems. Moreover, the most important properties of ion-exchange membranes, which are related to the membrane selectivity and electrical resistance, can be obtained by using electrochemical techniques. These properties depend on several factors, such as the membrane materials and structure, the characteristics of the electrolyte, as well as on kinetic concepts related to mass transfer processes.

Chronopotentiometry is a dynamic electrochemical technique which allows monitoring the variation with time of the concentration of electroactive species at the interface between an electrolyte and an ion-exchange membrane. The principle of chronopotentiometric experiments is based on the measurement of the voltage drop across a membrane system while a constant current is applied. The chronopotentiometric measurements provide an indirect measure of changes in the electrolyte composition occurring in the electrolyte/membrane interface, hence allowing us to study the concentration polarization phenomena.

3.5.1 Experimental setup and procedure

The experimental setup used for the chronopotentiometric experiments is composed of an electrodialysis cell which consists of three different compartments made of polyvinyl chloride. Each compartment has a volume capacity of 130 ml and upper apertures for the installation of the reference electrodes, the cathode and the anode. The electrodialysis cell was arranged as shown in Fig. 3.3, where an auxiliary anion-exchange membrane (Ionics AR 204-SZRA-412) is clamped between the anodic and the central compartment, and the cation-exchange membrane (Nafion 117) is clamped between the central and the cathodic compartment. The anion-exchange membrane was used in order to minimize the influence of the H^+ ions generated at the anode on the voltage measured through the cation-exchange membrane. The three compartments were filled with the same solution, so as to reduce the effect of diffusive transport between different compartments. The solution compositions used for the chronopotentiometric experiments are the same as those used in the ion uptake experiments, which are indicated in Tables 3.2-3.4. Prior to conduct the experiments the membranes were equilibrated with the salt counterions. For this purpose, the membranes were immersed in the salt solutions to be studied subsequently during at least 24 h and under stirring conditions. The effective membrane area in the chronopotentiometric experiments was 3.52 cm^2. Two Ag/AgCl reference electrodes were used to measure the voltage drop through the membrane under investigation, U_m. The reference electrodes were immersed in Luggin capillaries, with their tips close to the membrane surface (approximately at 1 mm of distance) in order to have access to the membrane/electrolyte interface. The experiments were conducted at room temperature (25ºC), in batch mode and without stirring. Two graphite bars were used as cathode and anode, and a potentiostat/galvanostat (Autolab PGSTAT 20, The Netherlands) was used to apply the current between both electrodes.

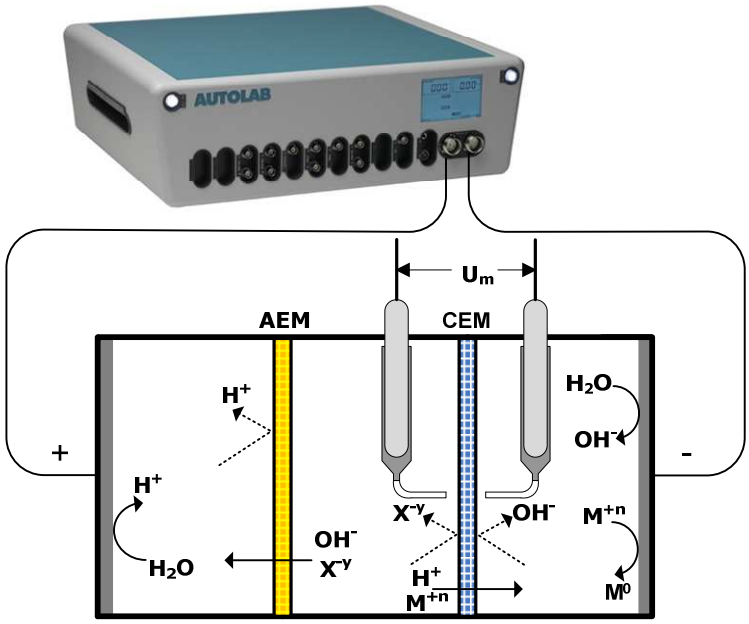

Figure 3.3. Schematic diagram of the three-cell electrodialysis setup used to conduct the chronopotentiometric experiments. (AEM: anion-exchange membrane, CEM: cation-exchange membrane).

In order to obtain the chronopotentiograms, different current pulses were imposed between cathode and anode. Each current pulse was applied for 300 s, whereas the relaxation of the system was allowed for at least other 300 s before a new pulse was applied. During the chronopotentiometric experiments, the response in U_m is registered. The term U_m includes the voltage drop corresponding to the membrane phase and that of the two adjoining solution layers. Accordingly, the measurement of U_m allows us to monitor the transition from the initial equilibrium to a final steady state reached in the system composed of the membrane and the adjacent electrolyte.

3.5.2 Chronopotentiometry

Due to the selectivity of ion-exchange membranes for counterions, the transport of counterions occurs faster through the membrane phase than in the electrolyte, where both counterions and coions carry the current. Consequently, when a driving force is applied between both sides of a membrane, gradients of concentration develop near the membrane/electrolyte interfaces [10]. Specifically, the concentration of counterions decreases near the membrane surface in the depleting compartment (the central

compartment in the case of the cation-exchange membrane shown in Fig. 3.3), whereas it increases in the concentrating compartment (cathodic compartment in the case of the cation-exchange membrane shown in Fig. 3.3). In other words, two diffusion boundary layers are developed in the vicinities of the membrane. The decrease in concentration of ionic species associated with the development of the diluting diffusion boundary layer leads to an increase in the voltage drop of the membrane system, which is registered in the chronopotentiograms.

Depending on the magnitude of the applied current, the development of the diffusion boundary layers is more or less severe and U_m evolves differently during the application of the current pulses. Figure 3.4 shows a schematic representation of the relationship between the applied signals in the form of direct current, the concentration polarization effects originated near the membrane/electrolyte interfaces, and the resulting response observed in the chronopotentiograms. At low applied current densities, the response in U_m is very fast and practically analogous to that of the current pulse. At the beginning of the current pulse an immediate increase in U_m is observed in the chronopotentiogram, which is associated with the ohmic resistance of the membrane system. Then, the increase in U_m with time during the course of the current pulse is very slight and U_m remains almost constant until the current ceases. However, as the current density is increased, the concentration of counterions at the depleting membrane surface decreases more notoriously. The increase in current can reach a limiting condition when the concentration of counterions near the membrane surface approaches zero. In that case, the scarcity of ions near the membrane depleting surface implies an increase in the electrical resistance of the membrane system and a steep increase in U_m is registered. The characteristic current density at which the concentration of counterions near the membrane depleting surface vanishes is commonly named as the limiting current density, i_{lim} [10,11]. If the current density is increased beyond the i_{lim} value, the sharp increase taking place in U_m is registered at shorter times because the depletion of ions occurs faster. Moreover, the thickness of the diffusion boundary layer, δ, may increase with increasing the excess beyond the i_{lim} value, and the final value of U_m may be also higher.

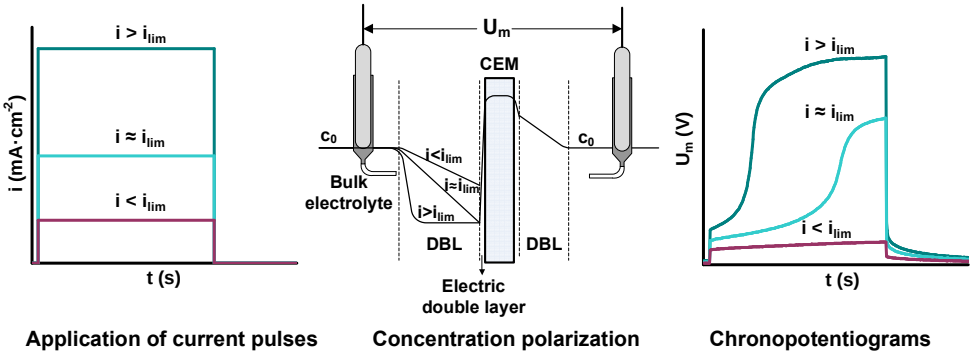

Figure 3.4. Correlation between the input signal of applied current, the profiles of counterion concentration near the membrane surface and the registered response of U_m. (CEM: cation-exchange membrane, DBL: diffusion boundary layer).

According to the different chronopotentiometric responses that are possible to obtain as a function of the applied current, the behavior of the membranes can be divided in three different current regimes: the regime of underlimiting current densities (also known as the quasi-ohmic domain), the behavior corresponding to current densities close to the i_{lim}, and the regime of overlimiting current densities. In addition, apart from the determination of the i_{lim} value and the steady state of the system at different current densities, chronopotentiometry also gives the dynamics by which the equilibrium is reached [12]. This allows us to separate the total voltage of the membrane system, U_m, into different contributions. The decomposition of the chronopotentiometric response corresponding to an ion-exchange membrane under the application of an overlimiting current is schematically represented in Fig. 3.5.

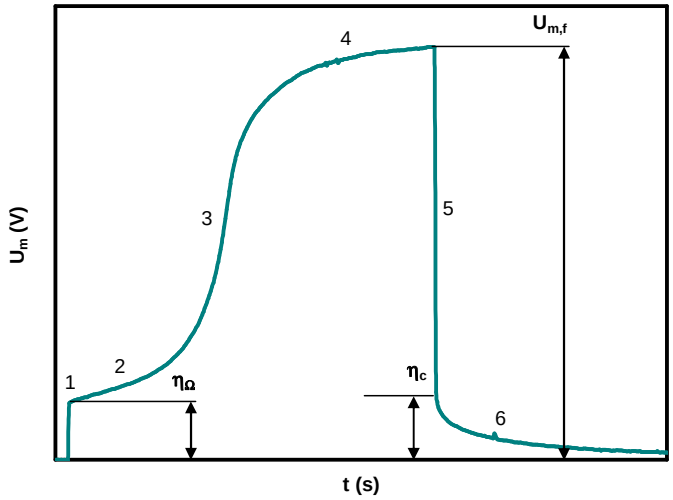

Figure 3.5. Schematic representation of the different regions appearing in chronopotentiometric curves registered at overlimiting currents.

The chronopotentiometric curves can be divided in the following six regions, as schematically indicated in Fig. 3.5:

- Region 1: the voltage drop across a membrane system composed by a cation-exchange membrane with identical solution composition at both its sides is zero when the system is not submitted to the imposition of current. As explained previously, when the application of current starts, an immediate increase in the voltage drop appears in the chronopotentiogram. This initial voltage drop corresponds to the ohmic contribution of the membrane system (η_Ω) [13,14].

- Region 2: during the first instants after reaching the ohmic overvoltage, U_m shows a moderate increase due to the development of small concentration gradients near the membrane/solution interfaces. In the case where an underlimiting current is applied, the voltage drop already levels off reaching the final value of U_m ($U_{m,f}$) and the region 3 is absent in the curves.

- Region 3: if the i_{lim} value is reached, the concentration of counterions vanishes in the depleting membrane/solution interface and the region 3 is registered in the chronopotentiogram, which is characterized by a sharp jump in the value of U_m.

- Region 4: after the acute increase in U_m, the voltage drop levels off and reaches the final steady state, thus remaining practically constant until the current ceases ($U_{m,f}$).

- Region 5: when the application of current ceases, U_m decreases abruptly reaching a certain voltage value different from zero. The voltage difference across the membrane system remaining immediately after the current is switched off represents the concentration overvoltage (η_c), which results from the different concentration profiles created at both sides of the membranes during the imposition of current [14,15].

- Region 6: the relaxation of the concentration profiles near the membrane system occurs in the last region of the curves, during which the voltage value of zero is restored in the system.

It must be noted that under the imposition of current densities far beyond the i_{lim} value, important information about the overlimiting mass transfer mechanisms can be obtained from the chronopotentiometric curves. However, these responses are very specific of each membrane/electrolyte systems and will be discussed in more detail in Chapter 4.3.

3.5.3 Calculation of the transport number

In addition to the information obtainable from the shape and voltage contributions of the chronopotentiograms, chronopotentiometry can also be used to determine the counterion transport number in the membrane phase. For this purpose, a characteristic parameter of the chronopotentiograms called the transition time has to be determined. The transition time (τ) indicates the moment at which the depletion of counterions at the depleting surface of the ion-exchange membrane takes place. This value can be obtained from the sharp increase observed in U_m when the i_{lim} values are surpassed. In the present Thesis the transition times were obtained by means of calculating the time corresponding to the maximum in the derivative of U_m with time, which corresponds to the instant when the steepest variation in U_m occurs. Fig. 3.6 shows an example of the determination of the transition time from a chronopotentiometric curve.

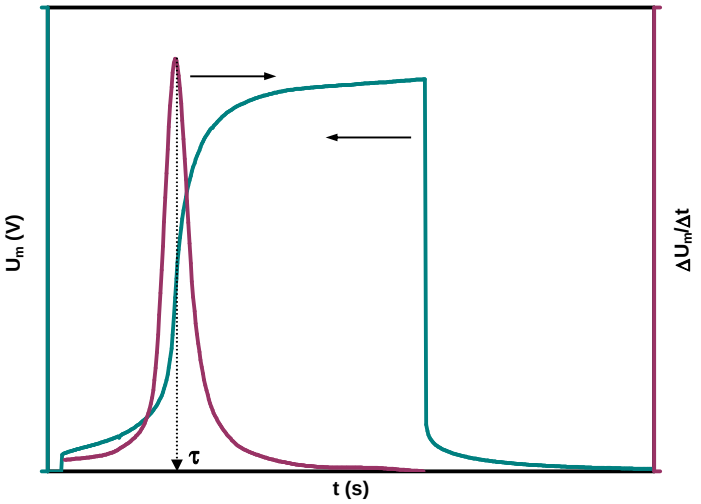

Figure 3.6. Determination of the transition time from the chronopotentiograms by means of the calculation of the maximum of the derivative of U_m with time.

The equations used to calculate the counterion transport number in the membrane phase are deduced as follows. First, let us consider a system composed of a flat cation-exchange membrane in vertical position and surrounded by a binary electrolyte in the absence of supporting electrolyte and without stirring, which is submitted to the application of a direct current. The variation of the concentration of counterions with time as a function of the distance from the surface of the membrane (x) can be described by Eq. (3.4):

$$\frac{\partial c_+}{\partial t} = -\frac{\partial J_+^s}{\partial x} \tag{3.4}$$

Where J_+^s represents the flux of cations in the solution layer next to the membrane. The convective transport of electroactive species from the bulk solution toward the membrane surface can be neglected and we can assume that the transport of counterions (in this case cations) occurs perpendicularly to the membrane surface and is principally due to diffusion and migration. Under these assumptions, J_+^s is described by Eq. (1.11), given in Chapter 1. In addition, the transport of counterions through the membrane phase (J_+^m) occurs principally by means of migration, and is described by Eq. (1.10).

At the depleting membrane/solution interface ($x=0$), J_+^s and J_+^m are equalized and the combination of Eq.(1.10) and (1.11) leads to the following expression:

$$\left(\frac{\partial c_+}{\partial x}\right)_{x=0} = \frac{i}{z_+ FD}\cdot(T_+ - t_+) \tag{3.5}$$

The relation that describes the concentration of counterions as a function of the distance from the membrane surface and time can be obtained from solving Eqs. (3.4) and (3.5). For this purpose, the Laplace transformation can be applied and the initial boundary condition $c_+(x,0)=c_0$ is used. This condition indicates that, at the beginning, the concentrations throughout the whole studied system are at equilibrium, and the concentration of counterions is the same at all points and equal to the initial electrolyte concentration c_0. The resulting solution is given by Eq.(3.6) [14,16]:

$$c_+(x,t)=c_0 - \frac{i}{z_+ FD}\cdot\left[(T_+ - t_+)\cdot 2\cdot\sqrt{\frac{Dt}{\pi}}\cdot\exp\left(-\frac{x^2}{4Dt}\right) - x\cdot erfc\left(\frac{x}{2\sqrt{Dt}}\right)\right] \tag{3.6}$$

At the membrane/solution interface, Eq. (3.6) is simplified and leads to the following expression:

$$c_+(0,t)=c_0 - \frac{i}{z_+ FD}\cdot(T_+ - t_+)\cdot 2\sqrt{\frac{Dt}{\pi}} \tag{3.7}$$

The expression that relates the transition time with the bulk electrolyte concentration and the applied current density can be obtained by making $c_+(0,t)=0$, which is also known as the Sand's equation (Eq. (3.8)).

$$\tau = \left(\frac{\pi D}{4}\right)\left(\frac{c_0 z_+ F}{T_+ - t_+}\right)^2 \frac{1}{i^2} \tag{3.8}$$

In consequence, if the transport number of the counterion in the electrolyte (t_+) and the diffusion coefficient of the salt (D) are known, and the transition times are obtained from the chronopotentiometric curves, the counterion transport number in the membrane

phase (T_+) can be determined from the slope of the representation of τ against c_o/i^2. Fig. 3.7 shows an example of different chronopotentiograms obtained at different current densities, where the typical decrease in the transition time is observed to occur as the current density increases. This dependence is in agreement with the Sand's equation and the T_+ value could be obtained from the chronopotentiometric results.

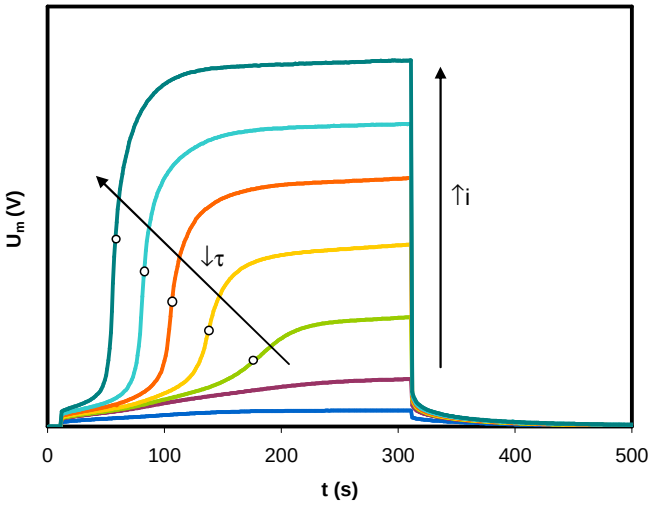

Figure 3.7. Effect of increasing the applied current density on the transition times determined by means of chronopotentiometry.

3.5.4 Current-voltage curves

The current-voltage curves of ion-exchange membrane systems are a necessary tool to characterize the membrane behavior over different ranges of current. The current-voltage curves indicate the relationship existing between the ionic current density and the steady voltage drop of the membrane system at different ranges of current density. The three characteristic types of membrane behavior can be observed in a typical current-voltage curve, such as that presented in Fig. 3.8. The different regions of electrochemical behavior of an ion-exchange membrane are explained below:

- Quasi-ohmic region: at low current densities (below the i_{lim} value) a quasi-ohmic relation defines the dependence between the applied current density and the voltage drop of the membrane system, U_m. In this region, the concentration

gradients generated at the depleting side of the membrane are not limiting for the ion transfer through the membrane, and the electrical resistance of the membrane system (R_1) can be calculated from the inverse of the slope of this region, as shown in Fig. 3.8.

- Plateau region: this region appears in the curves as the current density reaches the i_{lim} of the membrane system. When this occurs, the concentration gradients become more severe and the concentration of counterions at the depleting membrane/solution interface approaches zero. Consequently, the supply of counterions from the bulk solution toward the membrane surface is practically suppressed. In this region, the curve bends leading to a characteristic plateau. The electrical resistance of the membrane system increases considerably and, very small increments in the current density lead to drastic increases in the voltage drop of the membrane system. The i_{lim} value can be determined from the intersection between the tangents drawn for the quasi-ohmic and the plateau region, as shown schematically in Fig. 3.8.

- Overlimiting region: this region appears at an advanced stage of concentration polarization. When the voltage drop of the membrane/electrolyte system reaches a certain threshold, the system becomes unstable because of the strong electric field and the low ionic concentration at the depleting membrane/electrolyte interface. Under these circumstances, the ionic transfer through the membrane can be again enhanced due to the involvement of new mechanisms of ionic transfer. Among them, the most important are the formation of water dissociation products, the exaltation effect caused by OH^- and H^+ ions, gravitational convection and electroconvection [10]. These phenomena result in an additional supply of counterions to the membrane surface. As a consequence, the current rises again with the increase in the membrane voltage. The resistance of the membrane system in this region can be also approximated from the inverse of the slope of this region, which is usually known as the resistance of the third region (R_3).

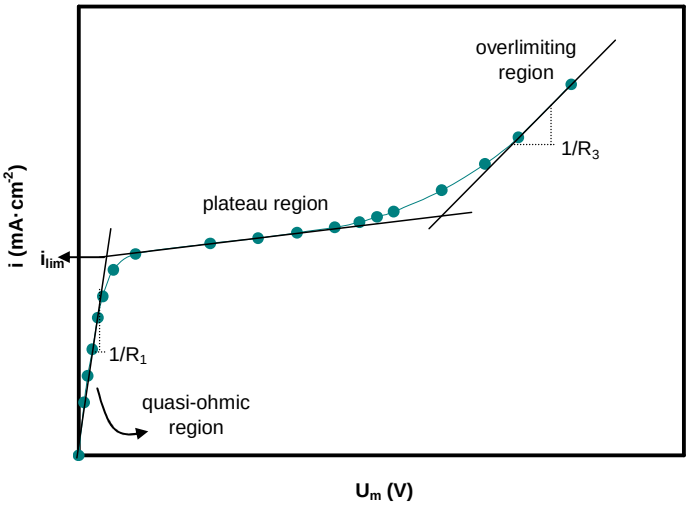

Figure 3.8. Typical current-voltage curve obtained for a cation exchange membrane showing the ohmic region, the plateau region and the overlimiting region.

The current-voltage curves of the studied membrane/electrolyte systems can be obtained from the chronopotentiometric curves. For this purpose, the final steady values of U_m ($U_{m,f}$) were plotted as a function of the current density of their corresponding current pulse. The translation of the chronopotentiometric results into a current-voltage curve is schematically represented in Fig. 3.9.

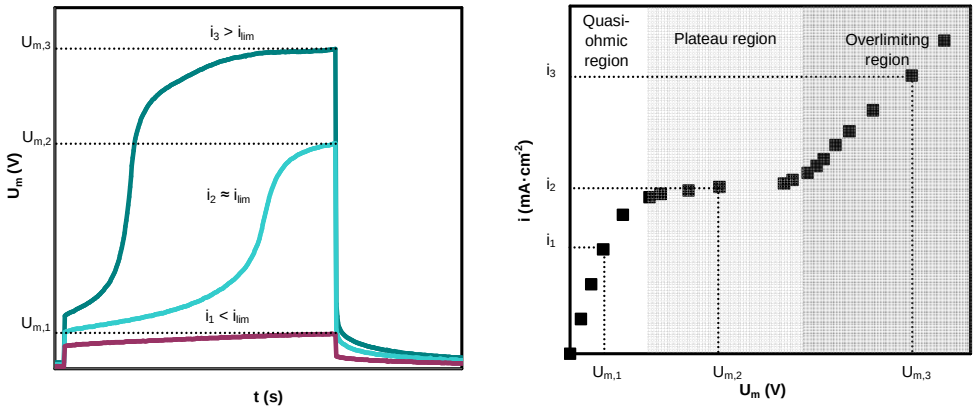

Figure 3.9. Correlation between the chronopotentiometric curves and the current-voltage curves.

3.6 Galvanostatic electrodialysis experiments

The conduction of electrodialysis experiments allows us to simulate the membrane behavior under conditions similar to those present in real processes. These experiments differ from other electrochemical techniques on the fact that the experiment duration is longer, which can serve to elucidate some transport phenomena not detected by other experimental techniques. Moreover, the practical interest of applying specific operating conditions can be assessed by conducting these experiments, because the evolution with time of the concentration of species can be measured, thus allowing the calculation of energy-related indicators, which are useful in order to get an idea about the energy consumption and the efficiency of the mass transfer processes.

3.6.1 Experimental setup and procedure

The experimental setup used for the electrodialysis experiments (shown in Fig. 3.10) was analogous to the setup used for conducting the chronopotentiometric experiments. It consists of three cylindrical compartments, between which the anion- and cation-exchange membranes were clamped. Each compartment has a volume capacity of 130 ml. However, in this case the effective membrane area was increased to 12.56 cm^2 in order to increase the ionic transfer rates through the membranes and promote concentration changes in each compartment measurably by means of AAS. All the experiments were carried out at room temperature (25ºC) and without recirculation. The three compartments were filled with the same solution, so as to reduce the effect of diffusive transport between different compartments. A constant current is imposed between two graphite electrodes by a potentiostat/galvanostat (Autolab, PGSTAT 20).

During the experimental tests, the applied current promotes the motion of different ions due to the electric field created within the electrodialysis cell. The ions with electronegative charge move from the central towards the anodic compartment crossing the anion-exchange membrane. At the same time, the anion-exchange membrane acts as a permselective barrier that impedes the passage of protons (generated at the anode as a consequence of the water oxidation reaction) toward the central compartment. Cationic species are transported through the cation-exchange membrane. Consequently, the concentration of metal ions increases in the cathodic compartment, whereas the central compartment becomes diluted with time. Each compartment possesses upper apertures

for taking the samples at different time periods and measuring the evolution of the concentration of ions with time.

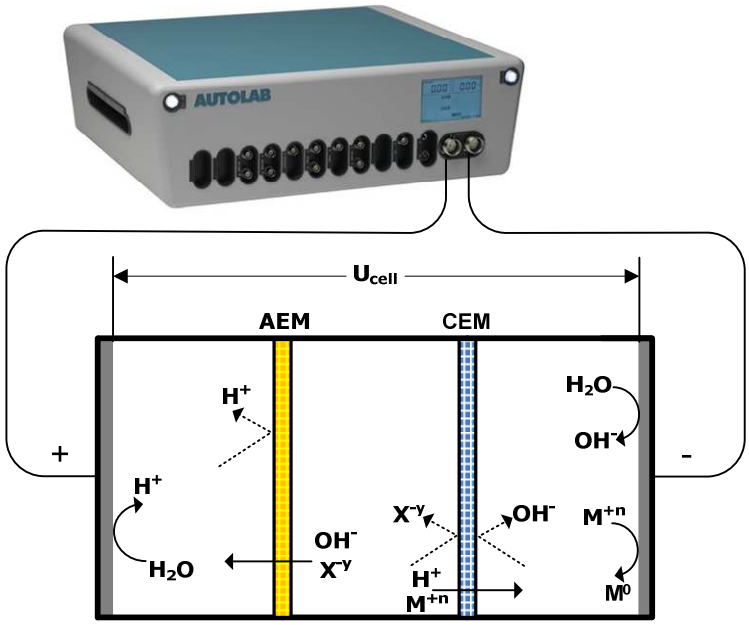

Figure 3.10. Schematic diagram of the three-compartment electrochemical cell used to conduct the galvanostatic experiments for the treatment of metal containing effluents. (AEM, anion-exchange membrane; CEM, cation-exchange membrane; U_{cell}, cell voltage drop)

The galvanostatic experiments correspond to the results presented in Chapter 4.4. For this study, the system composed of mixtures of $NiSO_4$ and CrO_3 was selected. The main objective of these experiments was to investigate the influence of the electrolyte composition on the transport of Ni^{2+} ions through the Nafion 117 membrane, and to study the influence of the applied current regime on the removal of Ni^{2+} ions from the central compartment. The compositions considered for this study are shown in Table 3.5, together with the applied current densities. The values of current density were selected by taking the i_{lim} values calculated for each composition as a reference. These values were obtained from the current-voltage curves previously registered. To study the effect of the CrO_3 concentration on the membrane selectivity in the underlimiting range of currents, a current corresponding to 75% of the most restrictive value of i_{lim} was selected for a constant concentration of $NiSO_4$ (i.e.: the i_{lim} corresponding to the solutions without CrO_3). To study the effect of the applied current regime on the transport of Ni^{2+} ions

through the membrane, values corresponding to 75, 100 and 125% of the i_{lim} corresponding to each solution composition were considered, as indicated in Table 3.5.

Table 3.5. Current densities applied during the galvanostatic experiments conducted for the section 4.4.

[$NiSO_4$]	[CrO_3]	Effect of CrO_3 on the transport of Ni^{2+} ions at underlimiting currents	Effect of the current regime on the transport of Ni^{2+} ions		
10^{-3}M	0M	75%·i_{lim} (10^{-3}M $NiSO_4$ + 0M CrO_3)	75%·i_{lim}	100%·i_{lim}	125%·i_{lim}
	10^{-3}M		75%·i_{lim}	100%·i_{lim}	125%·i_{lim}
	10^{-2}M		75%·i_{lim}	100%·i_{lim}	125%·i_{lim}
10^{-2}M	0M	75%·i_{lim} (10^{-2}M $NiSO_4$ + 0M CrO_3)	75%·i_{lim}	100%·i_{lim}	125%·i_{lim}
	10^{-3}M		75%·i_{lim}	100%·i_{lim}	125%·i_{lim}
	10^{-2}M		75%·i_{lim}	100%·i_{lim}	125%·i_{lim}

The experiments lasted for 6 h and samples were extracted every hour from the central compartment in order to register the decrease in the concentration of Ni^{2+} ions with time. These samples were diluted in order to obtain samples in the range of concentrations measurable by means of AAS. For the solutions with an initial concentration of 10^{-3}M $NiSO_4$, aliquots of 1 ml were extracted and diluted with distilled water in flasks of 10 ml volume capacity. For the solutions with an initial concentration of 10^{-2}M $NiSO_4$, aliquots of 1 ml were diluted with distilled water in flasks of 50 ml volume capacity. The specifications of the AAS measurements are indicated more precisely in Section 3.6.2.

Apart from the concentration of Ni(II) in the central compartment, the evolution of the cell voltage drop (U_{cell}) during the course of the experiment was also measured. U_{cell} corresponds to the voltage drop measured between the cathode and anode, as indicated in Fig. 3.10. In addition, the pH was also measured in each compartment at the end of the experiments. Both measured variables, the concentration of Ni(II) and the U_{cell} values, were subsequently used to quantify the performance of the electrodialysis operations. For this purpose, the figures of merit of the electromembrane reactor, which are explained below in section 3.6.3, were calculated.

3.6.2 Atomic absorption spectrometry

The concentration of metallic species in both the galvanostatic and the ion sorption experiments was determined by means of atomic absorption spectroscopy. For this purpose, an AAnalyst 100 atomic spectrometer (Perkin Elmer) was used. Except for the measurement of Na(I), which is sensitively determined by flame atomic emission spectrometry (AES), the rest of metals were determined by atomic absorption spectrometry (AAS). The conditions for the measurement of the metallic solutions are summarized in Table 3.6. The absorbance of different standard solutions was measured in the order of low to high concentrations and then the absorbance of the sample solutions was also measured.

Table 3.6. Measuring conditions for the determination of the concentrations of different metals by means of atomic absorption spectrometry.

Metal	Method	Standards	Wavelength (nm)	Slit width (nm)	Acetylene-oxidant ratio	Lamp current (mA)
Na(I)	AES	NaCl	589	0.2	2-4	-
Ni(II)	AAS	$NiSO_4$	351.5	0.2	2-4	17
Fe(III)	AAS	$Fe(NH_4)_2(SO_4)_2 \cdot 6H_2O$ (Mohr's salt)	248.3	0.2	2-4	5
Cr(III)	AAS	$K_2Cr_2O_7$	425.4	0.2	2-2	10

The atomic absorption measurements consist on focusing an incident light toward a flame that contains the analyte and determining the quantity of light that has been absorbed by the nebulized atoms. The absorbance follows a linear relationship with the concentration of analyte in the samples. Therefore, different calibration curves can be obtained for each specific ion. Fig. 3.11 shows an example of the calibration curves obtained for determining the concentration of each metallic ion used in the present Thesis. As can be observed, in all the cases good linear fittings are obtained. It must be noted that the case of Na(I) is particular because two different linear fittings can be represented at both low and high electrolyte concentrations.

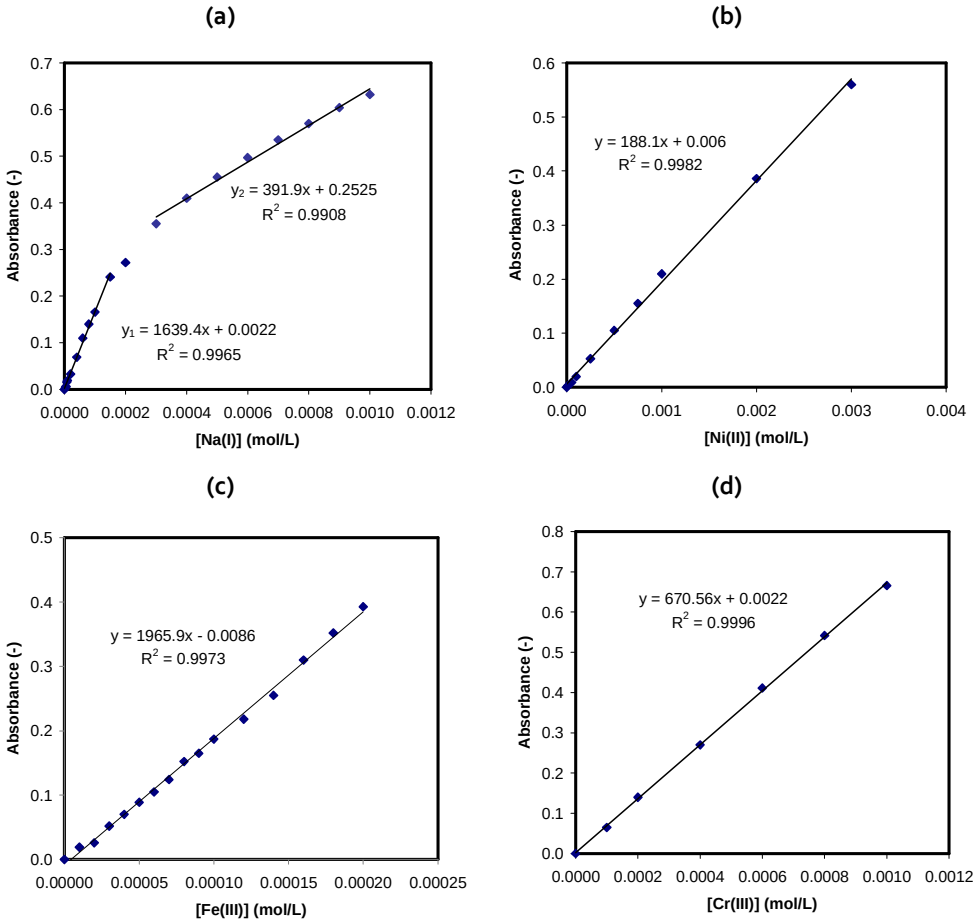

Figure 3.11. Examples of the calibration curves obtained for the determination of different metals. (a) Curve for solutions of Na(I), (b) Curve for solutions of Ni(II), (c) Curve for solutions of Fe(III), and (d) curve for solutions of Cr(III).

3.6.3 Figures of merit of an electromembrane reactor

Once determined the evolution with time of the concentration of species of interest in each compartment, different parameters indicative of the efficiency in the mass transfer and in the energy usage of an electrodialysis cell can be calculated. These parameters are usually referred as the figures of merit of an electromembrane reactor.

The fractional conversion (X), which relates the changes in the concentration of the species of interest in relation to the initial concentration, is calculated by means of Eq.

(3.9). The fractional conversion can also be known as the removal rate when it is calculated from the concentration variations occurring in the depleting compartment.

$$X(t)=\frac{c_0-c_t}{c_0}\times 100 \qquad (\%) \qquad (3.9)$$

In Eq. (3.9) c_0 is the initial concentration in the solution and c_t corresponds to the concentration of this species at a given time. Furthermore, the current efficiency (ϕ), which is an indicative of the mass transfer efficiency of the process and relates the current used to transfer the ions towards the cathodic compartment (in a cation-exchange membrane) with the total current input, was calculated by using the Eq. (3.10) [17]:

$$\phi(t)=\frac{nFV(c_0-c_t))}{\int_0^t I\,dt}\times 100 \qquad (\%) \qquad (3.10)$$

Where n is the number of equivalents exchanged per mole, V is the volume of the solution in the central compartment and I is the applied current. The space-time yield (η) is another parameter related to the achieved productivity that indicates the mass of ions removed per unit of volume and time and is defined by Eq. (3.11):

$$\eta(t)=\frac{M(c_0-c_t)}{t} \qquad (g\cdot l^{-1}\cdot h^{-1}) \qquad (3.11)$$

where M represents the molecular weight of the species of interest. Finally, the specific energy consumption (E_s) was also calculated using the following equation:

$$E_s(t)=\frac{\int_0^t U_{cell}\cdot I\,dt}{3600\cdot M\cdot V\cdot c_0\cdot X} \qquad (kW\cdot h\cdot kg^{-1}) \qquad (3.12)$$

Where U_{cell} is the cell voltage registered between the anode and cathode of the electrodialysis cell.

3.7 References

[1] K.A. Mauritz, R.B. Moore, State of understanding of Nafion, Chemical Reviews, 104 (2004) 4535-4586.

[2] K. Schmidt-Rohr, Q. Chen, Parallel cylindrical water nanochannels in Nafion fuel-cell membranes, Nature Materials, 7 (2008) 75-83.

[3] N.P. Berezina, N.A. Kononenko, O.A. Dyomina, N.P. Gnusin, Characterization of ion-exchange membrane materials: Properties vs structure, Advances in Colloid and Interface Science, 139 (2008) 3-28.

[4] Handbook of Raman Spectroscopy. From the research laboratory to the process line, CRC Press, 2001.

[5] C. Thibault, P. Huguet, P. Sistat, G. Pourcelly, Confocal Raman micro-spectroscopy and electrochemical investigation of anion transport through ion-exchange membranes, Desalination, 149 (2002) 429-433.

[6] S. Deabate, R. Fatnassi, P. Sistat, P. Huguet, In situ confocal-Raman measurement of water and methanol concentration profiles in Nafion® membrane under cross-transport conditions, Journal of Power Sources, 176 (2008) 39-45.

[7] X.T. Le, Contribution to the study of properties of Selemion AMV anion exchange membranes in acidic media, Electrochimica Acta, 108 (2013) 232-240.

[8] K.L. Huang, T.M. Holsen, J.R. Selman, Impurity partitioning in Nafion and ceramic separators used for purification of spent chromium plating solutions, Journal of Membrane Science, 210 (2002) 137-145.

[9] A.H. Galama, J.W. Post, M.A. Cohen Stuart, P.M. Biesheuvel, Validity of the Boltzmann equation to describe Donnan equilibrium at the membrane-solution interface, Journal of Membrane Science, 442 (2013) 131-139.

[10] V.V. Nikonenko, N.D. Pismenskaya, E.I. Belova, P. Sistat, P. Huguet, G. Pourcelly, C. Larchet, Intensive current transfer in membrane systems: Modelling, mechanisms and application in electrodialysis, Advances in Colloid and Interface Science, 160 (2010) 101-123.

[11] A.M. Peers, Membrane phenomena, Discussions of the Faraday Society, 24 (1956) 124-125.

[12] R. Ibanez, D.F. Stamatialis, M. Wessling, Role of membrane surface in concentration polarization at cation exchange membranes, Journal of Membrane Science, 239 (2004) 119-128.

[13] M. Taky, G. Pourcelly, A. Elmidaoui, Transport properties of a commercial cation-exchange membrane in contact with divalent cations or proton-divalent cation solutions during electrodialysis, Hydrometallurgy, 43 (1996) 63-78.

[14] A. Nicoara, L. Oniciu, Polarization at ion exchange membrane/electrolyte solution interface. V- Square wave chronopotentiometry, Revue Roumaine de Chimie, 44 (1999) 963-970.

[15] M. Taky, G. Pourcelly, F. Lebon, C. Gavach, Polarization phenomena at the interfaces between an electrolyte solution and an ion exchange membrane: Part I. Ion transfer with a cation exchange membrane, Journal of Electroanalytical Chemistry, 336 (1992) 171-194.

[16] R. Audinos, G. Pichelin, Characterization of electrodialysis membranes by chronopotentiometry, Desalination, 68 (1988) 251-263.

[17] S. Koter, A. Narebska, Current Efficiency and Transport Phenomena in Systems with Charged Membranes, Separation Science and Technology, 24 (1989) 1337-1354.

Chapter 4
RESULTS AND DISCUSSION

4.1 Transport of metal ions present in single salt solutions through cation-exchange membranes

4.1.1 Introduction

In this section of the results (4.1), the transport of multivalent metal ions through cation-exchange membranes is investigated. Multivalent heavy metals are both precious and hazardous. Therefore, the interest of this study is justified by the benefits that the treatment of metal containing wastewaters by means of electromembrane processes could imply for a variety of industries and, in general, for the environment.

First, we characterize the morphology and structure of the Nafion perfluorosulfonic membrane used in the Thesis. For this purpose, the chemical structure of Nafion is investigated by Raman microscopy, and the morphology of the membrane is visualized

using SEM. The sorption of different metal ions in equilibrium conditions by the membrane fixed charges is also measured.

Then, the transport of sulfate salts of different metals through the membranes is studied systematically by means of chronopotentiometry. The behavior of the Nafion membrane is first evaluated using solutions of monovalent metals (Na^+ ions). Subsequently, the transport of salts of divalent, Ni(II), and trivalent metals, Cr(III) and Fe(III), is studied and compared to that of monovalent sodium ions. For this purpose, the specific characteristics of multivalent metals (ion size, charge, equilibria of formation of complex species) are considered in order to identify the different phenomena that could take part in the process of formation of concentration polarization layers at the membrane/solution interface.

4.1.2 Structure and ion exchange equilibrium properties of Nafion membranes

4.1.2.1 Characterization of the membrane structure

The information about the morphology and internal structure of ion-exchange membranes is crucial in order to understand the manner in which the ionic transfer occurs through the membranes. In this section, the morphology of the membrane is visualized and characterized. The Raman spectrum of a sample of Nafion 117 immersed in water was obtained (see Fig. 4.1). In this figure we can see the characteristic peaks of the bonds present at both the polymer backbone and the charged groups of the Nafion membrane, which are tabulated in the literature [1]. For example, the twist and in plane bending vibration of the CF_2 bonds are associated to the peaks observed at 292 and 385 cm^{-1}, whereas the peak observed at 731 cm^{-1} is assigned to the symmetric stretching vibration of these groups. The vibrations associated with the membrane fixed charges are attributed to the bands appearing at higher Raman shifts: the stretching vibration of the C-S bond and the SO_3^- groups correspond to the peaks observed at 805 and 1060 cm^{-1}, respectively. The absence of additional characteristic peaks stems from the homogeneous structure of this membrane, which does not have polymer binder, impurities or reinforcements in their chemical composition.

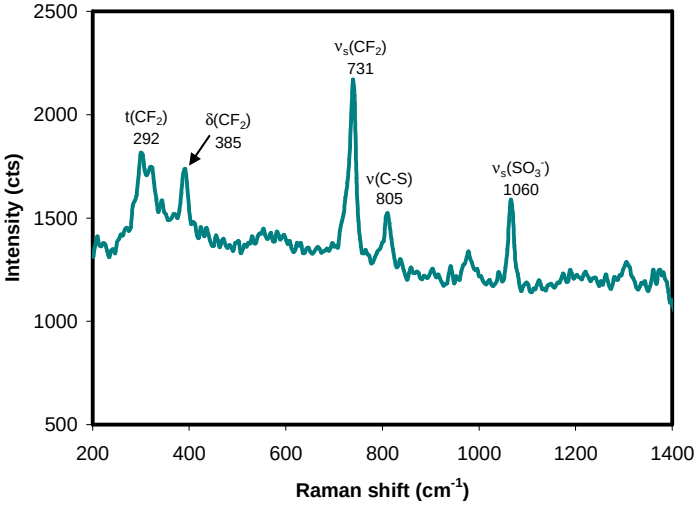

Fig. 4.1. Raman spectrum of the Nafion 117 membrane immersed in water.

The structure of the membranes was also visualized by means of scanning electron microscopy. The surface and cross section of Nafion 117 is shown in Fig. 4.2. Both pictures show a dense and uniform conformation of the membrane, where only one phase can be clearly visualized. In addition to this, the topology of the membrane surface is very flat, which is consequence of the fact that these membranes are synthesized by extrusion. This structure is typical of homogeneous ion-exchange membranes. Moreover, as explained above, the presence of agglomerates of polymer binder or the presence of reinforcing material (typically found in the case of heterogeneous membranes) is not identified in the pictures. Therefore the good properties in terms of mechanical stability and chemical durability seem to be exclusively due to the membrane matrix composed of perfluorinated polymer. Additionally, the ion conducting properties of Nafion may be due to the homogeneous distribution of the SO_3^- ion clusters within the membrane phase, as indicated previously in Fig. 3.1.

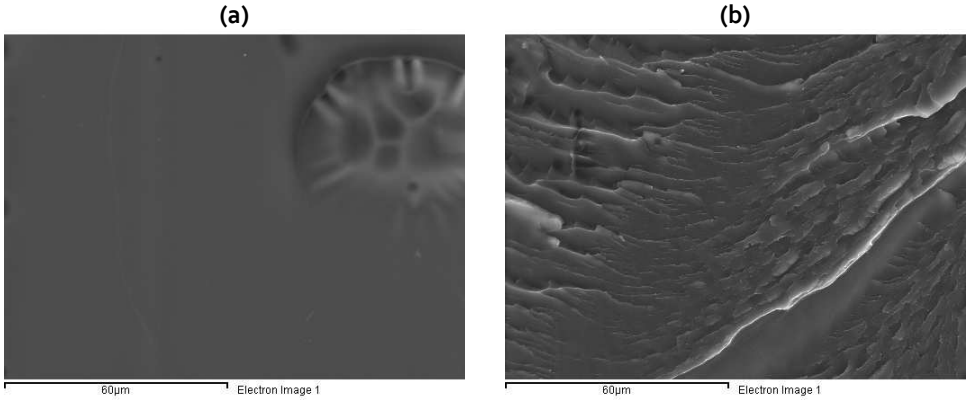

Fig. 4.2. SEM images obtained for the Nafion 117 membrane. (a) Picture of the membrane surface and (b) picture of the membrane cross-section.

4.1.2.2 Ion sorption equilibrium properties

The ion sorption equilibrium properties are important in order to know the affinity that the membrane fixed charges have for different ions. The procedure used to measure the quantity of ions exchanged in the membrane phase is explained in section 3.4 of the previous chapter. The concentration of ions in the membrane phase (c_m, expressed in mmol of ions per gram of dry membrane) is represented as a function of the concentration of the equilibrating solutions in Fig. 4.3. The metal having the highest concentration in the membrane phase is Na(I), followed in decreasing order of concentration by Ni(II), Fe(III) and Cr(III). The reason for the different results of ion uptake could stem from the different charge of each metal ion. Whereas each membrane sulfonate group can be equilibrated with one Na^+ ion; multivalent metal ions (i.e. Ni^{2+}, Fe^{3+} or Cr^{3+}) can be bound to more than one sulfonate group. With regard to the effect of the concentration of the equilibrating solution, in general the values of c_m remain constant with the external concentration. This indicates that all the membrane fixed charges are equilibrated with the electrolyte counterions, being the membrane saturated in counterions with independence of the concentration of the external solution. Only a significant decrease of c_m is obtained for the lowest concentration (10^{-3}M) in the case of Na^+ ions, which could be due to a lower affinity of the membrane for monovalent ions with very dilute solutions.

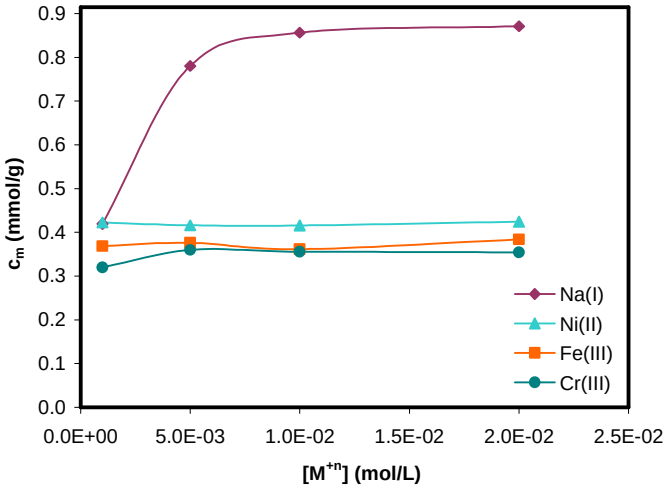

Fig. 4.3. Concentration of ions equilibrated in the membrane phase as a function of the concentration of metals in the equilibrating solution.

In order to evaluate the affinity of the membrane for different metal ions, the ion exchange capacity of the membrane was calculated by means of multiplying the c_m values by the valence of each ion. It is remarkable that the ion exchange capacity (expressed in miliequivalents per gram of dry membrane) calculated with Na_2SO_4 (0.89 meq/g) and $NiSO_4$ solutions (0.86 meq/g) is practically equal to the ion exchange capacity provided by the manufacturer (0.90 meq/g). These results reveal that each sulfonate group is bound to one Na^+ ion in the case of Na_2SO_4 solutions, and confirm that the membrane becomes saturated in electrolyte counterions. However, each Ni^{2+} ion is balancing two sulfonate groups when the membrane is immersed in $NiSO_4$ solutions.

On the contrary, the ion exchange capacity values calculated with solutions of trivalent metals ($Fe_2(SO_4)_3$ and $Cr_2(SO_4)_3$) exceed significantly the ion exchange capacity of the membranes, which reveals that the equilibrium between the membrane fixed charges and Fe(III) and Cr(III) is different from that observed for Na(I) and Ni(II) solutions. These different results indicate that, apart from free Fe^{3+} and Cr^{3+} ions, other charged Fe(III) and Cr(III) species could be equilibrating the membrane fixed charges. As it will be discussed below (see Fig. 4.31 and 4.32), if we assume that inside the membrane phase the OH^- ions are practically excluded and low pH values prevail, the main cationic species that can be balancing the SO_3^- groups are the free ions (Fe^{3+} and Cr^{3+}) and the complex ions $FeSO_4^+$ and $CrSO_4^+$. Accordingly, the fraction of membrane fixed charges equilibrated with each

type of ion could be calculated from solving the balance of moles and equivalents inside the membrane phase, which in the case of $Fe_2(SO_4)_3$ solutions are given by Eqs. (4.1) and (4.2):

$$c_{Fe(III),m} = c_{Fe^{3+},m} + c_{FeSO_4^+,m} \tag{4.1}$$

$$IEC = 0.89 meq/g = c_{Fe^{3+},m} \cdot z_{Fe^{3+}} + c_{FeSO_4^+,m} \cdot z_{FeSO_4^+} \tag{4.2}$$

Here IEC, $c_{Fe(III),m}$, $c_{j,m}$ and z_j refer to the ion exchange capacity of the membrane, the concentration of total iron and that of the ionic specie j in the membrane phase, and the charge of the specie j, respectively. The equations for $Cr_2(SO_4)_3$ solutions are analogous to Eqs. (4.1) and (4.2). The solution of the above equations indicates that approximately 90% of the membrane charges are equilibrated with Fe^{3+} ions, and 10% with $FeSO_4^+$. In the case of $Cr_2(SO_4)_3$ solutions, 75% of the charges are equilibrated with Cr^{3+} and 25% with $CrSO_4^+$. Another remarkable result is the fact that the equilibrium conditions inside the membrane phase do not vary significantly with the external concentration (as denoted by the constant values of c_m in Fig. 4.3), at least if the system is not under the influence of an applied electric field.

Finally, it is also interesting to compare the concentration of ions inside the membrane phase with the concentration of the external equilibrating solution. The partition coefficient calculated as the ratio between the concentrations of ions in the membrane to that in the external equilibrating solution, K (Eq. (3.3)), is represented in Fig. 4.4 as a function of the composition of the external electrolyte. In this case, since the membranes become saturated in counterions with independence of the external electrolyte concentration, the partition coefficients are significantly high for the lowest electrolyte concentrations. Then, the decrease of K with the external electrolyte concentration is attenuated for the highest concentrations.

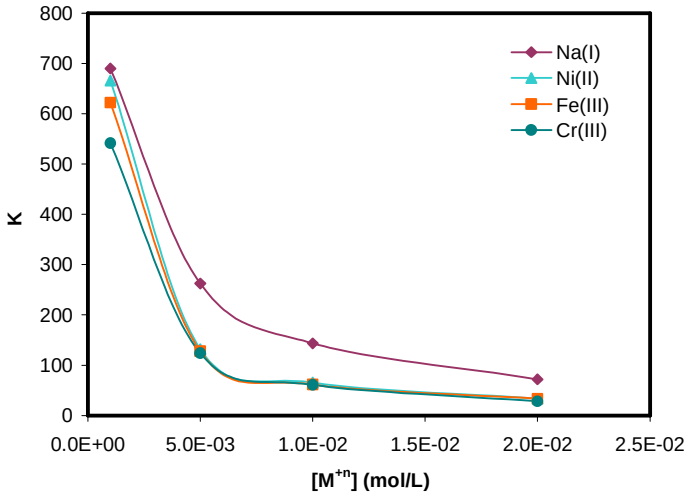

Fig. 4.4. Ion partition coefficient in the membrane phase as a function of the concentration of metals in the equilibrating solution.

4.1.3 Transport of monovalent ions

In this section, the electrochemical behavior of the Nafion 117 membrane is investigated using Na_2SO_4 solutions as the electrolyte. Na^+ is the most recurrent counterion used in the literature to characterize the ion transport through cation-exchange membranes. Therefore, the results obtained in this section can be used to compare the response of Nafion 117 to that of other membranes and to contrast it with that obtained with salts of multivalent metals.

4.1.3.1 Chronopotentiometric response

The chronopotentiometric response of the membrane was evaluated using Na_2SO_4 solutions of concentrations ranging from $5{\cdot}10^{-4}$M to 10^{-2}M, which correspond to a concentration of Na(I) of 10^{-3}M and $2{\cdot}10^{-2}$M, respectively.

The chronopotentiometric response obtained with the most diluted Na_2SO_4 solutions ($5{\cdot}10^{-4}$ M) for the underlimiting range of currents is presented in Fig. 4.5. In general, the behavior of the Nafion 117 membrane is analogous to the standard behavior typically observed in the literature for other ion-exchange membranes [2,3]. At very low values of

current density (i.e. 0.014 and 0.028 $mA \cdot cm^{-2}$), an almost plane response is observed in the chronopotentiograms and the increase of U_m with time is very slight. However, as pulses of higher current density are applied, U_m increases with time more notoriously. Since the membrane fixed charges induce selectivity for cations, the transport of Na^+ ions occurs faster in the membrane phase than in the bulk solution, where the current is carried by both cations and anions. As a consequence, the concentration of Na^+ ions decreases in the solution layer next to the membrane surface in the central compartment. This phenomenon results in an increase of the electrical resistance of the membrane system. If the current density is further increased, the concentration of Na^+ ions at the membrane surface can approach zero. In that case, the increase registered in U_m becomes very sharp, as can be seen in the curve obtained for 0.054 $mA \cdot cm^{-2}$.

The response of U_m once the current ceases was also registered during the experiments. When the current is switched off, the concentration of ionic species at the membrane/electrolyte interfaces is restored and the difference of potential measured across the membrane system diminishes asymptotically toward the initial value of zero. The time required for the U_m value to reach zero also increases with the applied current density. This fact is indicative of the effect of the current density on the concentration polarization phenomenon. As the current density increases, the concentration gradients developed near the membrane/electrolyte interfaces become stronger. Consequently, the first value of U_m registered immediately after the current has stopped increases with the current density and the back diffusion of species occurring thereafter takes place more slowly.

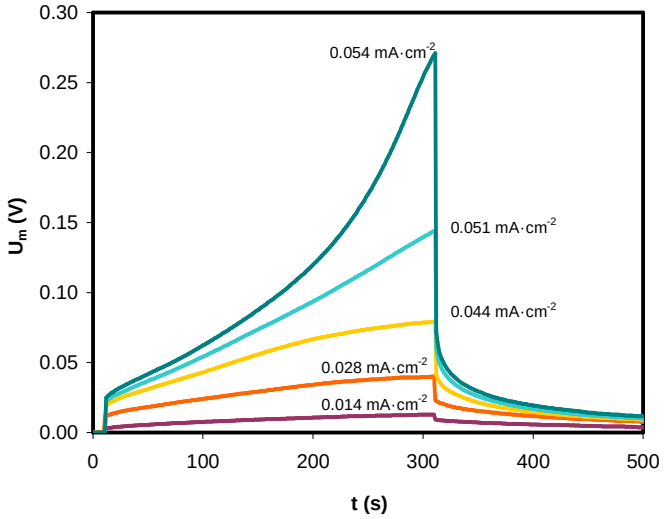

Fig. 4.5. Chronopotentiometric response obtained in the underlimiting range of currents for $5{\cdot}10^{-4}$ M Na_2SO_4 solutions.

The chronopotentiograms obtained in the range of overlimiting currents for $5{\cdot}10^{-4}$M Na_2SO_4 are presented in Fig. 4.6. When the concentration of counterions (in the present case Na^+ ions) is vanishing at the depleting membrane surface, a steep increase in U_m is observed in the chronopotentiograms. The jump registered in the voltage response occurs at a characteristic time known as the transition time, τ, which has been indicated in the figure for the current density of 0.059 mA·cm^{-2}. For times larger than τ, U_m levels off and is stabilized in an approximately constant value until the application of current ceases. As can be seen in the figure, the application of current densities beyond the i_{lim} induces the continuous depletion of ions in the diffusion boundary layer and this implies higher final U_m values. Moreover, in agreement with the Sand's equation previously presented in Chapter 3 (Eq. (3.8)), the transition time decreases for increasing current densities.

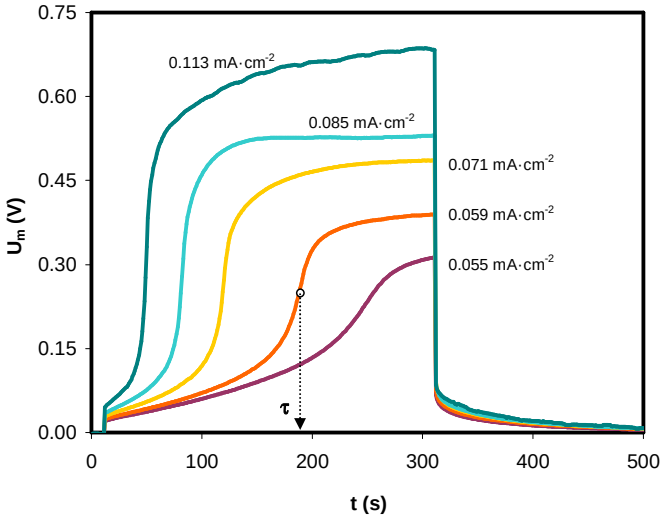

Fig. 4.6. Chronopotentiometric response obtained in the overlimiting range of currents for $5{\cdot}10^{-4}$ M Na_2SO_4 solutions.

Fig. 4.7 shows an example of the chronopotentiometric response obtained for more concentrated solutions of Na_2SO_4. The membrane behavior is analogous to that observed for lower concentrations (Figs. 4.5 and 4.6). As occurred with $5{\cdot}10^{-4}$M Na_2SO_4, at very low values of current density the increase in U_m is moderate. However, when the i_{lim} is reached, the inflexion point associated with the depletion of counterions near the membrane surface is also registered in the chronopotentiograms. For current densities that significantly exceed the i_{lim}, some oscillations can be observed in the last part of the chronopotentiograms. This feature typically appears at an advanced stage of concentration polarization, when the overlimiting mechanisms of current transfer have been enhanced. The coexistence of a strong applied electric field and high gradients of concentration near the membrane induces some hydrodynamic instabilities, which contribute to increase the mixing of the depleting diffusion boundary layer and to overcome the diffusive limitation of ion transport. However, this and other phenomena related to the emergence of the overlimiting transport of ions through the membranes are discussed in more detail in section 4.3.

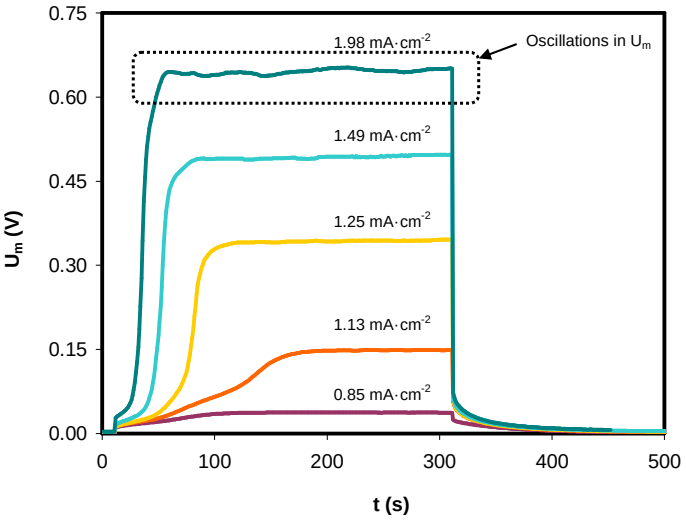

Fig. 4.7. Chronopotentiometric response obtained for 10^{-2} M Na_2SO_4 solutions.

The effect of the current density on the chronopotentiometric response obtained with solutions of different concentrations has been analyzed from Figs. 4.5 - 4.7. However, another interesting approach is to analyze the effect of the initial salt concentration on the response obtained for a constant value of current density, as shown in Fig. 4.8. From the almost plane response observed for 10^{-2}M Na_2SO_4 it is induced that the applied current density (0.71 mA·cm^{-2}) is below the i_{lim} of this membrane/electrolyte system. On the contrary, for lower electrolyte concentrations the same current density exceeds the i_{lim}, since U_m exhibits the inflexion point indicative that the concentration of counterions at the membrane depleting surface is vanishing. Nevertheless, once the voltage jump has occurred, the evolution of U_m with time is different in both cases. In the case of $5{\cdot}10^{-3}$M Na_2SO_4 solutions, after a sharp increase, U_m reaches a certain voltage value that remains stable and almost constant during the rest of the current pulse, whereas for the most diluted solutions of $2.5{\cdot}10^{-3}$M Na_2SO_4 the evolution of U_m with time shows the oscillations characteristic of overlimiting currents. These oscillations limit the increase of the membrane voltage drop, thus implying that the final value of U_m is practically the same for this concentration and for $5{\cdot}10^{-3}$M Na_2SO_4. Hence, these results illustrate how the overlimiting currents can reduce the electrical resistance of the membrane system and enhance the ion transport through the membrane.

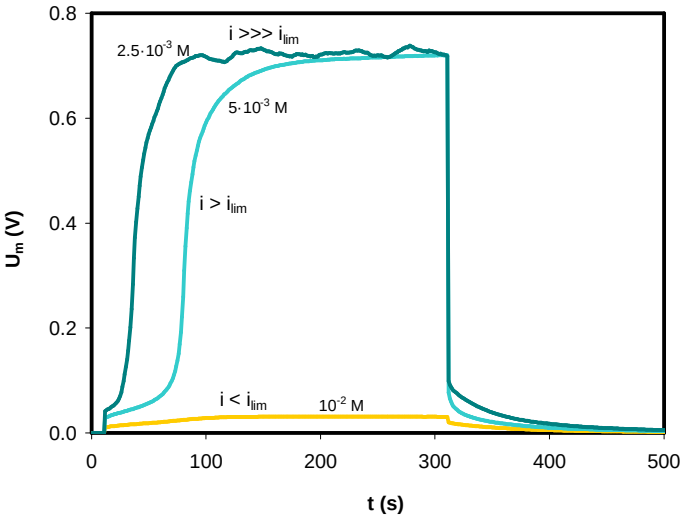

Fig. 4.8. Effect of the initial concentration of Na_2SO_4 on the chronopotentiometric response obtained under the application of a constant current density of 0.71 mA·cm^{-2}.

In conclusion, the response obtained with Na_2SO_4 solutions is analogous to that presented in other studies conducted with NaCl solutions, which may stem from the fact that Na_2SO_4 is a strong electrolyte and is almost completely dissociated into its forming ions, Na^+ and SO_4^{2-}. To verify this assumption, the speciation of Na_2SO_4 solutions was elucidated. For this purpose, the formation of complex species of Na^+ ions with SO_4^{2-} and OH^- ions as ligands was taken into account, as indicated in Eqs. (4.3) and (4.4) [4]:

$$Na^+ + OH^- \rightleftarrows NaOH \qquad \beta_1^{OH} = 10^{-0.2} \qquad (4.3)$$

$$Na^+ + SO_4^{2-} \rightleftarrows NaSO_4^- \qquad \beta_1^{SO_4} = 10^{0.7} \qquad (4.4)$$

Besides, SO_4^{2-} ions participate in protonation equilibria, which are described by Eqs. (4.5) and (4.6).

$$H_2SO_4 \rightleftarrows HSO_4^- + H^+ \qquad K_{H1} = 10^3 \qquad (4.5)$$

$$HSO_4^- \rightleftarrows SO_4^{2-} + H^+ \qquad K_{H2} = 10^{-1.99} \qquad (4.6)$$

The dissociation of water was also taken into account:

$H_2O \rightleftarrows H^+ + OH^-$ $\qquad K_W = 10^{-14}$ (4.7)

The stability constants of the different Na(I) complexes (β_i^{OH} and $\beta_i^{SO_4}$), the protonation equilibria for SO_4^{2-} ions (K_{Hi}), and the water dissociation constant (K_W) are defined by Eqs. (4.8)-(4.11), where M refers to the metal (in the present case Na):

$$\beta_i^{OH} = \frac{\left[M(OH)_i^{n-i}\right]}{\left[M^{+n}\right].\left[OH^-\right]^i} \tag{4.8}$$

$$\beta_i^{SO_4} = \frac{\left[M(SO_4)_i^{n-2i}\right]}{\left[M^{+n}\right].\left[SO_4^{2-}\right]^i} \tag{4.9}$$

$$K_{Hi} = \frac{\left[H^+\right].\left[H_{2-i}SO_4^{-i}\right]}{\left[H_{3-i}SO_4^{1-i}\right]} \tag{4.10}$$

$$K_W = \left[H^+\right].\left[OH^-\right] \tag{4.11}$$

The speciation diagram and the concentration of each complex in the equilibrium conditions are obtained from the previous equations, the mass balance of Na(I) and SO_4^{2-} ions given by Eqs. (4.12) and (4.13), and the proton balance given by Eq. (4.14):

$[Na(I)]_0 = [Na^+] + [NaOH] + [NaSO_4^-]$ (4.12)

$[SO_4^{2-}]_0 = [SO_4^{2-}] + [NaSO_4] + [HSO_4^-] + [H_2SO_4]$ (4.13)

$[H^+] = [OH^-] + [NaOH] - [HSO_4^-] - 2[H_2SO_4]$ (4.14)

Fig. 4.9(a) shows the speciation diagram of Na(I) species as a function of pH for $5{\cdot}10^{-4}$M Na_2SO_4. As commented previously, Na^+ ions predominate over other cationic species at the pH of the initial equilibrium conditions (pH_{eq}) and the formation of complex ions can be neglected. As the initial salt concentration is increased, the formation of $NaSO_4^-$ is more feasible. However, as can be seen in Fig. 4.9(b) for the most concentrated solutions, the concentration of complex ions is insignificant when compared to that of free Na^+ ions.

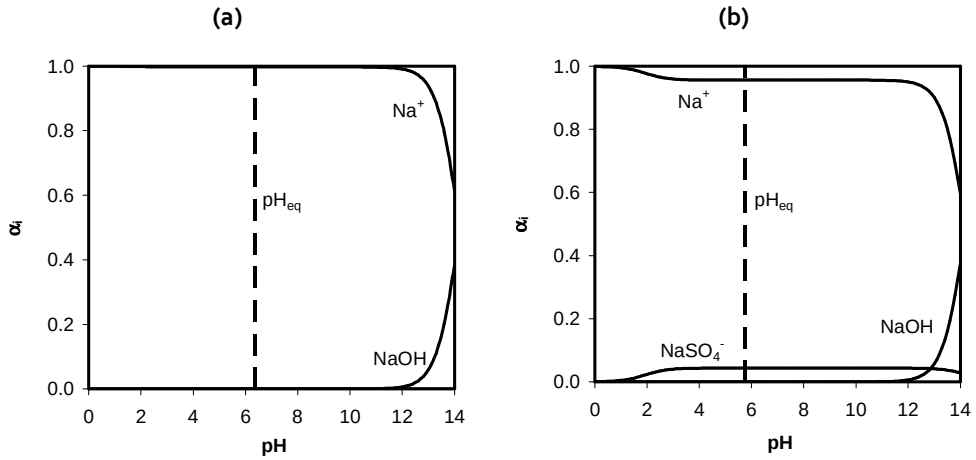

Fig. 4.9. Speciation diagram of (a) $5{\cdot}10^{-4}$M Na_2SO_4 solutions and (b) 10^{-2}M Na_2SO_4 solutions.

4.1.3.2 Calculation of the transport number of Na^+ ions through Nafion 117 membranes

As commented previously, chronopotentiometry allows us not only to obtain a qualitative notion about the ion transport phenomena taking place in a membrane/electrolyte system, but also the quantification of the transport of counterions by means of the calculation of the counterion transport number. This parameter is a measure of the membrane selectivity toward counterions. The transport number of Na^+ ions through the membrane phase (T_{Na^+}) indicates which part of the total charge transported through the membrane is carried by Na^+ ions. It can be calculated by using the Sand's equation (Eq. 3.8). For this purpose, the transition times, which indicate the time at which the steepest increase in U_m is registered, were obtained from the maximum in the derivative of U_m with time, as indicated in Fig. 4.10.

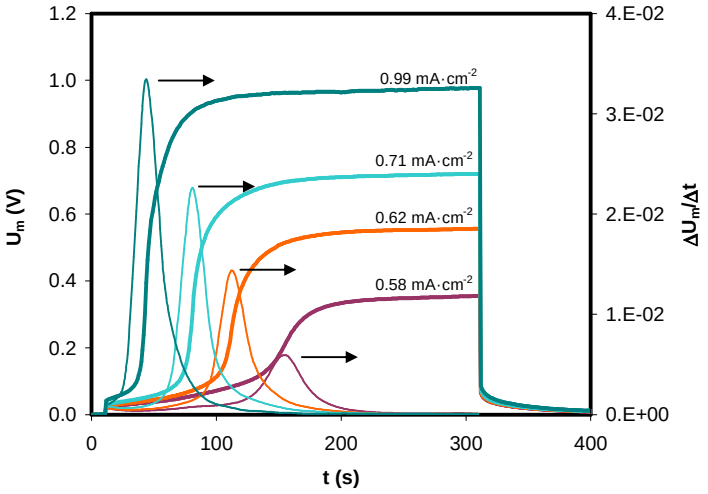

Fig. 4.10. Calculation of the transition times from the maximum in the derivative of U_m with time for the chronopotentiograms of $5{\cdot}10^{-3}$M Na_2SO_4.

Fig. 4.11 shows the linear relationship existing between the transition times τ and the parameter $(c_0/I)^2$ for the four salt concentrations tested. As seen from the graphic, the Sand's equation is accomplished accurately and, therefore, the counterion transport number through the membrane phase can be calculated from the slopes of the obtained linear fittings. For this purpose, the diffusion coefficient of Na_2SO_4 and the transport number of Na^+ ions in the solution phase were obtained from the molar (equivalent) conductivity data at infinite dilution. The ion diffusion coefficients (D_j) were calculated using the Nernst-Einstein equation, which is given by Eq. (4.15) [5]:

$$D_j = \frac{RT\lambda_j}{|z_j| \cdot F^2} \tag{4.15}$$

Here λ_j and z_j represent the molar conductivity at infinite dilution and the charge of the ion j, respectively. The diffusion coefficient of the salt can be calculated with Eq. (4.16):

$$D = \frac{(z_+ + |z_-|)D_+ D_-}{z_+ D_+ + |z_-| D_-} \tag{4.16}$$

Finally, the transport number of the counterions in the solution is calculated by means of Eq. (4.17):

$$t_+ = \frac{\lambda_+}{\lambda_+ + \lambda_-} \tag{4.17}$$

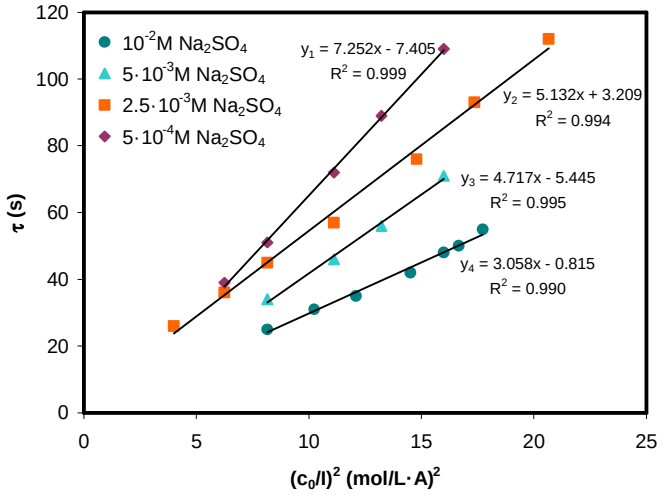

Fig. 4.11. Transition time, τ, as a function of $(c_0/I)^2$ for Na_2SO_4 solutions of varying concentration.

The membrane transport number of Na^+ ions calculated from the chronopotentiometric experiments is represented in Fig. 4.12 as a function of the initial Na(I) concentration. The results show that the T_{Na^+} values increase with the increase in the initial salt concentration and reach a maximum value of 0.99 for $2 \cdot 10^{-2}$M Na(I) solutions. This trend is in contradiction with the Donnan theory, which predicts a decrease in the counterion transport number with the increase in the salt concentration because of a weaker repulsion of the membrane fixed charges toward the solution coions (SO_4^{2-} ions). However, similar results were also obtained by Dlugolecki et al. with NaCl solutions, and the deviation from the expected behavior was attributed to the hydrodynamic instabilities in the diffusion boundary layer occurring specially at lower salt concentrations [6]. The formation of hydrodynamic instabilities in the overlimiting range of currents can imply higher experimental values for the transition time, which results in the lower T_{Na^+} values. The discrepancy between the expected and the obtained trend of the T_{Na^+} values with the electrolyte concentration could be also attributed to the dilution

effect taking place at very low concentrations, where the transport of water through the membrane could probably diminish the counterion transport number.

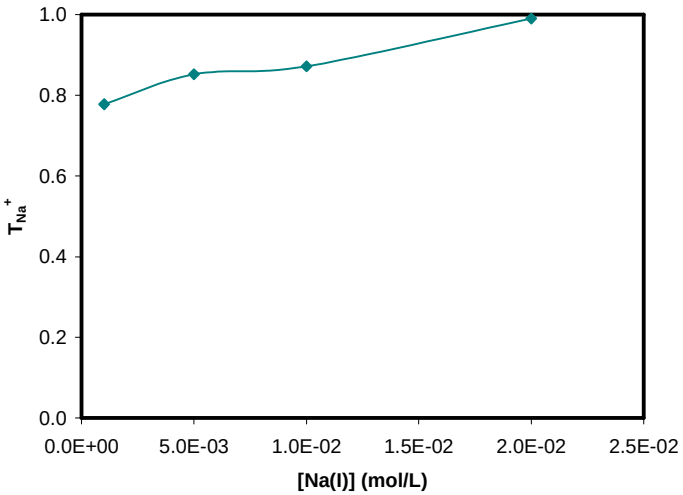

Fig. 4.12. Counterion transport number calculated from the experimental transition time as a function of the Na(I) concentration.

4.1.3.3 Current-voltage characteristics

The current-voltage curves obtained for Na_2SO_4 solutions are represented in Fig. 4.13 and 4.14 for diluted and concentrated solutions, respectively. The curves exhibit the shape typically found in the literature for NaCl solutions, where three regions of different membrane behavior can be clearly distinguished:

1. At very low current densities ($i<i_{lim}$), a linear dependence describes the relationship between current density and U_m. The behavior of the membrane system in this region responds to a quasi-ohmic pattern.

2. As the i_{lim} value is reached ($i \approx i_{lim}$), the transport of counterions in the depleting boundary layer is limited by diffusion. As a consequence, the concentration of counterions near the membrane surface is vanishing and the resistance of the membrane system increases, thus leading to a plateau in the current-voltage curves.

3. In the so-called overlimiting region ($i>i_{lim}$), the supply of ions to the membrane surface is again enhanced and the current density increases again with U_m.

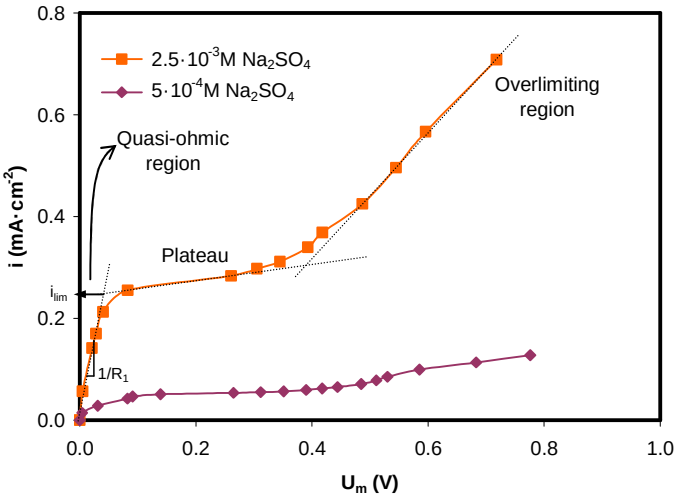

Fig. 4.13. Current-voltage curves obtained for diluted solutions of Na_2SO_4.

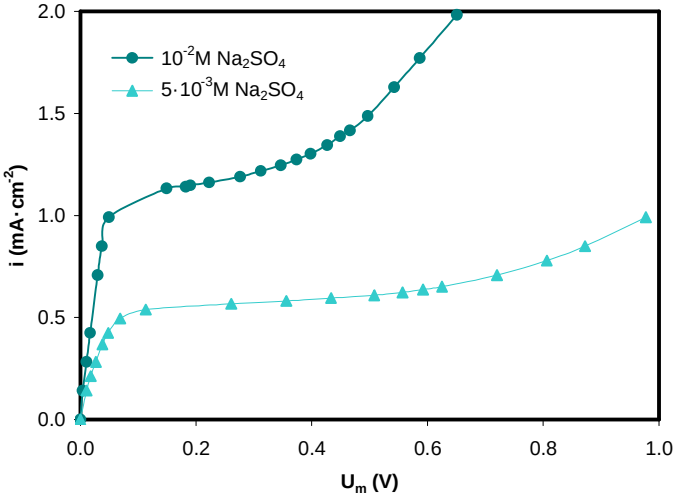

Fig. 4.14. Current-voltage curves obtained for concentrated solutions of Na_2SO_4.

One important current-voltage characteristic that can be obtained from the curves is the electrical resistance of the membrane system in the ohmic region (R_1), which is calculated from the inverse of the slope of this part of the curves. This parameter is related to the

amount of energy required to achieve the transport of ions through the membranes. Consequently, it is interesting to operate with membrane/electrolyte systems with low values of R_1 in order to achieve fast desalination rates for the minimum membrane area and power consumption.

In addition, the i_{lim} values can also be obtained from the intersection of the tangent lines drawn from the region of quasi-ohmic behavior and the plateau of the current-voltage curves (as indicated in Fig. 4.13). The i_{lim} values define the maximum current density that can be reached until the resistance of the membrane system increases notably due to the intensification of the concentration polarization phenomena. Therefore, overlimiting current densities have been typically avoided in order not to increase the power consumption of electrodialysis operations. However, it must be noted that, the possibility of operating at overlimiting current densities is gaining more attention in the recent time as an increasing number of studies are contributing to elucidate the mechanisms of overlimiting mass transfer. Nevertheless, the effects related to the use of overlimiting currents are out of the scope of this section and are discussed in detail in sections 4.3 and 4.4.

The values of R_1 and i_{lim} calculated for the different concentrations of Na_2SO_4 are summarized in Table 4.1 and are represented in Fig. 4.15 as a function of the Na(I) concentration. As expected, the values of R_1 decrease for increasing electrolyte concentrations, which is related to the increasing number of mobile ionic species being transported through the diffusion boundary layers and the membrane phase. Similar results were also obtained by other authors, which indicated that the significant increase in the resistance of the membrane system observed for diluted solutions was principally due to the contribution of the diffusion boundary layers [7,8]. With regard to the i_{lim} values, a linear increase describes their dependence with the initial salt concentration. This linear relationship follows the expected trend if, according to the Peers' equation (Eq. 1.13), other parameters such as the diffusion coefficient (D) and the thickness of the diffusion boundary layer (δ) are assumed invariant within the range of concentrations tested.

Table 4.1. Current-voltage characteristics obtained with Na_2SO_4 solutions.

	$5{\cdot}10^{-4}$M Na_2SO_4	$2.5{\cdot}10^{-3}$M Na_2SO_4	$5{\cdot}10^{-3}$M Na_2SO_4	10^{-2}M Na_2SO_4
R_1 ($\Omega \cdot cm^2$)	282.39	171.08	115.10	44.50
i_{lim} ($mA{\cdot}cm^{-2}$)	0.049	0.252	0.528	1.088

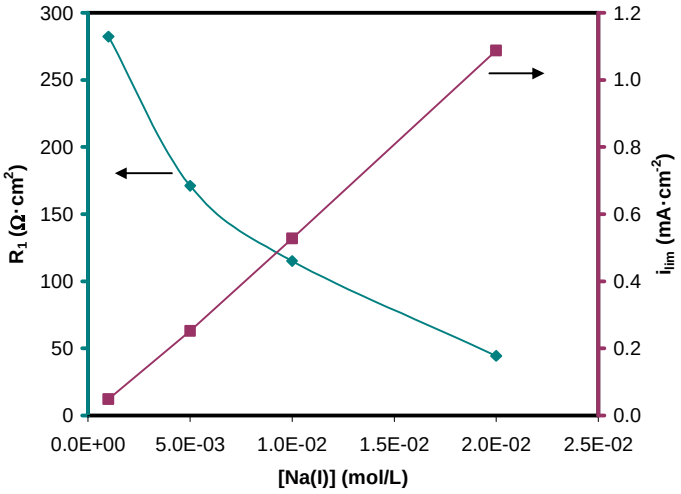

Fig. 4.15. Evolution of R_1 and i_{lim} as a function of the concentration of Na(I).

4.1.4 Transport of divalent ions

In this section, the transport of divalent ions through the Nafion 117 membrane is investigated. Nickel sulfate was selected as the electrolyte, since Ni(II) is present in some industrial effluents, such as spent nickel plating and chromium plating baths. In addition, large volumes of water become contaminated during the rinsing operations performed after the plating steps. These waters are hazardous effluents which cannot be directly discharged into the environment. Normally, the metals present in these effluents are precipitated forming a solid waste. However, their treatment by means of electromembrane processes could imply the recovery of nickel and its reuse as raw material in the plating process, as well as the recycling of large volumes of water to the rinsing steps.

4.1.4.1 Chronopotentiometric response

Different chronopotentiometric experiments were performed using $NiSO_4$ solutions having a concentration of metallic Ni(II) analogous to the concentrations of Na(I) considered previously. The chronopotentiometric response obtained for 10^{-3}M $NiSO_4$ solutions is presented in Fig. 4.16. The curves corresponding to underlimiting current densities are similar to those described previously for Na_2SO_4 solutions. As the i_{lim} is reached the sharp increase in U_m and the inflexion point associated with the depletion of counterions (in this case Ni^{2+} ions) near the membrane surface is also observed. However, as the current is increased beyond the i_{lim} values, other additional features that were not observed in the case of Na_2SO_4 solutions are detected in the chronopotentiograms. For the current densities that significantly exceed the i_{lim} value (i.e. 0.17, 0.23 and 0.25 $mA{\cdot}cm^{-2}$ in Fig. 4.16), a second increase in U_m takes place immediately after the registration of the first inflexion point. This second increase in U_m appears due to a further intensification of the concentration polarization phenomena, which is confirmed by the slower relaxation profile of the membrane potential once the current is stopped.

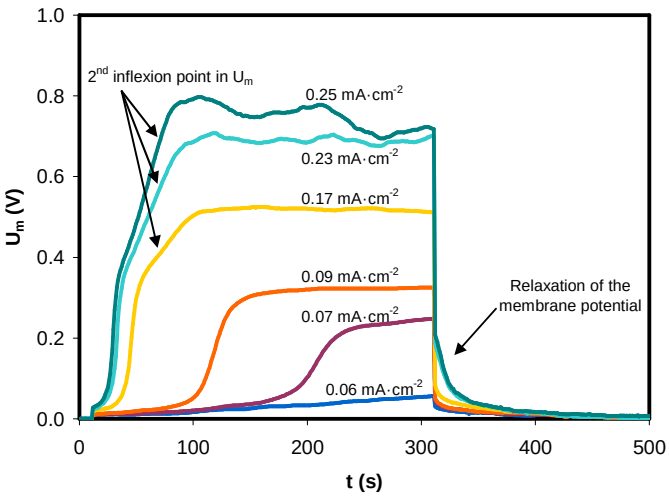

Fig. 4.16. Chronopotentiometric response obtained for 10^{-3}M $NiSO_4$ solutions.

Fig. 4.17 shows the chronopotentiometric response obtained for 10^{-2}M $NiSO_4$. These curves are significantly different from those obtained for more diluted solutions. Specifically, when the i_{lim} is surpassed U_m shows a second increase which is different from those observed in Fig. 4.16 for the highest applied currents. Whereas for the most diluted

solutions the second increase of U_m showed a clear inflexion point, in this case the increase of U_m takes place gradually. Moreover, the profile of the relaxation of U_m once the application of current ceases presents some peculiarities which were not obtained for underlimiting currents. At the first instants after the current is switched off U_m decreases very fast and reaches a plateau value considerably higher than zero. This plateau value is maintained almost constant during a few seconds and then U_m is restored slowly to zero. On the contrary, for lower current densities, the plateau in the relaxation of the membrane potential is not observed and U_m decreases asymptotically to zero more rapidly.

The voltage value remaining after switching off the current and the slow restoration of the membrane potential is a phenomenon characteristic of bipolar membranes and has been attributed in previous studies to the formation of water dissociation products [9,10]. Moreover, this behavior has been observed also in the case of monopolar cation-exchange membranes when a layer of metallic precipitates is formed at the anodic side of the membranes once the i_{lim} is surpassed [11,12]. In our case, it must be noted that the formation of precipitates at the anodic side of the membrane was verified at the end of these experiments. The inset photograph of Fig. 4.17 shows the nickel precipitates formed at the membrane surface, which have the characteristic green color of Ni(II) compounds. Therefore, the gradual increase of U_m and the plateau in the relaxation of the membrane potential registered for high overlimiting currents may be attributed to the formation of precipitates. The formation of precipitates and the features associated with this phenomenon were also observed in the chronopotentiograms obtained for $2 \cdot 10^{-2}$M $NiSO_4$. However, these results are not shown for the sake of clarity.

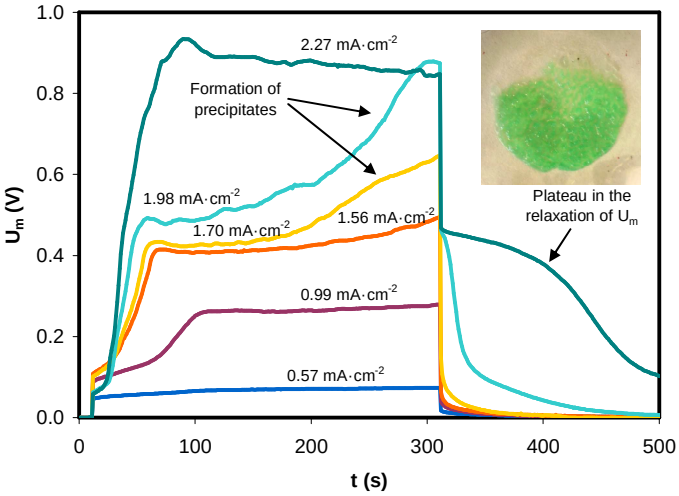

Fig. 4.17. Chronopotentiometric response obtained for 10^{-2}M $NiSO_4$ solutions. The inset photograph shows the precipitates formed at the surface of the membrane.

The presence of the second inflexion point in the curves obtained for the highest current densities of Fig. 4.16 and the formation of precipitates in the case of Fig. 4.17, as well as the different relaxation profiles of membrane potential can be explained in terms of the predominant species present in equilibrium conditions at the beginning of the experiments and during the imposition of current. As studied in previous works, the change in the pH values in the vicinities of the membrane could lead to the formation of complex species with different charge that alter the passage of ions through the membrane [11,13]. In order to elucidate the influence that the formation of complex ionic species can have on the shape of the chronopotentiograms, the speciation diagram for $NiSO_4$ solutions was obtained. Ni^{2+} ions can form complex species when they recombine with OH^- or SO_4^{2-} ions, as indicated in Eqs. (4.18)-(4.23) [4]:

$$Ni^{2+} + OH^- \rightleftarrows NiOH^+ \qquad \beta_1^{OH} = 10^{4.1} \qquad (4.18)$$

$$Ni^{2+} + 2OH^- \rightleftarrows Ni(OH)_2 \qquad \beta_2^{OH} = 10^{8} \qquad (4.19)$$

$$Ni^{2+} + 3OH^- \rightleftarrows Ni(OH)_3^- \qquad \beta_3^{OH} = 10^{11} \qquad (4.20)$$

$$Ni^{2+} + 4OH^- \rightleftarrows Ni(OH)_4^{2-} \qquad \beta_4^{OH} = 10^{12} \qquad (4.21)$$

$Ni^{2+} + SO_4^{2-} \rightleftarrows NiSO_4$ $\beta_1^{SO_4} = 10^{2.32}$ (4.22)

$Ni^{2+} + 2SO_4^{2-} \rightleftarrows Ni(SO_4)_2^{2-}$ $\beta_2^{SO_4} = 10^{1.42}$ (4.23)

Besides, the participation of SO_4^{2-} ions in protonation equilibria was also taken into account as explained previously in the case of Na_2SO_4 solutions (Eqs. (4.5) and (4.6)). The definition of the equilibrium constants for the formation of complex species is also analogous to that presented in Eqs. (4.8) and (4.9). However, since the formation of precipitates at the membrane surface was verified, the equilibrium of precipitation of Ni(II) was also considered:

$Ni(OH)_2\ (s) \rightleftarrows Ni^{2+} + 2OH^-$ $K_s\ (Ni(OH)_2) = 10^{-15.2}$ (4.24)

The solubility product constant (K_s) is defined in Eq. (4.25), where M^{+n} refers to Ni^{2+} ions in the present case:

$$K_s = \left[M^{+n}\right] \cdot \left[OH^-\right]^n \tag{4.25}$$

The mass balance of Ni(II) and SO_4^{2-} species along with the proton balance are described by Eqs. (4.26) – (4.28):

$[Ni(II)]_0 = [Ni^{2+}] + [NiOH^+] + [Ni(OH)_2] + [Ni(OH)_3^-] + [Ni(OH)_4^{2-}] + [NiSO_4] + [Ni(SO_4)_2^{2-}]$ (4.26)

$[SO_4^{2-}]_0 = [SO_4^{2-}] + [NiSO_4] + 2[Ni(SO_4)_2^{2-}] + [HSO_4^-] + [H_2SO_4]$ (4.27)

$[H^+] = [OH^-] + [NiOH^+] + 2[Ni(OH)_2] + 3[Ni(OH)_3^-] + 4[Ni(OH)_4^{2-}] - [HSO_4^-] - 2[H_2SO_4]$ (4.28)

The solubilitiy of Ni(II) species in aqueous solutions, s, was calculated as:

$s = [Ni^{2+}] + [NiOH^+] + [Ni(OH)_2] + [Ni(OH)_3^-] + [Ni(OH)_4^{2-}] + [NiSO_4] + [Ni(SO_4)_2^{2-}]$ (4.29)

The speciation diagram of 10^{-3}M $NiSO_4$ solutions is presented in Fig. 4.18 as a function of the pH, where the pH corresponding to the initial equilibrium conditions (pH_{eq}) is represented by a vertical dashed line. At the initial equilibrium conditions Ni^{2+} ions are the main cationic species present in the electrolyte. Therefore, the current transfer through the membrane may be mainly associated with the transport of Ni^{2+} ions and the first inflexion points appearing in the chronopotentiograms should correspond to their depletion from the membrane diluting surface. In addition, the second inflexion point observed in Fig. 4.16 for the highest applied currents could be associated with the depletion of other ionic species. Specifically, the concentration of the complex specie $NiSO_4$ is significant at the initial conditions of the experiments. Moreover, once the Ni^{2+} ions are depleted from the membrane surface, an important amount of protons can be transferred to the cathodic compartment. This phenomenon may promote the increase of the local pH at the anodic side of the membrane, thus shifting the initial pH value (pH_{eq}) to pH values at which the formation of hydroxilated species of nickel is favored. The dissociation of the complex specie $NiSO_4$ and the formation of $NiOH^+$ ions originated by changes in the pH near the membrane surface would imply the transport through the membrane of the generated cationic species. Therefore, the second inflexion point appeared in the chronopotentiograms for the highest applied currents can be attributed to the depletion of these ions.

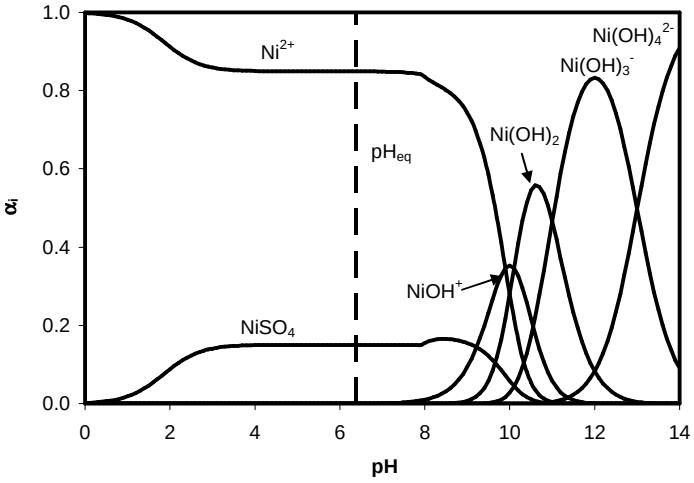

Fig. 4.18. Speciation diagram of 10^{-3}M $NiSO_4$ solutions.

In regard to the formation of precipitates verified for the most concentrated solutions of $NiSO_4$, the solubility plot of $NiSO_4$ solutions at different salt concentrations are presented in Fig. 4.19. It can be seen from the figure that the formation of $Ni(OH)_2$ precipitates starts when the pH reaches a value of 7.5 in the case of 10^{-2}M $NiSO_4$ solutions, while in the case of 10^{-3}M $NiSO_4$ solutions a pH value of 7.9 has to be reached. This difference together with the fact that the overlimiting currents are much higher for concentrated electrolytes may be the reason that explains the higher tendency toward the formation of precipitates observed for the highest concentrations of $NiSO_4$.

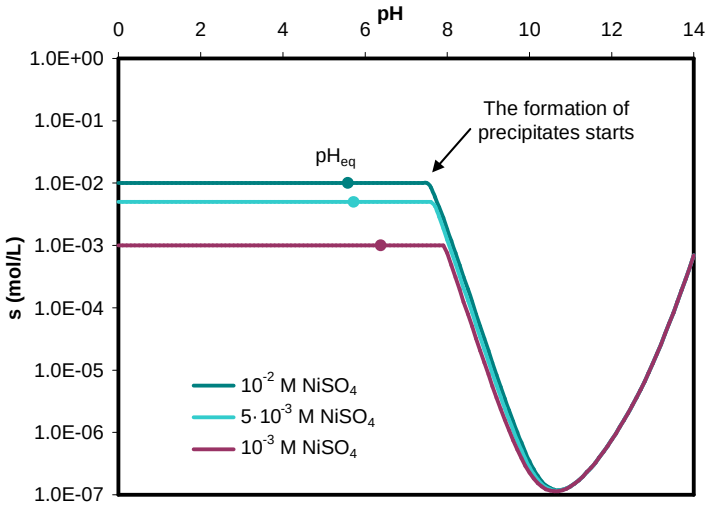

Fig. 4.19. Solubility plot of $NiSO_4$ solutions as a function of the salt concentration.

4.1.4.2 Calculation of the transport number of Ni^{2+} ions through Nafion 117 membranes

The membrane transport number of Ni^{2+} ions was also calculated from the transition times obtained from the chronopotentiometric curves. In this case, the transition times also followed a linear trend with the square of the inverse of the applied current, as can be seen in Fig. 4.20. Therefore, the Sand's equation is accomplished and the Ni^{2+} transport numbers can be calculated by means of chronopotentiometry, following the same procedure as that used for the Na_2SO_4 solutions.

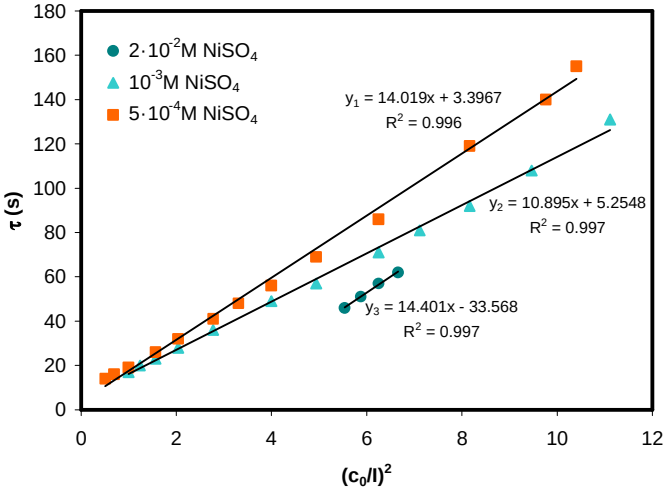

Fig. 4.20. Transition time, τ, as a function of $(c_0/I)^2$ for $NiSO_4$ solutions of varying concentration.

The evolution of the membrane transport number of Ni^{2+} ions (T_{Ni}^{2+}) as a function of the initial concentration is presented in Fig. 4.21. In this case, the T_{Ni}^{2+} value decreases for the lowest concentration, as occurred in the case of Na^+ ions (Fig. 4.12). Then, a maximum is reached for 10^{-3}M $NiSO_4$ solutions and T_{Ni}^{2+} decreases again with the increase in the concentration of Ni(II). Contrary to the trend observed for Na^+ ions, the decrease of the membrane selectivity with increasing the salt concentration is in agreement with the Donnan coion exclusion theory [14], which predicts a lowered coion exclusion (SO_4^{2-} ions in the present study) as a consequence of their invasion in the membrane phase at higher electrolyte concentrations. Analogous results were also obtained by other researchers with different electrolytes [2,15]. In addition, for the same metal ion concentration, the concentration of SO_4^{2-} ions in the case of a 1:1 electrolyte is twofold that of a 2:1 electrolyte, which could explain the different trends observed for Na_2SO_4 and $NiSO_4$.

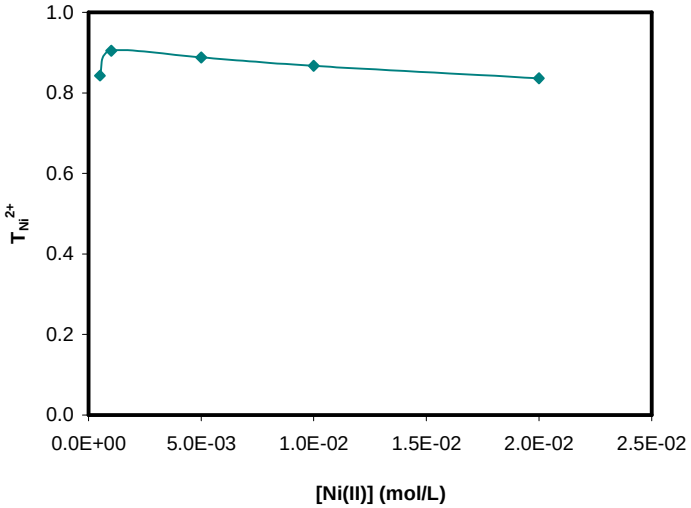

Fig. 4.21. Counterion transport number calculated from the experimental transition time as a function of the Ni(II) concentration.

4.1.4.3 Current-voltage characteristics

The current-voltage curves obtained for $NiSO_4$ solutions are presented in Fig. 4.22 and 4.23. The curves obtained for the more diluted solutions (Fig. 4.22) show the typical shape already explained for Na_2SO_4 solutions, where the region of quasi-ohmic behavior, the plateau and the overlimiting region can be clearly distinguished. Moreover the expected increase of the i_{lim} values with the electrolyte concentration can be clearly seen in the figure.

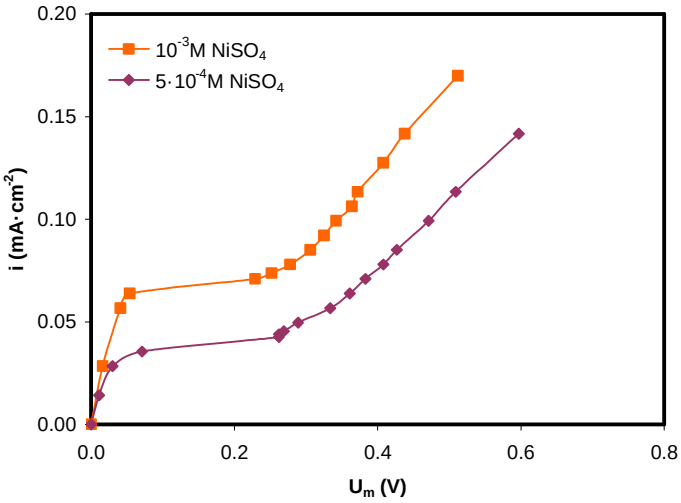

Fig. 4.22. Current-voltage curves obtained for diluted solutions of $NiSO_4$.

On the contrary, the shape of the curves obtained for more concentrated $NiSO_4$ solutions (Fig. 4.23) changes as the initial salt concentration is increased. Whereas the current-voltage curve obtained for $5{\cdot}10^{-3}$M $NiSO_4$ also exhibits the three characteristic regions of membrane behavior, the curve obtained for 10^{-2}M $NiSO_4$ exhibits some peculiarities. This curve shows two different plateaus and two limiting current densities (i_{lim1} and i_{lim2}). The first plateau corresponds to the current densities at which only one inflexion point was observed in the chronopotentiograms (e.g. 0.99 $mA{\cdot}cm^{-2}$ in Fig. 4.17). Therefore, this plateau is originated by the increase in the resistance of the membrane system caused by the depletion of Ni^{2+} ions near the membrane surface. The subsequent increase of current following the first plateau could be caused by overlimiting mass transfer phenomena. However, if the current is further increased, a second plateau is formed, which is much more prolonged and corresponds to the chronopotentiograms where the gradual increase in U_m was registered (e.g. 1.98 $mA{\cdot}cm^{-2}$ in Fig. 4.17). Therefore, the second plateau is formed due to the high electrical resistance of the precipitates deposited at the anodic side of the membrane. Finally, the last overlimiting region of this curve presents some scattering and is almost vertical. In this region the current increase is very acute and implies almost no increase in the membrane resistance. This membrane behavior could be attributed to the catalytic dissociation of water occurring at the interface between the precipitates and the membrane [11,12,16]. However, this phenomenon is analyzed in more detail in section 4.3.

In the case of $2{\cdot}10^{-2}$M $NiSO_4$ solutions, only one plateau can be seen in the current-voltage curves. Nevertheless, this plateau is very flat and long and also coincides with the formation of precipitates at the membrane surface. Therefore, this prolonged plateau seems to be the result of the overlapping of the two plateaus observed in the case of 10^{-2}M $NiSO_4$. The subsequent overlimiting region is also almost vertical, which seems to indicate that the main phenomenon causing the overlimiting region is the generation of new ionic species (H^+ and OH^- ions) as a result of the water splitting process catalyzed by the deposits of nickel hydroxide.

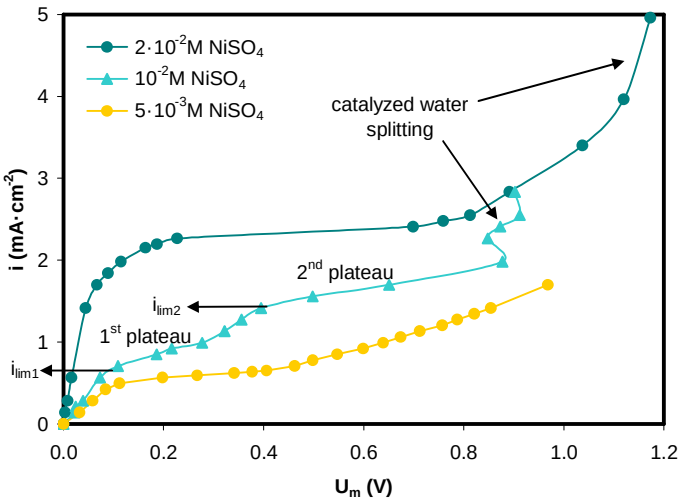

Fig. 4.23. Current-voltage curves obtained for concentrated solutions of $NiSO_4$.

The parameters obtained from the current-voltage curves are summarized in Table 4.2 and plotted in Fig. 4.24 as a function of the initial Ni(II) concentration. The trend followed by the R_1 and the i_{lim} values is similar to that observed in the case of Na_2SO_4 solutions (Fig. 4.15). The direct relationship between the initial concentration and the i_{lim} predicted by the Peers' equation is approximately accomplished with $NiSO_4$ solutions and the ohmic resistance calculated for the most diluted solutions is also significantly higher than that calculated for more concentrated solutions.

Table 4.2. Current-voltage characteristics obtained with $NiSO_4$ solutions.

	10^{-3}M $NiSO_4$	$5{\cdot}10^{-3}$M $NiSO_4$	10^{-2}M $NiSO_4$	$2{\cdot}10^{-2}$M $NiSO_4$
R_1 ($\Omega \cdot cm^2$)	735.25	196.81	129.20	104.47
i_{lim1} ($mA \cdot cm^{-2}$)	0.064	0.495	0.850	2.153
i_{lim2} ($mA \cdot cm^{-2}$)	-	-	1.416	2.153

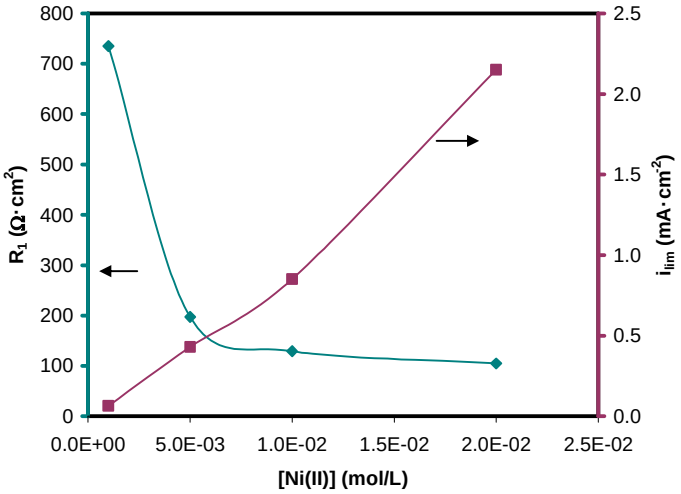

Fig. 4.24. Evolution of R_1 and i_{lim1} as a function of the concentration of Ni(II).

4.1.5 Transport of ions of trivalent metals

In this section the transport through cation-exchange membranes of ions present in single salt solutions of trivalent metals is studied. For this purpose, sulfate solutions of Cr(III) and Fe(III) of varying concentrations were prepared. These metals are commonly present as impurities in spent baths coming from metal finishing operations. Moreover, Cr(III) is also present in wastewaters generated in the leather tannery industry, and Fe(III) is typically found in the composition of acid mine drainage resulting from the exploitation of coal extracting sites. Therefore, the results obtained in this section could be of practical interest for some industries where the generation of wastewaters containing heavy metals causes important economical losses and environmental problems.

4.1.5.1 Chronopotentiometric response

For comparing purposes, we selected the same concentrations of metals than those studied previously with Na_2SO_4 and $NiSO_4$. The chronopotentiograms obtained for the more diluted solutions of $Fe_2(SO_4)_3$ ($5{\cdot}10^{-4}$M) are shown in Fig. 4.25. In these curves we can distinguish several inflexion points for the current densities higher than 0.71 mA·cm^{-2}. Hence, these results are similar to those presented previously for diluted $NiSO_4$ solutions. However, in the present case the two inflexion points can be elucidated for currents slightly higher than i_{lim}, whereas in the case of $NiSO_4$ solutions the second inflexion point was observed only at very high overlimiting currents. The elucidation of both inflexion points is difficult because they appear very close, being practically overlapped at the highest current densities. However, they can be seen more clearly in Fig. 4.26, where the derivative of U_m with time is represented in the right axis and the transition times corresponding to each maximum in $\Delta U_m / \Delta t$ are indicated.

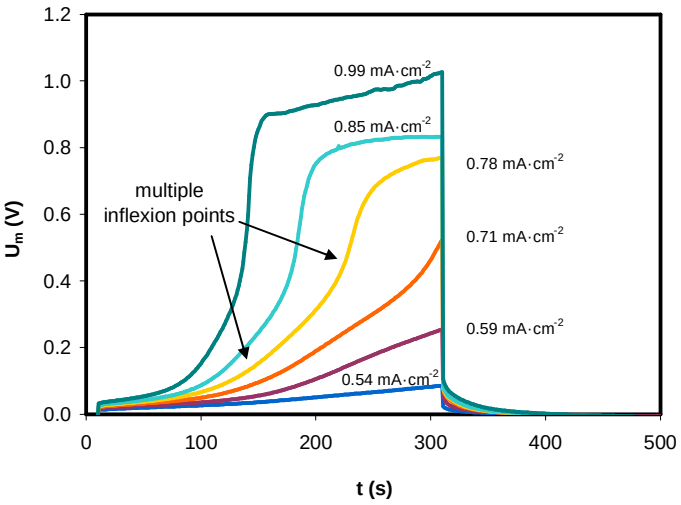

Fig. 4.25. Chronopotentiometric response obtained for $5{\cdot}10^{-4}$M $Fe_2(SO_4)_3$ solutions.

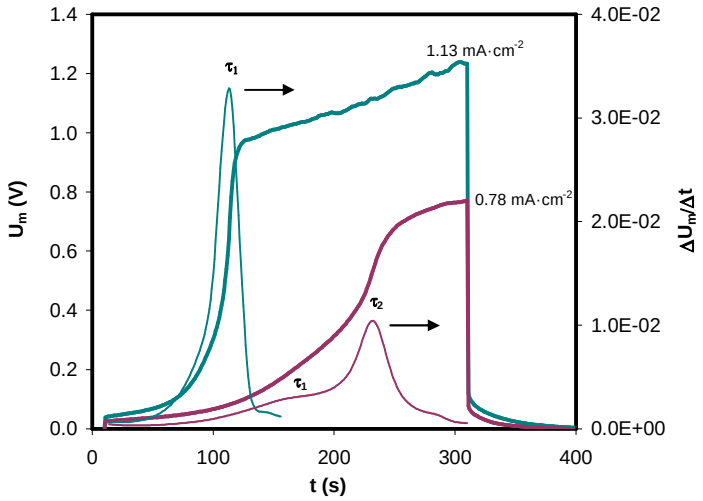

Fig. 4.26. Chronopotentiometric response obtained for $5{\cdot}10^{-4}$M $Fe_2(SO_4)_3$ solutions including the derivatives of U_m with time.

The response obtained for more concentrated solutions is presented in Fig. 4.27. In contrast with the results obtained for low concentrations, the curves obtained at low overlimiting currents (i.e. 7.08 mA·cm^{-2}) only present one inflexion point. However, at higher currents, a second increase in U_m is observed. This second increase lasts until the current is stopped, and the stabilization of U_m is not observed in the curves. As occurred with concentrated solutions of $NiSO_4$, the formation of a precipitate layer at the anodic side of the membrane was responsible for the gradual and prolonged increase of U_m, which in this case is more acute and reaches the magnitude of various volts. The inset photograph of Fig. 4.27 shows the orange precipitates of Fe(III) formed at the anodic side of the membrane. In addition, the relaxation profile of the membrane potential registered once the application of current ceases also shows a plateau. In this case, the plateau is smaller than that observed with $NiSO_4$ solutions, which probably indicates that the formation of water dissociation products is less intense than with Ni(II) solutions. In relation to this effect, it has to be noted that at the end of the experiments the layer of iron precipitates was removed from the membrane and it was observed that, conversely to what occurred with the precipitates of nickel, the precipitates of iron were present not only at the membrane surface but also inside the membrane.

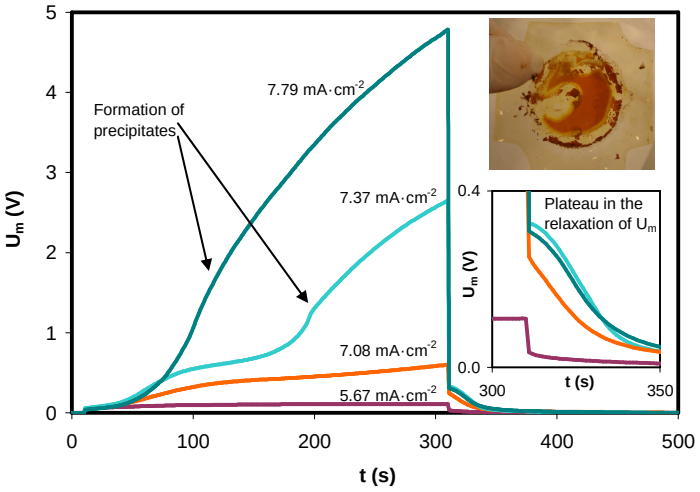

Fig. 4.27. Chronopotentiometric response obtained for 10^{-2}M $Fe_2(SO_4)_3$ solutions. The inset photograph shows the precipitates formed at the surface of the membrane.

In the case of diluted $Cr_2(SO_4)_3$ solutions (see Fig. 4.28), various inflexion points can be also distinguished for the highest current densities (i.e.: 0.64 and 0.99 mA·cm^{-2}). However, unlike the results obtained for $Fe_2(SO_4)_3$ solutions, the presence of the different inflexion points is more marked. For $2{\cdot}5{\cdot}10^{-3}$M solutions, the presence of the two inflexion points can be clearly elucidated from the derivative of U_m with time (see Fig. 4.29). Moreover, it can be also seen that both transition times decrease for increasing current densities, as predicted by the Sand's equation.

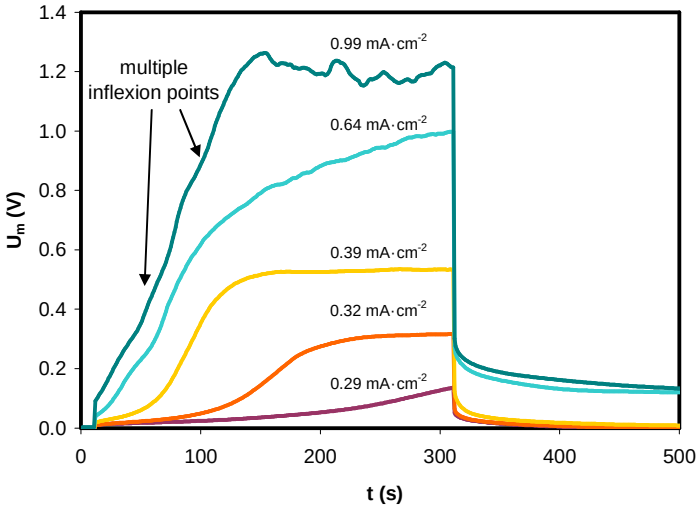

Fig. 4.28. Chronopotentiometric response obtained for $5{\cdot}10^{-4}$M $Cr_2(SO_4)_3$ solutions.

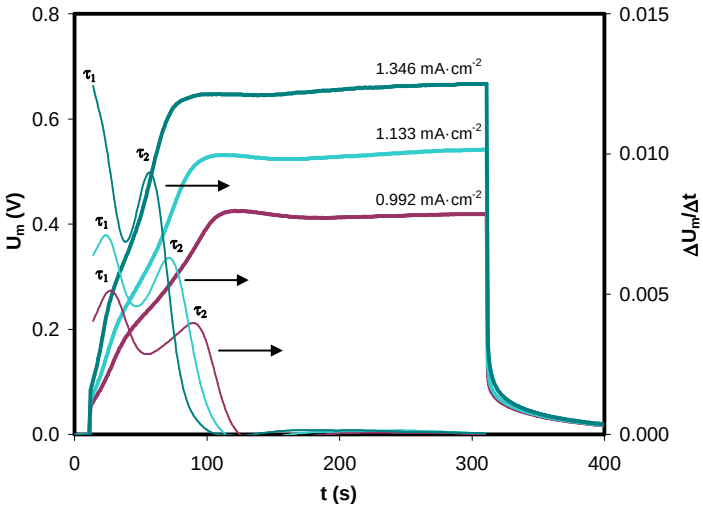

Fig. 4.29. Chronopotentiometric response obtained for $2.5{\cdot}10^{-3}$M $Cr_2(SO_4)_3$ solutions including the derivatives of U_m with time.

On the contrary, the chronopotentiometric curves obtained for more concentrated solutions of $Cr_2(SO_4)_3$ only show one inflexion point (see Fig. 4.30). In this case, the shape of the curves is very similar to that obtained for solutions of monovalent metals, especially for current densities slightly higher than i_{lim}. For the highest current densities (i.e. 4.249 and 6.374 mA·cm^{-2}) a maximum in U_m is registered a few seconds immediately

after the transition time, and beyond this point a decrease in U_m takes place until a steady value is reached. This response is typically attributed to the overlimiting mass transfer originated by gravitational convection, which is caused by the formation of strong concentration gradients at the membrane/solution interface. Finally, it must be noted that the formation of precipitates was not observed in the case of $Cr_2(SO_4)_3$ solutions. In congruence with this observation, the features previously attributed to the formation of precipitates were not detected in the chronopotentiometric curves. In the case of Cr(III) solutions, even for the highest values of applied current, the relaxation of the membrane potential once the current is stopped is very similar to the response observed for underlimiting current densities, as can be seen in Fig. 4.30. The different tendency of the membrane system to form metallic precipitates of Fe(III) and Cr(III) is explained below by means of comparing the solubility plots of the different solutions tested.

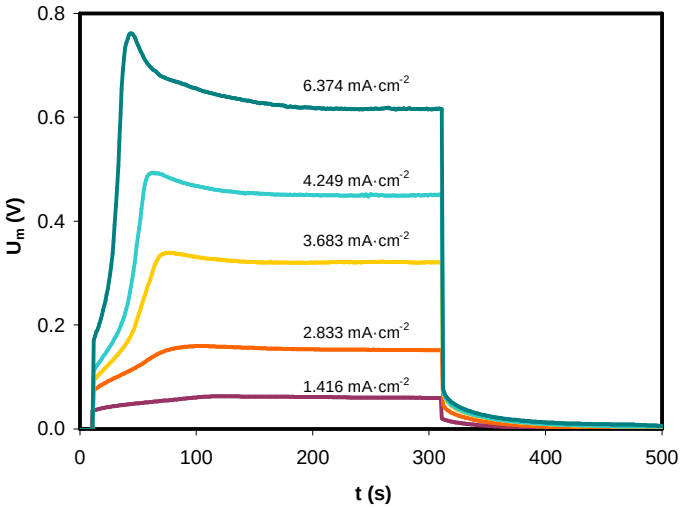

Fig. 4.30. Chronopotentiometric response obtained for 10^{-2}M $Cr_2(SO_4)_3$ solutions.

In order to elucidate the species responsible for the presence of several inflexion points registered in the chronopotentiograms, the speciation diagram of ferric and chromic sulfates was obtained. Fe^{3+} ions are involved in different equilibrium reactions with OH^- and SO_4^{2-} ions, as indicated by Eqs. (4.30)-(4.35):

$$Fe^{3+} + OH^- \rightleftarrows FeOH^{2+} \qquad \beta_1^{OH} = 10^{11.81} \qquad (4.30)$$

$$Fe^{3+} + 2OH^- \rightleftarrows Fe(OH)_2^+ \qquad \beta_2^{OH} = 10^{22.3} \qquad (4.31)$$

$Fe^{3+} + 3OH^- \rightleftarrows Fe(OH)_3$ $\beta_3^{OH} = 10^{30}$ (4.32)

$Fe^{3+} + 4OH^- \rightleftarrows Fe(OH)_4^-$ $\beta_4^{OH} = 10^{34.4}$ (4.33)

$Fe^{3+} + SO_4^{2-} \rightleftarrows FeSO_4^+$ $\beta_1^{SO_4} = 10^{4.04}$ (4.34)

$Fe^{3+} + 2SO_4^{2-} \rightleftarrows Fe(SO_4)_2^-$ $\beta_2^{SO_4} = 10^{5.38}$ (4.35)

Analogously, Cr(III) speciation is described by Eqs. (4.36)-(4.40):

$Cr^{3+} + OH^- \rightleftarrows CrOH^{2+}$ $\beta_1^{OH} = 10^{10.07}$ (4.36)

$Cr^{3+} + 2OH^- \rightleftarrows Cr(OH)_2^+$ $\beta_2^{OH} = 10^{18.3}$ (4.37)

$Cr^{3+} + 3OH^- \rightleftarrows Cr(OH)_3$ $\beta_3^{OH} = 10^{24}$ (4.38)

$Cr^{3+} + 4OH^- \rightleftarrows Cr(OH)_4^-$ $\beta_4^{OH} = 10^{28.6}$ (4.39)

$Cr^{3+} + SO_4^{2-} \rightleftarrows CrSO_4^+$ $\beta_1^{SO_4} = 10^{2.6}$ (4.40)

The protonation equilibria of SO_4^{2-} ions and the dissociation of water have also been taken into account in both cases (Eqs. (4.5)-(4.7)). Moreover, the formation of $Fe(OH)_3$ and $Cr(OH)_3$ precipitates could occur under certain conditions, which is given by Eq. (4.41) and (4.42), respectively:

$Fe(OH)_3\,(s) \rightleftarrows Fe^{3+} + 3OH^-$ $K_s\ (Fe(OH)_3) = 10^{-38.8}$ (4.41)

$Cr(OH)_3\,(s) \rightleftarrows Cr^{3+} + 3OH^-$ $K_s\ (Cr(OH)_3) = 6.3 \cdot 10^{-31}$ (4.42)

Once described the principal reactions in which Fe^{3+} ions can take part to form complex species, the speciation diagram of Fe(III) species can be obtained from the system of

equations formed by the mass balance of Fe(III), the mass balance of sulfates and the proton balance indicated by Eqs. (4.43)-(4.45), respectively:

$$[Fe(III)]_0 = [Fe^{3+}] + [FeOH^{2+}] + [Fe(OH)_2^{+}] + [Fe(OH)_3] + [Fe(OH)_4^{-}] + [FeSO_4^{+}] + [Fe(SO_4)_2^{-}] \quad (4.43)$$

$$[SO_4^{2-}]_0 = [SO_4^{2-}] + [FeSO_4^{+}] + 2[Fe(SO_4)_2^{-}] + [HSO_4^{-}] + [H_2SO_4] \quad (4.44)$$

$$[H^{+}] = [OH^{-}] + [FeOH^{2+}] + 2[Fe(OH)_2^{+}] + 3[Fe(OH)_3] + 4[Fe(OH)_4^{-}] - [HSO_4^{-}] - 2[H_2SO_4] \quad (4.45)$$

Analogously, the speciation diagrams of Cr(III) species can be obtained from the system formed by Eqs. (4.46)-(4.48):

$$[Cr(III)]_0 = [Cr^{3+}] + [CrOH^{2+}] + [Cr(OH)_2^{+}] + [Cr(OH)_3] + [Cr(OH)_4^{-}] + [CrSO_4^{+}] \quad (4.46)$$

$$[SO_4^{2-}]_0 = [SO_4^{2-}] + [CrSO_4^{+}] + [HSO_4^{-}] + [H_2SO_4] \quad (4.47)$$

$$[H^{+}] = [OH^{-}] + [CrOH^{2+}] + 2[Cr(OH)_2^{+}] + 3[Cr(OH)_3] + 4[Cr(OH)_4^{-}] - [HSO_4^{-}] - 2[H_2SO_4] \quad (4.48)$$

The speciation diagram of $5{\cdot}10^{-4}$M $Fe_2(SO_4)_3$ solutions is presented in Fig. 4.31(a) as a function of pH. At the initial equilibrium conditions (indicated in the diagram by the vertical dashed line of pH_{eq}), at least three cationic species coexist in the electrolyte. The ion with the highest concentration is $FeSO_4^{+}$, but the concentrations of Fe^{3+} and $FeOH^{2+}$ ions are also significant. Therefore, the multiple inflexion points registered in the chronopotentiograms of Fig. 4.25 should be due to the depletion of the different cationic species coexisting in the electrolyte. This situation is remarkably different from the speciation of Na_2SO_4 and $NiSO_4$ solutions. In the case of Na_2SO_4 solutions, the complex ion $NaSO_4^{-}$ is negatively charged and does not compete with the Na^{+} ions for the transport through the membrane. Regarding the $NiSO_4$ solutions, only the uncharged complex specie $NiSO_4$ coexists with the Ni^{2+} ions at the initial equilibrium conditions. This explains the fact that the elucidation of two inflection points in the chronopotentiograms obtained for $NiSO_4$ solutions was only observed at very high overlimiting currents, when the change from the initial equilibrium conditions favored the formation of hydroxilated species or the dissociation of $NiSO_4$. On the contrary, in the case of diluted $Fe_2(SO_4)_3$

solutions, since different cations coexist at the initial equilibrium conditions, the two transition times already appear at current densities slightly higher than i_{lim}.

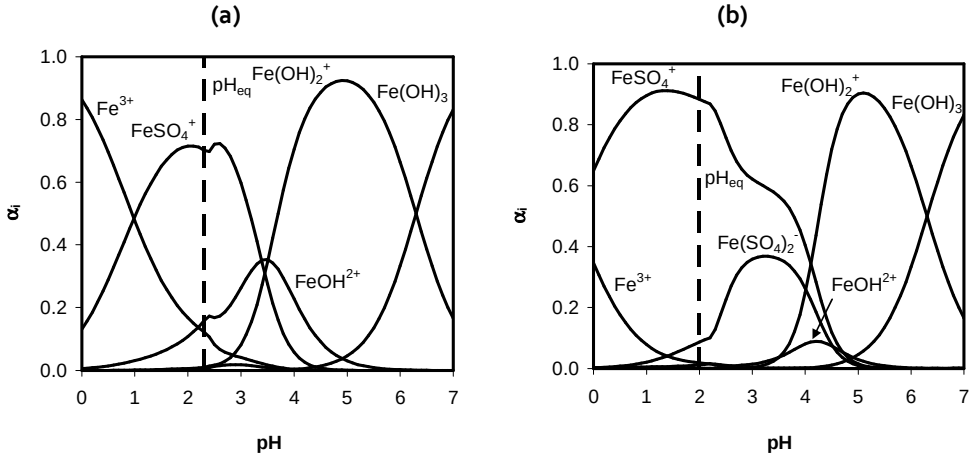

Fig. 4.31. Speciation diagram of (a) $5{\cdot}10^{-4}$M $Fe_2(SO_4)_3$ and (b) 10^{-2}M $Fe_2(SO_4)_3$ solutions.

As the initial salt concentration is increased, the equilibrium is displaced toward the formation of more $FeSO_4^+$ ions, and the concentration of free Fe^{3+} ions becomes insignificant, as can be seen in Fig. 4.31(b). Thus, the less important participation of Fe^{3+} ions in the ion transport through the membranes may be the reason for the absence of a second transition time in the chronopotentiograms obtained for more concentrated solutions of $Fe_2(SO_4)_3$ (Fig. 4.27).

The speciation diagram of $5{\cdot}10^{-4}$M $Cr_2(SO_4)_3$ solutions is shown in Fig. 4.32(a). As occurs with the diluted solutions of $Fe_2(SO_4)_3$, Cr^{3+} ions coexist in equilibrium conditions with the complex species $CrSO_4^+$ and $CrOH^{2+}$. However, in this case the concentration of the free Cr^{3+} ions is higher than the concentration of $CrSO_4^+$, which results in the well differentiated multiple inflexion points detected in the chronopotentiograms (Fig. 4.28). As the initial electrolyte concentration is increased this predominance is reverted because the formation of complex species with SO_4^{2-} ions is favored, as can be seen in Fig. 4.32(b). Therefore, the unique inflexion point detected for 10^{-2}M $Cr_2(SO_4)_3$ seems to be caused by the depletion of $CrSO_4^+$ ions (Fig. 4.30).

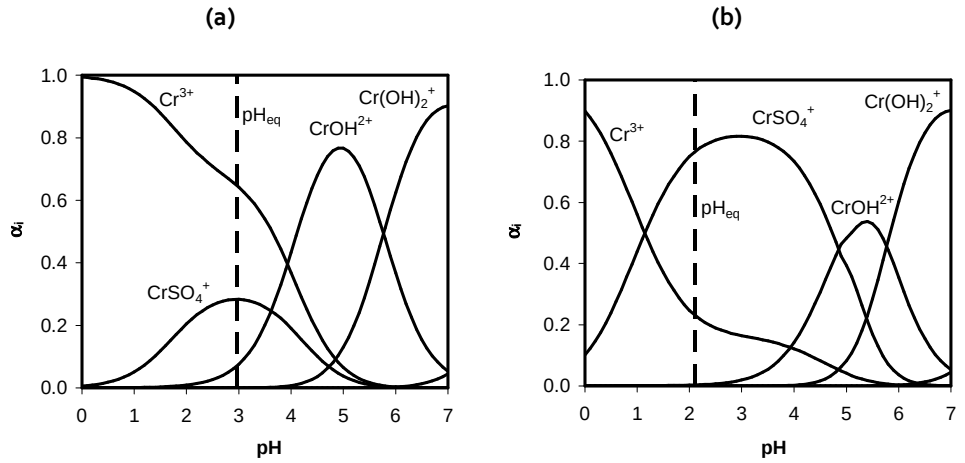

Fig. 4.32. Speciation diagram of (a) $5{\cdot}10^{-4}$M $Cr_2(SO_4)_3$ and (b) 10^{-2}M $Cr_2(SO_4)_3$ solutions.

In addition to the formation of several ionic species, the formation of precipitates can also be explained by calculating the solubility of $Fe(OH)_3$ and $Cr(OH)_3$, which are given by Eqs. (4.49) and (4.50), respectively:

$$s = [Fe^{3+}] + [FeOH^{2+}] + [Fe(OH)_2^{+}] + [Fe(OH)_3] + [Fe(OH)_4^{-}] + [FeSO_4^{+}] + [Fe(SO_4)_2^{-}] \quad (4.49)$$

$$s = [Cr^{3+}] + [CrOH^{2+}] + [Cr(OH)_2^{+}] + [Cr(OH)_3] + [Cr(OH)_4^{-}] + [CrSO_4^{+}] \quad (4.50)$$

The solubility plots of both $Cr_2(SO_4)_3$ and $Fe_2(SO_4)_3$ solutions for different salt concentrations are presented in Fig. 4.33 as a function of the pH, where the initial values of pH_{eq} are indicated with bold points. The formation of precipitates at the anodic surface of the cation-exchange membrane occurs when the local pH near the membrane surface increases and reaches a certain value at which the solubility of the metal species diminishes. In the case of $Fe_2(SO_4)_3$ the difference between the initial pH_{eq} of the solutions and the point at which the formation of $Fe(OH)_3$ precipitates starts is very small. Nevertheless, instead of occurring already at very low current densities, the formation of precipitates only occurs once the i_{lim} is surpassed. This observation probably indicates that the local pH at the diluting side of the membrane remains more or less constant until the depletion of Fe(III) species occurs. Then, the transport of H^+ ions through the membrane increases and the pH at the anodic side of the membrane increases too, thus causing the immediate formation of Fe(III) precipitates even at very low concentrations of Fe(III).

With regard to the formation of precipitates with the $Cr_2(SO_4)_3$ solutions, Cr^{3+} ions also have an important tendency to hydrolyze and the initial pH_{eq} values of these solutions are also acidic. However, the pH at which the solubility of Cr(III) species decreases and the precipitation of $Cr(OH)_3$ starts is higher than 5. This significant difference with respect to the initial pH_{eq} values would explain the absence of precipitates at the membrane surface verified at the end of the experiments. Therefore, the chronopotentiometric results obtained with $Cr_2(SO_4)_3$ solutions confirm that the local pH at the anodic side of the membrane did not increase above a pH value of 5 for all the current densities tested. In this sense, it must be noted that the final pH was measured after all the experiments and, in both cases ($Fe_2(SO_4)_3$ and $Cr_2(SO_4)_3$ solutions) it was confirmed that the pH in the central compartment remained almost constant and very similar to the initial pH_{eq} values. On the contrary, we could not measure the local pH in the vicinities of the membrane due to the characteristics of the electrochemical cell. The local pH in the vicinities of the membrane could vary significantly with respect to the pH measured in the bulk solution, which would be the reason for the formation of $Fe(OH)_3$ precipitates.

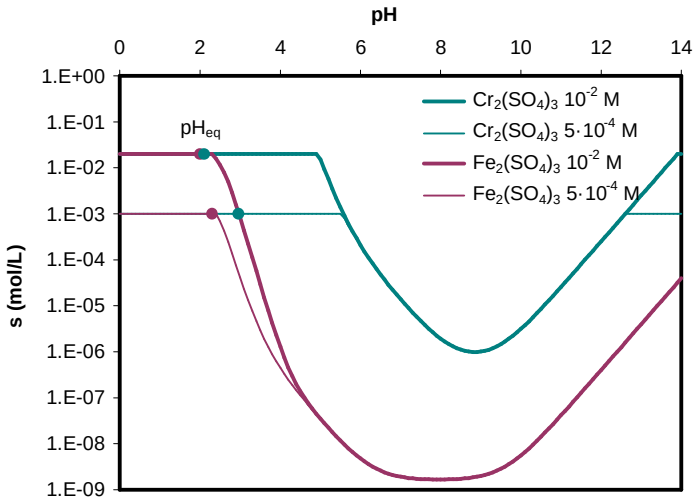

Fig. 4.33. Solubility plot for $Cr_2(SO_4)_3$ and $Fe_2(SO_4)_3$ solutions.

Finally, it must be noted that, in the case of Cr(III) and Fe(III) solutions, the speciation diagrams indicate a higher tendency of the electrolyte solutions to form positively charged complex species. These species compete for the ion transport through the membranes and, unfortunately entail more inaccuracies in the calculation of the Cr^{3+} and

Fe^{3+} ion transport numbers by means of chronopotentiometry. Consequently, this part has been neglected in the present section.

4.1.5.2 Current-voltage characteristics

In agreement with the chronopotentiometric results, the current-voltage curves obtained for solutions of trivalent metals also exhibit different features depending on the type of metal and the initial salt concentrations. The current-voltage curves obtained for diluted solutions of $Fe_2(SO_4)_3$ are presented in Fig. 4.34. The shape of the curves is analogous to that of Na_2SO_4 solutions, with the presence of the three characteristic regions: the region of quasi-ohmic behavior, the plateau, and the overlimiting region.

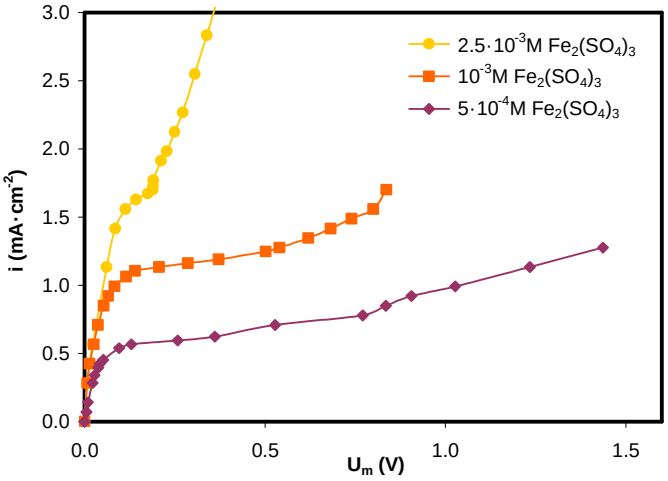

Fig. 4.34. Current-voltage curves obtained for diluted solutions of $Fe_2(SO_4)_3$

However, as observed previously in the chronopotentiometric curves, the increase of the initial concentration favors the formation of precipitates. The formation of precipitates gives rise to extended plateaus in the current-voltage curves obtained for concentrated solutions of $Fe_2(SO_4)_3$, which are shown in Fig. 4.35. This behavior is similar to the response obtained for concentrated solutions of $NiSO_4$, where the formation of precipitates also leads to long plateaus in the current-voltage curves. However, in this case the effect is much more drastic, since the plateau tends to very high values of U_m, even implying the suppression of the overlimiting region. These results indicate that the iron precipitates block the ionic transport through the membranes and limit the increase

in current density [2]. This difference with respect to the system of $NiSO_4$, where the plateau was followed by an almost vertical overlimiting region could be related to the different characteristics of both precipitates. In the case of $Ni(OH)_2$, the precipitate layer was formed at the membrane anodic surface. However, in the case of $Fe(OH)_3$, the precipitate layer formed at the membrane surface was accompanied by the precipitation of iron inside the membrane phase.

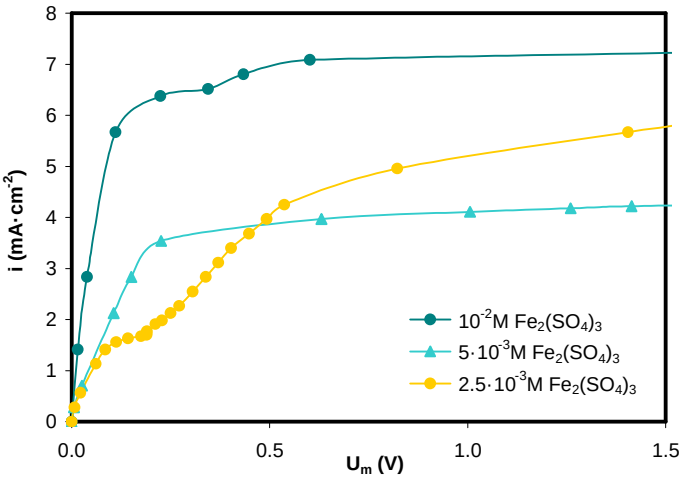

Fig. 4.35. Current-voltage curves obtained for concentrated solutions of $Fe_2(SO_4)_3$

The current-voltage curves obtained for diluted solutions of $Cr_2(SO_4)_3$ are shown in Fig. 4.36. These curves differ from the typical ones because they exhibit two characteristic limiting current densities (i_{lim1} and i_{lim2}) and two distinguished plateaus. For a better detection of both i_{lims} the representation of U_m/i against $1/i$, which is known as the Cowan-Brown plot [14,17,18], is represented in Fig. 4.37. In this figure, the change in the trend of the resistance of the membrane system indicates when the i_{lim1} and the i_{lim2} are reached, whereas a final decrease in U_m/i at high current densities indicates the enhancement of mass transfer in the overlimiting region. This unusual feature in the curves makes them similar to the current-voltage curves obtained by Pismenskaya et al. with weak electrolyte solutions [19]. If the chronopotentiometric results are correlated with the resulting current-voltage curves, it is found that the currents for which only the first transition time is detected coincide with the first plateau in the current-voltage curves, whereas the chronopotentiograms having multiple transition times correspond to the second plateau of the current-voltage curves. Therefore, it seems that the resistance of

the membrane system exhibits a first increase at low current densities when Cr^{3+} ions are depleted from the anodic diffusion boundary layer and a subsequent increase at higher currents when the depletion of other Cr(III) species occurs (i.e.: $CrSO_4^+$ and $CrOH^{2+}$ ions).

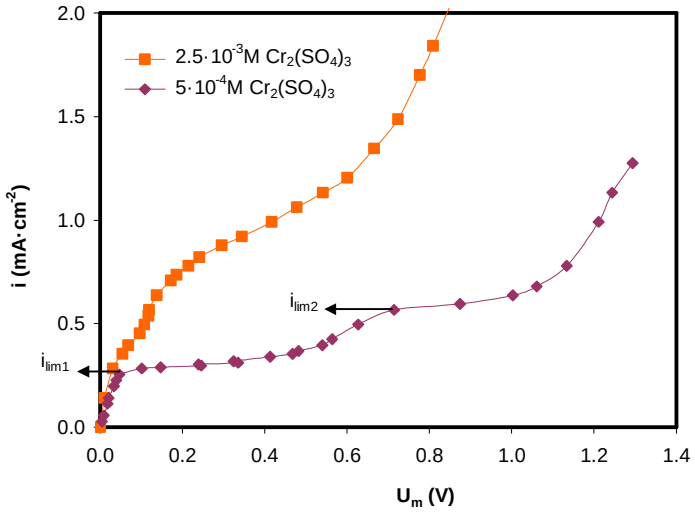

Fig. 4.36. Current-voltage curves obtained for diluted solutions of $Cr_2(SO_4)_3$.

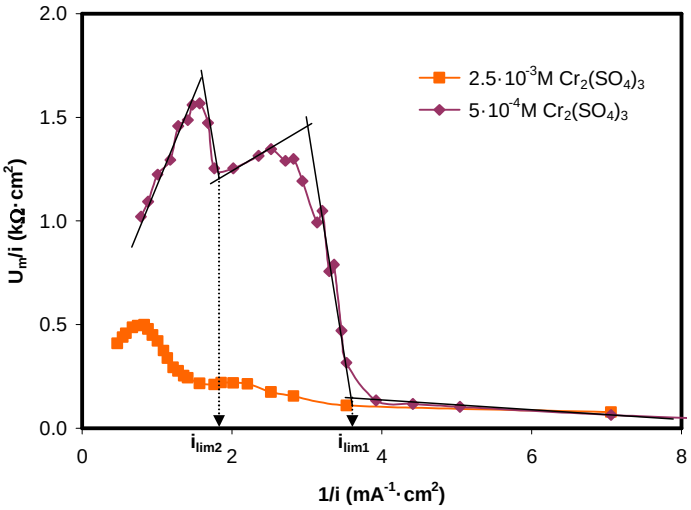

Fig. 4.37. Cowan-Brown plot obtained for diluted solutions of $Cr_2(SO_4)_3$.

The most remarkable characteristic of these curves is the unexpected decrease of the resistance taking place between both plateaus, which in this case are not overlapped. In

order to explain the membrane behavior for this range of currents where the current rises again with U_m, other processes different from the depletion of ions should be considered. In this regard, Pismenskaya et al. also reported an anomalous increase in the electrical conductivity of ion-exchange membranes equilibrated in ampholyte solutions with the dilution of the membrane external solution [20,21]. This behavior was attributed to an enrichment of the membrane pore solution in multicharged ions occurring due to the displacement of the equilibrium conditions inside the membrane phase.

In the systems considered in the present investigation, the main charge carrier inside the membrane phase can also change as the current is increased and the equilibrium conditions are altered in the depleting diffusion boundary layer. At low current densities, the membrane fixed charges should be preferentially equilibrated with Cr^{3+} ions (approximately 75% of the fixed charges are associated with Cr^{3+} ions), as deduced from the ion uptake equilibrium calculated in section 4.1.2.2. As the depletion of Cr^{3+} ions occurs in the diffusion boundary layer, the resistance of the membrane system increases (1st plateau) and the membrane phase becomes enriched in $CrSO_4^+$ ions. However, the fraction of coions inside the membrane phase changes when the dilution of the diffusion boundary layer is intensified. Due to the Donnan exclusion of coions, SO_4^{2-} and OH^- ions are more effectively expelled from the membrane phase in diluted solutions. As a consequence, the pH inside the membrane phase can be significantly lower than that of the external solution whereas the pSO_4 ($-\log[SO_4^{2-}]$) should be higher, thus promoting the dissociation of complex species inside the membrane and leading to the enrichment of the membrane phase in multicharged cations. In the system formed by $Cr_2(SO_4)_3$ solutions, the reaction shown in Eq. (4.51) would be displaced toward the formation of Cr^{3+} ions inside the membrane:

$$CrSO_4^+ \rightleftarrows Cr^{3+} + SO_4^{2-} \qquad (4.51)$$

According to previous studies, the electrical conductivity of ion-exchange membranes increases as the internal pore solution is enriched in multicharged ions [21]. Therefore, the increase in the equivalent fraction of Cr^{3+} ions in the membrane phase would explain the decrease of the resistance occurring between the two plateaus of the current-voltage curves. The Cr^{3+} ions resulting from the reaction (4.51) would be transferred to the cathodic compartment, whereas the sulfate anions return to the depleted diffusion boundary layer due to the coion excluding mechanism inside the membrane. If additional increments in the current density are applied, mass transfer limitations appear again and

the second limiting current (i_{lim2}) is reached. Finally, as denoted by the shape of the chronopotentiograms and confirmed by the overlimiting region appearing in the current-voltage curves, once the U_m surpasses the extension of the second plateau, other mass transfer mechanisms arise when intensive current density values ($i>i_{lim2}$) are applied and this promotes a facilitated supply of counterions to the membrane surface.

With regard to the more concentrated solutions of $Cr_2(SO_4)_3$ (see Fig. 4.38), only one i_{lim} is clearly observed in the current-voltage curves, which is in agreement with the unique transition time obtained in the chronopotentiograms (see Fig. 4.30). As commented above, an increase in the initial concentration favors the formation of the complex specie $CrSO_4^+$. The predominance of $CrSO_4^+$ ions is much larger, so that the contribution of Cr^{3+} to the transport through the membrane is less significant. Hence, when the depletion of $CrSO_4^+$ ions occurs in the diffusion boundary layer at the anodic side of the membrane, the plateau is formed in the current-voltage curves. Then, the overlimiting mechanisms of current activate the supply of these ions to the membrane surface before a significant conversion to Cr^{3+} ions occurs in the membrane phase, thus leading to the third region of the current-voltage curves.

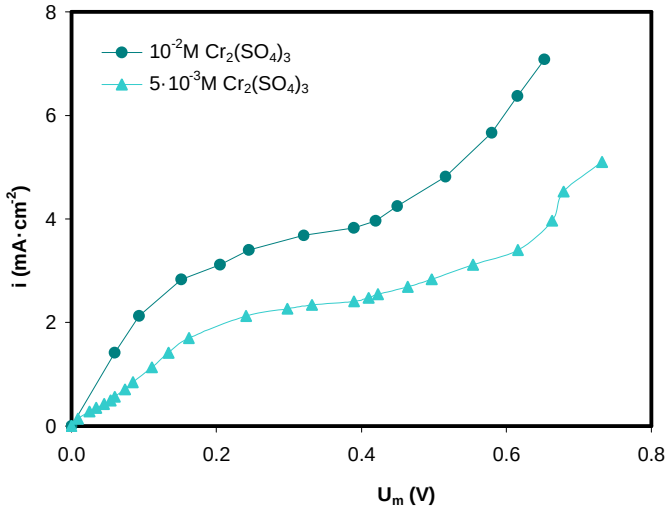

Fig. 4.38. Current-voltage curves obtained for concentrated solutions of $Cr_2(SO_4)_3$.

The values of R_1 and i_{lim} for the systems of trivalent metal sulfates are summarized in Table 4.3 and 4.4, where the values of i_{lim1} and i_{lim2} have been included for those systems in which various limiting currents were detected. The evolution of those parameters is

represented as a function of the initial metal concentration in Figs. 4.39 and 4.40. In both cases the evolution of R_1 is similar to the evolution observed for Na_2SO_4 and $NiSO_4$ solutions. The ohmic resistances of the membrane decrease with the increase in the electrolyte concentration, as it was expected, since the presence of more ionic species contributes to increase the membrane conductance. On the contrary, in the case of $Cr_2(SO_4)_3$ solutions the evolution of i_{lim} with the initial concentration does not follow the linear trend that would be expected from the Peers' equation. In this case, depending on the initial concentration the depletion of different cationic species can lead to various values of i_{lim}, as can be seen in Fig. 4.40, which differs from the linear trend observed with the other electrolytes.

Table 4.3. Current-voltage characteristics obtained with $Fe_2(SO_4)_3$ solutions.

	$5{\cdot}10^{-4}$M $Fe_2(SO_4)_3$	$2.5{\cdot}10^{-3}$M $Fe_2(SO_4)_3$	$5{\cdot}10^{-3}$M $Fe_2(SO_4)_3$	10^{-2}M $Fe_2(SO_4)_3$
R_1 ($\Omega{\cdot}cm^2$)	94.25	62.93	52.15	36.83
i_{lim} ($mA{\cdot}cm^{-2}$)	0.559	1.535	3.880	7.082

Table 4.4. Current-voltage characteristics obtained with $Cr_2(SO_4)_3$ solutions.

	$5{\cdot}10^{-4}$M $Cr_2(SO_4)_3$	$2.5{\cdot}10^{-3}$M $Cr_2(SO_4)_3$	$5{\cdot}10^{-3}$M $Cr_2(SO_4)_3$	10^{-2}M $Cr_2(SO_4)_3$
R_1 ($\Omega{\cdot}cm^2$)	180.33	112.501	63.538	43.842
i_{lim1} ($mA{\cdot}cm^{-2}$)	0.280	0.292	2.000	3.120
i_{lim2} ($mA{\cdot}cm^{-2}$)	0.566	0.736	2.000	3.120

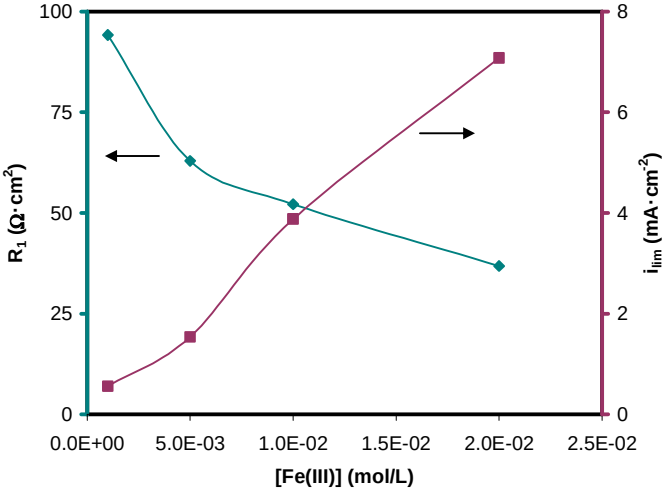

Fig. 4.39. Evolution of R_1 and i_{lim} as a function of the concentration of Fe(III).

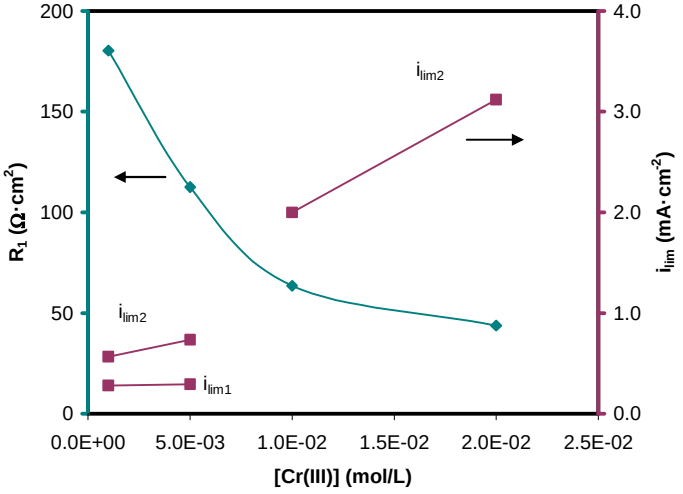

Fig. 4.40. Evolution of R_1, i_{lim1} and i_{lim2} as a function of the concentration of Cr(III).

4.1.6 Conclusions

In this chapter the transport of different metal ions through the Nafion 117 membrane has been investigated. Since the membrane transport properties are strongly correlated with their morphology and structural characteristics, the physical characterization of Nafion was conducted previously. The main conclusion from the membrane morphological characterization is described as follows:

- The SEM images showed that the Nafion 117 membrane has a dense and uniform conformation. Moreover, the fluorocarbon structure and the hydrophilic SO_3^- fixed charges characteristic of the Nafion membranes have been clearly identified in the Raman spectrum of the membrane, where the absence of other important peaks confirms that this membrane does not possess inert binder or polymer fillers in its structure.

After the structural characterization of Nafion, ion uptake experiments were conducted with single salt solutions of Na_2SO_4, $NiSO_4$, $Fe_2(SO_4)_3$ and $Cr_2(SO_4)_3$. The main conclusions obtained from these experiments are summarized below:

- The membrane absorbs a higher quantity of Na^+ ions in relation to other metals in equilibrium conditions (under the absence of an applied electric field). The higher amount of Na^+ ions inside the membrane phase with respect to other ions can be explained by the fact that each Na^+ ion is balancing the charge of one membrane fixed ionic group, whereas the multivalent ions could be bound to more than one membrane fixed charges.

- The comparison between the theoretical ion exchange capacity of the membranes and the concentration of ions equilibrating the membrane charges reveal that free Na^+ and Ni^{2+} ions are bound to the membrane fixed charges, when the membrane is immersed in Na_2SO_4 and $NiSO_4$ solutions, respectively. On the contrary, when the membrane is immersed in $Fe_2(SO_4)_3$ and $Cr_2(SO_4)_3$ solutions, the concentration of multivalent metals inside the membrane phase indicates that the membrane fixed charges are not exclusively balanced with free Fe^{3+} or Cr^{3+} ions. In these cases, the multivalent metals could be present inside the membrane phase also in the form of positively charged complex species, such as $FeSO_4^+$ or $CrSO_4^+$ ions.

- The membrane becomes generally saturated with solution counterions, since the concentration of metals in the membrane is independent of the equilibrating electrolyte concentration. These results lead to very high partition coefficients at low electrolyte concentrations.

The dynamics of the ion transport taking place through the membrane and the current-voltage curves were also obtained for the systems formed by the Nafion 117 membrane and different single salt solutions. The main conclusions obtained from these experiments are summarized as follows:

- The chronopotentiometric and current-voltage curves obtained for solutions of Na_2SO_4 are the typical ones obtained in previous studies with monovalent ions. The speciation diagrams of Na_2SO_4 solutions revealed that Na^+ ions are the predominant cationic species in the solutions, since Na_2SO_4 is a strong electrolyte. The current-voltage curves showed the three characteristic regions of membrane behavior: the quasi-ohmic region, the plateau formed when the concentration of Na^+ ions vanishes at the membrane depleting surface, and the overlimiting region with enhanced supply of ions to the membrane. As expected, the R_1 values decrease with an increase of the electrolyte concentration, since a higher amount of mobile ionic species are present in the diffusion boundary layers. On the contrary, the i_{lim} values increased linearly with the salt concentration, as predicted by the Peers' equation. The T_{Na^+} values also indicate that the cationic selectivity of the membrane immersed in single salt solutions is high, since T_{Na^+} values close to 0.9 were obtained.

- The chronopotentiometric curves obtained for $NiSO_4$ solutions are different from the typical ones obtained with Na_2SO_4. At low concentrations of $NiSO_4$ (10^{-3}M), the chronopotentiometric response obtained at high overlimiting currents shows two different increments in U_m with their related inflexion points. The first inflexion point is attributed to the depletion of Ni^{2+} ions from the anodic membrane surface when the i_{lim} is reached and the supply of counterions to the membrane is set under diffusion control. Once the i_{lim} is surpassed, the transport of H^+ ions through the membrane contributes to increase the local pH of the diffusion boundary layer, thus promoting the formation of $NiOH^+$ ions. Moreover, the dissociation of the complex species $NiSO_4$ could also take place. Therefore, the second inflexion point can be related

to the subsequent depletion of the cationic species generated at higher current densities ($NiOH^+$ and Ni^{2+} ions).

- In the case of concentrated solutions of $NiSO_4$ (10^{-2}M and $2{\cdot}10^{-2}$M), the formation of a precipitate layer of $Ni(OH)_2$ at the anodic membrane surface takes place when the i_{lim} is surpassed. This phenomenon was visualized at the end of the experiments and was also related to the observation of different chronopotentiometric features. A gradual increase in the membrane resistance takes place when the precipitates are formed and also a slower relaxation of the membrane potential occurs when the current is stopped. The formation of precipitates is promoted by the increase in the pH at the depleting diffusion boundary layer as a consequence of the application of high overlimiting currents. Once the precipitates are formed, the development of a quasi-bipolar membrane structure by the precipitate/membrane system favors the dissociation of water. The slower relaxation of U_m with time once the current is switched off, which is a feature typical of bipolar membranes, seems to be caused by the hindered recombination of the water dissociation products.

- The selectivity of the membrane is also high in the case of single salt solutions of $NiSO_4$, since the T_{Ni}^{2+} values are higher than 0.85 for all the salt concentrations. The slight decrease of T_{Ni}^{2+} observed for the highest concentrations of $NiSO_4$ could be attributed to a weaker Donnan exclusion for coions occurring at high concentrations.

- The current-voltage curves obtained with diluted $NiSO_4$ solutions have the three typical regions of membrane behavior. On the contrary, the curves obtained for those concentrations at which the formation of precipitates occurs show an extended plateau. Moreover, at overlimiting currents, the dissociation of water catalyzed by the $Ni(OH)_2$ precipitates implies an almost vertical increase of the current density. The trend of R_1 and i_{lim} with the initial electrolyte concentration is analogous to that observed in the case of Na_2SO_4 solutions.

- The speciation diagrams of diluted $Fe_2(SO_4)_3$ and $Cr_2(SO_4)_3$ solutions reveal the coexistence at the initial equilibrium conditions of various positively charged species. The successive depletion of each of these species at increasing current densities is elucidated from the observation of several transition times in the

chronopotentiometric curves. In the case of $Cr_2(SO_4)_3$ this phenomenon is more clear, since two different i_{lim} values were detected in the current-voltage curves (i_{lim1} and i_{lim2}). Moreover, in this case an unexpected decrease of the resistance of the membrane system is observed between i_{lim1} and i_{lim2}, which is probably caused by the dissociation of $CrSO_4^+$ ions and the subsequent enrichment of the membrane phase in multicharged ions (Cr^{3+} ions).

- Analogously to what occurred with concentrated $NiSO_4$ solutions, the formation of $Fe(OH)_3$ precipitates at the anodic side of the membranes also occurred with concentrations of $Fe_2(SO_4)_3$ higher than $2.5 \cdot 10^{-3}$M. However, these precipitates were formed not only at the membrane surface but also inside the inner membrane phase, which leads to the subsequent blockage of the ionic transport through the membrane and to extended plateaus in the current-voltage curves.

4.2 Competitive transport of metal ions present in multicomponent mixture solutions through cation-exchange membranes

4.2.1 Introduction

In traditional applications of ion-exchange membranes, such as the desalination of brackish water or the chlor-alkali industry, the electrolyte solutions usually contain one cation with a predominant concentration over that of other counterions [14,22]. Moreover, the utilization of membranes with binary cation systems is of major importance in emerging applications of electromembrane processes, such as the treatment of metal containing wastewaters. In this regard, the behavior of ion-exchange membranes can be severely affected by the electrolyte composition. For example, Okada et al. found out that the contamination of fuel cell membranes by impurity cations resulted in a decrease of their ionic conductivity [23]. In other cases it is important to avoid the permeation of specific ions through the membranes; as occurs with the vanadium redox flow batteries, where the transport of H^+ ions is desired but the vanadium crossover leads to a decrease of the coulombic efficiency of the batteries [24].

The competitive ion transport through ion-exchange membranes is also a fundamental aspect in the treatment of industrial effluents by electrodialysis. In certain situations it is interesting to promote the transport of the most valuable metal in order to obtain a product of high purity that could result in an added-value resource [13,25]. In other cases, the recovery of spent acids is the main objective of the treatment process and the transport of H^+ ions is desired over that of other metallic cations [26-29]. On the contrary, the general desalination of the effluent is preferred when the reclamation of large volumes of water is wanted [30,31]. However, in all these cases the competitive ion transport is accompanied by the formation of concentration gradients at the membrane/electrolyte interfaces. The concentration polarization phenomena can significantly affect both the selectivity and the electrical resistance of the membranes, thus determining also the energy consumption of the electrodialysis operations. Therefore, achieving a better understanding of the mass transport processes that determine the behavior of ion-exchange membranes in multicomponent mixtures is fundamental in order to develop electromembrane processes with optimal performances.

In this section (4.2), the competitive ion transport through the Nafion 117 cation-exchange membrane is investigated. Given the diversity of industrial wastewaters that can be treated by means of electrodialysis, two different practical cases have been considered:

- The first practical case considered is the treatment of spent rinse waters of nickel and chromium plating industries. These waters contain Ni(II) in the form of cationic impurities, which is considered a toxic pollutant, and may cause several health and environmental problems when discharged into natural watercourses [32]. Moreover, the spent rinse waters of the chromium electroplating industry contain important concentrations of Cr(VI), which has toxic and carcinogenic effects on different organs of the human body [33]. Basically, the composition of these effluents is characterized by the presence of metallic impurities in acidic solutions. As investigated in the previous chapter, the transport of multivalent Ni^{2+} ions through cation-exchange membranes presents some peculiar characteristics. Besides, H^{+} ions are also reported to have special transport properties, since they can be transported via the successive proton exchange between neighboring water molecules (Grotthuss mechanism [34]) and their mobility is 5-8 times larger than that of other ions [35]. Therefore, the study of the competitive ion transport between H^{+} and Ni^{2+} is interesting due to its potential application to the treatment of industrial wastewaters, and also as a fundamental aspect in the field of the membrane science.

- The second practical case considered is the treatment of acid mine drainage generated in coal mining sites. These solutions are composed of a mixture of several metallic cations in sulfuric acid media. Sometimes the recovery of precious metals is interesting from an economical point of view [36]. But in general, the treatment of acid mine drainage solutions is beneficial for the environment because these effluents imply potential hazards for natural watercourses. For this study we have selected an acid mine drainage generated in a coal extracting site, which contains Fe(III) and Na(I) as the main cationic contaminants. This study allows us to investigate the competitive ion transport between metal ions with different characteristics. On the one hand, Na^{+} is an alkali monovalent ion and has large diffusion coefficients and a small size. On the other hand, Fe^{3+} is a multivalent heavy metal ion and can give rise to the formation of several complex species of varying transport properties.

4.2.2 Competitive ion transport between protons and metal cations. Case of study: H^+ vs. Ni^{2+}

4.2.2.1 Introduction and applicability

In the present section the competitive transport of H^+ and Ni^{2+} ions through cation-exchange membranes is investigated. Both ions are present in spent acid baths generated in metal finishing operations. The metal finishing industry is known for its intensive water consumption [26], which stimulates the development of clean processes for the treatment of the spent effluents and the subsequent reuse of raw materials and water. To conduct this investigation, the composition of rinse waters of nickel and chromium plating industries has been considered.

In the plating process of metals, chromic acid is employed as a source of Cr(VI) in order to apply a corrosion resistant layer which protects the base material. For this purpose, Cr(VI), which is present in the plating baths in the form of anionic species such as chromate (CrO_4^{2-}), hydrochromate ($HCrO_4^-$) or dichromate ($Cr_2O_7^{2-}$), is reduced at the surface of the pieces being treated. During the plating process a slight amount of the metallic material is dissolved from the pieces in the form of ions, such as Ni^{2+}, Fe^{3+}, or Cr^{3+}. The main step of the process is then followed by a rinsing stage, during which hexavalent chromium and metallic impurities coming from the plating baths are transferred to the rinse waters, which have to be consequently replaced when a certain limit of cationic impurities is reached [25].

Among the available technologies that can be applied to treat spent rinse waters, electrodialysis offers many advantages in comparison with other methodologies. Chemical precipitation implies the addition of chemicals and the production of large quantities of sludge [37], the use of ion-exchange resins involves further operations to regenerate the ion exchangers, and reverse osmosis does not allow the separation of cationic contaminants from anionic species of Cr(VI). By contrast, electrodialytic techniques facilitate the simultaneous separation of ions of opposite charge and can make feasible both the reutilization of chromic acid free from cationic impurities [13] and the recirculation of water to the washing steps [25,38]. Fig. 4.41 shows a schematic representation of an electrodialysis cell coupled with the different steps of a chromium plating process. Once plated, the pieces are usually transported over a cascade rinsing, which is used for effecting water economies and reducing the volume of effluent [39,40].

The rinse water flows through a series of containers in the opposite direction to the workpieces, so that the first tank contains the most contaminated water. Once exhausted, the rinse waters can be circulated through an electrodialysis cell consisting of three compartments separated by an anion- and a cation-exchange membrane. The Cr(VI) and SO_4^{2-} ions are concentrated in the anodic compartment. Note that the recovery of SO_4^{2-} ions with the chromic acid is beneficial for the process, because SO_4^{2-} ions are used as catalysts in the plating process [13,41]. On the other hand, the cationic species would be transferred through the cation-exchange membrane toward the cathodic compartment. In this manner, the concentrated chromic acid could be reused in the plating process, whereas the regenerated rinse waters would be recycled to the rinsing steps. Finally, an important part of the metallic impurities removed from the rinse waters can be electrodeposited at the cathode, which could be recovered for other uses.

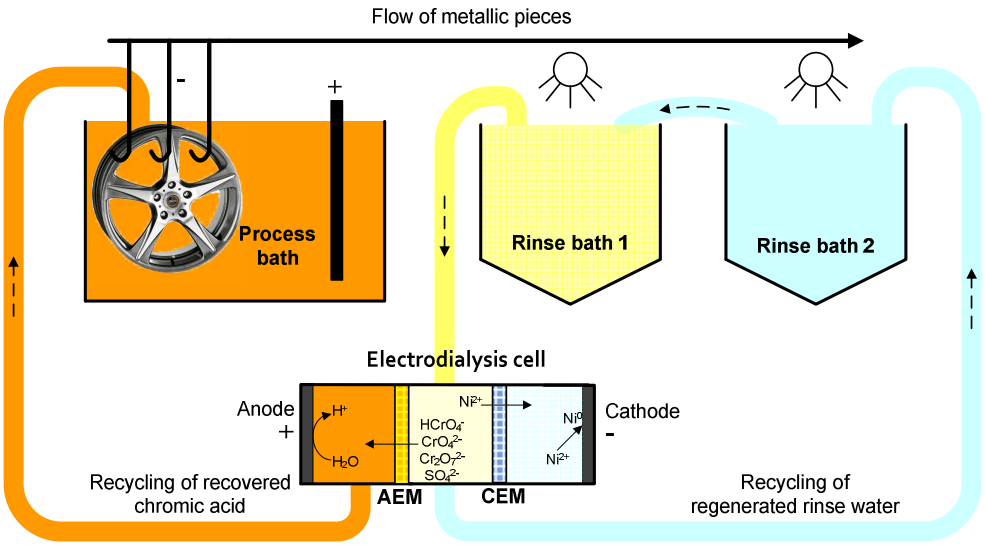

Fig. 4.41. Schematic representation of the process of chromium plating of metallic pieces with a double counter-flow cascade rinse system coupled with an electrodialysis cell for the treatment of the spent rinse waters.

The spent rinse waters generated in the metal finishing industry can contain toxic species in a wide concentration range, since their composition depends on the type of plating process and the previous history of the workpieces. For example, hard-chromium plating is applied directly to engineering pieces, whereas decorative chromium deposition is usually applied over nickel overcoats. Consequently, the spent rinse waters coming from the hard-chromium plating have predominant concentrations of Cr(VI), whereas a mixture of both Cr(VI) and Ni^{2+} is found in decorative chromium plating rinse waters. In

the case of nickel electroless plating, the presence of Ni^{2+} ions is much more significant. In Table 4.5 typical concentrations of spent rinse waters obtained from the literature are summarized.

Table 4.5. Typical concentrations of Cr(VI) and Ni(II) of spent rinse waters of chromium and nickel plating industries.

Cr(VI)	Ni(II)	pH	Finishing process	Reference
10^{-1}M	10^{-2}M	1.2	Chromium plating rinsing solution (synthetic)	[42]
$1.26 \cdot 10^{-2}$M	$7.32 \cdot 10^{-4}$M	-	Chromium plating rinsing solution (industrial effluent)	[43]
$4.81 \cdot 10^{-3}$ – $9.62 \cdot 10^{-3}$M	-	-	Chromium plating rinsing solution (reference values coming from multiple cascade rinse system)	[40]
-	$3.41 \cdot 10^{-2}$M	2-6	Nickel plating rinsing solution (synthetic)	[44]
-	$6.89 \cdot 10^{-4}$M	5.2	Nickel plating rinsing solution (synthetic)	[45]
-	$1.70 \cdot 10^{-3}$ – $3.41 \cdot 10^{-3}$M	-	Nickel plating rinsing solution (reference values coming from multiple cascade rinse system)	[40]

As commented above, the range of concentrations of both Ni(II) and Cr(VI) is wide and depends on the type of management of rinsing waters applied in each industry. Accordingly, we aim at performing a study covering a broad range of concentrations in order to evaluate the effect of the electrolyte composition on the competing transport of Ni^{2+} and H^{+} ions through cation-exchange membranes. Mixtures with concentrations of $NiSO_4$ ranging from $5 \cdot 10^{-4}$M to 10^{-2}M and concentrations of CrO_3 ranging from 0M to 10^{-2}M were considered for the present study. The combination of concentrations was indicated previously in more detail in Table 3.3 of the previous chapter.

4.2.2.2 Ion sorption experiments

As already performed with the single salt solutions (section 4.1), ion sorption experiments were also conducted with the mixtures of $NiSO_4$ and CrO_3. Fig. 4.42 shows the concentration of Ni^{2+} ions in the membrane phase in equilibrium conditions (c_m,

expressed in mmol of Ni^{2+} ions per gram of dry membrane) as a function of the external electrolyte composition. In analogy to the results obtained in section 4.1.2.2, when equilibrated with single salt solutions of $NiSO_4$, the membrane becomes practically saturated in Ni^{2+} ions and the values of c_m remain independent of the concentration of the equilibrating solution. Moreover, if the concentration of Ni^{2+} is converted into equivalents, c_m reaches the value of 0.86 meq/g, which is very close to the theoretical ion exchange capacity of the Nafion 117 membrane (0.90 meq/g). However, in the case of mixture solutions of $NiSO_4$ and CrO_3 the amount of fixed ion exchange sites equilibrated with Ni^{2+} ions decreases considerably for the lower $NiSO_4$ concentrations.

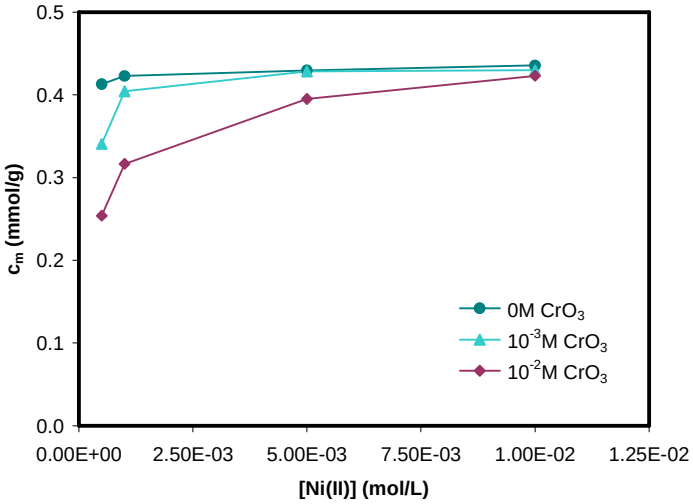

Fig. 4.42. Concentration of Ni^{2+} ions equilibrated in the membrane phase as a function of the composition of the equilibrating solution.

These results may be due to the presence of additional cations in the solutions of CrO_3, which compete with the Ni^{2+} ions for the membrane fixed charges. In this regard, the chromic acid formed when CrO_3 is dissolved in water, H_2CrO_4, releases H^+ ions to the solution. These ions could replace the Ni^{2+} ions and occupy an important part of the membrane fixed charges. The replacement of Ni^{2+} ions by H^+ ions in the membrane phase is more notorious for the solution mixtures having low $NiSO_4$ concentrations. However, as the concentration of $NiSO_4$ increases, the effect of the addition of CrO_3 is significantly attenuated. Fig. 4.43 shows the $[Ni^{2+}]/[H^+]$ ratio in the external electrolyte solution calculated for each composition from the speciation diagrams. The $[Ni^{2+}]/[H^+]$ ratio is in good agreement with the c_m values shown in Fig. 4.42. The solutions having $[Ni^{2+}]/[H^+]$

values below 1 correspond approximately to the c_m values that are below 0.4 mmol Ni(II)/g in Fig. 4.42.

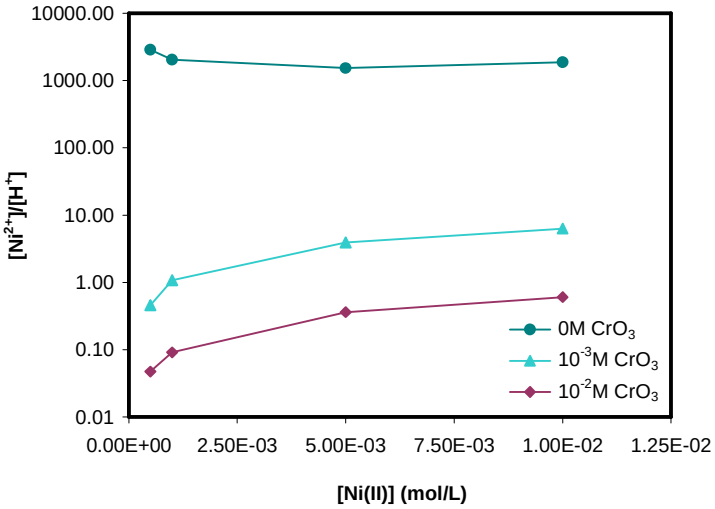

Fig. 4.43. Values of the $[Ni^{2+}]/[H^+]$ ratio in the electrolyte solution as a function of the composition of the mixtures of $NiSO_4$ and CrO_3.

Since the ion exchange capacity of the Nafion membrane is directly associated with the number of fixed sulfonate groups attached to the polymer backbone, we can assume that it remains invariable and independent of the composition of the external electrolyte. Based on this assumption, the fixed charges of the membrane can be bound either to Ni^{2+} or to H^+ ions, as these are the main counterions present in the mixtures of $NiSO_4$ and CrO_3. Therefore, we can estimate the number of fixed ion exchange sites equilibrated with H^+ ions from the difference between the ion exchange capacity of the membranes and the values of c_m obtained for the Ni^{2+} ions. By using this approach, the proportion of membrane fixed charges occupied by Ni^{2+} and H^+ ions was obtained for each electrolyte composition (see Fig. 4.44). As already discussed, for the solutions without CrO_3 the membrane practically becomes saturated in Ni^{2+} ions, and the fraction of fixed charges bound to H^+ ions increases gradually with the content of CrO_3. However, it must be pointed out, that in all cases the membrane absorbs preferentially Ni^{2+} ions, even for concentrations of CrO_3 exceeding that of $NiSO_4$. These results are in agreement with previous studies dealing with the absorption equilibrium of cation-exchange membranes in mixtures of acids and metals [46-48]. More specifically, several authors obtained similar results in different cation-exchange membranes equilibrated in electrolyte

systems of H^+/Ni^{2+} ions [23,49]. The higher preference of cation-exchange membranes for multivalent ions has been usually attributed to the larger electrostatic attraction between multivalent ions and the fixed ion exchange sites of opposite polarity [46,47].

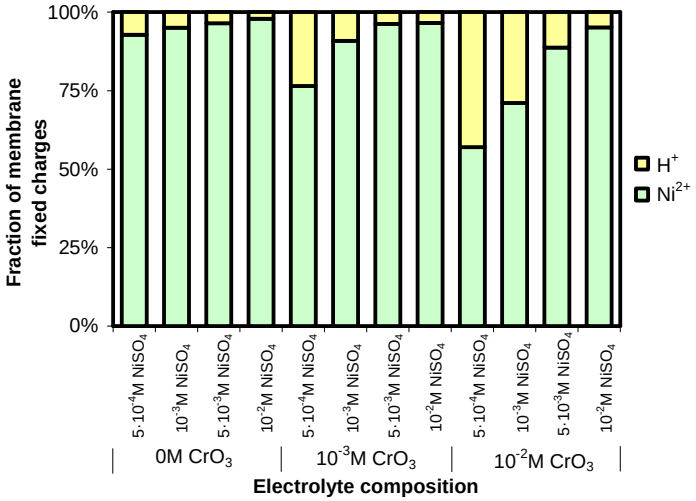

Fig. 4.44. Fraction of membrane fixed charges equilibrated with each ion (Ni^{2+} or H^+) present in the different electrolyte compositions tested.

4.2.2.3 Chronopotentiometric response

The effect of the addition of CrO_3 to the $NiSO_4$ solutions on the ion transport through the Nafion 117 membrane can be analyzed from the comparison of the chronopotentiograms obtained for mixture solutions and those obtained for single salt solutions of $NiSO_4$ (presented in section 4.1). The chronopotentiometric response obtained for the mixtures of 10^{-3}M $NiSO_4$ and 10^{-3}M CrO_3 is shown in Fig. 4.45. The curves present a shape similar to that obtained for 10^{-3}M $NiSO_4$. At low values of current density (i.e.: 0.21 mA·cm^{-2}) the increase of U_m with time is moderate but, when the i_{lim} is surpassed ($i \geq 0.27$ mA·cm^{-2}) the chronopotentiograms exhibit the steep increase of U_m associated with the depletion of Ni^{2+} ions. Then, the subsequent evolution of U_m until the steady state is reached is different depending on the current density. As observed for the single salt solutions of $NiSO_4$, at current densities moderately higher than the i_{lim} the evolution of U_m for times larger than the transition time is almost flat; whereas at very high current densities, the

curves present fluctuations related to the destabilizing effect of electroconvection on the diffusion boundary layers.

Despite the similarities observed between the curves obtained for the mixtures with 10^{-3}M CrO_3 and the curves corresponding to single salt solutions of $NiSO_4$, it must be said that the current densities at which each chronopotentiometric feature is detected is significantly higher for the mixture solutions. For example, the curve obtained at 0.21 mA·cm^{-2} in Fig. 4.45 clearly corresponds to the quasi-ohmic regime of currents, whereas the same current density would belong to the overlimiting regime of currents for 10^{-3}M $NiSO_4$ (see Fig. 4.16). Therefore, the addition of CrO_3 promotes a delay in the development of the concentration polarization phenomena related to the depletion of Ni^{2+} ions. This influence may be due to the presence of H^+ ions released by the chromic acid, which act as additional charge carriers and compete with the Ni^{2+} ions for the transport through the membranes. Specifically, the pH values measured for 10^{-3}M CrO_3 solutions are approximately 3, which confirms that the H^+ ions may be the main cationic species competing with the Ni^{2+} ions for the transport through the membrane. Nevertheless, the formation of other ionic species due to the addition of CrO_3 is also considered and discussed below.

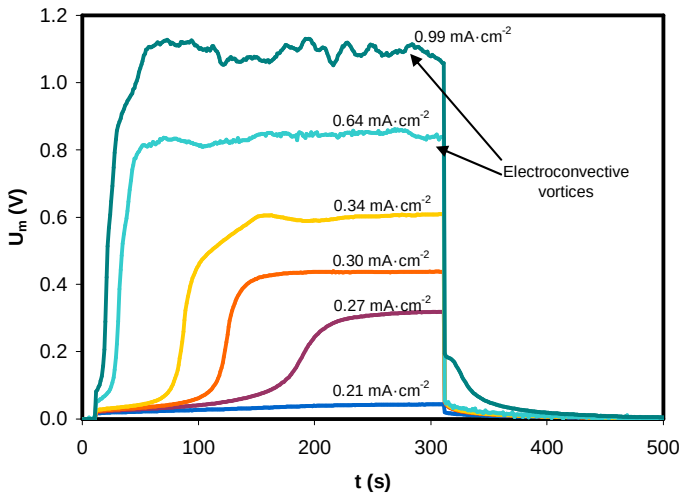

Fig. 4.45. Chronopotentiometric response obtained for mixtures of 10^{-3}M $NiSO_4$ and 10^{-3}M CrO_3.

Fig. 4.46 shows the curves obtained for the mixtures of 10^{-2}M $NiSO_4$ and 10^{-3}M CrO_3. For a constant CrO_3 concentration of 10^{-3}M, the effect of increasing the concentration of $NiSO_4$ is also similar to that observed for the single salt solutions. The chronopotentiograms corresponding to high overlimiting currents present a second increase in U_m at times higher than the transition time. Moreover, these curves also exhibit a slow restoration of the membrane potential once the current ceases. As occurred with the 10^{-2}M $NiSO_4$ solutions, the formation of precipitates at the depleting membrane surface induces an increase in the electrical resistance of the membrane system, which is responsible for the continuous increase in U_m observed in the curves. The inset photograph of Fig. 4.46 shows the precipitate formed at the membrane surface. The texture of this precipitate is the same as that of $Ni(OH)_2$ (Fig. 4.17), however, it has the characteristic color of chromic acid solutions. Since the metallic hydroxides catalyze the dissociation of water, the hindered transport of H^+ and OH^- ions through the precipitate layer and their slower recombination in the diffusion boundary layers originates the plateau observed in the relaxation of U_m.

With regard to the magnitude of currents at which the different chronopotentiometric characteristics are registered, in this case the effect of the addition of chromic acid is not as important as with more diluted solutions of $NiSO_4$. For 10^{-2}M $NiSO_4$ solutions, the addition of 10^{-3}M CrO_3 increases very slightly the values of current density at which the transition times and the formation of precipitates were detected. This could be caused by the fact that in this case the concentration of $NiSO_4$ is higher than the concentration of CrO_3.

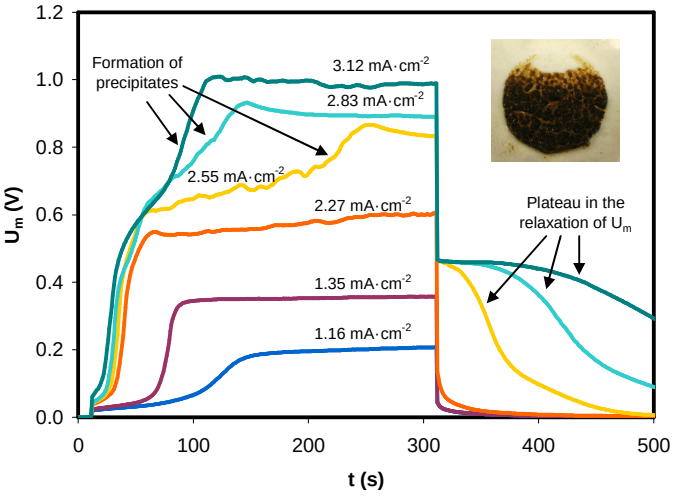

Fig. 4.46. Chronopotentiometric response obtained for mixtures of 10^{-2}M $NiSO_4$ and 10^{-3}M CrO_3. The inset photograph shows the precipitates formed at the surface of the membrane.

A further increase in the concentration of CrO_3 has similar effects at both low and high concentrations of $NiSO_4$, as can be seen in Figs. 4.47 and 4.48. The current densities at which the depletion of ions and the overlimiting features appear are significantly higher for the mixture solutions than for the single salt solutions of $NiSO_4$. The competence between H^+ and Ni^{2+} ions in 10^{-2}M CrO_3 solutions is stronger, because the pH is more acidic (pH ≈ 2). Moreover, in this case the formation of precipitates was not observed during the experiments and neither detected in the chronopotentiometric curves, since, as shown in Fig. 4.47 and 4.48, the curves do not exhibit the continuous increase in U_m and the slow restoration of the membrane potential related to this phenomenon.

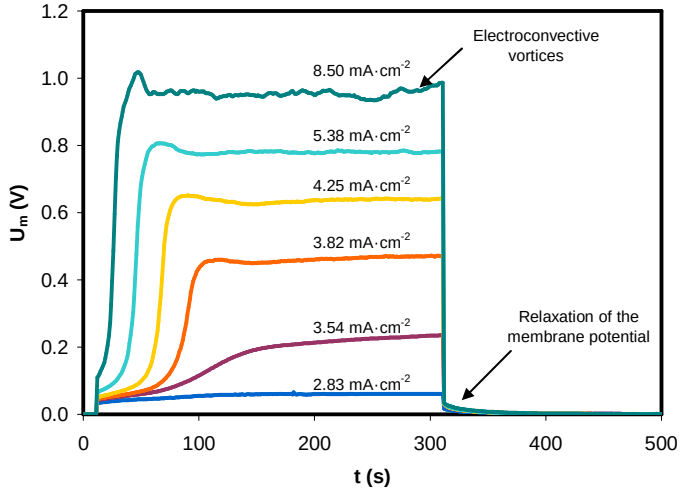

Fig. 4.47. Chronopotentiometric response obtained for mixtures of 10^{-3}M $NiSO_4$ and 10^{-2}M CrO_3.

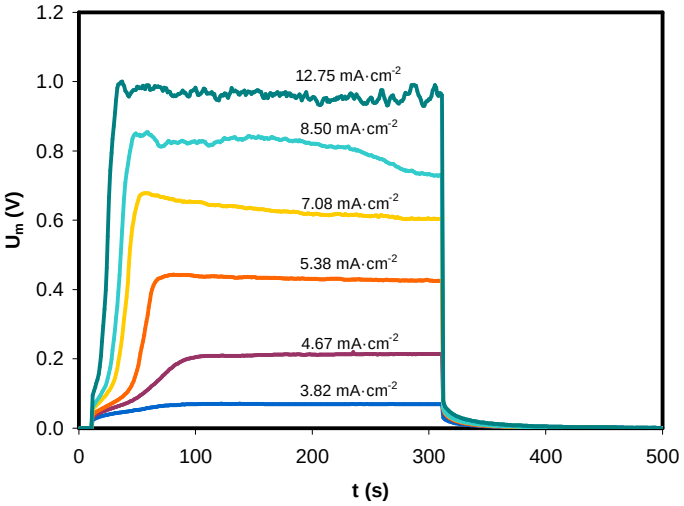

Fig. 4.48. Chronopotentiometric response obtained for mixtures of 10^{-2}M $NiSO_4$ and 10^{-2}M CrO_3.

In order to correlate the different chronopotentiometric responses with the ionic composition of the mixtures of CrO_3 and $NiSO_4$, the concentrations in equilibrium conditions of each ionic species were calculated. The reactions of formation of Ni(II) complex species are the same as those used in section 4.1 (Eqs. (4.18)-(4.24)). However,

the presence of CrO_3 implies the formation of additional ions, thus altering the equilibrium conditions. When CrO_3 is dissolved in water, it forms chromic acid (H_2CrO_4), as indicated by Eq. (4.52):

$$CrO_3\,(s) + H_2O \rightarrow H_2CrO_4\,(aq.) \tag{4.52}$$

The chromic acid undergoes hydrolysis reactions, which are given by Eqs. (4.53) and (4.54) [50]:

$$H_2CrO_4 \rightleftarrows HCrO_4^- + H^+ \qquad K_1 = 10^{-0.75} \tag{4.53}$$

$$HCrO_4^- \rightleftarrows CrO_4^{2-} + H^+ \qquad K_2 = 10^{-6.45} \tag{4.54}$$

Moreover, $HCrO_4^-$ ions have tendency to dimerize and form dichromate ions:

$$2HCrO_4^- \rightleftarrows Cr_2O_7^{2-} + H_2O \qquad k_{22} = 10^{2.2} \tag{4.55}$$

The equilibrium constants K_i and k_{22} are defined by Eq. (4.56) and (4.57), respectively:

$$K_i = \frac{\left[H^+\right]\cdot\left[H_{2-i}CrO_4^{-i}\right]}{\left[H_{3-i}CrO_4^{1-i}\right]} \tag{4.56}$$

$$k_{22} = \frac{\left[Cr_2O_7^{2-}\right]}{\left[HCrO_4^-\right]^2} \tag{4.57}$$

To calculate the concentrations of each species in equilibrium conditions, the system of equations formed by the previously defined equilibrium relations, the mass balance of Ni(II) species (Eq. (4.26) in section 4.1), the mass balance of sulfates (Eq. (4.27) in section 4.1), the mass balance of Cr(VI) species indicated by Eq. (4.58) and the proton balance indicated by Eq.(4.59) was solved:

$$[Cr(VI)]_0 = [H_2CrO_4] + [HCrO_4^-] + [CrO_4^{2-}] + 2[Cr_2O_7^{2-}] \tag{4.58}$$

$$[H^+] = [OH^-] + [Ni(OH)^+] + 2[Ni(OH)_2] + 3[Ni(OH)_3^-] + 4[Ni(OH)_4^{2-}] - [HSO_4^-] - 2[H_2SO_4] + 2[Cr_2O_7^{2-}] + 2[CrO_4^{2-}] + [HCrO_4^-] \tag{4.59}$$

The speciation of Cr(VI) species is presented in Fig. 4.49. We can see that the addition of CrO_3 implies an acidification of the electrolyte (pH_{eq}≈2-3). For an initial concentration of 10^{-3}M CrO_3 the predominant species are $HCrO_4^-$ ions, whereas an increase in the concentration of CrO_3 favors the formation of $Cr_2O_7^{2-}$ ions. However, all the ionic species of Cr(VI) are anionic and, therefore, do not compete with the Ni^{2+} ions for the transport through the cation-exchange membrane. Hence, the main effect of CrO_3 on the transport of ions through the membranes is caused by the increased concentration of H^+ ions in the electrolyte.

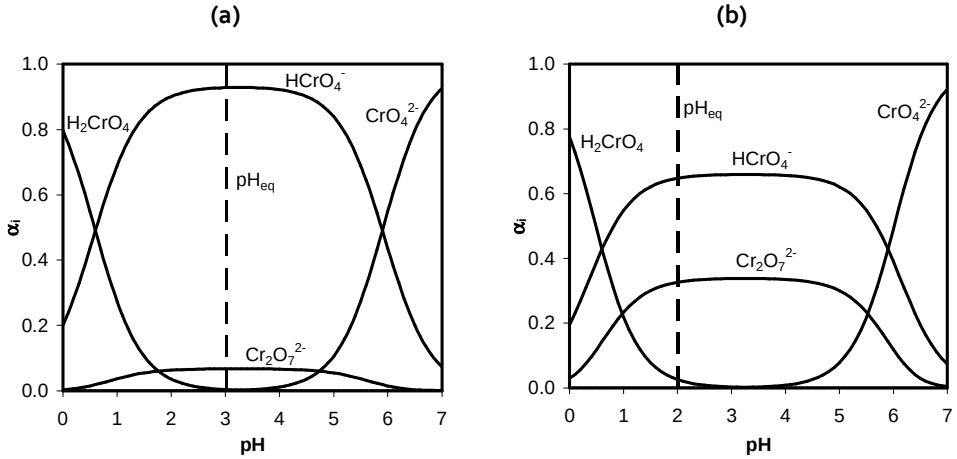

Fig. 4.49. Speciation diagram of CrO_3 solutions (a) with an initial concentration of 10^{-3}M, and (b) with an initial concentration of 10^{-2}M.

The speciation diagram of Ni(II) for 10^{-3}M $NiSO_4$ and varying concentrations of CrO_3 is shown in Fig. 4.50. As commented above, the speciation of Ni(II) is not significantly altered due to the addition of CrO_3. The main Ni(II) species are Ni^{2+} ions and the complex species $NiSO_4$. However, the pH_{eq} values decrease gradually as the concentration of CrO_3 is increased. Therefore, the transport of H^+ ions through the membrane may be the principal reason for the delayed depletion of Ni^{2+} ions observed for the mixture solutions. Since H^+ ions compete with Ni^{2+} ions for the transport through the membranes, the current densities at which the concentration polarization phenomena develop increase notoriously. In addition to this effect, the acidic pH values of chromic acid solutions also contribute to prevent the formation of metallic precipitates at the membrane surface, since the local pH near the membrane/electrolyte interface does not reach the values at which the formation of precipitates starts (pH≈7.9).

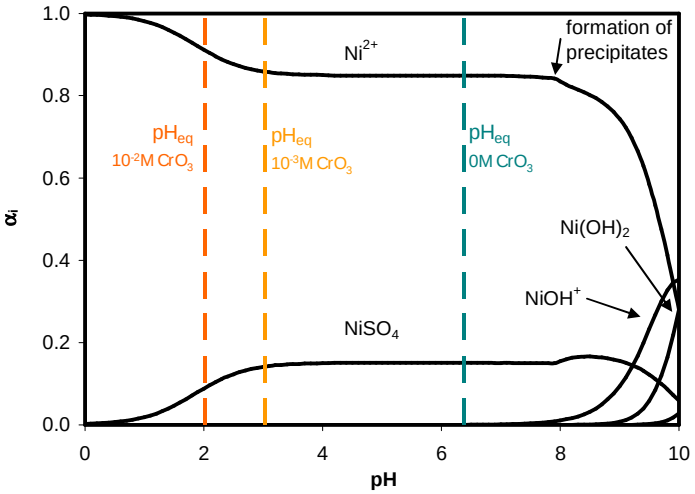

Fig. 4.50. Speciation diagram of 10^{-3}M $NiSO_4$ and initial equilibrium conditions for varying concentrations of CrO_3.

4.2.2.4 Current-voltage characteristics

The current-voltage curves obtained for the mixtures of 10^{-3}M CrO_3 and varying concentrations of $NiSO_4$ are presented in Fig. 4.51. First of all we can see that all the curves present the three typical regions of membrane behavior (quasi-ohmic, plateau and overlimiting region), except the one obtained for the mixture of 10^{-2}M $NiSO_4$ and 10^{-3}M CrO_3. In that case, apart from the plateau formed due to depletion of Ni^{2+} ions, the curves exhibit a second plateau at higher current densities. This curve is analogous to the curve obtained for 10^{-2}M $NiSO_4$ in the absence of CrO_3. The formation of precipitates at the anodic side of the membrane and the related increase in U_m observed in the chronopotentiometric curves is therefore the phenomenon responsible for the second plateau.

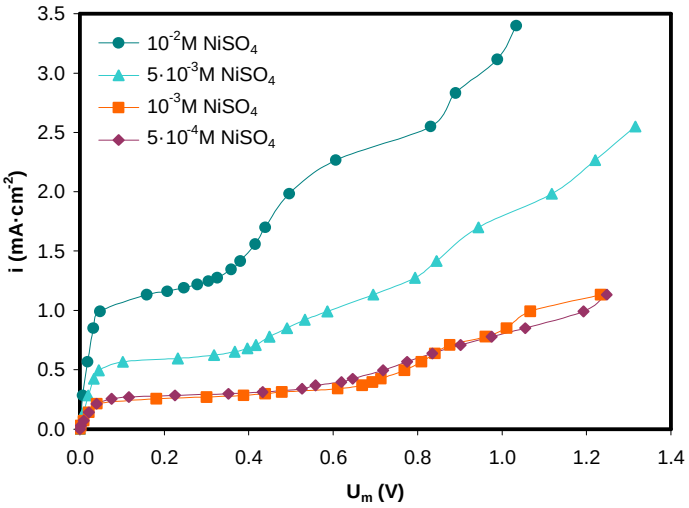

Fig. 4.51. Current-voltage curves obtained for mixtures of 10^{-3}M CrO_3 and $NiSO_4$ of different concentrations.

The curves obtained for 10^{-2}M CrO_3 solutions and varying concentrations of $NiSO_4$ are presented in Fig. 4.52. Since in this case the formation of precipitates was not observed, the four curves show the three characteristic regions. The effect of the acidic pH values resulting from the addition of CrO_3 can be clearly seen from Fig. 4.53, where the solubility plot of 10^{-2}M $NiSO_4$ solutions is presented together with the pH_{eq} values for each CrO_3 concentration. As the concentration of CrO_3 increases, the initial pH_{eq} values become lower and higher current densities can be applied before a precipitate layer is formed at the anodic side of the membrane.

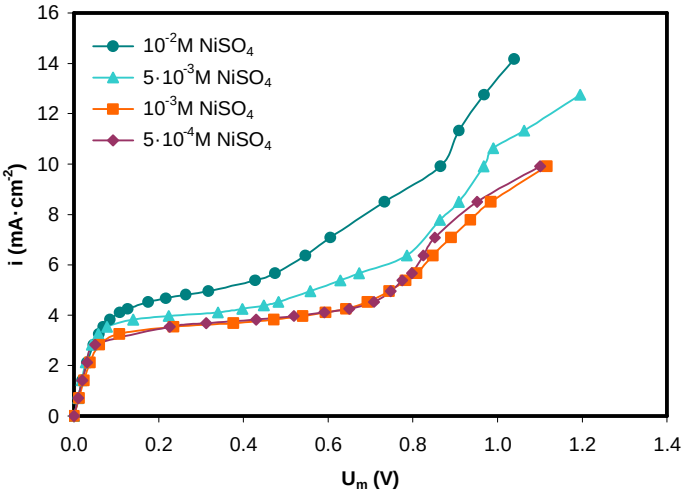

Fig. 4.52. Current-voltage curves obtained for mixtures of 10^{-2}M CrO_3 and $NiSO_4$ of different concentrations.

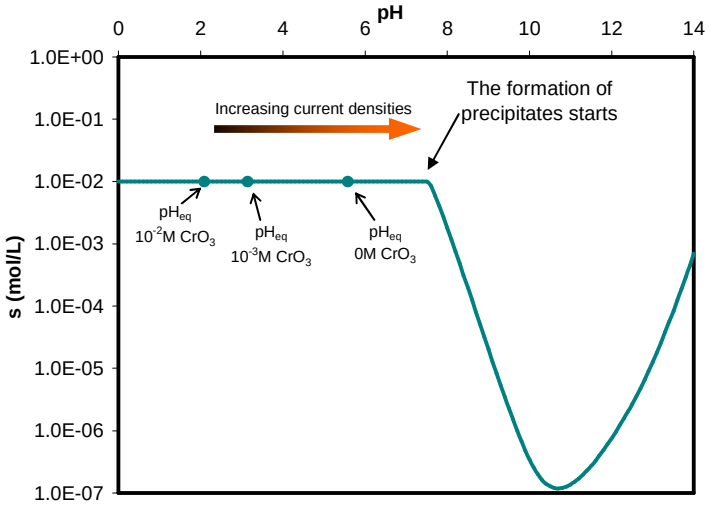

Fig. 4.53. Solubility plot for 10^{-2}M $NiSO_4$ solutions and initial pH_{eq} values for varying concentrations of CrO_3.

The current-voltage characteristics obtained from each curve are indicated in Table 4.6. Despite the fact that almost all the curves are similar in shape, we can observe some differences depending on the electrolyte composition. The first difference with respect to the single salt solutions is the evolution of the i_{lim} values with the electrolyte composition. Although in general the i_{lim} values increase with the $NiSO_4$ concentration, this increase is

different depending on the CrO_3 concentration. This means that the development of concentration polarization is affected by the relative predominance of ions in the multicomponent mixtures. As discussed above, the main cationic species in the mixtures are Ni^{2+} and H^+ ions. However, since only one transition time is detected in each chronopotentiometric curve, we assume that the ions being depleted from the membrane surface at the diluting compartment are Ni^{2+}. Specifically, the diffusion coefficient of H^+ ions ($9.311 \cdot 10^{-5}$ $cm^2 s^{-1}$) is several times higher than the coefficient of Ni^{2+} ions ($0.661 \cdot 10^{-5}$ $cm^2 s^{-1}$) [5]. Therefore, the supply of the more mobile H^+ ions from the bulk solution to the membrane is greater, whereas the supply of Ni^{2+} ions to the membrane is more likely to be restricted by diffusive limitations. Hence, the higher i_{lim} values obtained for the mixtures can be considered a consequence of the delay in the depletion of Ni^{2+} ions caused by the important proportion of current carried by H^+ ions through the membrane.

In fact, with 10^{-3}M CrO_3 solutions two levels of i_{lim} could be distinguished: the curves with a $NiSO_4$ concentration lower than or equal to the CrO_3 concentration have i_{lim} values around 0.25 $mA \cdot cm^{-2}$; and the i_{lim} increases more notoriously with the concentration of $NiSO_4$ for the curves in which the $NiSO_4$ concentration exceeds that of CrO_3. In concordance, in the case of 10^{-2}M CrO_3 solutions, the increase in the i_{lim} values with the Ni^{2+} concentration is slight (as observed in Fig. 4.52), since for all the mixtures the concentration of CrO_3 is at least the same as the $NiSO_4$ concentration.

Table 4.6. Current-voltage characteristics obtained for different mixtures of CrO_3 and $NiSO_4$ solutions.

0M CrO_3	**$5 \cdot 10^{-4}$M $NiSO_4$**	**10^{-3}M $NiSO_4$**	**$5 \cdot 10^{-3}$M $NiSO_4$**	**10^{-2}M $NiSO_4$**
R_1 ($\Omega \cdot cm^2$)	1084.07	735.25	196.81	129.20
i_{lim} ($mA \cdot cm^{-2}$)	0.035	0.064	0.495	0.850
10^{-3}M CrO_3	**$5 \cdot 10^{-4}$M $NiSO_4$**	**10^{-3}M $NiSO_4$**	**$5 \cdot 10^{-3}$M $NiSO_4$**	**10^{-2}M $NiSO_4$**
R_1 ($\Omega \cdot cm^2$)	188.24	193.11	78.17	38.58
i_{lim} ($mA \cdot cm^{-2}$)	0.255	0.255	0.567	1.130
10^{-2}M CrO_3	**$5 \cdot 10^{-4}$M $NiSO_4$**	**10^{-3}M $NiSO_4$**	**$5 \cdot 10^{-3}$M $NiSO_4$**	**10^{-2}M $NiSO_4$**
R_1 ($\Omega \cdot cm^2$)	18.99	17.82	14.55	14.45
i_{lim} ($mA \cdot cm^{-2}$)	3.26	3.26	3.82	4.24

With regard to the influence of the electrolyte composition on the ohmic resistance (R_1), a general decrease in the R_1 values is produced with the increase of both the $NiSO_4$ and CrO_3 concentration. Fig. 4.54 shows the relation between the ohmic resistance of each system and the equivalent cationic charge in equilibrium conditions (Q_+), which is defined in Eq. (4.60) as follows:

$$Q_+ = \sum_j |z_j| \cdot c_j \qquad (4.60)$$

where z_j and c_j are the electrochemical valence and the concentration in equilibrium conditions of each cation, respectively. From the Fig. 4.54 it is seen that the values of R_1 decrease abruptly with Q_+ when the equivalent cationic charge is lower than 0.01. Above this value, the decrease of R_1 with Q_+ is slighter, with values of R_1 close to 10 $\Omega \cdot cm^2$. Similar results were also obtained in previous studies [6,11,51]. Sang et al. explained this trend of the R_1 values with the electrolyte concentration on the basis that at higher electrolyte concentrations, the amount of cations in the medium rises and they can easily escape from the fixed charges of the membrane, thus contributing to a higher conductivity in the diffusion boundary layer [51]. The important contribution of the diffusion boundary layer to the ohmic resistances measured at low electrolyte concentrations was also suggested as the main reason for the increased R_1 values obtained in previous studies [8]. In the present case, the R_1 values measured in the absence of CrO_3 increase significantly also due to the absence of the more mobile H^+ ions in solution.

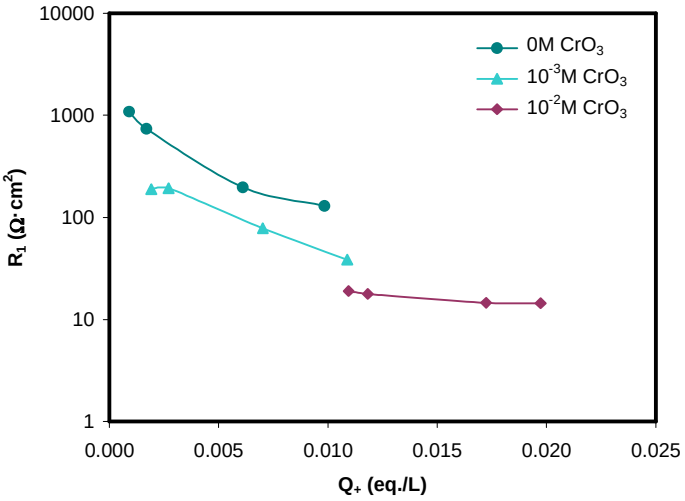

Fig. 4.54. Resistance of the membrane system as a function of the equivalent cationic charge at the initial equilibrium conditions.

4.2.2.5 Calculation of the transport number of Ni^{2+} ions through Nafion 117 membranes

As mentioned above, chronopotentiometry can also be used to quantify the selectivity of ion-exchange membranes for specific counterions. In the present section, the Ni^{2+} transport number through the membrane phase (T_{Ni}^{2+}) is calculated by means of chronopotentiometry. For this purpose, the transition times, τ, which are related to the vanishing of the Ni^{2+} concentration at the depleting side of the membrane, were calculated from each chronopotentiometric curve. The τ values were calculated as the instant at which the steepest increase in U_m is registered, and are plotted as a function of the parameter $(c_0/I)^2$ for the mixtures with 10^{-3}M and 10^{-2}M CrO_3 in Figs. 4.55 and 4.56, respectively. The obtained curves show a high linearity (R^2>0.99); thereby the experimental data is properly described by the Sand's equation for the range of concentrations of $NiSO_4$ and CrO_3 studied.

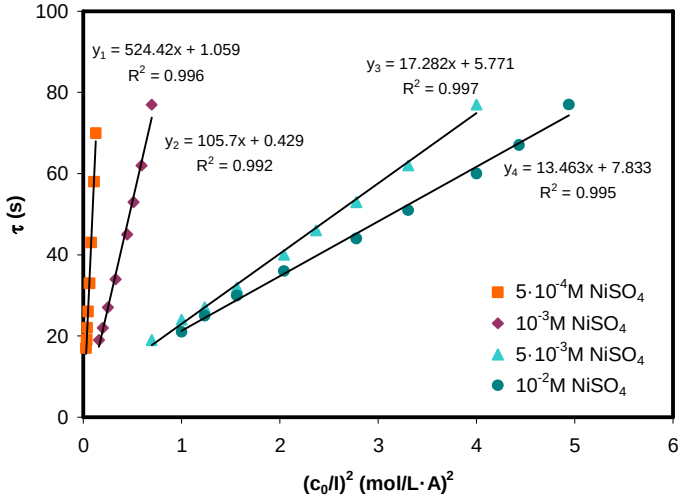

Fig. 4.55. Transition time, τ, as a function of $(c_0/l)^2$ for the mixtures of 10^{-3}M CrO_3 and varying concentrations of $NiSO_4$.

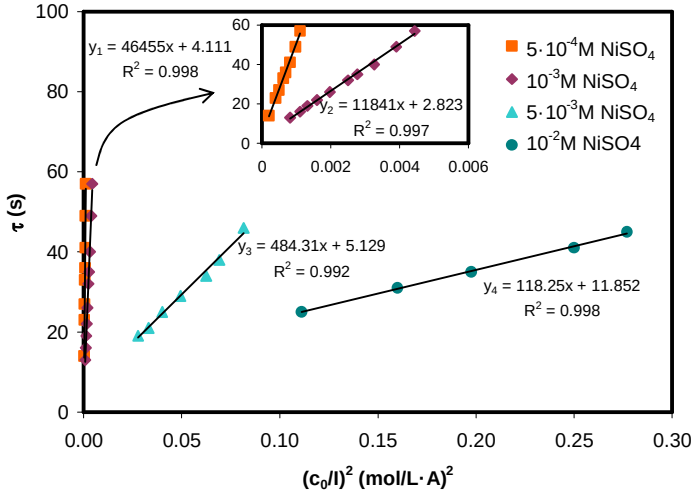

Fig. 4.56. Transition time, τ, as a function of $(c_0/l)^2$ for the mixtures of 10^{-2}M CrO_3 and varying concentrations of $NiSO_4$.

The T_{Ni}^{2+} values were calculated by substituting the slopes obtained from Figs. 4.55 and 4.56 in the Sand's equation (Eq. (3.8)). Fig. 4.57 shows the relationship between the T_{Ni}^{2+} values and the concentration of $NiSO_4$ for different concentrations of CrO_3. As already

commented in section 4.1, in the absence of CrO_3 the T_{Ni}^{2+} values are close to 0.9 for the entire range of concentrations of $NiSO_4$. Only a slight decrease of T_{Ni}^{2+} was observed at higher electrolyte concentrations as a consequence of the weaker Donnan exclusion of coions. On the contrary, for the mixtures of $NiSO_4$ and CrO_3 the evolution of T_{Ni}^{2+} with the concentration of $NiSO_4$ is the opposite. As expected, the H^+ ions provided by the chromic acid compete with the Ni^{2+} ions for the fixed ion-exchange sites of the membrane; which leads to decreased T_{Ni}^{2+} values with the addition of CrO_3. The decrease observed in the T_{Ni}^{2+} values is very important in the mixture solutions with low concentrations of $NiSO_4$. Then, for a constant CrO_3 concentration, the nickel transport number increases with the $NiSO_4$ concentration. These results are in agreement with the ion sorption equilibria presented in section 4.2.2.2, that showed a strong dependence between the ion partition in the membrane phase and the composition of the external equilibrating solution.

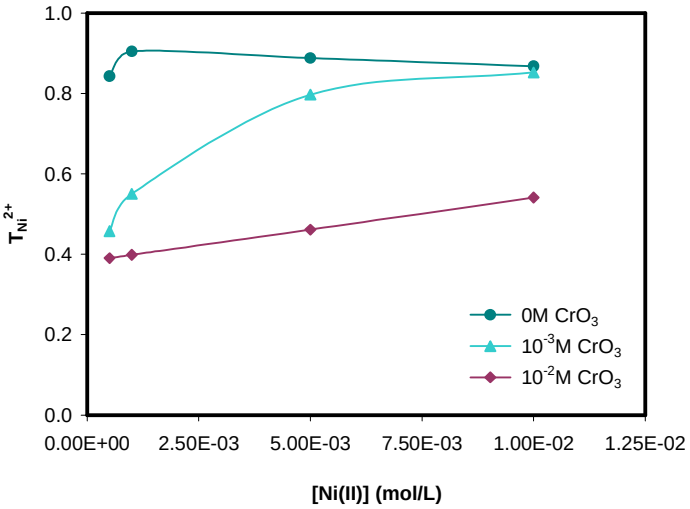

Fig. 4.57. Nickel transport number calculated for the different mixtures of CrO_3 and $NiSO_4$ tested.

In order to analyze in more detail the effect of the external electrolyte composition on the membrane selectivity, the results of T_{Ni}^{2+} are depicted in Fig. 4.58 as a function of the $[Ni^{2+}]/[H^+]$ ratio in equilibrium conditions for each CrO_3 concentration. From this figure, we can see that, when the concentration of H^+ ions in the external electrolyte solution is higher than the concentration of Ni^{2+} ions (ratios lower than 1), the T_{Ni}^{2+} values are close to 0.4. This implies that, even though the transport of H^+ ions is predominant, still an important fraction of the current passed through the membrane is associated with the

transport of Ni^{2+} ions. For $[Ni^{2+}]/[H^+]$ ratios exceeding the unity, the nickel transport number in the membrane increases considerably and, in the absence of CrO_3, the current passed through the membrane is mainly transported by Ni^{2+} ions (T_{Ni}^{2+} > 0.9). The important contribution of Ni^{2+} ions to the current transfer through the membrane when the $[Ni^{2+}]/[H^+]$ ratio is very low, and the increase in the T_{Ni}^{2+} values when the concentration of Ni^{2+} ions in the solution exceeds the concentration of H^+ ions may be caused by the strong attracting forces existing between the ion-exchange groups of the membrane and the divalent Ni^{2+} ions, as deduced from the ion sorption experiments. Moreover, it can be clearly seen that there is a strong correlation between the T_{Ni}^{2+} values and the $[Ni^{2+}]/[H^+]$ ratio, since the functions obtained for the mixtures of $NiSO_4$ and CrO_3 follow an increasing trend and overlap for similar $[Ni^{2+}]/[H^+]$ values.

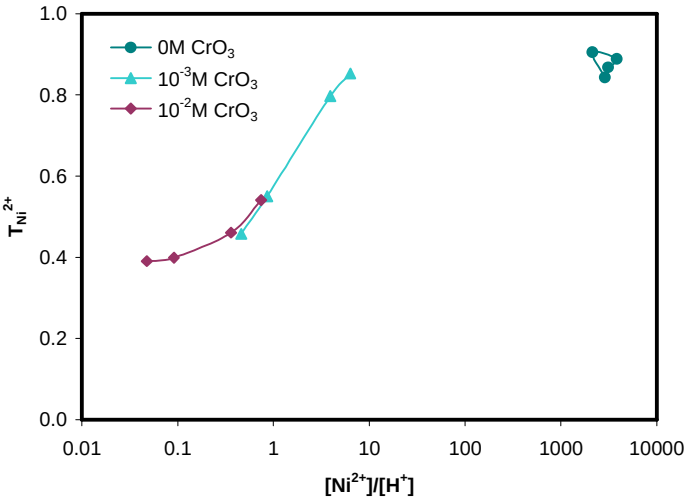

Fig. 4.58. Effect of the initial $[Ni^{2+}]/[H^+]$ ratio in solution on the value of T_{Ni}^{2+}.

4.2.3 Competitive ion transport between metal ions of different valence. Case of study: Na(I) vs. Fe(III)

4.2.3.1 Introduction and applicability

In the present section the competitive transport of metals of different valence through cation-exchange membranes is investigated. The coexistence of various metal ions is common in numerous effluents that can be treated by electrodialysis techniques. To conduct this investigation the treatment of acid mine drainage solutions is considered as a practical case of study, since these solutions are composed of a mixture of ions and their treatment by electrodialysis could imply important environmental advantages.

Acid mine drainage solutions are generated in coal extracting sites as a consequence of the natural oxidation of pyrite (FeS_2) [52]. These solutions are rich in sulfate ions and present significant concentrations of two types of metal:

(a) Transition metals, such as Fe(III), which have to be removed from the effluents in order to protect the natural ecosystems from their hazards and toxic effects.

(b) Alkali and alkaline earth metal ions, such as Na^+ or Ca^{2+}, which have to be removed to decrease the salinity of the effluents discharged to the environment.

The hazards associated with these effluents stem from their acidic pH values and the toxicological effects of heavy metals on aquatic ecosystems [53]. The most conventional technique used to diminish the environmental impacts of acid mine drainage consists on the addition of limes to neutralize the drainage and precipitate the metals [54]. As a consequence, a ferruginous solid waste is generated. Therefore, this treatment technology implies the addition of reagents and space requirements for the disposal of the solid wastes. In this sense, the application of electrodialysis could imply important advantages, because the addition of reagents and the generation of solid waste are minimized. As an example, Fig. 4.59 shows an electrodialysis cell with a configuration that could be used to treat acid mine drainage solutions. This cell consists of three compartments separated by an anion-exchange membrane and a cation-exchange membrane. The transport of cationic species through the cation-exchange membrane contributes to reduce the contaminant charge of the effluent. Moreover, the transport of SO_4^{2-} ions toward the anodic compartment together with the generation of H^+ ions at the anode would allow the recovery of sulfuric acid. The recovered sulfuric acid could be used

as a resource to offset the treatment costs, thus resulting in another advantage of using electrodialysis techniques.

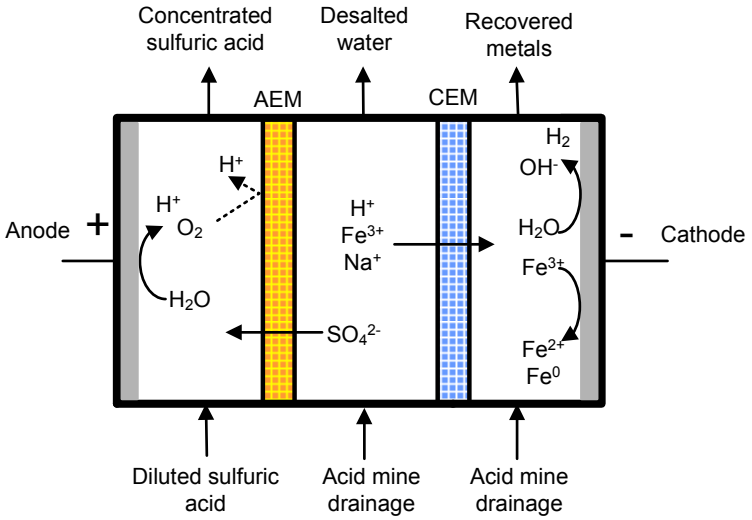

Fig. 4.59. Schematic representation of an electrodialysis cell used to treat acid mine drainage solutions. (AEM: anion-exchange membrane, CEM: cation-exchange membrane).

The composition of acid mine drainage solutions of a coal extracting site placed in Criciúma (Brazil) was taken as a basis for the present investigation [31]. The composition of the acid mine drainage solution is summarized in Table 4.7.

Table 4.7. Composition of the acid mine drainage solutions taken as a reference. The concentrations of each species is given in mol·L^{-1}.

pH	[Na^+]	[K^+]	[Mg^{2+}]	[Ca^{2+}]	[Fe^{3+}]	[Mn^{2+}]	[Cl^-]	[SO_4^{2-}]
2.48	0.017	0.004	0.006	0.006	0.037	0.001	0.008	0.082

The highest concentration in multivalent metals is that of trivalent iron, and the presence of SO_4^{2-} ions is predominating over other anions. Moreover, in order to evaluate the competitive transport of different cations through the membranes, the presence of Na^+ ions was also considered. The concentration of the other ions present in the acid mine drainage is significantly lower and was neglected for the sake of simplicity. Accordingly, we prepared synthetic mixtures of 0.02M $Fe_2(SO_4)_3$ and 0.01M Na_2SO_4, which correspond to similar concentrations to those determined in the acid mine drainage solutions. The present study was also extended to equimolar solutions of Na(I) and Fe(III), and the

results obtained with the mixtures were compared to the behavior of the membrane immersed in single salt solutions of Na(I) and Fe(III).

4.2.3.2 Ion sorption experiments

Ion sorption experiments were conducted in order to determine the affinity of the fixed ion-exchange sites of the membrane for metal cations of different valence. Fig. 4.6o shows the concentration of ions equilibrated in the membrane phase, c_m, as a function of the external electrolyte composition. The results reveal a marked preference of the membrane fixed charges for Fe(III) over Na(I). As the concentration of Na^+ ions in the solution increases, the concentration of Fe(III) in the membrane phase decreases slightly. On the contrary, the increase of Na^+ ions equilibrated with the membrane fixed charges increases more notoriously. This effect could be associated with the fact that each Fe^{3+} could be bound to more than one fixed charge, thus being replaced by several Na^+ ions when the concentration of Na_2SO_4 in the equilibrating solution increases.

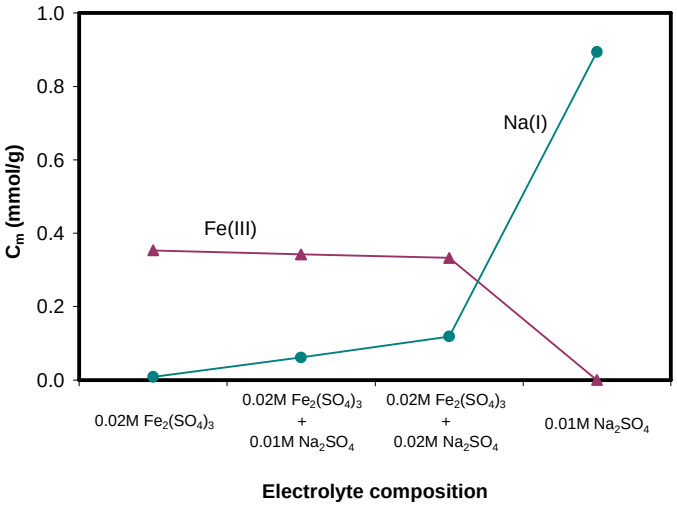

Fig. 4.6o. Concentration of ions equilibrated in the membrane phase as a function of the composition of the equilibrating solution.

The relationship between the [Na(I)]/[Fe(III)] ratio in the membrane phase with the [Na(I)]/[Fe(III)] ratio in the equilibrating solution is represented in Fig. 4.61. The increase in the proportion of Na^+ ions in the membrane phase is linear with the increase in the concentration of Na_2SO_4 in the equilibrating solution. However, the predominance of

Fe(III) is still very significant even when the membranes are equilibrated in equimolar solutions of Na(I) and Fe(III). These results corroborate that the fixed charges of the membrane exert stronger attractive forces for multivalent ions than for monovalent ones. Similar conclusions were obtained from previous studies where it was found that the membranes absorb preferentially multicharged ions when they are immersed in multicomponent solutions [55,56].

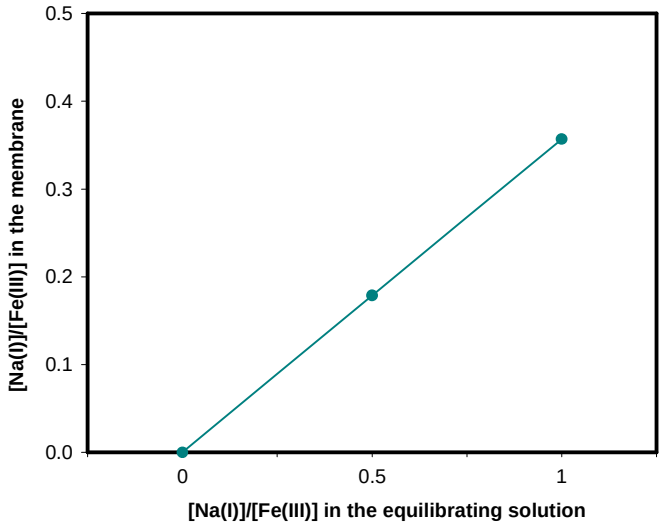

Fig. 4.61. [Na(I)]/[Fe(III)] ratio in the membrane phase as a function of the [Na(I)]/[Fe(III)] ratio in the equilibrating solution.

Another remarkable result is the different correlation between the c_m values obtained for each solution and the ion exchange capacity of the membranes. The values of c_m obtained with Na_2SO_4 (0.89 meq/g) almost matches the value of ion exchange capacity provided by the manufacturers (0.90 meq/g), which is in congruence with the results obtained previously in section 4.1.2.2. On the contrary, if we consider that Fe(III) is in the form of Fe^{3+} inside the membrane phase (with a valence of z=3), the equivalents bound to the membrane fixed charges would exceed the theoretical ion exchange capacity of the membrane. Consequently, these results indicate that other Fe(III) ions apart from Fe^{3+} are present inside the membrane. At the acidic pH values prevailing inside the membrane phase, $FeSO_4^+$ ions are together with Fe^{3+} ions the unique Fe(III) species that could be equilibrating the fixed charges of the membrane. In consequence, to calculate the specific concentration of each ion, the system of equations formed by the mass balances of Fe(III)

species inside the membrane and the balance of the equivalents equilibrating the membrane fixed sites (Eqs. (4.61) and (4.62) was solved:

$$c_{Fe(III),m} = c_{Fe^{3+},m} + c_{FeSO_4^+,m} \tag{4.61}$$

$$IEC = 0.89\,meq/g = c_{Na^+,m} \cdot z_{Na^+} + c_{FeSO_4^+,m} \cdot z_{FeSO_4^+} + c_{Fe^{3+},m} \cdot z_{Fe^{3+}} \tag{4.62}$$

Where $c_{Fe(III),m}$, $c_{j,m}$ and $z_{j,m}$ refer to the concentration of total iron in the membrane phase, and the concentration in the membrane and the valence of the ionic specie j, respectively. The results obtained are plotted in Fig. 4.62, where the percentage of membrane fixed charges bound to each ion (Fe^{3+}, $FeSO_4^+$ or Na^+) is represented as a function of the composition of the equilibrating solution. From this graphic we can see that the addition of Na_2SO_4 to the solutions containing $Fe_2(SO_4)_3$ reduces the amount of fixed ion exchange sites occupied by Fe(III) species. However, the increasing concentrations of Na_2SO_4 in the equilibrating solution also alters the speciation of Fe(III) inside the membrane phase, since it decreases the proportion of Fe^{3+} ions, but increases the amount of fixed charges bound to $FeSO_4^+$ ions. This effect could be due to the displacement of the equilibrium in the equilibrating electrolyte, because the increase in the concentration of Na_2SO_4 also implies an increase in the amount of SO_4^{2-} ions in the solution, hence displacing the equilibrium toward the formation of more $FeSO_4^+$ ions. In addition, as the concentration of SO_4^{2-} ions in solution increases, the Donnan coion exclusion is less effective, and more $FeSO_4^+$ ions occupy the membrane fixed charges.

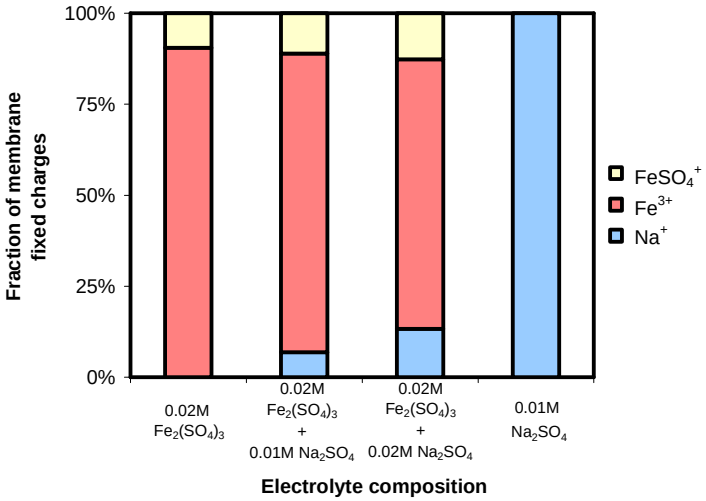

Fig. 4.62. Fraction of membrane fixed charges equilibrated with each ion (Fe^{3+}, $FeSO_4^+$ or Na^+) present in the different electrolyte compositions tested.

4.2.3.3 Chronopotentiometric response

The chronopotentiometric response of the membranes immersed in mixtures of Na_2SO_4 and $Fe_2(SO_4)_3$ was investigated and compared to the behavior of the membranes immersed in single salt solutions of Na_2SO_4 and $Fe_2(SO_4)_3$. The chronopotentiometric and current-voltage characteristics obtained with 0.01M Na_2SO_4 (presented in section 4.1) were the typical ones described in the literature for monovalent counterions. However, the membranes immersed in $Fe_2(SO_4)_3$ exhibited different behavior depending on the initial salt concentration. The concentration of Fe(III) of the acid mine drainage solutions is higher than those studied in the previous section (4.1). Consequently, additional chronopotentiometric measurements were conducted with 0.02M $Fe_2(SO_4)_3$ solutions.

The response obtained for 0.02M $Fe_2(SO_4)_3$ in the underlimiting range of currents is presented in Fig. 4.63. Within the underlimiting range of currents the shape of the chronopotentiograms also changes depending on the magnitude of applied current. At low current densities (i.e. 5.67 $mA{\cdot}cm^{-2}$), the evolution of U_m with time is almost plane. However, for higher current densities (e.g. 14.16 $mA{\cdot}cm^{-2}$) the chronopotentiometric response shows an atypical behavior. From the first instants of the current pulse U_m increases during a few seconds and then, after reaching a maximum value, decreases again with time. The maximum and the subsequent decrease in U_m become more

pronounced as the current is increased, which implies a reduction in the electrical resistance of the membrane system for high underlimiting currents. This membrane behavior is markedly different from that observed with monovalent cations, where the continuous depletion of counterions near the membranes leads to a gradual increase of the electrical resistance with current density. Finally, when the i_{lim} value is approached (i.e. 17.00 mA·cm^{-2}), the depletion of counterions at the anodic side of the membrane is intensified and a sharp increase in U_m is registered.

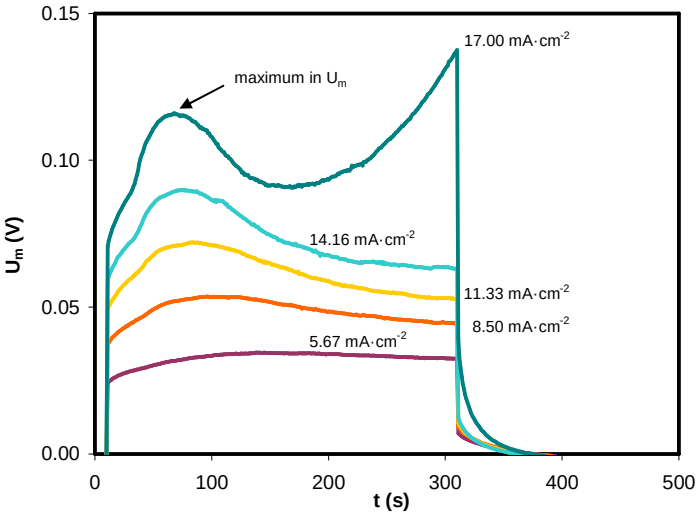

Fig. 4.63. Chronopotentiometric response obtained in the underlimiting range of currents for 0.02M $Fe_2(SO_4)_3$.

The response obtained in the overlimiting range of currents is shown in Fig. 4.64. For current densities slightly exceeding the i_{lim} (e.g. 17.14 and 17.28 mA·cm^{-2}), U_m increases at the transition time due to the vanishing of Fe(III) species near the membrane depleting surface. Subsequently, U_m levels off and reaches a steady value which remains approximately constant until the end of the current pulse. However, at the current density of 17.56 mA·cm^{-2} an important increase in U_m was registered at times larger than the transition time. In analogy with the results obtained in section 4.1 for 0.01M $Fe_2(SO_4)_3$ solutions, this increase is continued and reaches the magnitude of various volts, hence being also related to the formation of a precipitate layer at the anodic side of the membrane. The continued growth of the precipitate layer taking place while the current is applied is the main contribution to the increased electrical resistance of the membrane.

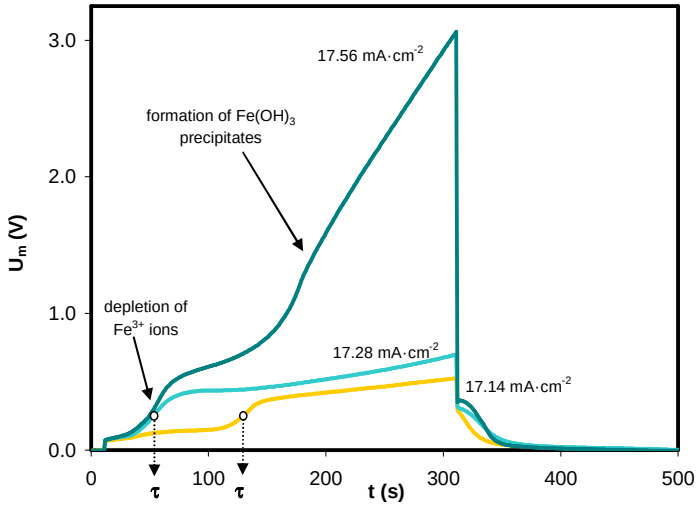

Fig. 4.64. Chronopotentiometric response obtained in the overlimiting range of currents for 0.02M $Fe_2(SO_4)_3$ solutions.

As explained above, the dynamics of the ionic transport taking place within the underlimiting regime of currents with 0.02M $Fe_2(SO_4)_3$ solutions is markedly different from the results obtained for more diluted solutions. A similar chronopotentiometric response showing the maximum and subsequent decrease in U_m was also observed by Taky et al. when they studied the transport of Cr(III) through cation-exchange membranes [57]. In that case, a change in the species being transported through the membranes was suggested as the reason for this atypical response. Therefore, in order to clarify the different behavior observed for high and low electrolyte concentrations, the speciation diagrams of 0.001M and 0.02M $Fe_2(SO_4)_3$ solutions are compared in Figs. 4.65 and 4.66, respectively. For 0.001M $Fe_2(SO_4)_3$ three different cationic species coexist at the initial equilibrium conditions: $FeSO_4^+$, Fe^{3+} and $FeOH^{2+}$. In consequence, when the cation-exchange membrane immersed in diluted solutions of $Fe_2(SO_4)_3$ is submitted to an electric field, the more mobile Fe^{3+} ions, which have larger diffusion coefficients than $FeSO_4^+$ ions (see Table 4.8), are more likely to carry the ionic current through the membranes within the range of underlimiting currents. On the contrary, in the case of 0.02M $Fe_2(SO_4)_3$ solutions (Fig. 4.66) $FeSO_4^+$ ions are the main cationic species at the initial equilibrium conditions and the concentration of Fe^{3+} ions is practically negligible. Therefore, at low polarization levels, the contribution of Fe^{3+} ions to the ionic transfer through the membranes may be insignificant.

However, when the concentration polarization is intensified, the equilibrium conditions in the diffusion boundary layer can be altered, thus changing the ions being supplied to the membrane surface. In the present case, the maximum in U_m appearing immediately after starting the current pulses of Fig. 4.63 may be induced by the overlapping of two different effects. First, as the $FeSO_4^+$ ions are transported through the membrane, they would replace the Fe^{3+} ions that are initially balancing the fixed charges of the membrane (see Fig. 4.62). On the other hand, as the diffusion boundary layer becomes more diluted, the $FeSO_4^+$ ions present in the membrane region tend to dissociate and form Fe^{3+} and SO_4^{2-} ions, as indicated in Eq. (4.63):

$$FeSO_4^+ \rightleftarrows Fe^{3+} + SO_4^{2-} \tag{4.63}$$

The displacement of the above reaction toward the dissociation of $FeSO_4^+$ would thus imply a change from $FeSO_4^+$ to Fe^{3+} ions as the main charge carriers through the membrane.

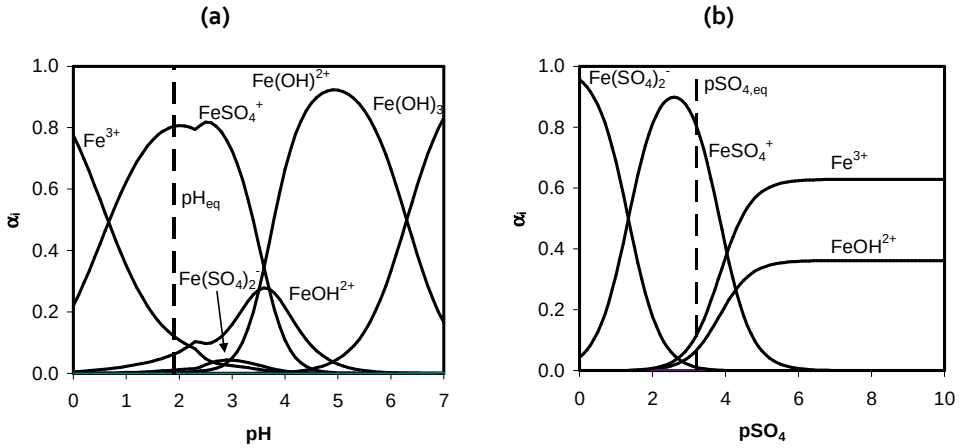

Fig. 4.65. Speciation diagram of Fe(III) species present in 0.001M $Fe_2(SO_4)_3$ solutions. (a) Speciation diagram as a function of pH and (b) as a function of pSO_4.

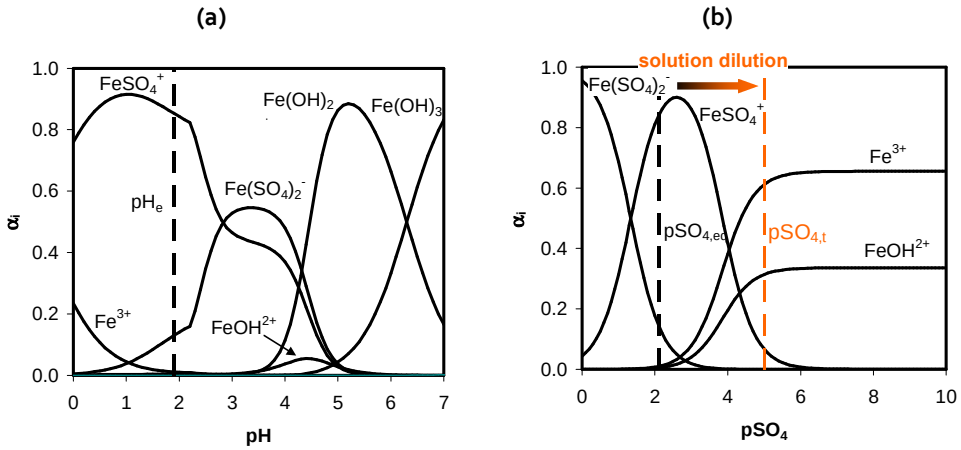

Fig. 4.66. Speciation diagram of Fe(III) species present in 0.02M $Fe_2(SO_4)_3$ solutions. (a) Speciation diagram as a function of pH and (b) as a function of pSO_4.

Therefore, under sufficiently intense polarization conditions, the displacement from the initial equilibrium state in the depleting solution layer ($pSO_{4,eq}$) toward higher pSO_4 values (for example $pSO_{4,t}$ in Fig. 4.66(b)) implies the enrichment in multicharged ions of the membrane region. Both Fe^{3+} and SO_4^{2-} ions are much more mobile than the monovalent $FeSO_4^+$ complex ion, as can be deduced from the diffusion coefficients presented in Table 4.8. Furthermore, the higher mobility and charge of Fe^{3+} and SO_4^{2-} ions implies an even more pronounced increase in the ionic conductivities, which may confirm the role of these ions on the gradual decrease observed in U_m for increasing current densities. In analogy to our results, a similar effect was obtained in preceding studies where the electrical conductivity of ion-exchange membranes increased as a result of an enrichment of the membrane phase in multicharged ions [20,21]. Hence, the diffusion boundary layers of membrane systems in contact with weak electrolytes can be regarded as a dynamic reaction layer where the displacement of the equilibrium conditions can alter the ionic species being transported through the membranes. Fig. 4.67 shows a schematic representation of the phenomenon of dissociation of $FeSO_4^+$ ions near the membrane/solution interface as a consequence of the application of a sufficiently strong electric field. The Fe^{3+} ions resulting from the dissociation of $FeSO_4^+$ ions would pass through the membrane, whereas the SO_4^{2-} ions return back to the diffusion boundary layer, thus contributing to increase its conductivity.

Table 4.8. Diffusion coefficient (D_j) and ionic conductivity (λ_i) at infinite dilution of various ionic species present in the solutions (Taken from [5,58]).

	10^{-9} D_j ($m^2 \cdot s^{-1}$)	λ_i ($mS \cdot m^2 \cdot mol^{-1}$)
Na^+	1.334	5.01
Fe^{3+}	0.604	20.40
SO_4^{2-}	1.065	16.00
$FeSO_4^+$	0.201	0.76

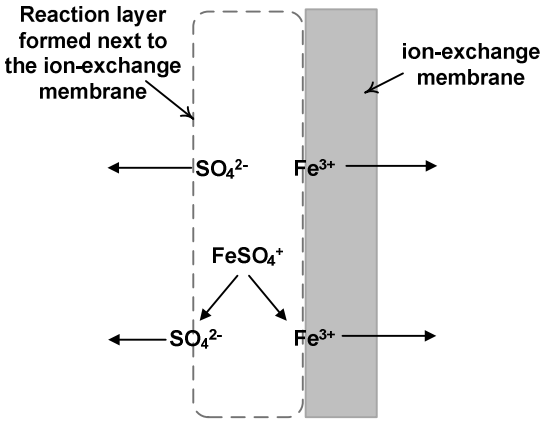

Fig. 4.67. Schematic representation of the reaction layer formed next to the membranes once the diffusion layer becomes diluted.

The results obtained for the mixtures of 0.02M $Fe_2(SO_4)_3$ and 0.01M Na_2SO_4 at low and high current densities are presented in Figs. 4.68 and 4.69, respectively. The chronopotentiometric curves of Fig. 4.68 already exhibit an inflexion point and an increase in U_m at very low current densities (i.e. 4.11 and 4.96 $mA \cdot cm^{-2}$), which was not observed in the case of 0.02M $Fe_2(SO_4)_3$ solutions. Therefore, this first inflexion point seems to be related to the presence of Na^+ ions in the electrolyte and their transport through the membranes. For higher current densities ($i \geq 5$ $mA \cdot cm^{-2}$) a slight decrease in U_m after reaching a maximum is also observed in the curves. In this case the dissociation of $FeSO_4^+$ ions occurring when the depleting diffusion boundary layer becomes more diluted seems to be also the reason for the decrease of U_m with time.

At higher current densities ($i \geq 14$ $mA \cdot cm^{-2}$, Fig. 4.69), the evolution of U_m after the first inflexion point changes and, instead of decreasing, increases gradually with time.

Moreover, the restoration of U_m to zero during the relaxation of the membrane system is also slower, as can be seen in the magnified view included in Fig. 4.69. Therefore, the increase in U_m occurring at higher current densities could be associated with the formation of precipitates, which were observed at the end of the experiment. However, the presence of Na^+ ions in the mixture solutions seems to attenuate the magnitude of the increase in U_m. The results obtained with equimolar mixtures of sodium and iron (0.02M $Fe_2(SO_4)_3$ and 0.02M Na_2SO_4) were analogous to those presented in Figs. 4.68 and 4.69. Accordingly, the chronopotentiograms are not presented and the effect of increasing the concentration of Na^+ ions on the membrane behavior will be analyzed in detail from the differences observed in the current-voltage curves.

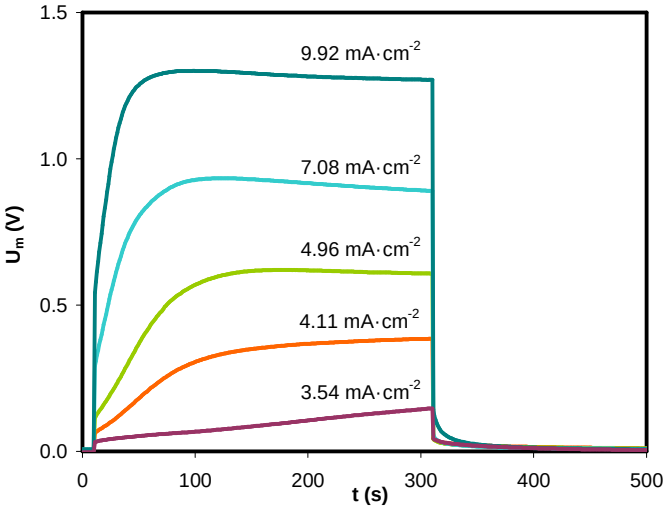

Fig. 4.68. Chronopotentiometric response obtained in the underlimiting range of currents for mixtures of 0.02M $Fe_2(SO_4)_3$ and 0.01M Na_2SO_4.

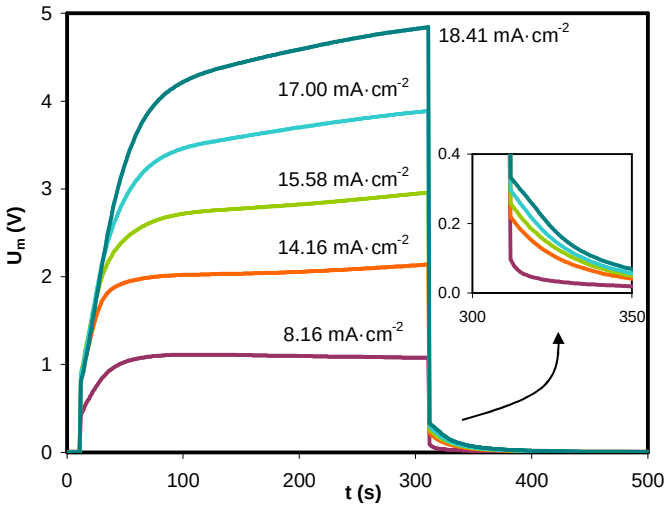

Fig. 4.69. Chronopotentiometric response obtained in the overlimiting range of currents for mixtures of 0.02M $Fe_2(SO_4)_3$ and 0.01M Na_2SO_4.

4.2.3.4 Current-voltage characteristics

The current-voltage curves obtained for 0.02M $Fe_2(SO_4)_3$ solutions and varying concentrations of Na_2SO_4 are presented in Fig. 4.70. In regard to the curves obtained for single salt solutions of 0.02M $Fe_2(SO_4)_3$, some singular characteristics make them different from those obtained for more diluted solutions. First, the quasi-ohmic region exhibits a change of slope, which coincides with the current densities for which U_m decreased in the chronopotentiograms (see the magnified curve included in Fig. 4.70). Accordingly, two different electrical resistances have been calculated: R_1 for the low current densities and R_2 for the high current densities. As stated previously, the shift from the initial equilibrium state which gives rise to the dissociation of $FeSO_4^+$ ions into the more conductive Fe^{3+} and SO_4^{2-} ions causes a reduction of the electrical resistance of the membrane for increasing current densities. Then, the quasi-ohmic region is followed by an extended plateau, which is developed when the deposits of $Fe(OH)_3$ are formed at the membrane surface, thus implying the blockage of the ion transport and increasing the membrane resistance.

The curves obtained for the mixtures of $Fe_2(SO_4)_3$ and Na_2SO_4 exhibit four regions of different membrane behavior. The first one corresponds to the range of low current

densities in which a quasi-ohmic behavior prevails. Then, the quasi-ohmic region extends until the i_{lim} is reached and is followed by a plateau region, which coincides with the current densities at which the first inflexion points in U_m are observed in the chronopotentiograms (i = 4.11 mA·cm^{-2} in Fig. 4.68). This first i_{lim} (i_{lim1}) may be associated with the depletion of Na^+ ions at the membrane surface, since the plateau is not observed with single salt solutions of 0.02M $Fe_2(SO_4)_3$. The correspondence between the first plateau and the depletion of Na^+ ions at the depleting membrane surface is also corroborated by the increase in the i_{lim1} values that is almost proportional to the increase in the concentration of Na^+ ions in the electrolyte. For current densities higher than i_{lim1}, a third region where the current density increases again with U_m follows the first plateau. As occurred with single salt solutions of Fe(III), the conversion of $FeSO_4^+$ ions (coming from the bulk solution and reaching the reaction layer next to the membrane) into the more mobile Fe^{3+} and SO_4^{2-} ions also induces an increased conductance of the membranes. Finally, the second i_{lim} (i_{lim2}), which leads to the second plateau, is determined by the formation of precipitates at the anodic side of the membrane.

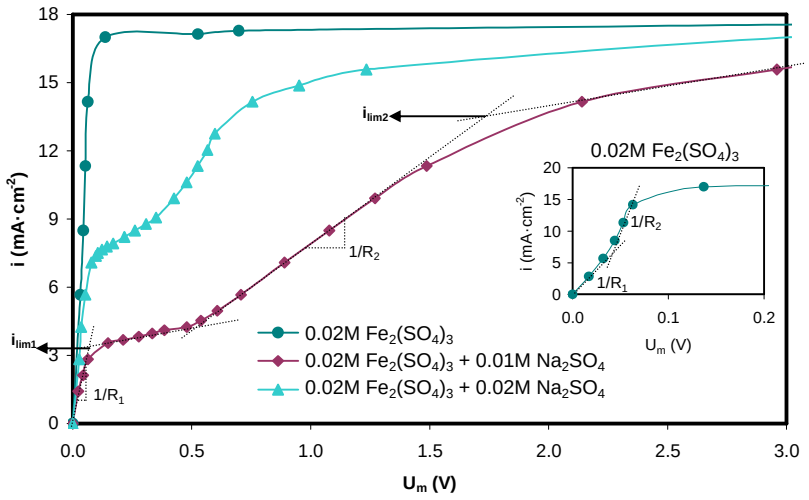

4.70. Current-voltage curves obtained for 0.02M $Fe_2(SO_4)_3$ solutions with varying concentrations of Na_2SO_4.

The current-voltage parameters calculated from the curves are presented in Table 4.9, where the parameters corresponding to 10^{-2}M Na_2SO_4 solutions obtained in section 4.1 are also included. The values of electrical resistance at low and high current densities (where R_2 refers to the region following the first plateau for the mixture solutions) also

reveal the different behavior of the membranes when they are immersed in single salt and mixture solutions. Whereas the values of R_2 obtained for 0.02M $Fe_2(SO_4)_3$ are lower than R_1, this trend is the opposite with the mixture solutions. As already explained, with the concentrated solutions of $Fe_2(SO_4)_3$, the dissociation of $FeSO_4^+$ ions into the more conductive Fe^{3+} and SO_4^{2-} ions is the reason for the decrease in the electrical resistance at high current densities. However, with the mixture solutions the contribution of Na^+ ions to the ion transport at low current densities and their depletion in the diffusion boundary layer for currents higher than i_{lim1} lead to values of R_1 lower than R_2.

Table 4.9. Current-voltage characteristics obtained from the experiments conducted with different solutions.

	$2{\cdot}10^{-2}$M $Fe_2(SO_4)_3$	**$2{\cdot}10^{-2}$M $Fe_2(SO_4)_3$ + 10^{-2}M Na_2SO_4**	**$2{\cdot}10^{-2}$M $Fe_2(SO_4)_3$ + $2{\cdot}10^{-2}$M Na_2SO_4**	**10^{-2}M Na_2SO_4**
R_1 ($\Omega \cdot cm^2$)	5.65	22.60	9.16	44.50
R_2 ($\Omega \cdot cm^2$)	3.61	136.42	61.47	-
i_{lim1} ($mA{\cdot}cm^{-2}$)	17.00	3.40	7.44	1.09
i_{lim2} ($mA{\cdot}cm^{-2}$)	-	13.61	15.15	-

Moreover, the differences in the electrical resistances obtained for single salt solutions of $Fe_2(SO_4)_3$ and mixtures of Na_2SO_4 and $Fe_2(SO_4)_3$ are also remarkable. For a constant concentration of 0.02M $Fe_2(SO_4)_3$ the addition of Na_2SO_4 instead of reducing the electrical resistance of the membrane system, leads to an increase in the R_1 values for the mixture of 0.02M $Fe_2(SO_4)_3$ and 0.01M Na_2SO_4. Then, for the equimolar mixture (0.02M $Fe_2(SO_4)_3$ + 0.02M Na_2SO_4) the values of R_1 decrease again. This trend can be clearly seen in Fig. 4.71. In order to explain this behavior, we have to consider all the contributions to the voltage drop measured between the reference electrodes. The U_m value includes the voltage drop through the membrane phase and the voltage drop of the diffusion boundary layers. The former is determined by the ion exchange capacity of the membranes and the ions balancing the membrane fixed charges; whereas the latter decreases with the electrolyte concentration (higher concentrations imply higher conductivities and lower voltage drops). With regard to the first contribution, a decrease in the electrical resistance of ion-exchange membranes with the dilution of the external solution was also observed in previous studies conducted with weak electrolytes [20,21]. This behavior was attributed to an enrichment of the membrane phase in multivalent cations as the electrolyte became diluted, which has been reported to originate an

increased membrane electrical conductivity [20]. In the present study, an increase in the concentration of Na_2SO_4 involves the addition of more SO_4^{2-} ions, which displace the equilibrium toward the formation of $FeSO_4^+$ and $Fe(SO_4)_2^-$ ions and decrease the concentration of free Fe^{3+} ions (as can be seen from the concentration of species obtained for 0.02M $Fe_2(SO_4)_3$ solutions and varying concentrations of Na_2SO_4 shown in Table 4.10). Moreover, as already seen from the ion uptake equilibrium (Fig. 4.62), the number of membrane fixed charges bound to Fe^{3+} ions decreases as the concentration of Na_2SO_4 increases. Therefore, this seems to be the reason for the high values of R_1 observed for the mixtures of 0.02M $Fe_2(SO_4)_3$ and 0.01M Na_2SO_4. The decrease in R_1 obtained for a further increase in the concentration of Na_2SO_4 can be explained by the more important contribution of the conductivity of the diffusion boundary layers, which in this case may compensate the decrease in the amount of membrane fixed charges bound to multivalent ions.

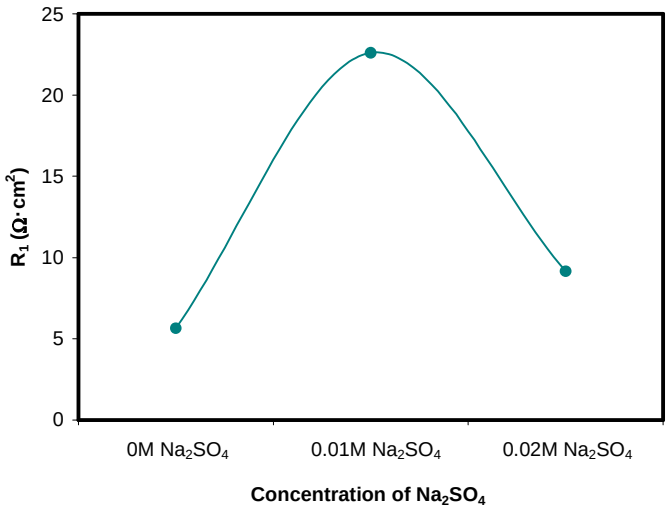

Fig. 4.71. Evolution of the electrical resistance of the membrane systems composed of the Nafion 117 membrane and 0.02M $Fe_2(SO_4)_3$ solutions with varying concentrations of Na_2SO_4.

Table 4.10. Concentration of ionic species present in single salt solutions of Na_2SO_4, $Fe_2(SO_4)_3$ and multicomponent mixtures of both salts. The concentrations are given in $mol \cdot L^{-1}$.

	$[Fe^{3+}]$	$[FeSO_4^+]$	$[Fe(SO_4)_2^-]$	$[FeOH^{2+}]$	$[Na^+]$	$[NaSO_4^-]$	$[SO_4^{2-}]$	$[HSO_4^{2-}]$
0.01M Na_2SO_4	-	-	-	-	$1.91 \cdot 10^{-2}$	$8.76 \cdot 10^{-4}$	$9.14 \cdot 10^{-3}$	$1.82 \cdot 10^{-11}$
0.02M $Fe_2(SO_4)_3$	$4.84 \cdot 10^{-4}$	$3.41 \cdot 10^{-2}$	$5.19 \cdot 10^{-3}$	$2.30 \cdot 10^{-4}$	-	-	$6.95 \cdot 10^{-3}$	$8.55 \cdot 10^{-3}$
0.02M $Fe_2(SO_4)_3$ + 0.01M Na_2SO_4	$2.95 \cdot 10^{-4}$	$3.24 \cdot 10^{-2}$	$7.11 \cdot 10^{-3}$	$1.51 \cdot 10^{-4}$	$1.90 \cdot 10^{-2}$	$9.56 \cdot 10^{-4}$	$1.00 \cdot 10^{-2}$	$1.23 \cdot 10^{-2}$
0.02M $Fe_2(SO_4)_3$ + 0.02M Na_2SO_4	$2.16 \cdot 10^{-4}$	$3.09 \cdot 10^{-2}$	$8.81 \cdot 10^{-3}$	$1.11 \cdot 10^{-4}$	$3.75 \cdot 10^{-2}$	$2.46 \cdot 10^{-3}$	$1.31 \cdot 10^{-2}$	$1.61 \cdot 10^{-2}$

With respect to the values of i_{lim}, they can be also compared in order to analyze the selectivity of the membrane at different current densities. As commented above, when the i_{lim1} is reached the supply of Na^+ ions to the surface of the membrane is limited by diffusion and their contribution to the membrane conductance diminishes at current densities higher than i_{lim1}. This hypothesis is supported by the fact that a twofold increase in the concentration of Na_2SO_4 also implies an almost twofold increase in the i_{lim1} values. Therefore, it seems that Na^+ and Fe(III) species are transported simultaneously at currents lower than i_{lim1}, but the transport of Na^+ ions occurs faster due to their higher diffusion coefficients (see Table 4.8). Once the supply of Na^+ ions to the membrane surface is set under diffusion control, the transport of Fe^{3+} ions through the membrane is greater and, in consequence, Fe^{3+} ions become the main charge carriers at high current densities ($i > i_{lim1}$). Fig. 4.72 shows a scheme of the concentration profiles of both species in the depleting diffusion boundary layer when current densities higher than i_{lim1} are applied to the membrane system.

The ability of the Nafion 117 membrane to separate ions of different valence depending on the applied current density could have practical implications for certain processes where the recovery of a specific valuable metal and its separation from other cations of different valence is desired. Moreover, the effect of the current density on the permselectivity of these membranes could be used in combination with other existing strategies in order to achieve a highly effective separation between different cations present in multicomponent industrial effluents [59,60].

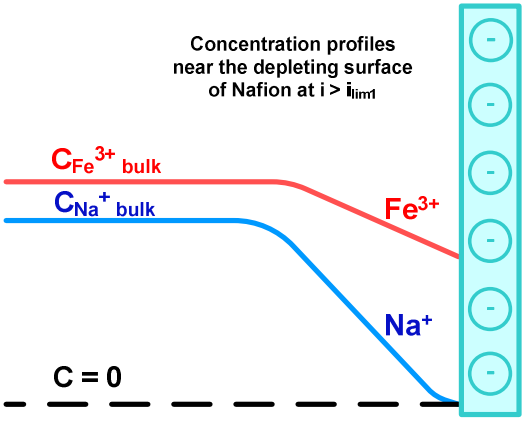

Fig. 4.72. Schematic representation of the diffusion boundary layer next to a Nafion 117 membrane at current densities higher than i_{lim1}.

4.2.4 Conclusions

The competitive cation uptake and transport through the Nafion 117 membrane has been investigated in the present section. The main conclusions regarding the competitive ion transport between H^+ and Ni^{2+} ions, which are present in the rinse waters generated in various metal finishing industries, are summarized as follows:

- The ion uptake experiments have shown that the membrane fixed charges have an important preference for Ni^{2+} ions over H^+ ions. When the membranes are equilibrated with single salt solutions of $NiSO_4$ they become saturated in Ni^{2+} ions. If the concentration of CrO_3 is higher than that of $NiSO_4$, the amount of fixed charges bound to H^+ ions becomes more significant but; even for the highest content of CrO_3 in the equilibrating solution, the fraction of membrane fixed charges balanced with Ni^{2+} ions is predominant. These results stem from the stronger attractive forces existing between the membrane fixed charges and multivalent ions.

- The addition of CrO_3 to $NiSO_4$ solutions implies an important increase in the concentration of H^+ ions. The transport competition between H^+ and Ni^{2+} ions delays the depletion of Ni^{2+} ions, which occurs for higher current densities in the mixture solutions. Moreover, the acidic pH values of the 10^{-2}M CrO_3 solutions prevent the formation of $Ni(OH)_2$ precipitates at the anodic side of the membrane.

- The i_{lim} values increase with both the concentration of $NiSO_4$ and CrO_3; however, when the concentration of $NiSO_4$ is higher than that of CrO_3, the i_{lim} increases more notoriously with the concentration of $NiSO_4$. Although two cationic species coexist in the electrolyte (Ni^{2+} and H^+ ions), only one i_{lim} was observed in the current-voltage curves. This result can be explained by the fact that the depletion of H^+ ions is less likely to occur, since H^+ ions have higher mobility and their supply from the bulk solution to the diffusion boundary layer occurs faster in relation to the supply of Ni^{2+} ions.

- The ohmic resistance of the membrane systems, R_1, exhibits a sharp decrease with the equivalent cationic charge (Q_+) for the most diluted solutions. This decreasing trend is somewhat attenuated as the concentration of CrO_3 increases. These results denote an important contribution of the resistance of the diffusion boundary layers to the total ohmic resistance at low electrolyte concentrations.

- The selectivity of the membranes for Ni^{2+} ions is very high in single salt solutions of $NiSO_4$. For the mixture solutions with low $[Ni^{2+}]/[H^+]$ ratios the T_{Ni}^{2+} values decrease considerably; however, the contribution of Ni^{2+} as current carriers is still important. For $[Ni^{2+}]/[H^+]$ ratios exceeding the unity, the current passed through the membrane is mainly transported by Ni^{2+} ions, with T_{Ni}^{2+} values approaching 0.9.

With regard to the competitive ion transport between Fe(III) species and Na^+ ions, which are typically found in acid mine drainage solutions, the main conclusions are outlined below:

- The membrane uptake of Fe(III) was higher than that of Na^+ ions, which is also in congruence with the hypothesis that the membrane fixed charges have stronger electrostatic interactions with multicharged ions. The majority of Fe(III) balanced with the membrane fixed charges is in the form of Fe^{3+} ions; however, $FeSO_4^+$ ions are also involved in the equilibrium uptake of the membranes. The addition of Na_2SO_4 to the $Fe_2(SO_4)_3$ solutions implies an increase in the concentration of SO_4^{2-} ions and displaces the equilibrium toward the formation of more $FeSO_4^+$ ions, whose concentration inside the membrane phase increases too with the concentration of Na_2SO_4.

- The chronopotentiometric curves obtained for both 0.02M $Fe_2(SO_4)_3$ and mixtures of $Fe_2(SO_4)_3$ and Na_2SO_4 showed a decrease in U_m with time for the range of high underlimiting currents. This change is originated by a shift in the equilibrium conditions in the diffusion boundary layers as the polarization of the membrane system is intensified and the external solution becomes diluted. The dissociation of $FeSO_4^+$ ions into the more conductive and mobile Fe^{3+} and SO_4^{2-} ions is favored at higher current densities, which leads to a reduction of the electrical resistance of the membrane system.

- At high current densities the formation of $Fe(OH)_3$ precipitates occurs for both $Fe_2(SO_4)_3$ solutions and mixtures of $Fe_2(SO_4)_3$ and Na_2SO_4. This phenomenon can be detected from a sharp increase in U_m with time in the chronopotentiometric curves. The precipitate layer was also visually confirmed at the anodic side of the membranes. The only difference between the single salt solutions and the mixtures is the attenuated increase of U_m when the precipitates are formed due to the presence of the more mobile Na^+ ions.

- The current-voltage curves obtained for the mixtures of $Fe_2(SO_4)_3$ and Na_2SO_4 show two i_{lim} values and their corresponding plateaus. The first i_{lim} (i_{lim1}) is approximately proportional to the concentration of Na^+ ions, so that it is associated with the depletion of Na^+ ions at low current densities. When the second i_{lim} (i_{lim2}) is reached, the precipitation of $Fe(OH)_3$ starts and leads to an extended plateau. The presence of two i_{lim} values defines two regions of predominant transport of different ions. At currents lower than i_{lim1} the transport of Na^+ and $FeSO_4^+$ ions occurs simultaneously. However, the transport of Na^+ ions may be faster, since their concentration is vanishing from the depleting membrane surface when the i_{lim1} is reached. At currents higher than i_{lim1}, once Na^+ ions are depleted from the membrane surface, Fe^{3+} ions are the main charge carriers through the membrane. These results indicate that the faster diffusion of Na^+ ions plays a more important role than the higher ion uptake of Fe(III) species by the membrane.

- The comparison between the values of R_1 obtained for each membrane system reveal a strong relationship between the membrane conductivity and the type of ions bound to the membrane fixed charges. For a constant concentration of 0.02M $Fe_2(SO_4)_3$, the R_1 values show a maximum with the addition of Na_2SO_4. These results indicate that the membrane conductance is higher when the fixed

charges are balanced with multivalent ions (Fe^{3+}). On the contrary, for the mixtures of 0.02M $Fe_2(SO_4)_3$ and 0.02M Na_2SO_4, the R_1 values decrease due to the more important increase in the conductivity of the diffusion boundary layers.

4.3 Investigation of the mechanisms of overlimiting mass transfer

4.3.1 Introduction

The mass transfer through ion-exchange membranes tends to be the governing step in electrodialysis. As commented in previous sections, the fixed charges attached to the structure of the membranes favor the transport of counterions in detriment of that of coions, which leads to the development of concentration gradients at the membrane/solution interfaces. When the ion concentration approaches zero at the membrane depleting surface, the transmembrane ion flux does not increase even if the applied electric field is further intensified. At this stage the i_{lim} has been reached and the supply of ions to the membrane is set under diffusion control.

The phenomenon of concentration polarization is common to all membrane processes: electro- as well as pressure-driven ones [61]. In both cases, the concentration polarization leads to the saturation of the transmembrane flux for increasing driving forces, as can be schematically seen in Fig. 4.73. However, electrodialysis membranes differ from other types of membranes in the fact that they allow a further increase of the current density beyond the i_{lim} if a certain threshold in the voltage drop is surpassed, as indicated in Fig. 4.73(b) [62]. This peculiarity of ion-exchange membranes is still not well understood and has engaged the interest for ion-exchange membranes of multiple research groups.

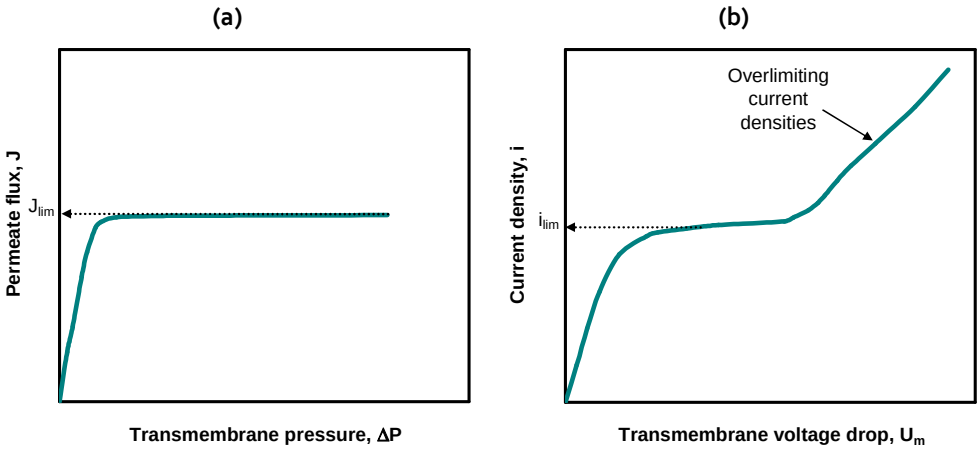

Fig. 4.73. Comparison between the characteristic curves ion flux vs. driving force for (a) pressure-driven membrane and (b) electrodialysis membranes.

Since the overlimiting currents cannot be explained by the concentration polarization theory, they were initially attributed to the generation of water splitting products due to the polarization of water molecules occurring near the membrane fixed charges under the influence of strong electric fields [63]. Besides, the presence of OH^- and H^+ ions in the diffusion boundary layer could also imply an attraction of the salt ions to the membrane surface and contribute to increase the current, which is known as the exaltation effect [61]. The hypothesis of increased water splitting was also consistent with the pH variations experimentally observed in some electrodialysis experiments. Accordingly, the water splitting was assumed as common to all electrodialysis systems and the overlimiting currents were considered detrimental for the transport of salt counterions through the membranes. In consequence, the use of overlimiting currents has been traditionally avoided because it was considered to imply a waste of energy and a decrease in the current efficiency [64].

Nevertheless, more recent studies have proven that the increase in current above the i_{lim} values cannot be entirely attributed to the water dissociation products [65]. Whereas an important catalytic activity toward the dissociation of water has been proven in strong ionizable groups present in anion-exchange membranes (e.g. tertiary amines) [66,67]; a nearly absent dissociation of water was verified in cation-exchange membranes with sulfonate groups [68]. This has implied the formulation of additional interpretations in order to explain the origin of the overlimiting currents in electrodialysis, such as the implication of convective phenomena. In this regard, the non-uniform distribution of the

electrolyte concentration in the vicinities of the membranes when the i_{lim} is reached can induce the phenomenon of gravitational convection [69]. In addition, the application of strong electric fields can also derive in a current induced destabilization of the diffusion boundary layer, which is known as electroconvection [70]. In both cases, an additional supply of ions from the bulk solution to the membrane surface would initiate the overlimiting currents. To summarize, the main mechanisms causing the overlimiting currents are indicated in Fig. 4.74.

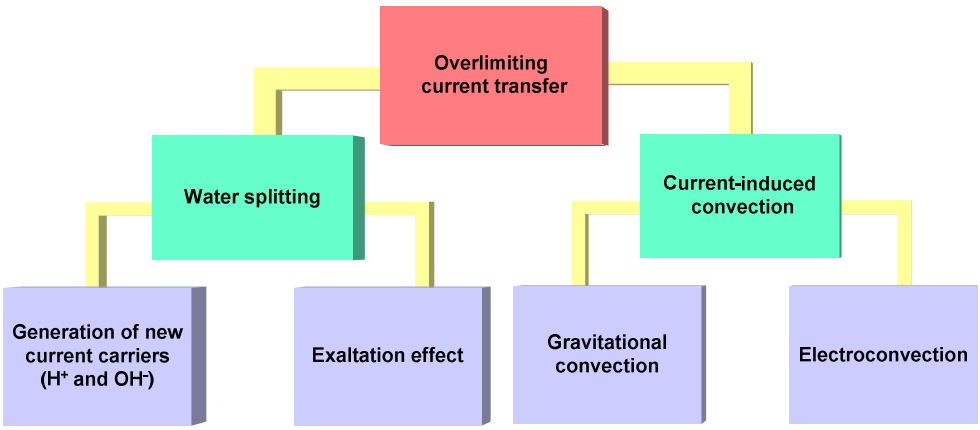

Fig. 4.74. Schematic diagram of different overlimiting current transfer mechanisms (Adapted from [69]).

As indicated in Fig. 4.74, the increased ionic flux beyond the i_{lim} is mainly carried by the ions of interest (salt counterions) when coupled convection phenomena are responsible for promoting the overlimiting currents. Consequently the utilization of intensive current regimes can broaden the possibilities of electrodialysis to new procedures and applications. In electromembrane processes, it is economically interesting to attain the highest desalination rates for a given membrane area and for the minimum operating times [71]. This could be achieved by operating at the highest current density that could ensure good current efficiency for the transfer of salt counterions through the membrane. Therefore, it is fundamental to achieve a better understanding of the origin of the membrane overlimiting conductance in order to elucidate if the operation at overlimiting currents could be advisable.

In this section (4.3), the principles causing each type of overlimiting mechanism of current transfer are discussed. Then, the dynamics by which the overlimiting currents are reached are assessed by means of chronopotentiometry, which is a powerful tool in order to

distinguish which overlimiting mass transfer mechanism predominates over the rest. Finally, the effect of the overlimiting phenomena on the steady state behavior of the membranes and the effect of the electrolyte on the type of overlimiting mechanism are analyzed. This could be used in order to evaluate the convenience of applying overlimiting currents, which could extend the use of electrodialysis to new modes of operation that could be promising for the treatment of metal containing effluents.

4.3.2 Mechanisms of overlimiting mass transfer

4.3.2.1 Water splitting

The splitting of water molecules in protons and hydroxide ions was the first phenomenon used to explain the overlimiting currents in electrodialysis, owing to the experimental detection of pH changes in electrodialysis cells. The reaction of dissociation of water occurs in aqueous solutions, as described by the following equation:

$$H_2O \rightleftarrows H^+ + OH^- \tag{4.64}$$

However, the rate of dissociation of water in aqueous solutions can be significantly incremented in the presence of ion-exchange membranes. Simons suggested that the dissociation of water can occur due to protonation and deprotonation reactions of the membrane fixed charges [72]. These reactions are obviously favored when an intense electric field is applied, the concentration polarization becomes very severe and the concentration of salt counterions almost vanishes at the depleting membrane surface, hence leaving the membrane fixed charges uncompensated [71]. Under these circumstances the water molecules are attracted and polarized by the membrane fixed charges and initiate the dissociation of water. In the case of a cation-exchange membrane having fixed anionic groups, A, the dissociation of water would occur according to the following reactions:

$$AH + H_2O \underset{k_{-1}}{\overset{k_1}{\leftrightarrow}} A^- + H_3O^+ \tag{4.65}$$

$$A^- + H_2O \underset{k_{-2}}{\overset{k_2}{\leftrightarrow}} AH + OH^- \tag{4.66}$$

These chain reactions take place in a very thin reaction layer (10-100 Å) called the space charge region [71]. The water splitting products are then transported in opposite directions owing to the applied electric field. The protons would be transported through the cation-exchange membrane whereas the OH^- ions migrate back across the depleting diffusion boundary layer.

The rate of dissociation at different ion-exchange membranes would therefore depend on the values of their corresponding reaction constants. The backward reactions of recombination (k_{-1} and k_{-2}) are normally rapid, whereas the direct reactions of dissociation depend on the nature of the membrane fixed charges, which can be expressed as a function of the K_a (acid-dissociation equilibrium constant) according to:

$$k_1 = k_{-1} \cdot K_a \tag{4.67}$$

$$k_2 = k_{-2} \cdot \frac{K_w}{K_a} \tag{4.68}$$

where K_w is the constant of the water dissociation reaction, which was previously defined in Eqs. (4.7) and (4.11). Therefore, the limiting reaction that determines the extent of the water dissociation depends on the K_a of the membrane functional groups. Accordingly, several authors have ordered different membrane fixed charges in order of increasing tendency for the water splitting reaction by comparing their rate limiting constants ($k_{\lim}$), which are presented in Table 4.11. For example, according to Table 4.11, the catalytic dissociation of water should be much higher in phosphonic acid groups than in sulfonic acid groups:

Table 4.11. Series of catalytic activity of functional groups of different ion-exchange membranes in order of increasing rate constants for the dissociation of water [73].

	$-N^+(CH_3)_3$	$-SO_3^-$	PO_3H^-	=NH	$-NH_2^+$	≡NH≡	$-COO^-$	$-PO_3^{2-}$
$k_{\lim}$ (s^{-1})	0	$3 \cdot 10^{-3}$	$3 \cdot 10^{-2}$	10^{-1}	10^{-1}	1	10	10^2

Finally, it must be also noted that the dissociation of water can be incremented by the specific conditions of each electrodialysis cell. For example, it has been suggested that the strength of the electric field accelerates the rotation of water molecules and increases

the mobility of the H^+ and OH^- ions, hence boosting the chain reactions of (4.65) and (4.66) [68]. Moreover, it has been proven that the formation of deposits of metal hydroxides at the surface of cation-exchange membranes can also increase the strength of the electric field in the reaction layer formed near the depleting surface of the membranes [74]. Therefore, in order to ascertain if the dissociation of water accounts for the major part of the current density exceeding the i_{lim}, all the above factors should be specifically evaluated for each membrane/electrolyte system.

4.3.2.2 Exaltation effect

The term "exaltation effect" is attributed to an increase in the migration of salt counterions occurring as a result of the modification of the electric field due to the presence of new ionic species, which are the product of reactions taking place next to a liquid/solid interface (ion-exchange membrane or electrode). This effect was first reported in the form of an increase of the limiting current density related to the reduction of metals in electrodes, which is associated with the OH^- ions produced by the reduction of water [75,76]. It is assumed that the OH^- ions generated attract salt counterions from the bulk solution, thus causing the increase of limiting currents.

In the case of ion-exchange membranes, the dissociation of water molecules occurring via protonation/deprotonation reactions of the membrane fixed sites can also imply an increase in the current migration of salt counterions. In the specific case of a cation-exchange membrane, the OH^- ions released to the depleting diffusion boundary layer would exert attractive forces on the cations present in the solution bulk [61,77]. When this occurs, the exalted current density of counterions is given by an equation different from the Peers' equation (Eq. (1.13)), which takes into account the transport of counterions attracted by the water splitting products. The limiting current density for the salt counterions is predicted by Eq. (4.69), which was proposed by Kharkats [75,77-80]:

$$i_{\lim j} = \frac{2D_j c_0}{\delta} + \frac{D_j}{D_w} i_w \tag{4.69}$$

Where D_j is the diffusion coefficient of the salt counterion j, D_w and i_w are the diffusion coefficient and the current density of the water splitting product (OH^- ion in the case of a cation-exchange membrane). As can be seen in Eq. (4.69) the current associated with the transport of the salt counterion increases due to the generation of water splitting

products, which attract positively charged salt cations from the solution bulk towards the interface [81]. However, due to the comparatively higher mobility of OH^- ions in relation to that of metal ions, the contribution of the exaltation effect is rather small (low values of D_j / D_w) [78]. Moreover, it has to be taken into account that this effect is restricted to those cases where intense water splitting exists [69].

4.3.2.3 Gravitational convection

Gravitational convection is a type of natural convection caused by volume forces that arise when a non-uniform distribution of solution density is present at the membrane/solution interface. In the specific case of ion-exchange membranes being exposed to the influence of an electric field, when concentration polarization develops, substantial density differences are created between the solution in the bulk and next to the membrane. This non-uniform distribution of solution density causes an Archimedean volume force which brings the solution in motion, thus implying the distortion and mixing of the diffusion boundary layers. The volume force displaces the heavier solution (bulk solution) towards the lighter solution (depleted boundary layer), thus implying an additional supply of salt counterions to the membrane depleting surface and allowing an increase in the current density above the i_{lim}.

The distortion of the diffusion boundary layer by gravitational convection was investigated by Larchet et al. [82]. It has been found that the thickness of the diffusion boundary layer decreases significantly when the gravitational convection is activated. However, the emergence of gravitational convection is promoted under certain circumstances. Gravitational convection is more likely and important in electrolyte systems with higher concentrations, since the density gradients formed between the solution bulk and the membrane depleting surface are larger. In addition, the onset of gravitational convection also depends on the properties of the electrolyte and the dimensional characteristics of the electrodialysis unit. Gravitational convection is favored by high intermembrane distances, electrolytes of low viscosity and strong electric fields. The orientation of the membrane/solution interface in the gravitational earth field has been also reported to affect the development of gravitational convection. In systems with the membranes placed in horizontal position, gravitational convection is unfeasible as the lighter solution is placed below the membrane. On the contrary, when the lighter solution is placed above the membrane, the tendency of gravitational convection to emerge is

evaluated by calculating the dimensionless Rayleigh number, which is given by Eq. (4.70) [78,80,83]:

$$Ra = \frac{\Delta\rho}{\rho}\frac{gX^3}{\nu D} \tag{4.70}$$

In Eq. (4.70) $\Delta\rho$ is the change in the solution density ρ, which occurs between the upper and lower portions of a layer of thickness X, in which the change in the solution density occurs; g is the gravitational acceleration; ν is the kinematic solution viscosity; and D is the diffusion coefficient of the electrolyte. If the Ra number exceeds a critical threshold (Ra_{cr} of 1708), the volume with a negative density gradient floats up with acceleration [78]. On the contrary, if the Ra_{cr} is not exceeded, the system is stable and no gravitational convection develops.

Nevertheless, ion-exchange membranes are usually installed in vertical position in electrodialysis cells and, therefore, the solution density gradient is horizontal. In that case, the gravitational convection generally emerges without threshold, i.e.: it develops always and increases gradually with the current [78]. This phenomenon has been widely studied with NaCl or KCl solutions, but to our knowledge, there are not many studies regarding the development of gravitational convection with systems of heavy metal ions. In this regard, the relative importance of gravitational convection on the overlimiting conductance of the membranes could be greater with solutions containing multivalent metals, since the density gradients formed at the solution/membrane interfaces are larger for lower molar electrolyte concentrations. The solutions used in our study have concentrations relatively lower than those for which gravitational convection is significant in systems of NaCl [61,80]. Therefore, it is also interesting to investigate if this type of coupled convection has an important role in diluted solutions of heavy metal ions.

4.3.2.4 Electroconvection

Electroconvection is a type of current induced convection which develops at an advanced stage of concentration polarization as a consequence of the interaction between a strong electric field and the electrical non-uniformities present at the depleting diffusion layer of a membrane/electrolyte system. This phenomenon has been considered the main transport mechanism originating the overlimiting currents in electrodialysis systems. The role of electroconvection seems to be comparatively large in diluted systems where the

gravitational convection is not present and in electrodialytic cells where the dissociation of water is nearly absent. Consequently, in the recent years a large number of investigations have been conducted in order to clarify the origin of electroconvection and to design electrodialysis systems which foster the electroconvective regime.

Different mathematical approaches have been used to explain the overlimiting conductance of ion-exchange membranes due to electroconvection. The structure of the diffusion boundary layer plays a fundamental role in the onset of electroconvection. The diffusion boundary layer can be divided into two different parts: the electroneutral zone adjacent to the bulk solution, and the space charge region adjacent to the membrane surface. The space charge region is attributed to the quasi-equilibrium diffuse electric double layer in solution. The different mathematical models used to describe the ion transport in the diffusion boundary layers are based on the extended Nernst-Planck equation, which is given in Eq. (4.71). Moreover, at overlimiting currents the Poisson equation, which relates the electric potential ϕ to the space charge density ρ_e has to be taken into account (Eq. (4.72) [61]:

$$\vec{J}_j = -D_j\left(\nabla c_j + z_j c_j \frac{F}{RT}\nabla\phi\right) + c_j\vec{V} \tag{4.71}$$

$$\varepsilon\varepsilon_0\nabla^2\phi = -\rho_e = -F(c_+ + c_H - c_- - c_{OH}) \tag{4.72}$$

Where $\vec{J}_j$, is the ion flux density, ϕ is the electric potential, $\vec{V}$ is the fluid velocity vector, ε_0 is the dielectric permittivity of vacuum and ε is the relative permittivity of the medium. Rubinstein and Shtilman were the first who solved the extended Nerst-Planck equation for overlimiting currents [84]. They found out that the solution of these equations implied an increase with the current density of the space charge region thickness, becoming comparable to the thickness of the diffusion boundary layer. Therefore, the flux density of the salt counterion grows due to the decrease in the electroneutral part thickness of the diffusion boundary layer. When an electric force is directed normally to the space charge located near the interface, an excess pressure arises within the space charge region. This excess pressure displaces the liquid out from the space charge region in tangential direction towards zones with lower pressure (i.e. lower space charge). When moving, the displaced fluid meets inertial resistance of static liquid layers that changes the direction of the moving fluid towards the solution bulk. As a

result, a pair of vortices rotating in opposite senses appears. The two vortices generated at the entrance of membrane charged nanopore are illustrated schematically in Fig. 4.75.

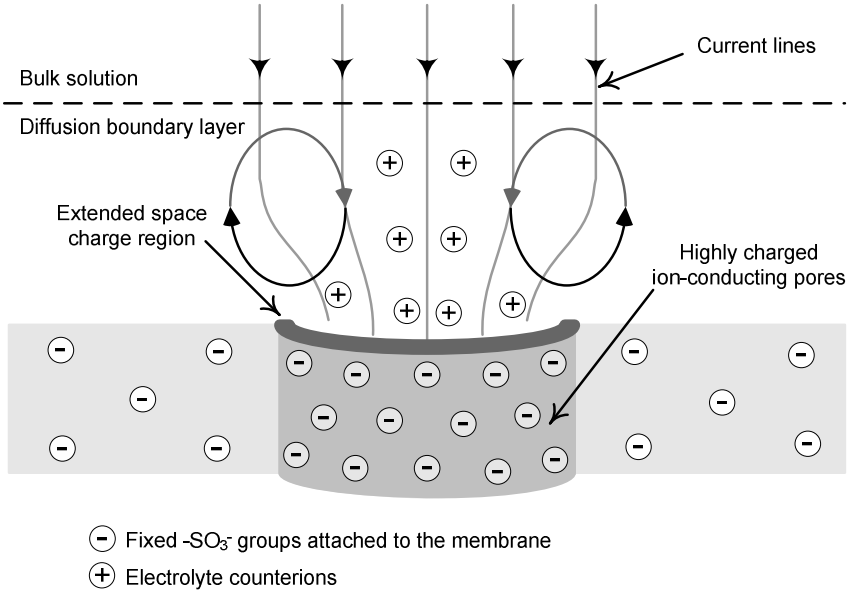

Fig. 4.75. Electroconvective vortices generated at the depleting surface of an ion-exchange membrane.

Rubinstein and Zaltzmann developed the theory of the fluid slip at a permselective membrane, which revealed that there is a certain threshold value of the membrane voltage ($U_{m,threshold}$), which corresponds to the transition from stability to instability [70]. Electroconvection developing from this instability results in the destruction of the diffusion boundary layer and causes the overlimiting currents. At U_m values of the order of magnitude of $U_{m,threshold}$ the oscillations of the electroconvective vortices are periodic, thus becoming steady-state or even decaying with time. However, the effect of the electroconvective vortices can increase if this threshold is substantially exceeded because they become chaotic [61,81]. Maletzki et al. reported that the overlimiting current contained also alternate current components (excess current noise) in the low frequency range, which also increase in magnitude with U_m [67].

In addition to the mathematical modeling and theoretical predictions used to justify and explain the role of electroconvection on the overlimiting transmembrane conductance, also some experimental evidence of the electroconvective vortices has been obtained. Rubinstein et al. developed an electrodialysis cell that allowed the direct visualization of

the electroconvective vortices [85]. Kwak et al. also developed a microscale electrodialysis cell incorporating a microscopic fluorescence imaging device to allow the visualization of the electroconvective vortices [86]. Chronopotentiometry has been also utilized as a useful tool to identify the onset of electroconvection, since the registration of some membrane voltage oscillations with time have been attributed to the emergence of electroconvective vortices [62,80,87].

Due to the obvious advantages and improvements that electroconvection could imply for electromembrane separation processes, different approaches have been used to increase the ability of ion-exchange membranes to initiate electroconvection. These include the surface modification of membranes in order to vary the hydrophobicity of the membrane surface and the increase of the degree of heterogeneity of the membranes [88]. Both surface and conductive heterogeneities have been introduced into ion-exchange membranes in order to enhance electroconvection [62,89]. However, it has been also reported that the electrolyte properties can also trigger the onset of the overlimiting currents by shifting it to lower voltages. It has been reported that solvents of greater permittivity or higher bulk ionic concentrations could imply a more rapid growth of overlimiting currents [90]. Also the size of the counterions has been reported to affect the intensity of electroconvection [91]. Therefore, the present study could be useful to identify the role of multivalent heavy metal ions on the formation and development of electroconvective instabilities. The principle of electroconvection to transform electrical energy in mechanical energy has also increased the scope of utilization of overlimiting current regimes in the field of micro- and nanofluidics [61,92-94].

4.3.3 Study of the overlimiting currents by means of chronopotentiometry and current-voltage curves

4.3.3.1 Dynamics of ion transport in membrane systems operated at overlimiting currents

In order to evaluate the viability and the technical feasibility of applying overlimiting currents in electrodialysis systems, it is crucial to know which overlimiting mass transfer mechanism predominates in each situation. For this purpose, an exhaustive analysis of the chronopotentiometric response of each membrane system can be of major utility. Chronopotentiometry is a powerful tool which allows us not only to obtain the final steady state of a membrane system, but also the dynamics by which this steady state is

reached [87]. Therefore, a qualitative interpretation of the chronopotentiograms obtained in the previous sections (4.1 and 4.2) would allow us to identify the main mechanisms of overlimiting current transfer predominating in each system.

There are some chronopotentiometric features that can be directly attributed to specific overlimiting mass transfer mechanisms. Fig. 4.76 shows different examples of chronopotentiometric curves obtained at overlimiting currents, which are explained as follows:

- Fig. 4.76(a) shows the curves typically obtained when the formation of precipitates takes place at the surface of a cation-exchange membrane. The formation of precipitates implies the increase of the electrical resistance of the membrane system due to the hindered transport of ions through the precipitate layer. The increase in the electrical resistance is manifested in the form of an increase of U_m with time as the precipitate layer thickness grows.

- Fig. 4.76(b) shows a curve typical of bipolar membranes, which is also registered after the formation of a layer of precipitates at the surface of the membranes. The plateau formed in the curves is attributed to the hindered recombination reaction of OH^- and H^+ ions formed at the bipolar junction composed of the membrane and the precipitate layer.

- The curve shown in Fig. 4.76(c) is usually formed when gravitational convection is the main overlimiting mass transfer mechanism. These curves show a maximum in U_m which is formed initially when a current density higher than i_{lim} is applied and intense concentration gradients are developed near the membrane. Subsequently, the differences in density between the depleted layers and the bulk solution activate the gravitational convection and lead to a decrease in the thickness of the boundary layers. This phenomenon is registered in the chronopotentiograms as a gradual decrease of U_m with time.

- The curves shown in Fig. 4.76(d) are typical of systems where electroconvection is the main mechanism of overlimiting mass transfer. The formation of electroconvective vortices produces a distortion of the diffusion boundary layer, which leads to chaotic fluctuations in the voltage drop through the membrane. Therefore, the oscillations in U_m with time registered in the chronopotentiograms reveal the predominance of electroconvection.

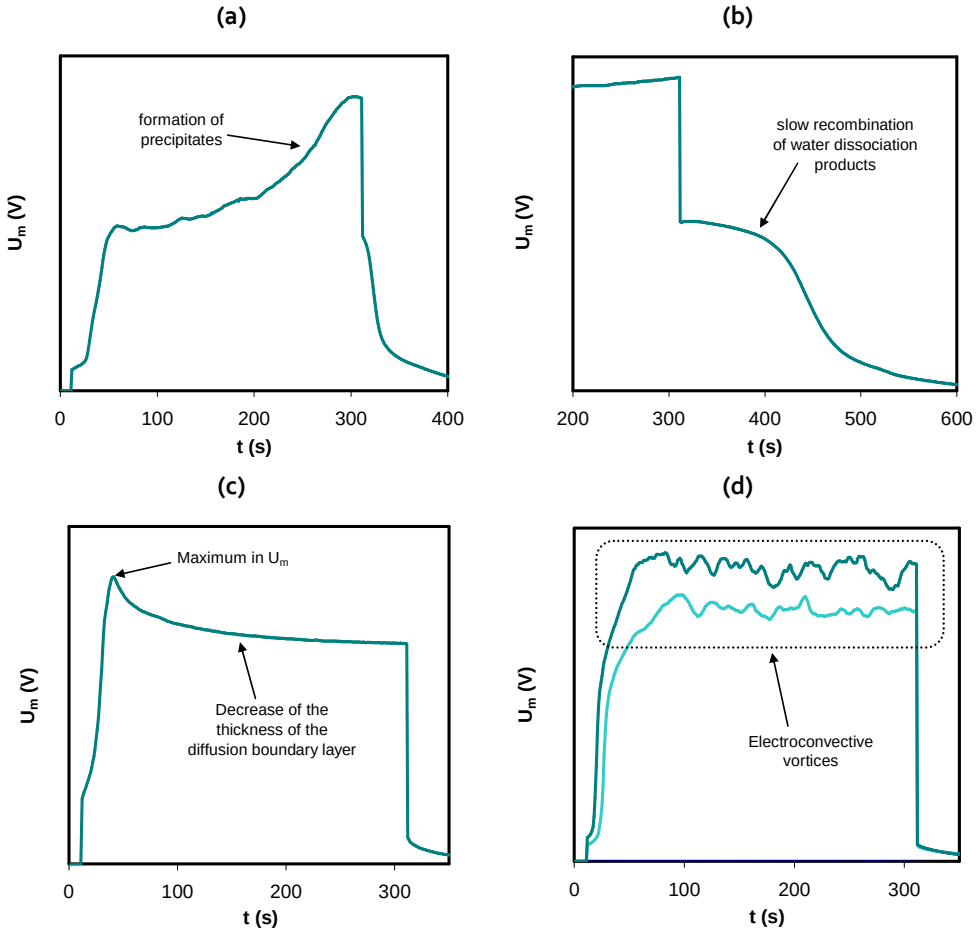

Fig. 4.76. Chronopotentiometric features caused by different overlimiting mass transfer phenomena: (a) Sharp increase of U_m due to the formation of precipitates, (b) relaxation profile of U_m as a consequence of the accelerated water splitting originated at the bipolar junction formed between a cation-exchange membrane and the deposits of metal hydroxide precipitates, (c) maximum and subsequent decrease in U_m caused by a decrease of the thickness of the diffusion boundary layer due to the emergence of gravitational convection, (d) oscillations in U_m due to the electroconvective vortices.

4.3.3.2 Steady state of membrane systems operating at overlimiting currents

The current-voltage curves of ion-exchange membranes represent the steady state relationship between the current and the membrane voltage drop. They can also be very useful to identify the differences between the mechanisms of overlimiting mass transfer and to estimate if the application of overlimiting currents could be beneficial for the mass transfer and the energy consumption in an electrodialysis cell.

Fig. 4.77 shows different current-voltage curves typical of membrane systems where different overlimiting mass transfer mechanisms predominate. The curves are normalized by dividing the current density by their corresponding i_{lim}. In the case of the membranes where the formation of precipitates occurs (curves (a) and (b)), very long plateaus are developed. However, curves (a) and (b) represent two different types of behavior: curves showing a rapid increase in current in the overlimiting region and curves with extended plateaus (without overlimiting region). The former case is typical of membrane systems where the precipitate layer formed at the membrane surface does not entirely block the ionic transport and can catalyze the water dissociation at the bipolar interface formed by the precipitate and the membrane. The rapid increase in current and the very low electrical resistance of the overlimiting region is indicative of an increased amount of ionic species present in the membrane region, which is not only due to ion transport, but also due to the catalytic generation of new species; in this case H^+ and OH^- ions. On the contrary, the latter case occurs when the precipitate layer does not have high catalytic activity for the dissociation of water or blocks the pores of the membrane. In this case, the electrical resistance of the membrane system grows without threshold.

The other two curves presented in Fig. 4.77 (curves (c) and (d)) are typical of systems in which the overlimiting conductance is propitiated principally by coupled convection. However both curves differ significantly in the length of their plateaus. This different behavior is due to a different tendency for the initiation of the overlimiting currents. In this regard, the length of the plateau region has been typically used as a parameter to assess the propensity with which an electrolyte/membrane system reaches the overlimiting regime of currents. In this sense, the plateau length can be regarded as a measure of the energy input that has to be supplied to a membrane system in order to onset the generation of electroconvective vortices or the gravitational convection. Obviously, in systems with shorter plateaus the application of overlimiting currents would improve more importantly the performance of electrodialysis systems, since increased

mass transfer rates could be achieved with lower energy consumptions. Accordingly, this parameter will be used in the present section to evaluate the effect of the electrolyte composition on the overlimiting currents.

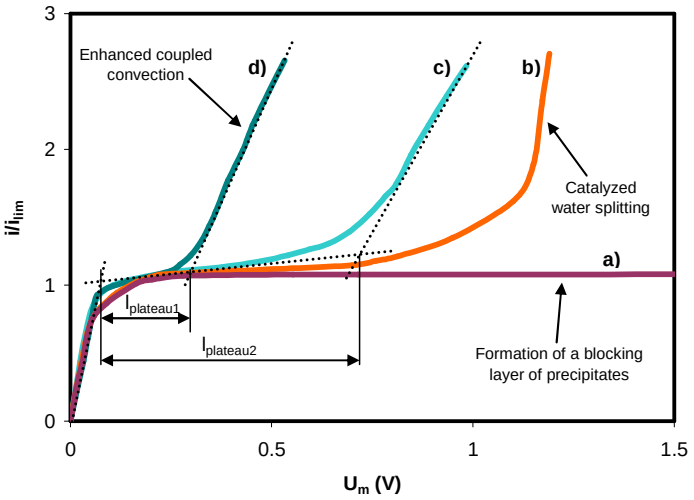

Fig. 4.77. Different current-voltage curves obtained for cation-exchange membranes: (a) cation-exchange membrane without overlimiting current, (b) cation-exchange membrane with enhanced water splitting, (c) and (d) cation-exchange membranes with enhanced coupled convection.

4.3.4 Overlimiting currents originated by water splitting products

From all the electrolyte/membrane systems studied in the previous chapters, only significant pH changes were registered in those cases where metallic precipitates were formed at the membrane surface. For example, Fig. 4.78 shows a detailed current-voltage curve obtained for diluted $NiSO_4$ solutions which includes the evolution of pH in each compartment. It must be remembered, that the formation of precipitates at the membrane surface was not observed at the end of this experiment and was neither detected in the electrochemical curves. In agreement with this, the pH in each compartment remains practically constant when overlimiting currents are applied. Only a variation of the pH in the anodic and central compartment was registered at very low current densities, which could be probably caused by some proton leakage occurring through the anion-exchange membrane. Similar pH evolutions were also obtained with

solutions of Na_2SO_4, $Cr_2(SO_4)_3$ and $Fe_2(SO_4)_3$ where the formation of precipitates was absent.

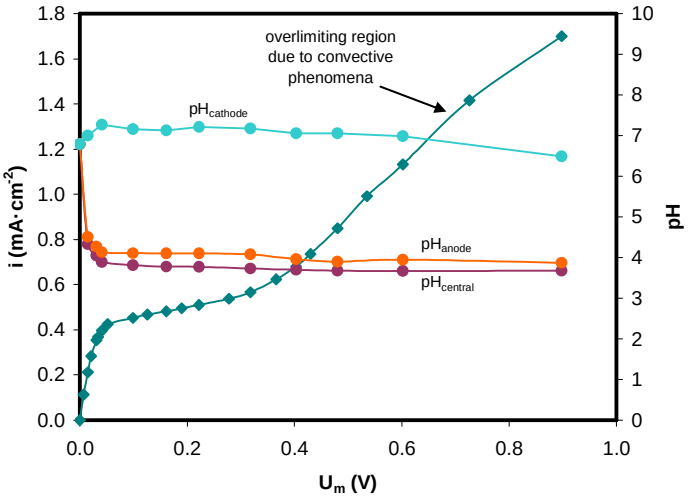

Fig. 4.78. Current voltage curve and pH evolution in each compartment registered for $5{\cdot}10^{-3}$M $NiSO_4$ solutions.

These results are also coincident with previous works, which report insignificant pH changes in systems of cation-exchange membranes [73]. As can be deduced from the low values of $k_{\lim}$ corresponding to the sulfonate groups of Nafion 117 presented in Table 4.11, the catalytic dissociation of water at Nafion membranes is very low, even when the applied current significantly exceeds the i_{lim}. Therefore, the dissociation of water has been normally neglected in membranes having sulfonate groups as fixed charges, because this phenomenon can only represent a minimal part of the important increment in current density obtained above the i_{lim} [65,66]. On the contrary, the rates of water dissociation are usually larger in systems of anion-exchange membranes. This difference is usually attributed to the presence of secondary and tertiary amine groups attached to the structure of anion-exchange membranes [72,95].

In contrast with the response presented in Fig. 4.78, a different type of pH evolution was registered for those cases where the formation of precipitates occurred (concentrated solutions of $NiSO_4$ and $Fe_2(SO_4)_3$). Fig. 4.79 shows a current-voltage curve obtained for concentrated solutions of $NiSO_4$, which includes the detailed pH evolution in each compartment of the electrodialysis cell. We can see that the pH in each compartment

also remains approximately constant in the central and cathodic compartments (at both sides of the cation-exchange membrane) when the i_{lim} is reached (plateau of the current-voltage curve). However, the emergence of overlimiting currents coincides with an important decrease of the pH in the cathodic compartment, which fails from an initial value of 7.3 to a value of 3.5. These results evidence the activation of a violent water splitting process taking place once the precipitates of $Ni(OH)_2$ are formed at the anodic side of the membrane. The H^+ ions generated at the interface between the precipitate layer and the cation-exchange membrane are transported through the membrane phase, thus contributing to increase the current beyond the i_{lim} and decrease the pH in the cathodic compartment. On the contrary, the OH^- ions generated do not imply a significant increase of the pH in the central compartment, which could be caused by their contribution to the growth of the precipitate layer.

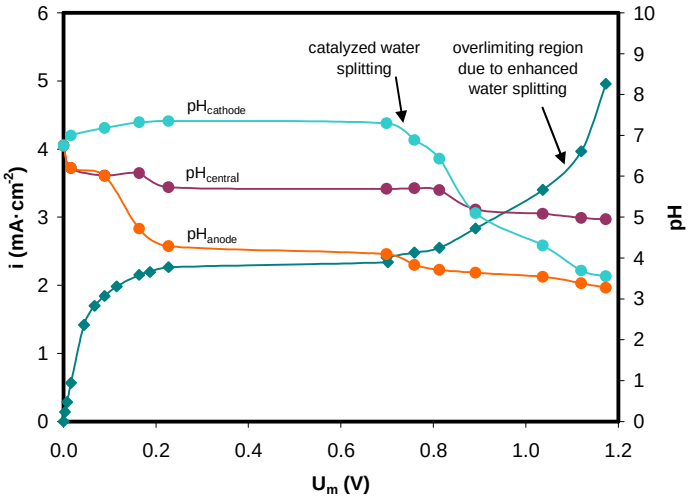

Fig. 4.79. Current-voltage curve and pH evolution in each compartment registered for $2{\cdot}10^{-2}$M $NiSO_4$ solutions.

The occurrence of violent water splitting due to the deposition of metal hydroxides at the surface of cation-exchange membranes has been reported in previous studies [73,74,96]. To explain the drastic increase in water splitting associated with the presence of precipitates at the membrane surface Mel'nikov developed a model based on the following cascade reactions of catalytic water dissociation [97]:

$$M^{+n} + nOH^- \rightleftarrows M(OH)_n \qquad (4.73)$$

$$M(OH)_n + 2H_2O \underset{k_{-1}}{\overset{k_1}{\leftrightarrow}} M(OH)_{n-1}^{+} + OH^- \quad (4.74)$$

$$M(OH)_{n-1}^{+} + 2H_2O \underset{k_{-2}}{\overset{k_2}{\leftrightarrow}} M(OH)_n + H_3O^+ \quad (4.75)$$

Based on these reactions, the series of catalytic activity for the water dissociation of Table 4.11 was completed in Table 4.12 with the inclusion of the catalytic activity of transition metal compounds, which includes the precipitates of $Ni(OH)_2$ and $Fe(OH)_3$ formed during our chronopotentiometric experiments [97].

Table 4.12. Series of catalytic activity of functional groups of different ion-exchange membranes and metal hydroxides in order of increasing rate constants for the dissociation of water [73].

	$N^+(CH_3)_3$	SO_3^-	$Ni(OH)_2$	PO_3H^-	=NH	NH_2^+	≡NH≡	COO^-	PO_3^{2-}	$Fe(OH)_3$
$k_{\lim}$ (s^{-1})	0	$3{\cdot}10^{-3}$	$5.6{\cdot}10^{-3}$	$3{\cdot}10^{-2}$	10^{-1}	10^{-1}	1	10	10^2	$1.1{\cdot}10^3$

As can be seen from Table 4.12, the $k_{\lim}$ of $Ni(OH)_2$ is only moderately higher than that of the membrane sulfonate groups. Therefore, it seems that the significantly different water splitting behavior observed in the presence of $Ni(OH)_2$ precipitates cannot be only attributed to their normal catalytic activity, and may be somehow incremented due to the electric field effects. In this sense, some researchers have related the enhanced water splitting capability of membranes having deposits of metallic hydroxides to the formation of a quasi-bipolar structure at the junction between the membrane and the metal hydroxides [16,74]. The bipolar junction constitutes a space charge region (depleted double layer) where the electric fields are very strong, thus contributing to the exponential increase of the water splitting rates with the applied current density [74,98]. Fig. 4.8o shows a schematic representation of the electric fields generated at the interface between the immobilized metal hydroxides and the membrane. In addition to the increased electric fields prevailing at the bipolar junction, the tendency for dissociating water is also enhanced by the simultaneous polarization of water molecules by the positively charged precipitate layer and by the negatively charged membrane sulfonate groups. As a consequence, the water molecules present around the membrane fixed charges must be strongly oriented so that the water structure may be more easily

broken. As already commented, the H^+ ions generated contribute to decrease the acidity of the cathodic compartment, whereas the OH^- ions are mainly consumed in the formation of a thicker precipitate layer of metal hydroxides.

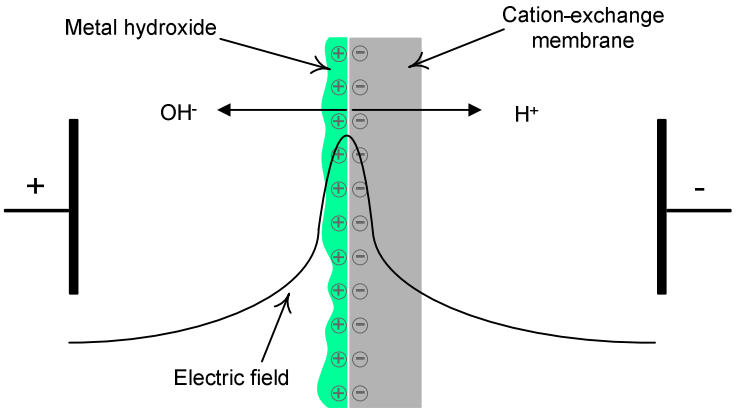

Fig. 4.80. Water dissociation at the quasi-bipolar interface/structure formed between metal hydroxides and a cation-exchange membrane.

In addition to the above discussion, a more evident proof of the quasi-bipolar behavior of the membranes having a precipitate layer is the response obtained from the chronopotentiometric experiments. As already mentioned in section 4.3.3.1, when the application of current ceases; the membrane potential decreases to a plateau value and remains almost constant during a few seconds before approaching zero. This response is typical of systems with bipolar membranes, where the dissociation of water is very intense [9].

Fig. 4.81 shows the response of the relaxation of the potential corresponding to a membrane having an attached layer of $Ni(OH)_2$ precipitates. These curves were registered after the application of different overlimiting currents. The potential remaining immediately after switching off the current is consequence of the strong concentration profiles of H^+, OH^- and salt ions in the membrane system resulting from the enhanced water splitting. At the first instants after the current interruption, uncompensated charges exist at the interface between the membrane and the bipolar junction and very large field strengths are present [10]. Afterwards, the membrane potential is restored to zero as the recombination of H^+ and OH^- ions occurs at the precipitate/membrane interface. However, the recombination reaction is limited by the rate of replacement in the membrane phase of H^+ ions by the salt counterions. As a consequence, the plateau extends over longer times and the membrane potential decreases very slowly with time.

However, when the diffusion processes in the membrane have relaxed the concentration profiles of the water splitting products, the recombination of H^+ and OH^- ions is almost exhausted and a sharp decrease of U_m is registered in the curves. The time at which the steepest decrease in U_m takes place is a parameter characteristic of bipolar membranes known as the discharging time, t_D (indicated in Fig. 4.81 for the curve corresponding to a current density of 2.83 $mA \cdot cm^{-2}$).

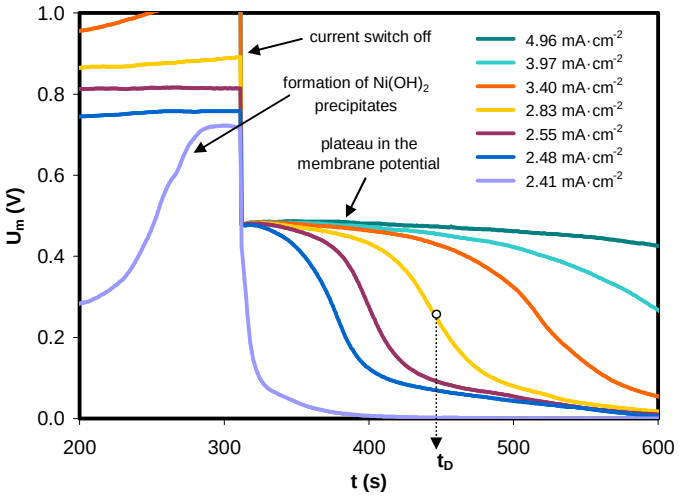

Fig. 4.81. Relaxation of membrane potential registered after the application of overlimiting currents to a system formed by a Nafion 117 membrane and $2 \cdot 10^{-2}$M $NiSO_4$ solutions.

From the different curves presented in Fig. 4.81 we can see that the plateaus become more prolonged (i.e. the t_D increases) as the applied current increases. This trend could be due to the higher concentration of water dissociation products achieved for higher current densities. Once the current is stopped, the H^+ and OH^- ions produced at the bipolar interface need longer times to complete the recombination reaction. On the contrary, the potential value at which the plateau is formed is practically the same (around 0.46 V) with independence of the applied current density.

The effect of the addition of CrO_3 to the $NiSO_4$ solutions can be examined from Fig. 4.82. As commented in section 4.2, the addition of CrO_3 does not change the speciation of Ni(II) species, but implies an acidification of the electrolyte and increases the i_{lim}. Therefore, the current densities needed to form the precipitate layer and boost the

catalytic dissociation of water also increase with the addition of CrO_3. As a consequence, for a constant current density the discharging times, t_D, decrease with the addition of CrO_3. Moreover, the process of replacement of H^+ for Ni^{2+} ions in the membrane until the equilibrium is attained is also faster in the case of the mixtures because the equilibrium partition in the membrane phase differs from the equilibrium corresponding to $NiSO_4$ solutions (as already proven from the ion uptake equilibriums obtained in section 4.2.2.2). In this case we can also observe that the potential reached at the beginning of the plateau is also about 0.46 V, thus corroborating the fact that the precipitate formed is the same (i.e. $Ni(OH)_2$) with independence of the presence of CrO_3 in the electrolyte.

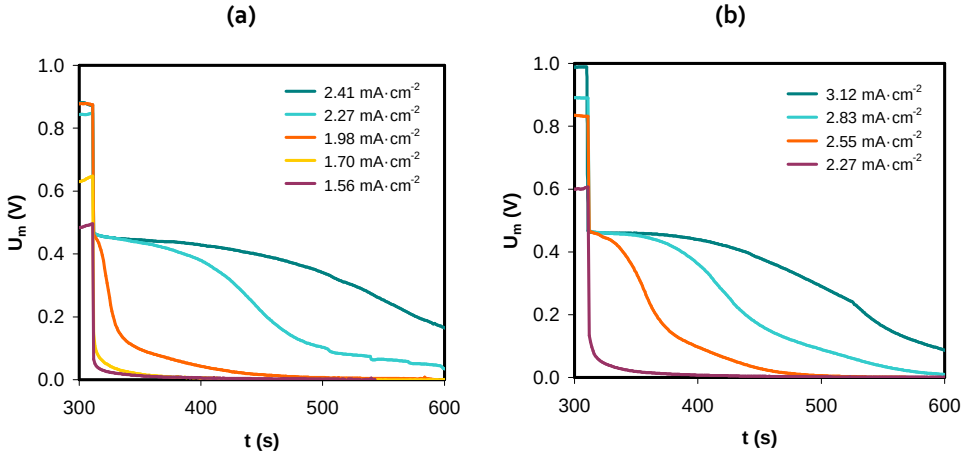

Fig. 4.82. Relaxation of membrane potential registered after the application of overlimiting currents to a system formed by a Nafion 117 membrane and (a) 10^{-2}M $NiSO_4$ solutions and (b) mixtures of 10^{-2}M $NiSO_4$ and 10^{-3}M CrO_3.

With respect to the behavior observed with the precipitates of $Fe(OH)_3$, a series of results obtained with different compositions are presented in Fig. 4.83. The effect of the applied current density can be clearly seen from the different graphics. For a given electrolyte concentration the discharging time increases for higher current densities as a consequence of the increased water splitting rates, as occurred with the $NiSO_4$ solutions. With regard to the effect of the electrolyte concentration, Figs. 4.83 (a)-(c) show the relaxation profiles of the membrane potential for different electrolyte concentrations. At lower electrolyte concentrations (Fig. 4.83 (a)) the relaxation of the concentration profiles in the membrane system are slower and the plateaus extend over longer times. However, as the concentration is increased (Fig. 4.83 (b) and (c)) the values of t_D decrease notoriously because the amount of mobile species increases and their diffusion through the membrane phase occurs more rapidly. Moreover, in the case of $Fe_2(SO_4)_3$ solutions

the initial potential value registered when the current is switched off also changes with the initial salt concentration. For diluted solutions (Fig. 4.83 (a) and (b)) the potential takes a value of approximately 0.27 V, whereas it increases to values higher than 0.3 for more concentrated solutions (Figs. 4.83 (c) and (d)). The conformation of a more dense and compact precipitate layer with the most concentration solutions could be the phenomenon responsible for this difference. Finally, there is also an effect of the addition of Na_2SO_4 to the $Fe_2(SO_4)_3$ solutions because the plateaus formed are shorter in this case (Fig. 4.83 (d)). Since Na^+ ions are also involved in the relaxation of the concentration profiles, it seems that their higher mobility leads to a faster replacement of the H^+ ions bound to the membrane fixed charges, hence allowing a faster recombination between H^+ and OH^- ions at the bipolar junction and anticipating the restoration of U_m to zero.

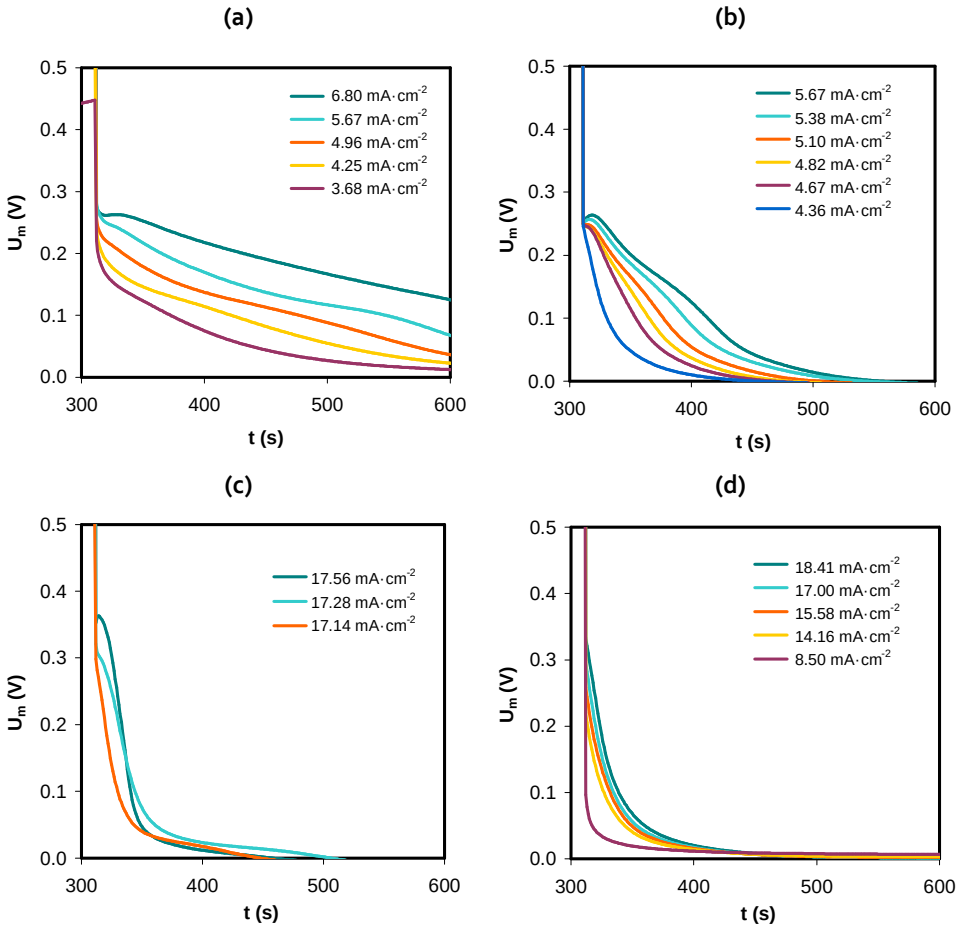

Fig. 4.83. Relaxation of membrane potential registered after the application of overlimiting currents to a system formed by a Nafion 117 membrane and (a) $2.5 \cdot 10^{-3}$M $Fe_2(SO_4)_3$ solutions, (b) $5 \cdot 10^{-3}$M $Fe_2(SO_4)_3$ solutions, (c) $2 \cdot 10^{-2}$M $Fe_2(SO_4)_3$ solutions and (d) mixtures of $2 \cdot 10^{-2}$M $Fe_2(SO_4)_3$ and 10^{-2}M Na_2SO_4.

In addition to the restoration of the membrane potential, the process of formation of precipitates was also identified by a continuous increase of U_m with time in the chronopotentiograms. The chronopotentiometric curves, presented in Fig. 4.84, reveal a different behavior of the systems of $NiSO_4$ and $Fe_2(SO_4)_3$. In the case of $NiSO_4$ solutions, the formation of $Ni(OH)_2$ precipitates at the membrane surface is accompanied by an increase of U_m with time. However, the increase in U_m is limited and, once the precipitate layer is formed, the dissociation of water implies the stabilization or even a decrease of U_m. On the contrary, when the precipitates of $Fe(OH)_3$ are formed, the increase in U_m is continued as the current is being applied. This difference was also observed in the

current-voltage curves, where the overlimiting region was suppressed for concentrated solutions of $Fe_2(SO_4)_3$, and their shape was analogous to that shown in Fig. 4.77(a), as previously discussed (see the current-voltage curves of concentrated $Fe_2(SO_4)_3$ solutions shown in Fig. 4.35 and 4.70). It seems that the bipolar structure formed by the membrane and the precipitates of iron has lower water dissociation capabilities, which is contradictory with the high values of $k_{\lim}$ of $Fe(OH)_3$ (Table 4.12). As the current is applied the layer of $Fe(OH)_3$ precipitates continues growing and becomes thicker, hence leading to an increase in U_m that reaches the magnitude of various volts. This different response seems to be related to the different conformation of both precipitates, which is discussed below.

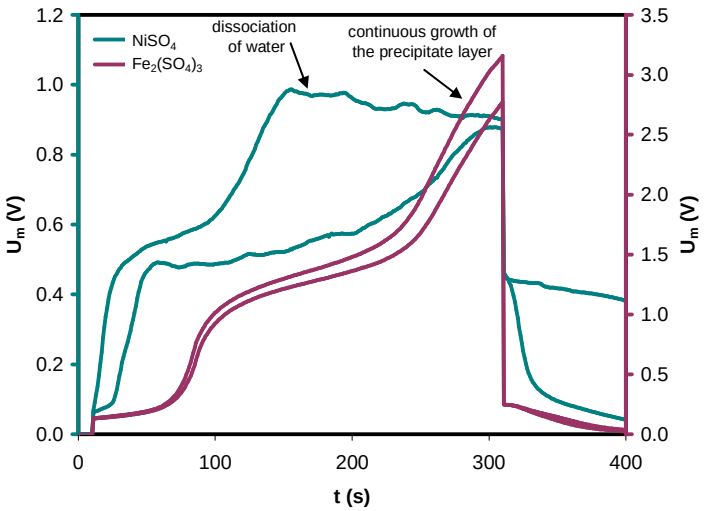

Figure 4.84. Comparison between the sharp increase in U_m occurring during the formation of deposits of $Ni(OH)_2$ and $Fe(OH)_3$ at the anodic surface of the Nafion 117 membrane (Note that, depending on the electrolyte, each curve is read in different y-axis).

Fig. 4.85 shows the aspect of the precipitates of $Ni(OH)_2$ and $Fe(OH)_3$ formed at the membrane surface during the chronopotentiometric experiments. The precipitates of $Ni(OH)_2$ show a granulated and irregular morphology. Moreover, they could be easily removed from the membrane after the experiments. On the contrary, the $Fe(OH)_3$ precipitates are formed not only at the surface of the membrane but also inside the inner membrane structure. The morphology of these precipitates is very dense and compact, as can be seen in Fig. 4.85 (b). Therefore, the continued increase in U_m registered when the $Fe(OH)_3$ precipitates are formed seems to be directly related to the blockage of

membrane pores by the hydroxide deposits, which reduce the water splitting rates and lead to a notorious increase of the membrane resistance.

As a concluding remark, we would like to note that the formation of precipitates is a phenomenon that should be avoided in electrodialysis units operated with the purpose of desalinating effluents, owing to the decrease in the salt counterion transport through the membrane and to the related increase of the energy consumption. However, the water splitting capabilities of the metallic deposits formed at the surface of ion-exchange membranes has found application in other uses of electrodialysis. For example, this phenomenon has been used as a strategy to optimize the water splitting behavior of bipolar membranes, which are specially designed for the recovery of acids and bases from aqueous effluents [74,99]. In addition, the phenomena related to the membrane potential remaining after ceasing the application of current has been also investigated in order to use bipolar membranes in alternative energy storage systems [100].

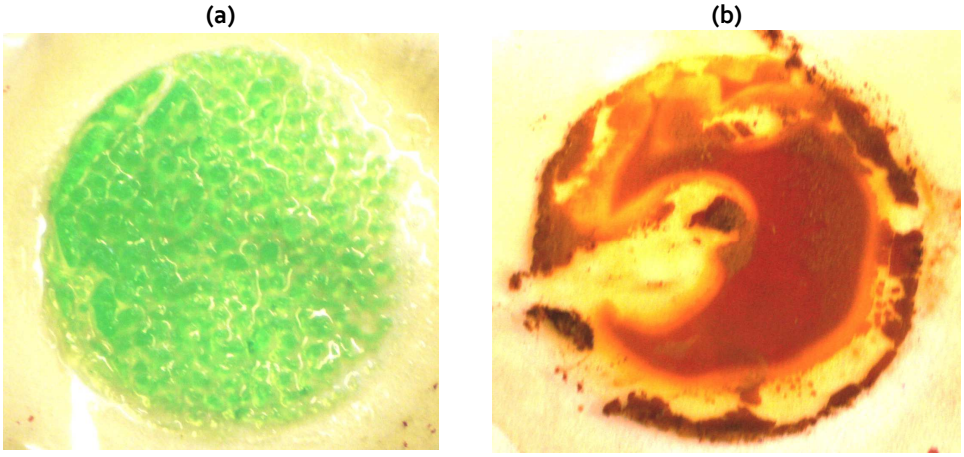

Figure 4.85. Pictures showing the precipitates formed at the surface of the Nafion 117 membrane: (a) $Ni(OH)_2$ precipitates and (b) $Fe(OH)_3$ precipitates.

4.3.5 Overlimiting currents originated by enhanced convective phenomena

4.3.5.1 Electroconvection and gravitational convection

The inducement of overlimiting currents by enhanced convective phenomena is one of the most topical research subjects in the field of electrodialysis. Since it has been conclusively proven that the overlimiting currents in cation-exchange membranes are mainly caused by other phenomena different from water splitting, many investigations have been carried out in order to clarify the origin of the overlimiting currents. Several indications suggest that the emergence of the overlimiting currents is mainly related to the destabilization of the diffusion boundary layers by convective processes occurring at an advanced stage of concentration polarization [81]. Both gravitational convection and electroconvection represent the main mechanisms of current-induced convection in ion-exchange membranes. Since both mechanisms involve an increase in the transport of salt counterions, different strategies are being investigated in order to induce their use in advanced modes of electrodialysis.

Despite the fact that gravitational convection and electroconvection predominate at specific conditions of the electrodialysis cells, in many occasions they are coupled and it is difficult to evaluate them separately. Consequently, in this section both phenomena are investigated together. The results obtained with $Cr_2(SO_4)_3$ solutions are appropriate to study the effect of the electrolyte concentration on the emergence of coupled convection, since for these solutions the formation of precipitates was absent in all cases. Fig. 4.86 shows various chronopotentiometric curves registered for diluted solutions of $Cr_2(SO_4)_3$ ($5{\cdot}10^{-4}$M) at overlimiting currents. For current densities slightly higher than the i_{lim} (i.e.: 0.32 and 0.40 mA·cm^{-2}) the evolution of U_m at times larger than the transition time is almost plane. However, when the excess beyond the i_{lim} is more important (0.60 and 0.64 mA·cm^{-2}), a further increase in U_m takes place. This response is associated with an intensification of the concentration polarization, which promotes the emergence of hydrodynamic instabilities at higher current densities. In the present case the onset of electroconvection is the phenomenon causing hydrodynamic instabilities, which are manifested in the form of chaotic oscillations in U_m. Furthermore, the magnitude of the oscillations becomes larger with the increase in the current density, even reaching the magnitude of 0.2 V for the current density of 1.28 mA·cm^{-2}. The slower relaxation of the membrane potential registered for the highest currents also confirms the relationship

existing between the intensification of the concentration polarization and the overlimiting features.

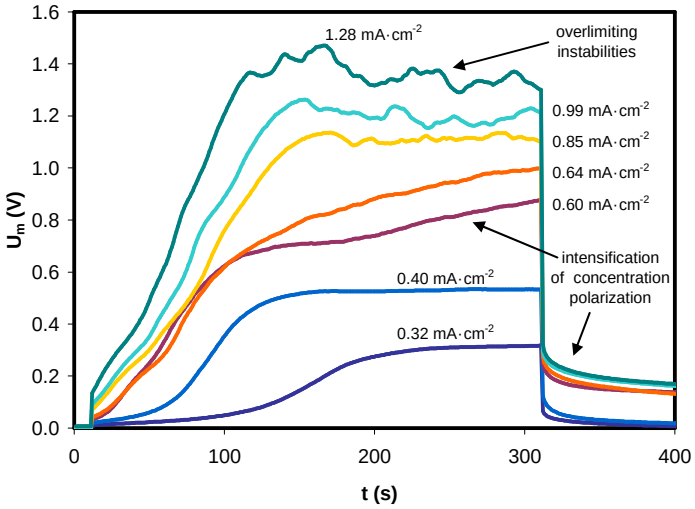

Fig. 4.86. Chronopotentiometric response obtained in the overlimiting range of currents for $5{\cdot}10^{-4}$M $Cr_2(SO_4)_3$ solutions.

The effect of an increase in the electrolyte concentration can be evaluated by comparing Figs. 4.86 and 4.87, which shows the chronopotentiometric response obtained for $5{\cdot}10^{-3}$M $Cr_2(SO_4)_3$. Whereas for the lower electrolyte concentration only the phenomenon of electroconvection was clearly confirmed, an increase of the salt concentration also implies the emergence of gravitational convection. Specifically, the curves of Fig. 4.87 show a maximum in U_m which is registered immediately after the transition time. Then U_m decreases until an approximately steady value is reached. Several authors have related this type of chronopotentiometric response to the development of gravitational convection [61,65,82]. Gravitational convection appears especially in concentrated electrolytes as a consequence of the development of high concentration gradients near a membrane/solution interface under the influence of an electric field. Once the concentration gradients are developed, an Archimedes volume force emerges and reactivates the supply of salt counterions from the bulk solution to the membrane surface. Consequently, the emergence of gravitational convection leads to a decrease of the thickness of the diffusion boundary layer, which is manifested in the form of the decrease in U_m in the chronopotentiograms. For the highest overlimiting currents presented in Fig. 4.87 the maximum in U_m becomes more pronounced and also coincides

with the oscillations related to electroconvection. This kind of response evidences the coexistence of both types of convective mechanisms of overlimiting mass transfer [78].

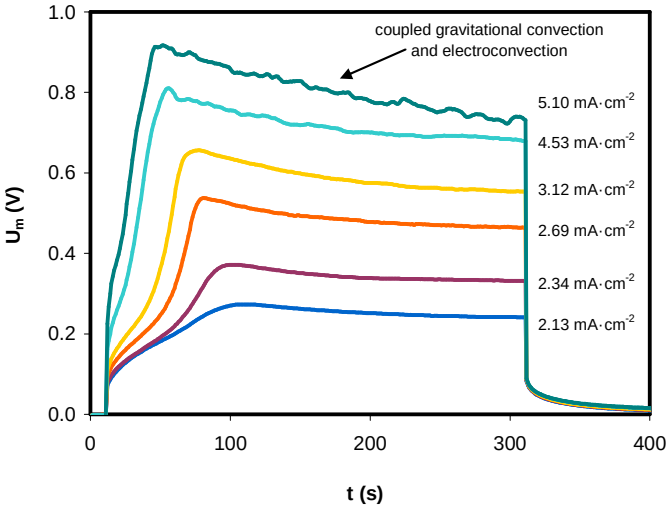

Fig. 4.87. Chronopotentiometric response obtained in the overlimiting range of currents for $5 \cdot 10^{-3}$M $Cr_2(SO_4)_3$ solutions.

The results obtained for 10^{-2}M $Cr_2(SO_4)_3$ are shown in Fig. 4.88. An additional increase of the electrolyte concentration leads to the intensification of gravitational convection. In this case the maximum is very marked because the density gradients created near the membrane are higher than those developed for lower concentrations. Moreover, the oscillations in the voltage drop originated by the electroconvective vortices are not present in the curves. It seems that for increasing electrolyte concentrations, the necessary condition for the emergence of gravitational convection is already achieved for moderate current densities. However, an additional intensification of the applied electric field is required for the development of electroconvective vortices.

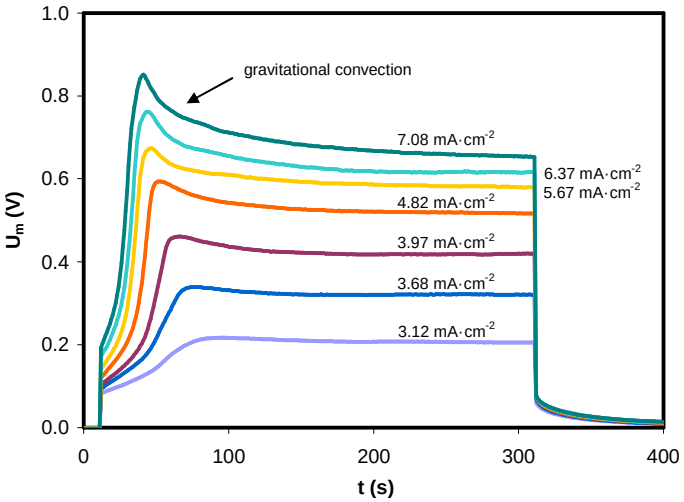

Fig. 4.88. Chronopotentiometric response obtained in the overlimiting range of currents for 10^{-2}M $Cr_2(SO_4)_3$ solutions.

The results obtained for mixtures of $NiSO_4$ and CrO_3 are quite similar to those presented for $Cr_2(SO_4)_3$. Fig. 4.89 shows the response obtained for the mixtures of 10^{-2}M $NiSO_4$ and 10^{-2}M CrO_3, where the features related to gravitational convection and electroconvection can be clearly seen. At low overlimiting currents the steady state of U_m is reached very fast after the registration of the transition time and the subsequent response remains plane until the end of the current pulse. However, when the current density exceeds in more than 1.5 times the i_{lim}, the decrease in U_m associated to the emergence of gravitational convection can be distinguished in the curves. In addition, this curve also exhibits very small oscillations. With an additional increase of current density ($2 \cdot i_{lim}$), both chronopotentiometric features can be clearly identified in the curves: the gradual decrease of U_m due to gravitational convection is accompanied by oscillations in the curve associated with electroconvective vortices. Finally, at very high overlimiting currents ($3 \cdot i_{lim}$) the effect of electroconvection predominates to such an extent that the role of gravitational convection is not detected in the curves. It seems that the strong electric fields create the necessary conditions for the early development of electroconvection, which takes place even before the gradients of concentration necessary to initiate the gravitational convection could be formed.

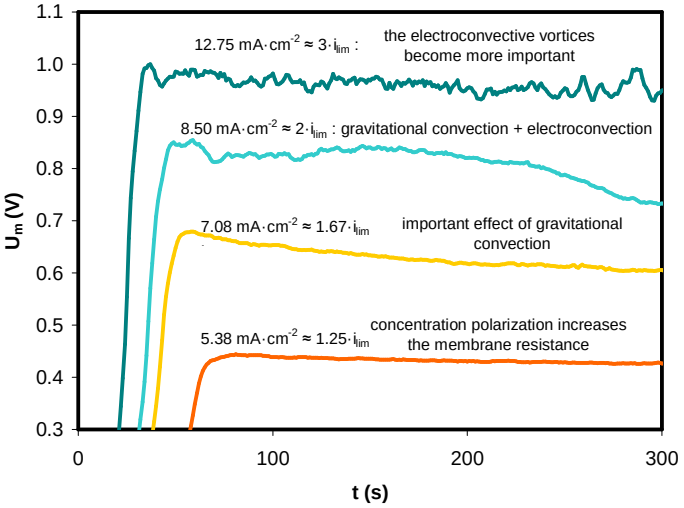

Fig. 4.89. Chronopotentiometric response obtained in the overlimiting range of currents for the mixtures of 10^{-2}M $NiSO_4$ and 10^{-2}M CrO_3.

As already seen in previous figures (Fig. 4.86-4.89), the magnitude of the electroconvective vortices increases with the current density. This effect is clearly seen in Fig. 4.90, which shows a magnification of the upper part of chronopotentiograms obtained at overlimiting currents. At low overlimiting currents and times larger than the transition time the evolution of U_m with time is flat. However, even though the oscillations in U_m are not manifested in the chronopotentiograms, there may exist already a distortion of the diffusion boundary layer by electroconvection, since the transition to the overlimiting region in the current-voltage curve has already occurred for these current densities. As the current is further increased, the oscillations in U_m start to become noticeable due to the generation of larger electroconvective vortices. Larger electroconvective vortices bring higher volumes of fluid into motion, thus promoting a greater supply of counterions from the bulk solution to the membrane surface and an increased distortion of the diffusion boundary layer. The amplitude of the oscillations increases gradually, thus becoming very notorious for the highest applied currents. This effect is very clear for the two highest curves shown in Fig. 4.90, which are practically overlapped despite the fact that they are obtained at significantly different current densities.

The results obtained for Na_2SO_4 and diluted solutions of $Fe_2(SO_4)_3$ are similar to those obtained for $Cr_2(SO_4)_3$ and diluted solutions of $NiSO_4$, where the role of electroconvection

was clearly seen, but the maximum in U_m formed due to gravitational convection was not detected. Consequently, these results have been omitted for the sake of conciseness. On the contrary, the overlimiting behavior obtained for concentrated solutions of $Fe_2(SO_4)_3$ is the characteristic one related to the formation of precipitates, as has been discussed above.

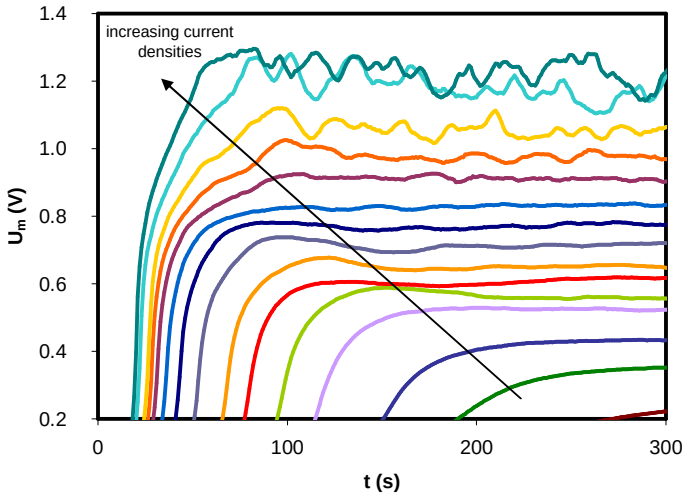

Fig. 4.90. Chronopotentiometric response obtained in the range of overlimiting currents for the mixtures of $5{\cdot}10^{-4}$M $NiSO_4$ and 10^{-3}M CrO_3.

Although the chronopotentiometric features characteristic of electroconvection and gravitational convection were registered for both $Cr_2(SO_4)_3$ and $NiSO_4$ solutions, there are some differences between the overlimiting behavior of both electrolytes. The decrease in U_m due to gravitational convection was more important in the case of $Cr_2(SO_4)_3$ solutions, whereas the relative importance of the electroconvective vortices is greater in the presence of $NiSO_4$. This different behavior could stem from the different density of both electrolytes. In the case of $Cr_2(SO_4)_3$ solutions, the amount of sulfates is higher than for $NiSO_4$ solutions and the magnitude of the density gradients generated at the diffusion boundary layer should be also greater, hence implying a more important role of gravitational convection. On the contrary, gravitational convection becomes significantly attenuated with $NiSO_4$ solutions as the current density increases. In $NiSO_4$ solutions the earlier onset of electroconvective vortices may destroy the diffusion boundary layer and impede the development of higher density gradients, which is the necessary condition to initiate the gravitational convection.

The relative predominance of each type of current-induced convection can also be analyzed by plotting the difference between the maximum value reached in the chronopotentiograms, $U_{m,max}$, and the final value registered, $U_{m,f}$, as a function of the ratio of the applied current density to the limiting one (i/i_{lim}), as shown in Figs. 4.91 and 4.92. The synergic effect of both types of convective supply of ions to the membrane surface is evident for the $Cr_2(SO_4)_3$ solutions (Fig. 4.91). At current densities below the limiting value the decrease in the voltage drop during the chronopotentiometric measurements were already registered (positive values of ($U_{m.max} - U_{m,f}$)). This is caused by the emergence of important density gradients causing gravitational convection, which is in agreement with previous studies that report the initiation of gravitational convection even at current densities below the i_{lim} [78]. If current densities around $1.5 \cdot i_{lim}$ are applied, an important increase in ($U_{m,max} - U_{m,f}$) is observed. This increase does not follow a clear pattern and the values of ($U_{m,max} - U_{m,f}$) show a significant scatter. On the contrary, for i/i_{lim} values higher than 2 the decrease in U_m obeys again a linear dependence with the applied current, which coincides with the increase of the magnitude of the electroconvective vortices. The obtained results may be explained as follows: at currents below or slightly higher than i_{lim} the contribution of gravitational convection is the main mechanism causing a decrease in both the diffusion boundary layer thickness and the membrane voltage drop; for $1<i/i_{lim}<2$ the observed scatter seems to indicate the initiation of steady electroconvective vortices and gravitational convection is intensified, whereas for $i/i_{lim}>2$ the vortices due to electroconvection become chaotic and its contribution to the decrease in U_m is summed to that of gravitational convection.

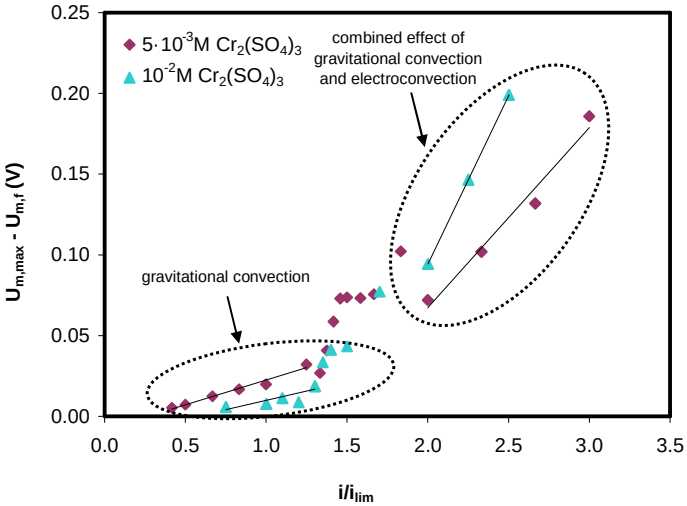

Fig. 4.91. Plot of the difference ($U_{m,max} - U_{m,f}$) obtained from the chronopotentiometric curves as a function of the i/i_{lim} parameter for different concentrations of $Cr_2(SO_4)_3$.

The relationship between the parameters ($U_{m,max} - U_{m,f}$) and i/i_{lim} obtained for $NiSO_4$ solutions (shown in Fig. 4.92) is different from that obtained for $Cr_2(SO_4)_3$. In this case, the maximum in U_m related to gravitational convection is not detected until the i_{lim} is surpassed, which may be due to the lower density gradients generated with $NiSO_4$ solutions. Moreover, the role of electroconvection becomes more important as the concentration polarization is intensified. As commented previously, the application of high overlimiting currents anticipates the development of electroconvection and increases the magnitude of the vortices to such an extent that the gravitational convection becomes attenuated. As a result, the maximum in U_m is not registered in the chronopotentiograms for current densities higher than $1.5 \cdot i_{lim}$, and the values of ($U_{m,max} - U_{m,f}$) become lower and scattered.

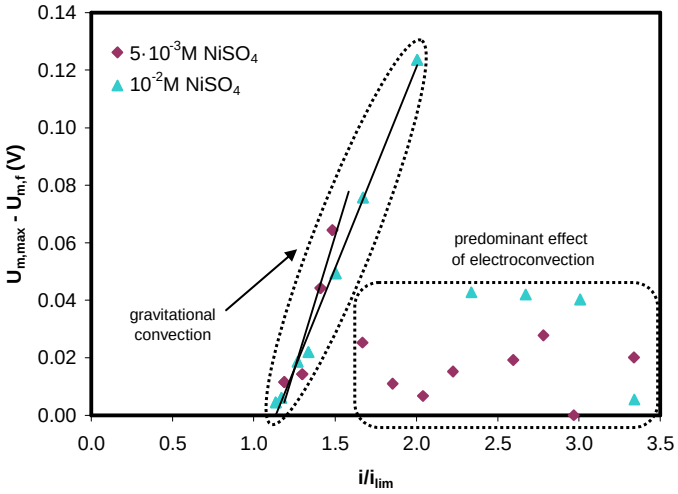

Fig. 4.92. Plot of the difference ($U_{m,max} - U_{m,f}$) obtained from the chronopotentiometric curves as a function of the i/i_{lim} parameter for different concentrations of $NiSO_4$ in 10^{-2}M CrO_3 solutions.

The chronopotentiometric results explained above are in agreement with previous studies conducted to characterize the nature of the overlimiting current transfer in systems of cation-exchange membranes [65,69,78,101]. In general, at low electrolyte concentrations the participation of electroconvection on the overlimiting conductance of the membranes is predominating, whereas the role of gravitational convection becomes more important at higher electrolyte concentrations. In addition, both types of coupled convection can also coexist in concentrated electrolytes when very strong electric fields are applied. Nevertheless, some different features have been elucidated for solutions containing multivalent metals. In this sense, the fact that an important participation of gravitational convection has been observed for very low electrolyte concentrations is quite noticeable, since the emergence of gravitational convection in salts of alkaline metals, such as NaCl, is considered to occur only for concentrations higher than 0.02M [80]. This difference could probably stem from the presence of heavy metals in the electrolyte. The higher molecular weight of the salts of multivalent metals favors the development of high density gradients for molar concentrations considerably lower than those of NaCl for which the gravitational convection was previously reported. This difference could result in a more advantageous application of overlimiting currents to treat metal containing effluents, in relation to the desalination of brine or brackish waters. Accordingly, this effect of the electrolyte composition on the initiation of the overlimiting currents is analyzed in more detail below.

4.3.5.2 Role of M^{+n} ions on coupled convection

The effects of operating electrodialysis units at overlimiting currents depend not only on which mechanisms promote the overlimiting conductance but also on the threshold in the membrane voltage drop that has to be surpassed to reach the overlimiting regime. If the increase in the mass transfer occurs at the expense of considerable higher energy consumptions, the application of overlimiting currents is not advisable. On the contrary, if the increased mass transfer rates are achieved without implying an excessive dissipation of energy in the membrane region, the operation at overlimiting currents could be beneficial for the desalination process. Related to this, the length of the plateau region of the current-voltage curves ($l_{plateau}$) can be regarded as a measure of the energy needed in order to change the mass transfer mechanism in the solution layer adjacent to the membrane from diffusion to coupled convection. Therefore, we can evaluate the convenience of applying overlimiting currents by investigating the influence of the electrolyte composition on the $l_{plateau}$ values.

Fig. 4.93 shows two current-voltage curves obtained for different concentrations of $Cr_2(SO_4)_3$ with the values of current density normalized by the corresponding values of i_{lim} (i/i_{lim}). As can be seen from the graphic, increasing electrolyte concentrations lead to shorter plateaus in the current-voltage curves. This effect in the case of $Cr_2(SO_4)_3$ solutions could derive from the fact that the density gradients needed to initiate the gravitational convection are formed at lower membrane voltage drops for higher electrolyte concentrations. The results obtained for mixtures of CrO_3 and $NiSO_4$ solutions show a similar trend (Fig. 4.94), with decreasing values of $l_{plateau}$ as the electrolyte concentration increases. However, in this case the overlimiting region of the current-voltage curves is different for lower and higher electrolyte concentrations. The curve obtained for 10^{-2}M $NiSO_4$ shows two differentiated slopes in the overlimiting region: the slope is lower at low overlimiting currents; whereas at higher overlimiting currents the electrical resistance of the membrane system decreases notoriously. It also seems that the facilitated initiation of gravitational convection in concentrated electrolytes contributes to decrease the $l_{plateau}$. However, the increase in the current density is not as important as that promoted by the electroconvective vortices of higher amplitude generated at high overlimiting currents.

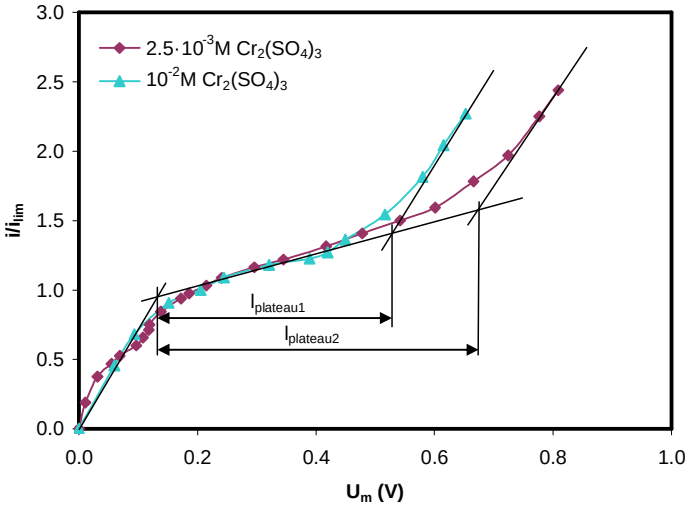

Fig. 4.93. Normalized current-voltage curves obtained for different concentrations of $Cr_2(SO_4)_3$.

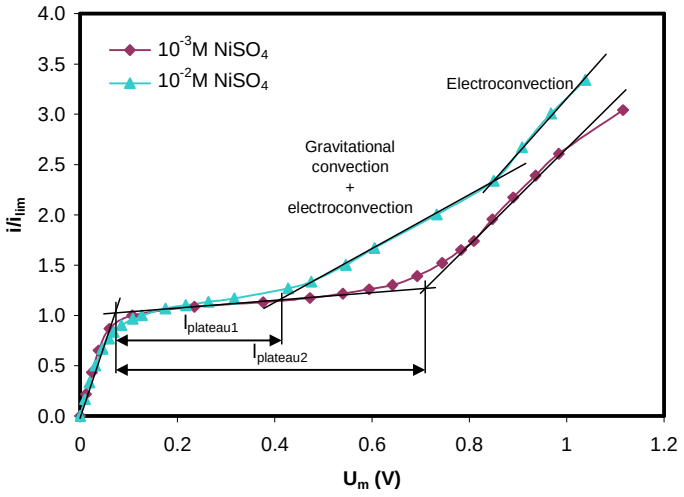

Fig. 4.94. Normalized current-voltage curves obtained for mixtures of 10^{-2}M CrO_3 and two different concentrations of $NiSO_4$.

The $I_{plateau}$ values obtained for different single salt solutions of Na_2SO_4, $NiSO_4$, $Fe_2(SO_4)_3$ and $Cr_2(SO_4)_3$ are represented in Fig. 4.95. Note that the $I_{plateau}$ values corresponding to those compositions where precipitates were formed and the overlimiting region was not caused by coupled convection have been omitted (concentrated solutions of $Fe_2(SO_4)_3$

and $NiSO_4$). The results show that the $I_{plateau}$ values obtained for $Cr_2(SO_4)_3$ solutions are higher than those obtained for $Fe_2(SO_4)_3$ and $NiSO_4$. As reported in previous studies, the plateau length can be significantly affected by the size of the counterions that are involved in the emergence of the overlimiting conductance [91,102]. The Stokes radius of the membrane counterions is usually used for comparison purposes. The Stokes radius (d) represents the radius of a hard sphere that diffuses at the same rate as the molecule, which includes hydration and shape effects; and is calculated according to Eq. (4.76).

$$d = \frac{k_B T}{6\pi\eta D_j} \tag{4.76}$$

Where k_B, T, η and D_j are the Boltzmann's constant, the temperature, the solution viscosity and the diffusion coefficient of the ion j. The Stokes radius of each ion has been included in Table 4.13. It is remarkable that Ni^{2+} ions, although having lower charge, have larger Stokes radius than Cr^{3+} ions. This is caused by the different hydration shells of both ions. The difference in Stokes radius is in congruence with the shorter $I_{plateau}$ values obtained for $NiSO_4$ solutions. Since the electroconvection is promoted by the motion of counterions propitiated by strong electric fields, those ions having larger Stokes radius would involve the motion of larger volumes of fluid. As a result, the destabilization of the diffusion boundary layer occurs earlier in the case of cations of larger size.

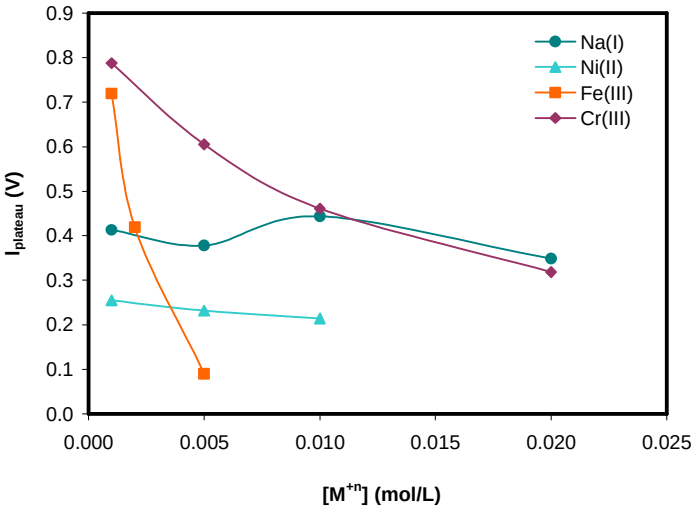

Fig. 4.95. Effect of the electrolyte concentration on the $I_{plateau}$ values obtained for solutions of Na_2SO_4, $NiSO_4$, $Fe_2(SO_4)_3$ and $Cr_2(SO_4)_3$.

Table 4.13. Stokes radius calculated for the different metal ions investigated.

Cation	Stokes radius (nm)
Na^{+}	0.184
Ni^{2+}	0.371
Fe^{3+}	0.406
Cr^{3+}	0.309

In regard to the effect of the electrolyte concentration, in general, the $I_{plateau}$ values follow a decreasing trend with the electrolyte concentration. Nevertheless this trend is more marked in the case of trivalent metals (Cr(III) and Fe(III)). These results indicate that higher concentration of metal ions also favor an early onset of the overlimiting currents for lower membrane voltage drops. In the case of $Cr_2(SO_4)_3$ the increasing role of gravitational convection could contribute to the decreasing $I_{plateau}$ values. However, as commented previously, the decrease of I_{plateu} values may not be entirely associated to gravitational convection, since electroconvection can also develop for concentrated electrolytes even without being manifested in the form of oscillations of U_m in the chronopotentiograms. Note that the oscillations in U_m may not be detected by the tips of the reference electrodes when the electroconvective vortices are small. Therefore, the decreasing trend of the $I_{plateau}$ with the electrolyte concentration could be caused by both types of convection. The tendency of coupled convection to appear, and analogously, the decrease of the length of the plateau region, have been compared for different electrolytes in the literature by means of the calculation of the Péclet dimensionless number (Pe), which quantifies the contribution of convection to the transport related to diffusion [102]. The Pe number is calculated by means of Eq. (4.77)

$$Pe = 6\pi\left(r_0^2 d / \lambda^3\right) \tag{4.77}$$

where r_0, d and λ account for the Debye length, the Stokes radius and the mean interionic distance, respectively [102,103]. The Debye length is given by Eq. (4.78), where ε_r, ε_0 and k_B stand for the relative static permittivity, the electric constant and the Boltzmann constant respectively [104,105]. T, N_A, e, c_j and z_j represent the temperature, the Avogadro's number, the electronic charge, the concentration and charge of the ion j, respectively:

$$r_0 = \left(\frac{\varepsilon_r \varepsilon_0 k_B T}{e^2 N_A \sum_i c_i z_i^2} \right)^{1/2} \quad (4.78)$$

Finally, the mean interionic distance can be calculated by means of Eq. (4.79), where c refers to the ionic concentration of the electrolyte.

$$\lambda = \left(\frac{1}{N_A c} \right)^{1/3} \quad (4.79)$$

The decrease of the plateau length with the salt concentration observed in our results differs from the observations of other authors in the literature, which found that there was no influence of the electrolyte concentration on the plateau length and the Péclet number [70,102]. This might stem from the fact that the binary salts considered in those studies dissociate completely in their respective anions and cations, and therefore the terms corresponding to the electrolyte concentration in r_0 (Eq. (4.78) and λ (Eq. (4.79) are cancelled when applying Eq.(4.77). On the contrary, in systems composed of sulfate salts of multivalent cations, the chemical equilibria induce the formation of various complex species with different ionic charge. As a consequence, both concentration terms may change differently with the changes in the initial salt concentration. The Pe number was calculated for each electrolyte solution and concentration and is presented in Fig. 4.96. The Pe number remains almost independent of the concentration for nickel and sodium sulfates because they are almost completely dissociated in their free anions and cations for the range of concentrations considered. On the contrary, a significant increase is observed for Cr(III) and Fe(III) solutions with the electrolyte concentration. This observation would in part justify the results of plateau length observed in the current-voltage curves for the sulfate salts of trivalent metals (Fig. 4.95). Moreover, similar decreasing trends of the $l_{plateau}$ values with the electrolyte concentration were also found in previous studies [106,107]. Kim and Lawler attributed the effect of the electrolyte concentration to an increase in the amount of ionic charge created in the space charge region [90].

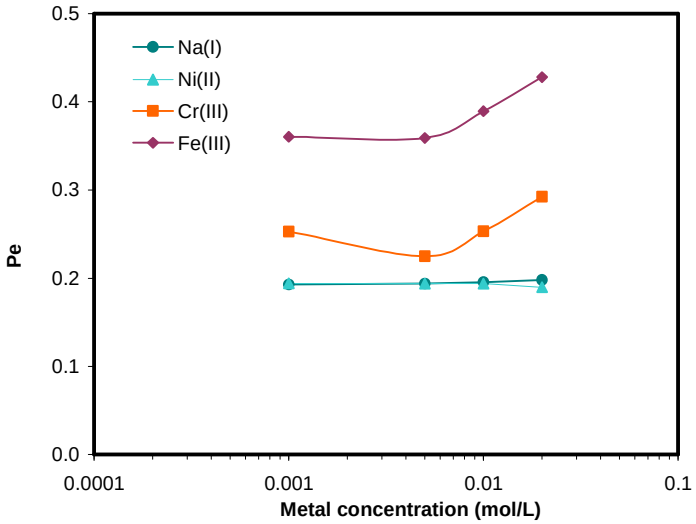

Fig. 4.96. Evolution of the Pe number for different electrolytes as a function of the metal concentration.

4.3.5.3 Role of H^+ ions on coupled convection

Apart from the role of heavy metal ions on the initiation of convective phenomena at overlimiting currents, the participation of H^+ ions in the overlimiting currents can also be studied by comparing the current-voltage curves obtained for the mixtures of $NiSO_4$ and CrO_3. It must be remembered that CrO_3 forms chromic acid when dissolved in water (H_2CrO_4). As a result, the concentration of H^+ ions is approximately the same as that of CrO_3 (i.e.: solutions of 10^{-3}M and 10^{-2}M CrO_3 have pH values of 3 and 2, respectively). Fig. 4.97 shows the normalized current-voltage curves obtained for solutions with a constant concentration of $NiSO_4$ (10^{-3}M) and varying concentrations of CrO_3. The effect of increasing the concentration of H^+ ions in the electrolyte is the contrary to that observed for the concentration of heavy metal ions, since the plateaus of the current-voltage curves become larger as the concentration of H^+ ions increases.

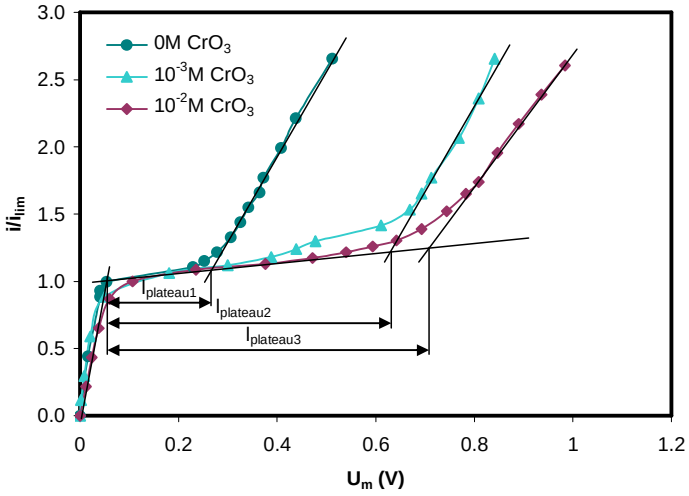

Fig. 4.97. Normalized current-voltage curves obtained for mixtures of 10^{-3}M $NiSO_4$ and different concentrations of CrO_3.

Fig. 4.98 shows the relationship between the $I_{plateau}$ values and the concentration of Ni(II) for different CrO_3 concentrations. As reported previously, the values of $I_{plateau}$ decrease with the concentration of $NiSO_4$. Moreover, this decrease becomes more notorious for the mixtures with CrO_3 than for single salt solutions of $NiSO_4$. This increased effect of the concentration of Ni^{2+} probably stems from the competitive ion transport between H^+ and Ni^{2+} ions. On the contrary, the largest $I_{plateau}$ values were obtained for the solutions with the highest concentration of CrO_3. This behavior reveals an unfavorable effect of the concentration of H^+ ions on the onset of coupled convection.

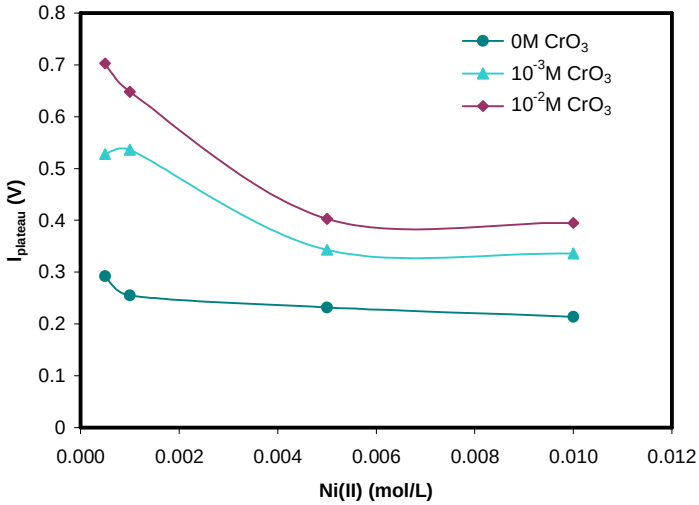

Fig. 4.98. Effect of the electrolyte concentration on the $I_{plateau}$ values obtained for mixtures of $NiSO_4$ and CrO_3.

This effect is attenuated as the amount of Ni^{2+} ions increases in the electrolyte and the participation of Ni^{2+} ions in the transmembrane current transfer gains importance. The negative influence of H^+ ions on the onset of electroconvection was also reported by Choi et al. [102]. In that case, it was found that the plateaus of the current-voltage curves obtained for HCl solutions were significantly larger than those obtained for chlorides of metal ions. These results could be also explained by considering the Stokes radius of H^+ ions, which is 0.026 nm, and therefore, considerably lower than those reported in Table 4.13 for heavy metal ions. When a certain electric noise initiates the destabilization of the electric field and sets in motion the first counterion molecule in the diffusion boundary layer, the propagation of the electroconvective vortices is more likely to occur for weaker electric fields when ions of greater size are involved. In this regard, Fig. 4.99 shows the hydrated shell of Ni^{2+} ions, which includes six surrounding molecules of water. It is consistent to think that a small perturbation to an ion with large hydration spheres would imply the collision of this ion with a considerable amount of surrounding fluid, thus involving the motion of greater fluid volumes and leading to an easy propagation of the electroconvective vortices. On the contrary, when the size of the counterion is much smaller, the initial instabilities would be more easily mitigated, hence being necessary the application of stronger electric fields in order to initiate the chaotic distortion of the diffusion boundary layer by the electroconvective vortices.

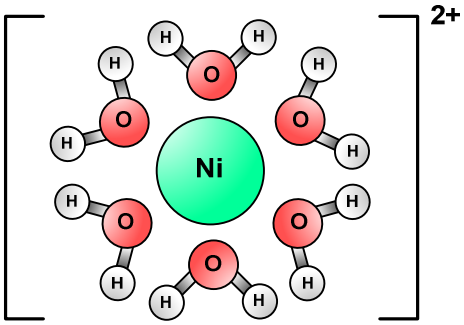

Fig. 4.99. Schematic representation of the hydration shell of Ni^{2+} ions giving rise to the hexaaquo $[Ni(H_2O)_6]^{2+}$ ions.

In addition to the lower Stokes radius of H^+ ions, the abnormal transport properties of H^+ ions have also been pointed out as the reason for the large $l_{plateau}$ values obtained for increasing concentrations of H^+ ions. Protons are mainly transported by "tunneling" from one water molecule to another according to the Grotthuss mechanism. Fig. 4.100 shows a schematic representation of the Grotthuss mechanism of proton conduction in aqueous solutions. An excess proton diffuses through the network of water molecules by forming and breaking bonds with associated water molecules. This mechanism is in part responsible for the higher proton mobility and conductivity of H^+ ions [108]. In addition, under the imposition of an electric field the molecules of water become polarized and the ion conduction increases notably. However, as can be seen in Fig. 4.100 the transport of H^+ ions in aqueous solutions by means of the Grotthuss mechanism does not involve the settling of large volumes of fluid in motion, hence delaying the commencement of electroconvective vortices. In addition, the H^+ ions also force the salt counterions out of the space charge region, which hampers electroconvection [78,91,109]. As a result, the disruption of the diffusion boundary layer is more difficult and the resistance of the membrane system remains high until significantly strong electric fields are applied to the system. This effect can be clearly seen from the results presented for the mixtures of $NiSO_4$ and CrO_3 in Fig. 4.98: as the $[Ni^{2+}]/[H^+]$ ratio increases, the presence of H^+ ions in the space charge region should be lower, thus leading to shorter $l_{plateau}$ values.

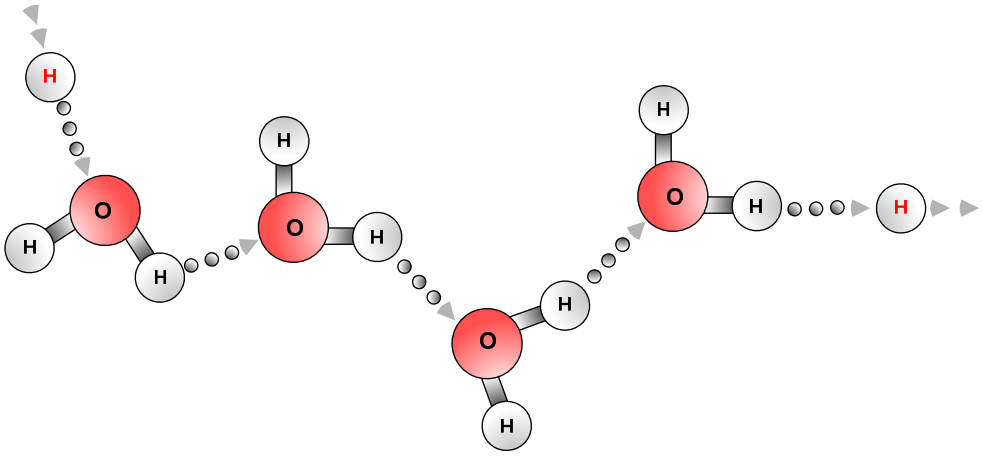

Fig. 4.100. Grotthuss mechanism of proton conduction in aqueous solutions.

In summary, from the results above presented we can conclude that the application of overlimiting currents can be more or less advantageous in terms of energy consumption depending on the composition of the electrolyte. The achievement of overlimiting currents occurs at the expense of an extra energy input to the membrane system, which is substantially reduced when heavy metal cations participate in the hydrodynamic destabilization of the diffusion boundary layers. On the contrary, high concentrations of H^+ ions in the electrolyte hinder the overlimiting coupled convection, which requires higher membrane voltage drops in order to become important.

The obtained results could have important practical implications in the treatment of metal containing effluents. As commented above, in electrodialysis it is desired to achieve fast desalination rates for the minimum operating times and membrane areas. Therefore, the use of overlimiting currents could be advantageous if the energy efficiency of the process is maintained above a certain threshold. Accordingly, in order to achieve a good management of industrial waste effluents, their composition and the ions involved in the concentration polarization mechanisms should deserve special attention. However, in order to decide when a spent industrial bath has to be treated and regenerated and which current is the optimum, other operating parameters are also important, such as the changes of conductivity, the fouling of the membranes or the electrode reactions. Consequently, the use of overlimiting currents in long-term experiments will be addressed in the following section (section 4.4).

4.3.6 Conclusions

In this Chapter, the mechanisms of overlimiting current transfer through ion-exchange membranes have been investigated by comparing the different chronopotentiometric responses and current-voltage curves obtained in sections 4.1 and 4.2. The predominance of each mechanism of overlimiting conductance has been evaluated as a function of the electrolyte composition. The main conclusions related to the dissociation of water in membrane systems are summarized below:

- The dissociation of water is in general insignificant for the systems formed by Nafion 117 membranes with different metallic solutions, unless the formation of precipitates at the membrane surface occurs. This behavior has been contrasted by measuring the pH variations in the compartments of the electrodialysis cell and by contrasting the chronopotentiometric features detected in the curves. The formation of metal hydroxides occurred with concentrated solutions of $NiSO_4$ and $Fe_2(SO_4)_3$.

- The formation of precipitates is associated with a gradual increase of U_m with time in the chronopotentiometric curves. The precipitate layers increase the resistance of the membrane, which leads to current-voltage curves with extended plateaus.

- The relaxation of the membrane after the application of current gives a hint about the catalytic dissociation of water occurred at the bipolar interface between the precipitate layers and the membranes. When catalytic water splitting occurs, a plateau is formed in the relaxation profile of the membranes due to the hindered recombination of H^+ and OH^- ions. Longer plateaus, associated with higher water splitting rates, were obtained with more diluted solutions and at higher current densities.

- The conformation and morphology of the precipitates affects the ion transport trough the membranes. $Fe(OH)_3$ precipitates were very compact and were also formed in the internal membrane matrix, thus causing a blockage of pores and leading to current-voltage curves without overlimiting region. On the other hand, $Ni(OH)_2$ precipitates were granulated and did not imply the blockage of

the membrane pores. The current-voltage curves obtained for the membranes with $Ni(OH)_2$ precipitates showed flat extended plateaus followed by an overlimiting region of rapid current growth, which was attributed to the accelerated water splitting.

The main conclusions related to coupled convective phenomena are the following:

- Both gravitational convection and electroconvection are responsible for the overlimiting conductance of the membrane/electrolyte systems investigated. Whereas electroconvection is more significant in diluted solutions, gravitational convection predominates in concentrated ones. Furthermore, both types of convection can coexist at high electrolyte concentrations and current densities.

- The relative effect of both gravitational convection and electroconvection can be evaluated by representing the values of $(U_{m,max} - U_{m,f})$ against the i/i_{lim} ratio. In $Cr_2(SO_4)_3$ solutions, the decrease of the thickness of the boundary layer due to gravitational convection already occurs at i/i_{lim} values close to 1. However, the role of electroconvection predominates for values of i/i_{lim} higher than 2. In the case of $NiSO_4$, electroconvection is more important in relation to gravitational convection, and the values of $(U_{m,max} - U_{m,f})$ become scattered at values of i/i_{lim} higher than 2.

- Increasing concentrations of metal ions led to shorter $I_{plateau}$ values. This trend proves the enhancement of overlimiting currents by heavy metal ions having large Stokes radius. The emergence of gravitational convection for low $I_{plateau}$ values could stem from the fact that the density gradients generated in electrodialysis cells are higher in the case of heavy metal ions. With regard to the anticipated onset of electroconvective vortices, the larger Stokes radius of heavy metal ions involves the motion of larger fluid volumes, hence contributing to the initiation of chaotic electroconvective vortices for lower $I_{plateau}$ values.

- An increase in the concentration of H^+ ions has the opposite effect of an increase in the concentration of heavy metal ions, since the $I_{plateau}$ values increase notoriously with the concentration of CrO_3. The Grotthuss mechanism of proton conduction in aqueous systems seems to be the reason for these results. This

mechanism consists on the proton hopping between neighboring molecules of water, hence not involving the motion of large fluid volumes.

4.4 Effects of the electrolyte composition and the current regime on the performance of electrodialysis

4.4.1 Introduction

In the previous sections (4.1, 4.2 and 4.3) the fundaments of the transport mechanisms of metal ions through cation-exchange membranes have been investigated by means of ion sorption and electrochemical techniques. Nevertheless, despite the useful information that can be easily obtained from the chronopotentiometric results, these experiments have relatively short time duration. For that reason, some important phenomena that could be associated with long-term effects were not taken into account. Therefore, the experiments of the present section (section 4.4), which consist on galvanostatic electrodialysis experiments of 6 h duration, are focused on the corroboration of the previous results and also on elucidating possible long-term effects arising in an electrodialysis cell. Some of these effects could be the gradual change in the electrolyte conductivity as the desalting compartments become more diluted, or the possible formation of precipitates. Moreover, these experiments would serve as a tool to assess the practical viability of applying overlimiting currents, since the rates of transport of electrolyte counterions will be measured experimentally.

The system composed of mixture solutions of $NiSO_4$ and CrO_3 has been selected for conducting this study because it allows us to simultaneously investigate the competitive ion transport through the membrane in mixture solutions and the effects of the current regime on the electrodialysis performance. With regard to the membrane selectivity, the study conducted in section 4.2.2 with mixtures of $NiSO_4$ and CrO_3 showed that the transport number of Ni^{2+} ions through the membrane decreases as the concentration of CrO_3 increases in relation to that of $NiSO_4$. With the galvanostatic experiments of longer duration we want to confirm the previous results about the membrane selectivity, evaluate possible changes in the membrane selectivity with time as the diluted compartment becomes depleted and investigate any long-term effects that could arise during the course of electrodialysis operations.

With regard to the mechanisms of overlimiting current transfer, the chronopotentiometric study performed in section 4.3 showed that electroconvection was the mechanism of overlimiting mass transfer that predominates with mixtures of $NiSO_4$

and CrO_3. Moreover, it was observed that the electrolyte composition has a meaningful effect on the overlimiting membrane current transfer, since the overlimiting currents were activated for low membrane voltage drops in the case of solutions having a high concentration of heavy metals and a low concentration of H^+ ions. With the experiments planned in this section we aim to evaluate the effects of the mass transfer regime on the performance of an electrodialysis process by taking into account long-term operational effects that could arise during galvanostatic experiments. Moreover, the convenience of applying overlimiting currents would be assessed by means of calculating energy-related indicators, such as the current efficiency of the Ni^{2+} transport through the membrane or the energy consumption of the electrodialysis cells. In relation to this, some relevant characteristics and parameters previously obtained for the solutions considered in the present section are indicated in Table 4.14.

Table 4.14. Composition of the solution mixtures selected for the galvanostatic experiments and values of the current-voltage parameters for each solution composition.

$[NiSO_4]$	$[CrO_3]$	i_{lim} (mA·cm^{-2})	$I_{plateau}$ (V)	pH_o	$[Ni^{2+}]/[H^+]$
10^{-3}M	0 M	0.064	0.255	6.40	2036.61
	10^{-3}M	0.255	0.536	2.99	1.08
	10^{-2}M	3.260	0.648	2.00	0.09
10^{-2}M	0M	0.850	0.214	5.80	1874.33
	10^{-3}M	1.130	0.336	3.06	6.34
	10^{-2}M	4.240	0.395	2.05	0.61

According to the different objectives, the structure of this section (4.4) is organized as follows:

- First, the selectivity of the membranes in the underlimiting range of currents is evaluated. In order to analyze the effect of the concentration of CrO_3 on the transport of Ni^{2+} ions through the Nafion 117 membrane, the same value of applied current density is applied to treat solutions of a constant concentration of $NiSO_4$ and varying concentrations of CrO_3. In this case, the most restrictive i_{lim} was considered.

- Subsequently, the potential of electrodialysis operations is also studied. Since the i_{lim} values strongly depend on the concentration and composition of the electrolyte, experiments at 75%·i_{lim} were conducted with the different solutions.

These results would allow us to investigate the mass transfer rates that could be achieved in mixture solutions of $NiSO_4$ and CrO_3 within the underlimiting range of currents.

- Finally, the effect of applying overlimiting currents was investigated. For this purpose, several experiments were carried out at current densities corresponding to 75%, 100% and 125% of the i_{lim} value of each solution composition. The transfer of Ni^{2+} ions through the cation-exchange membrane is measured in order to ascertain if the application of currents above the i_{lim} implies an increase of the mass transfer rates of electrolyte counterions through the membranes. Finally, the convenience of applying overlimiting currents would be evaluated taking into account energy-related indicators such as the current efficiency for the transport of Ni^{2+} ions through the membranes, or the specific energy consumed in the transport of Ni^{2+} ions.

The experimental conditions and the setup used to conduct the galvanostatic experiments were schematically shown in section 3.6 of Chapter 3 (Fig. 3.10). In order to evaluate the energy consumption of the process, the cell voltage (U_{cell}) measured between the anode and cathode was registered. According to the values of i_{lim} obtained for each solution composition (Table 4.14), and the range of applied current densities that were planned for this section (Table 3.5), the values of current density applied in the experiments are summarized in Table 4.15.

Table 4.15. Values of current densities applied during the galvanostatic experiments of 6 h duration.

$[NiSO_4]$	$[CrO_3]$	Effect of CrO_3 on the transport of Ni^{2+} ions at underlimiting currents	Effect of the current regime on the transport of Ni^{2+} ions		
10^{-3}M	0M	0.048 mA·cm^{-2}	0.048 mA·cm^{-2}	0.064 mA·cm^{-2}	0.080 mA·cm^{-2}
	10^{-3}M		0.191 mA·cm^{-2}	0.255 mA·cm^{-2}	0.319 mA·cm^{-2}
	10^{-2}M		2.445 mA·cm^{-2}	3.260 mA·cm^{-2}	4.075 mA·cm^{-2}
10^{-2}M	0M	0.638 mA·cm^{-2}	0.638 mA·cm^{-2}	0.850 mA·cm^{-2}	1.063 mA·cm^{-2}
	10^{-3}M		0.848 mA·cm^{-2}	1.130 mA·cm^{-2}	1.413 mA·cm^{-2}
	10^{-2}M		3.180 mA·cm^{-2}	4.240 mA·cm^{-2}	5.300 mA·cm^{-2}

4.4.2 Effect of the electrolyte composition on the membrane behavior at underlimiting currents

4.4.2.1 Electrodialysis performance with different compositions at a constant current

First, the applied current was selected in order not to exceed the i_{lim} value and minimize possible parasitic processes which could reduce the current efficiency for the nickel removal. In this manner, the competing transport through the cation-exchange membrane between Ni^{2+} and H^+ ions can be studied for varying concentrations of $NiSO_4$ and CrO_3. For the experiments carried out with 10^{-2} M $NiSO_4$ solutions and different CrO_3 concentrations the current density was set to 75% of the i_{lim} obtained with the single salt solutions of 10^{-2} M $NiSO_4$ (0.85 mA·cm^{-2}), as this was the most restrictive value of i_{lim} calculated for this group of compositions. Thus, the effect of CrO_3 on the nickel removal is studied under a constant value of applied current density. The same criterion was used for the experiments carried out with 10^{-3} M $NiSO_4$ solutions and different CrO_3 concentrations (in this case the most restrictive i_{lim} was 0.064 mA·cm^{-2}).

Fig. 4.101 shows the evolution with time of the parameters measured during the experiments conducted with 10^{-2}M $NiSO_4$ solutions and varying CrO_3 concentrations. As expected, the concentration of Ni^{2+} ions in the central compartment of the electrodialysis cell decreases with time (Fig. 4.101(a)). However, for a constant concentration of $NiSO_4$, the increase in the initial CrO_3 concentration leads to a decrease of the transport of Ni^{2+} ions through the membrane. On the contrary, the values of cell voltage (U_{cell}) decrease with the increase of the CrO_3 concentration (Fig. 4.101(b)), which is mainly caused by the higher conductivity of the electrolyte. The values of U_{cell} show a slightly increasing evolution with time, which stems from the decrease of conductivity in the central compartment, where the concentration of cations (H^+ and Ni^{2+}) and anions ($Cr_2O_7^{2-}$, CrO_4^{2-}, $HCrO_4^-$, SO_4^{2-}) decreases as they are transported through the cation- and anion-exchange membrane, respectively. The results corresponding to 10^{-3}M $NiSO_4$ solutions and varying concentrations of CrO_3 are presented in Fig. 4.102. In this case, the parameters show similar trends than those observed for 10^{-2}M $NiSO_4$ solutions.

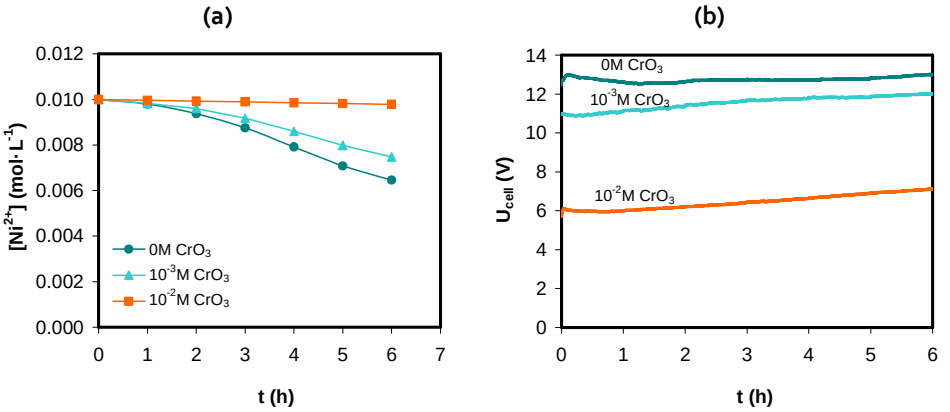

Figure 4.101. Results obtained with 10^{-2}M $NiSO_4$ solutions and varying concentrations of CrO_3 under the application of a current density of 0.638 mA·cm^{-2}. (a) Evolution of the concentration of Ni^{2+} ions in the central compartment and (b) evolution of the cell voltage.

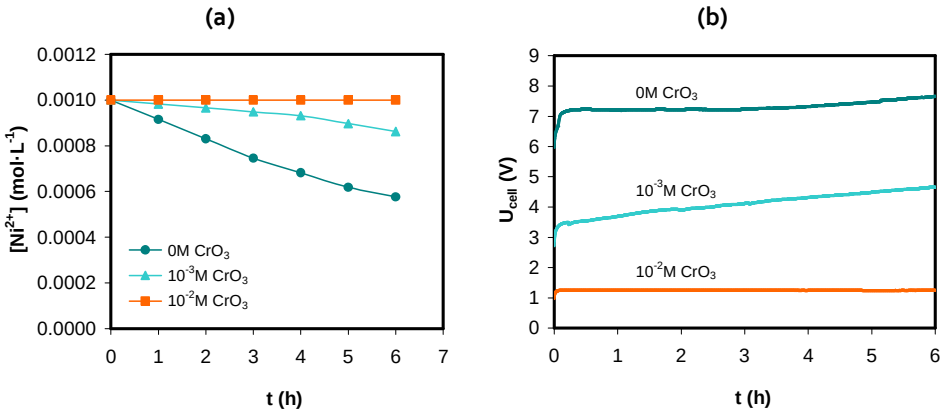

Figure 4.102. Results obtained with 10^{-3}M $NiSO_4$ solutions and varying concentrations of CrO_3 under the application of a current density of 0.048 mA·cm^{-2}. (a) Evolution of the concentration of Ni^{2+} ions in the central compartment and (b) evolution of the cell voltage.

In order to evaluate the performance of the electrodialysis cell, the variables measured in the experiments ([Ni^{2+}] and U_{cell}) were used to calculate the figures of merit of each galvanostatic operation, namely: the fractional conversion or removal degree of Ni^{2+} ions in the central compartment, X, (Eq. (3.9)), the current efficiency for the transport of Ni^{2+} ions through the membrane, ϕ, (Eq. (3.10)), the space-time yield, η, (Eq. (3.11)), and the specific energy consumption inverted to transport each gram of Ni(II) through the membrane, E_s, (Eq.(3.12)). The evolution of the nickel removal rate with time for each group of three experiments is presented in Fig. 4.103. On the basis of the constant ionic transfer dictated by the same value of applied current, the experimental results shown in Fig. 4.103(a) corroborate the negative effect of CrO_3 on the transfer of cationic nickel through the membrane. After six hours of galvanostatic electrodialysis with 10^{-2}M $NiSO_4$ solutions in the absence of CrO_3, 35% of the initial Ni(II) can be removed from the central compartment. Conversely, the presence of CrO_3 with a concentration of 10^{-3}M involves a reduction of the removal degree to a value lower than 25%. Moreover, if the initial CrO_3 concentration reaches the concentration of $NiSO_4$ (i.e.: 10^{-2} M CrO_3), the transfer of Ni^{2+} through the membrane is practically disabled due to the higher concentration of H^+ ions. When the concentration of $NiSO_4$ is 10^{-3} M (see Fig. 4.103(b)), if solutions without CrO_3 are considered, the rate of removal took the value of 42% at 6 hours. The similar values of removal degree for different $NiSO_4$ concentrations in the absence of CrO_3 is justified by the increase in the i_{lim} values and therefore of the applied current with the electrolyte concentration. Looking at the same graphic, if a concentration of chromic acid of 10^{-3}M is

reached, the nickel removal rate decreases to 14%. Finally, with an increase of the concentration of chromic acid to 10^{-2}M, the removal rate is reduced practically to zero, as occurred with 10^{-2}M $NiSO_4$ solutions. Nevertheless, the effect of the chromic acid concentration on the evolution of the nickel removal rate is more notorious in the case of 10^{-3}M $NiSO_4$ solutions. This difference is due to the competition of H^+ with Ni^{2+} ions, which is more meaningful when the content of protons reaches or exceeds that of the Ni^{2+} ions.

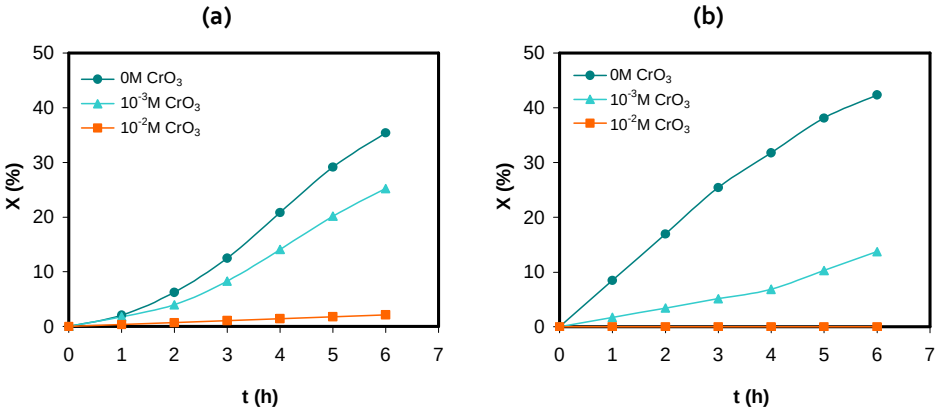

Figure 4.103. Nickel renoval rate (X) vs. time for different CrO_3 concentrations in (a) 10^{-2}M $NiSO_4$ solutions (i = 0.638 mA·cm^{-2}) and (b) 10^{-3}M $NiSO_4$ solutions (i = 0.048 mA·cm^{-2})

The results of current efficiency calculated from the previous experiments are shown in Fig. 4.104. With 10^{-2}M $NiSO_4$ solutions, the values of current efficiency decrease gradually with the increase of the chromic acid concentration (Fig. 4.104(a)). The values of ϕ obtained with 10^{-3}M $NiSO_4$ solutions follow the same dependence with the chromic acid concentration (Fig. 4.104(b)). For this nickel sulfate concentration the current efficiency abruptly decreases with the concentration of chromic acid: it decreases from a value of 80% in the absence of CrO_3 to values around 20% with 10^{-3}M CrO_3 solutions and reaches zero with a concentration of CrO_3 of 10^{-2}M. The reduction in the ϕ values with increasing concentrations of CrO_3 is consequence of the reduced transport of Ni^{2+} ions as more protons are transferred through the membrane. Apart from this, if solutions without CrO_3 are compared, the change of $NiSO_4$ concentration from 10^{-2}M to 10^{-3}M implies an increase in the current efficiency from 40% to 80%. The reduction in the current efficiency with the nickel sulfate concentration could be explained in terms of a reduction of the passage of the ions of interest through the membrane due to a diminished exclusion of

SO_4^{2-} ions. In fact, it is reported that the repulsion of coions by the membrane fixed charges decreases with the electrolyte concentration and implies a decreased transport of counterions [2,15,110]. Moreover, these results are in congruence with the decreasing trend of $T_{Ni^{2+}}$ with the increase in the electrolyte concentration calculated in section 4.2 (see Fig. 4.57). In addition to the weakened coion exclusion occurring at increasing electrolyte concentrations, in the case of nickel sulfate solutions, the recombination of Ni^{2+} ions with SO_4^{2-} ions to form the complex specie $NiSO_4$ is enhanced at high electrolyte concentrations. This complex specie, without a net charge, could be also responsible for the reduction of the transport of Ni^{2+} ions through the membrane. Besides this, the increasing evolution of ϕ values with time in most of the cases reveals a reduction of the hindrance of the transport of Ni^{2+} ions originated by the decrease in the concentration of SO_4^{2-} ions with time in the central compartment. As more SO_4^{2-} ions are transported to the anodic compartment, the complex specie $NiSO_4$ dissociates in the central compartment to give Ni^{2+} and SO_4^{2-} ions. Therefore, the higher supply of Ni^{2+} to the depleting surface of the cation-exchange membrane would cause the increasing values of ϕ with time obtained in Fig. 4.104(a).

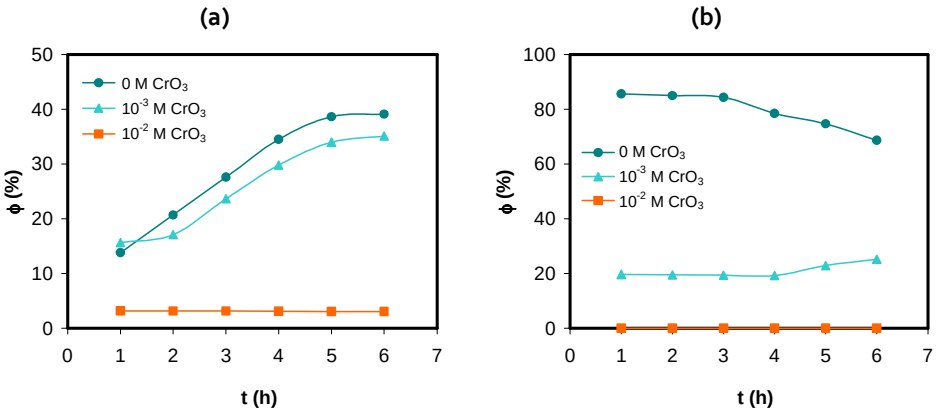

Figure 4.104. Current efficiency of nickel (ϕ) vs. time for different CrO_3 concentrations in (a) 10^{-2}M $NiSO_4$ solutions (i = 0.638 mA·cm^{-2}) and (b) 10^{-3}M $NiSO_4$ solutions (i = 0.048 mA·cm^{-2})

The values of space-time yield and specific energy consumption are depicted in Figs. 4.105 and 4.106, respectively. The space-time yield is generally higher in the case of 10^{-2}M $NiSO_4$ solutions, as expected since the values of applied current are higher because the i_{lim} increases with the electrolyte concentration. Furthermore, in Fig. 4.105 an increasing trend of η with time shown in some curves confirms the major importance of the

presence of the complex specie $NiSO_4$ and SO_4^{2-} ions in the case of solutions in which the concentration of $NiSO_4$ is higher. In these cases, the reduction with time of the SO_4^{2-} ion concentration in the central compartment allows for a higher selectivity of the membrane for Ni^{2+} ions with the course of the experiment.

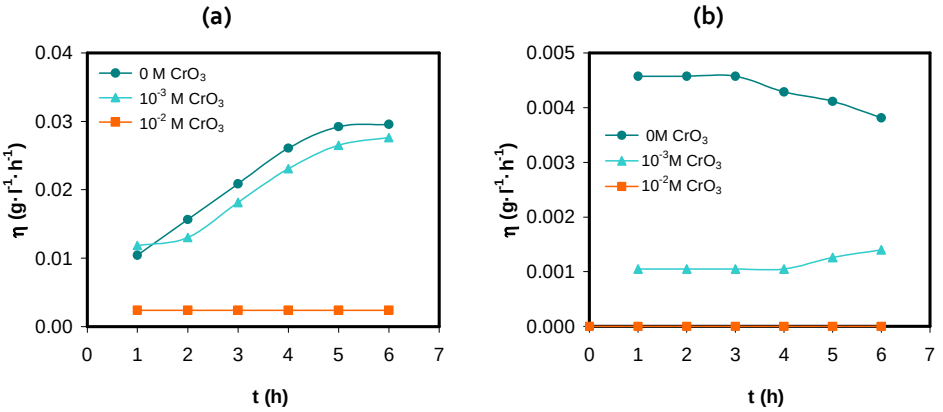

Figure 4.105. Space-time yield of nickel (η) vs. time for different CrO_3 concentrations in (a) 10^{-2}M $NiSO_4$ solutions (i = 0.638 mA·cm^{-2}) and (b) 10^{-3}M $NiSO_4$ solutions (i = 0.048 mA·cm^{-2})

With regard to the specific energy consumption, from Fig. 4.106 it is seen that the removal of nickel requires less energy in the case of low $NiSO_4$ concentrations, which is in concordance with the lower values of current that have to be applied for these solutions to work in the underlimiting range. This is also a consequence of the lower U_{cell} values registered for 10^{-3}M $NiSO_4$ with respect to the values registered for 10^{-2}M $NiSO_4$ solutions. With 10^{-2}M $NiSO_4$ solutions, around 30 kW·h/kg are consumed when the chromic acid concentration is below 10^{-3}M. For an increase in the concentration of CrO_3 to 10^{-2}M the specific energy grows abruptly until values higher than 150 Kw·h/kg. With this parameter it is also observed that 10^{-3}M $NiSO_4$ solutions are much more sensitive to the concentration of CrO_3 in the electrolyte, as the energy becomes almost twofold when changing from 0M to 10^{-3}M CrO_3 solutions and cannot be calculated for a CrO_3 concentration of 10^{-2}M because the transport of Ni^{2+} was insignificant. From the results shown in Fig. 4.106 it is also possible to ascertain which effect is more significant from the dependence of E_s with time, that of the presence of SO_4^{2-} ions or that due to CrO_3. When the influence of the complex $NiSO_4$ in the solution together with the reduced repulsion of SO_4^{2-} ions by the membrane is more meaningful, a descending trend is observed in the curves, since the transport of Ni^{2+} ions increases as the SO_4^{2-} concentration diminishes

with time in the central compartment. However, when the concentration of CrO_3 is higher, the competence of H^+ with Ni^{2+} ions hides the positive effect of a diminishing SO_4^{2-} ion concentration and implies an increasing evolution of the specific energy consumption with time.

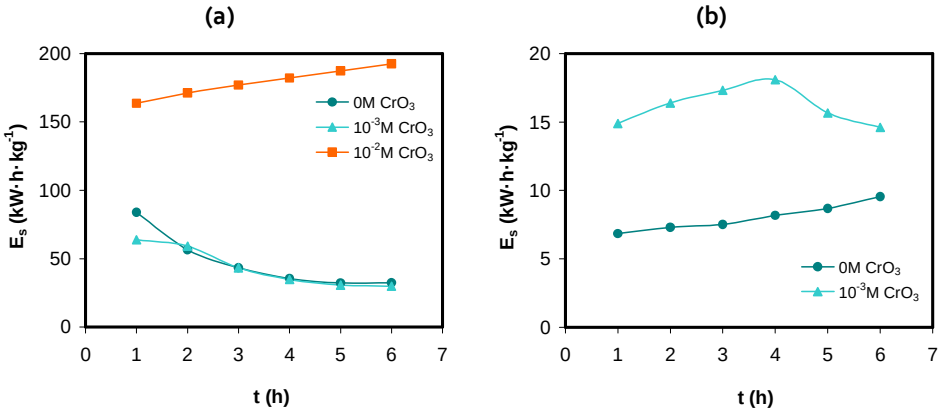

Figure 4.106. Specific energy consumption (E_s) vs. time for different CrO_3 concentrations in (a) 10^{-2}M $NiSO_4$ solutions (i = 0.638 mA·cm^{-2}) and (b) 10^{-3}M $NiSO_4$ solutions (i = 0.048 mA·cm^{-2})

To summarize, it can be concluded that the trends observed in the galvanostatic experiments of 6-hour duration confirm the results of T_{Ni}^{2+} obtained in section 4.2.2.5. The competitive ion transport between Ni^{2+} and H^+ ions determines the efficiency of the removal of Ni^{2+} ions from the central compartment of the electrodialysis cell. This competition takes place in the solution layers next to the membrane due to the higher mobility of H^+ ions ($D_{H^+} = 9.311 \cdot 10^{-5} cm^2 s^{-1}$) in relation to that of Ni^{2+} ions ($D_{Ni^{2+}} = 0.661 \cdot 10^{-5} cm^2 s^{-1}$), which would imply a comparatively higher supply of H^+ ions to the membrane surface when the concentration of both ions in the bulk solution is similar [5]. However, the competing ion transport also takes place inside the membrane phase. As reported in previous studies, the affinity of the fixed charges of Nafion 117 and other cation-exchange membranes for cations increases with their valence, which is known as the valence effect [23,46,47,49]. However, as described in the literature and also reported in the ion uptake experiments presented in section 4.2.2.2 (Figs. 4.42 and 4.43), changes in the pH of the electrolyte also affect the partitioning of Ni^{2+} ions in the membrane [55]. In this respect, the initial pH of the solutions, which is specified in Table 4.14, took values around 3 when the concentration of CrO_3 is 10^{-3}M and values of 2 when

the concentration of CrO_3 increased to 10^{-2}M. Moreover, the decreased partition of Ni^{2+} ions in the membrane phase as a consequence of the increased concentration of H^+ ions could be aggravated as the rate of supply of ions to the membrane is altered due to the development of concentration polarization resulting from the application of current.

4.4.2.2 Electrodialysis performance at 75%·i_{lim} for each solution composition

In order to contrast the potential of the electrodialytic treatment of metal containing effluents of different compositions, additional galvanostatic experiments of 6 h were performed with an imposed current density of 75% of the i_{lim} obtained for each electrolyte. By comparing the obtained results it is possible to elucidate which composition leads to better electrodialytic performance within its corresponding underlimiting range of currents. It must be noted that the experiments with the mixtures of 10^{-3}M $NiSO_4$ and 10^{-2}M CrO_3 could not be performed because the high electrical resistance of the cell at the corresponding applied current implied very high U_{cell} values, which exceeded the bearable conditions of the galvanostat.

In Fig. 1.107 the evolution of the removal degree of Ni^{2+} with time is depicted for each experiment. The results show that applying a constant current equal to 75% of the i_{lim} corresponding to each solution makes possible an increase of the passage of Ni^{2+} ions through the membrane with respect to the experiments of the previous section. Especially significant are the cases of 10^{-2}M CrO_3 solutions, where the passage of Ni^{2+} through the membrane was inappreciable when the applied current was 75% of the i_{lim} corresponding to the single salt solutions without CrO_3. The removal degree increases with the presence of CrO_3 in the composition of the solutions because the range of limiting currents increases with the presence of this species. In this respect, removal rates close to 80% were obtained with solutions having the same concentration of $NiSO_4$ and CrO_3.

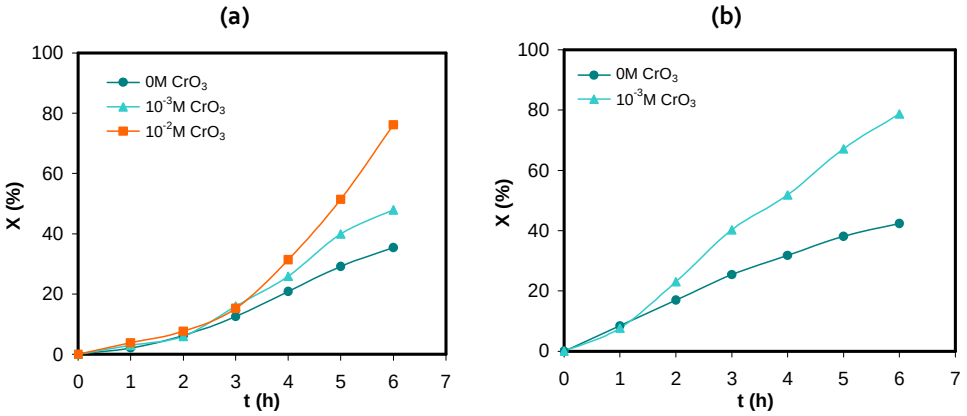

Figure 4.107. Nickel removal rate (X) vs. time for different CrO_3 concentrations in (a) 10^{-2}M $NiSO_4$ solutions and (b) 10^{-3}M $NiSO_4$ solutions. (The applied current corresponds to $0.75 \cdot i_{lim}$ en each case)

The rest of figures of merit obtained from these experiments are shown in Figs. 4.108-4.110. As the concentration of CrO_3 increases, ϕ values decrease because an important portion of current is employed to transfer H^+ ions through the membrane. This decrease is less important in the case of 10^{-2}M $NiSO_4$ solutions (Fig. 4.105(a)), because Ni^{2+} ions are the predominant specie both in the solution and inside the membrane. As expected, the increase of the removal rates resulting from applying higher currents with solutions containing CrO_3 is achieved at the expense of lower values of ϕ. Nevertheless, the values of current efficiency are very similar to those obtained previously in the section 4.4.2.1, as it was expected, since in both cases underlimiting currents were imposed. Furthermore, in most cases the current efficiency increases with time due to the decrease of the concentration of coions in the central compartment and also due to the faster passage of H^+ ions compared to that of Ni^{2+} ions. Since protons are more mobile than Ni^{2+} ions, their passage takes place at shorter times. Therefore, at increasing times the transport of Ni^{2+} ions to the membrane surface would predominate, thus causing the improvement of the current efficiency with time.

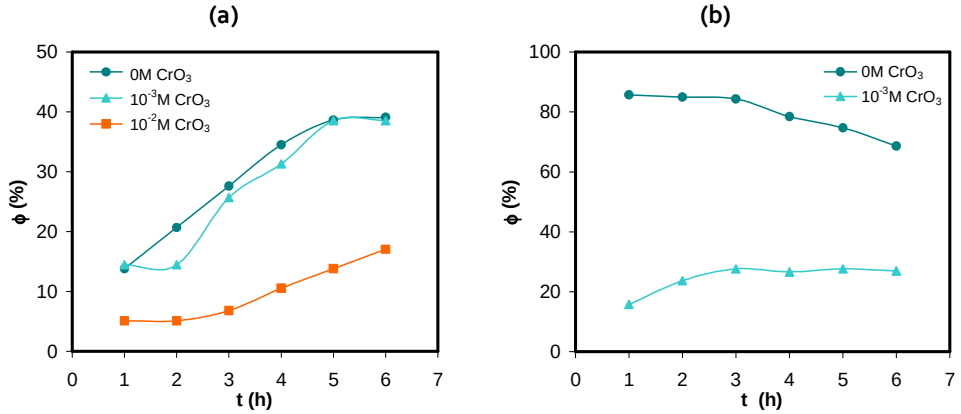

Figure 4.108. Current efficiency of nickel (ϕ) vs. time for different CrO_3 concentrations in (a) 10^{-2}M $NiSO_4$ solutions and (b) 10^{-3}M $NiSO_4$ solutions. (The applied current corresponds to $0.75 \cdot i_{lim}$ en each case)

With regard to the results of space-time yield (Fig. 4.109), the η values increase with the concentration of both $NiSO_4$ and CrO_3, which is basically derived from the different applied currents, which are determined by the i_{lim} values obtained previously for each composition. Since the i_{lim} values increase with the presence of electroactive species that can be transported through the membrane (Ni^{2+} and H^+ ions), the values of η were also expected to increase with the electrolyte concentration.

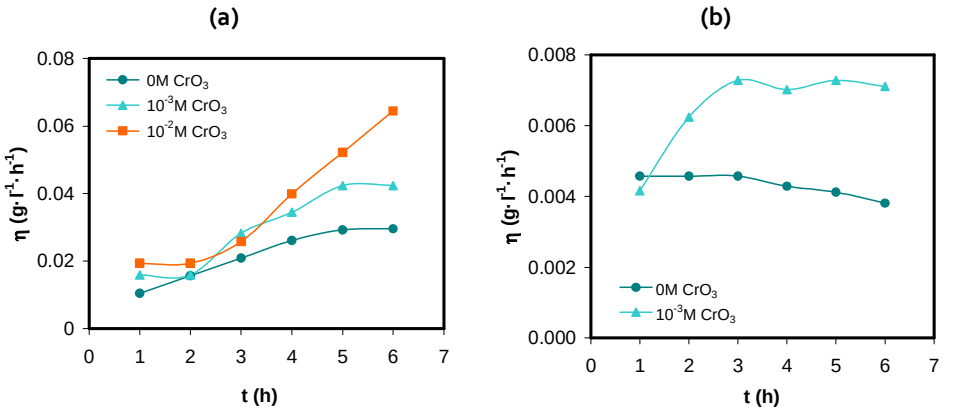

Figure 4.109. Space-time yield of nickel (η) vs. time for different CrO_3 concentrations in (a) 10^{-2}M $NiSO_4$ solutions and (b) 10^{-3}M $NiSO_4$ solutions. (The applied current corresponds to $0.75 \cdot i_{lim}$ en each case)

In terms of specific energy consumption, the values of E_s obtained for solutions with equal concentrations of CrO_3 and $NiSO_4$ increase notoriously with respect to the values obtained in the previous section. For example, E_s values are higher than 100 kW·h/kg with solutions of a concentration of 10^{-2}M of both $NiSO_4$ and CrO_3 (see Fig.4.110(a)) and values higher than 40 kW·h/kg in the case of solutions mixing 10^{-2}M $NiSO_4$ and 10^{-2}M CrO_3 (see Fig. 4.110(b)). Therefore, despite the increase in the values of nickel removal rate and space-time yield with the concentration of species, this occurs at the expense of an additional cost related to increased values of energy consumption. These results are consequence of the high U_{cell} values registered for higher applied currents.

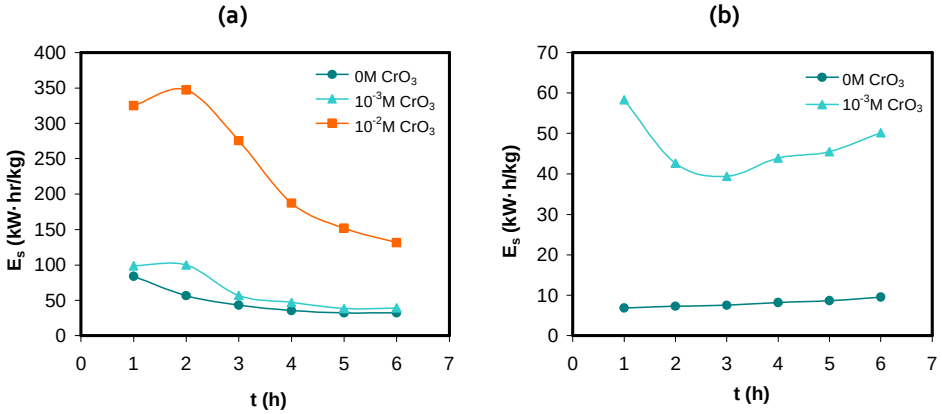

Figure 4.110. Specific energy consumption (E_s) vs. time for different CrO_3 concentrations in (a) 10^{-2}M $NiSO_4$ solutions and (b) 10^{-3}M $NiSO_4$ solutions. (The applied current corresponds to $0.75 \cdot i_{lim}$ en each case)

In general, the results obtained in this section indicate that the potential of electrodialytic recovery of nickel can be increased within the underlimiting range of currents in the case of solutions mixing $NiSO_4$ and CrO_3 because the i_{lim} values are higher for these solutions. In effect, the removal rates of Ni^{2+} are significantly higher than those obtained in the previous section, where lower current densities were applied. Moreover, the current efficiency remained in the same order of magnitude within the underlimiting range of currents. Nevertheless, the increase in the transfer of Ni^{2+} through the membrane implies higher specific energy consumptions, which is related to the higher U_{cell} values registered when higher currents are applied.

4.4.3 Effect of the current regime

Once the effect of the concentration of $NiSO_4$ and CrO_3 on the transference of Ni^{2+} ions through the cation-exchange membrane has been studied under the application of underlimiting currents, the effect of the current regime is also investigated. For this purpose, galvanostatic experiments conducted at values of 75, 100 and 125% of the i_{lim} calculated for each composition were carried out. As occurred in the previous section, the experiments corresponding to the mixture solution of 10^{-3}M $NiSO_4$ and 10^{-2}M CrO_3 could not be conducted because the U_{cell} values were higher than the limits bearable by the galvanostat.

The results obtained with 10^{-2}M $NiSO_4$ solutions are presented as a function of the time of galvanostatic operation in Fig. 4.111. The nickel removal rates (X , Fig. 4.111(a)) increase with the range of applied currents. More specifically, the nickel removal rate reached after the 6 h of operation was 35%, 71% and 83% for increasing values of current density. These results prove that the overlimiting currents are associated with an increase in the transport of the electrolyte counterions (Ni^{2+} ions) through the membrane, even though conditions of intensive concentration polarization may predominate in the depleting diffusion boundary layer. Therefore, coupled convection may be the phenomenon causing an additional supply of Ni^{2+} ions to the membrane at intensive current regimes, whereas the transport of new current carriers (H^+ and OH^- ions resulting from the dissociation of water) would be irrelevant. It has to be pointed out that during the experiments carried out at 75%·i_{lim}, overlimiting current phenomena could also take place at a certain time if the electrolyte concentration in the central compartment decreased to such an extent that the actual i_{lim} would reach the value of the applied current density.

Regarding the evolution of the cell voltage with time; the results show a different evolution of this parameter depending on the current regime. The cell voltage can be considered as the sum of different contributions: the resistance of the solution present in the different compartments, the resistance of the electrodes, the resistance of the ion-exchange membranes and that of the boundary layers next to the membranes. In Fig. 4.111(b) an increase in U_{cell} is observed in every case at different time values. Under the application of 75%·i_{lim}, the cell voltage increases from 13.2 V at two hours of operation to 14.4 V after four hours. However, at overlimiting currents the increase in the cell voltage occurs at the beginning of the experiments. Hence, this important increase in the cell voltage can be mainly attributed to the counterion depletion at the interface between the

membrane and the solution in the central compartment, which originates a solution layer of high electric resistance. After the first increase, the values of cell voltage are stabilized or even decrease with time depending on the applied current. This decrease can be associated with an additional supply of ions to the membrane caused by electroconvection. Specifically, electroconvection would imply the mixing of the depleting boundary layer, hence reducing the resistance of the depleted solution near the membrane. Finally, cell voltage values increase with time at the end of the experiments due to the decrease in the conductivity of the central compartment. This increase in U_{cell} is significantly higher in the case of 125%·i_{lim}, which could be probably due to the formation of precipitates.

The evolution of the current efficiency and specific energy consumption with time obtained for 10^{-2}M $NiSO_4$ solutions is presented in Fig. 4.111(c)-(d). Current efficiency values rise in every case during the duration of the experiments. Nevertheless, the final values of current efficiency are significantly higher in the case of applying currents of 100 and 125%·i_{lim}, reaching an efficiency around 60% in both cases. In contrast, the values of ϕ achieved with underlimiting currents are lower than 40%, which corroborates the positive effect of electroconvection on the process. The formation of electroconvective vortices of higher height when stronger electric fields are applied would be the phenomenon responsible for an increased supply of Ni^{2+} ions from the bulk solution to the membrane. The increased transport of Ni^{2+} ions through the membrane occurring at larger times also implies a decrease of the E_s values, as shown in Fig. 4.111(d). The E_s values obtained for the experiment conducted at underlimiting currents are higher than those obtained at overlimiting currents. However, the values of E_s of the three curves become closer with time, in a range between 20-35 kW·h/kg at the end of the experiments. The difference between the three curves decreases with time because in the case of overlimiting currents the resistance in the central compartment rises more notoriously due to the intensive ion depletion. This entails a significant increase in the U_{cell} values, which attenuates the decrease of E_s, even though their current efficiencies are higher than those achieved at 75%·i_{lim}.

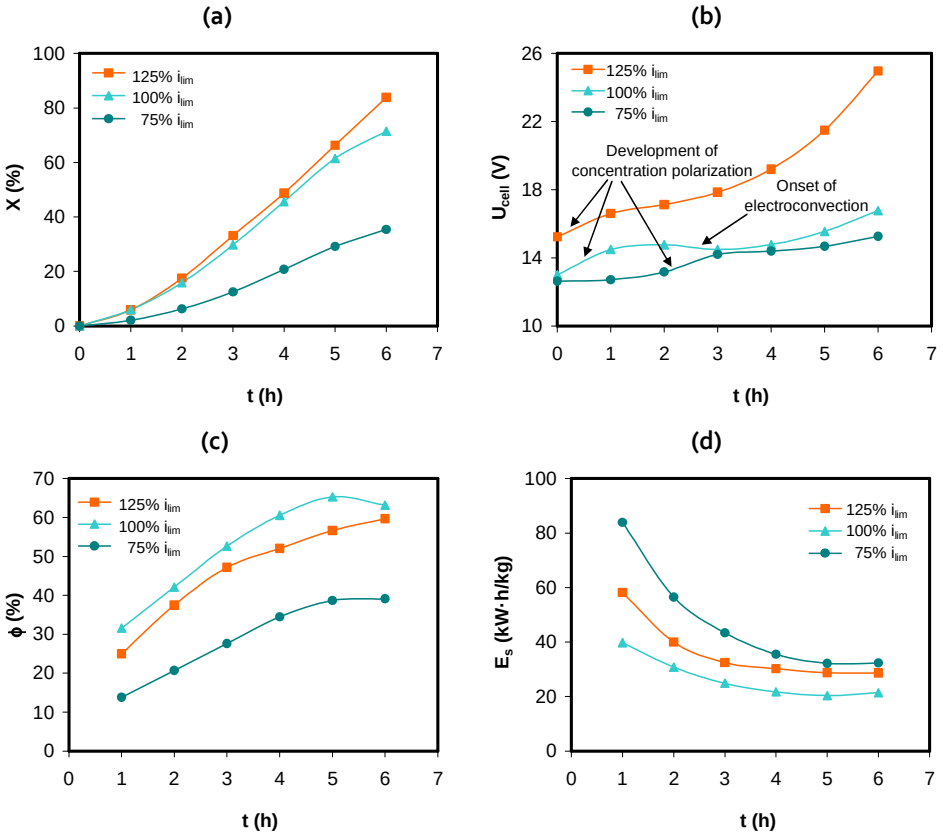

Figure 4.111. Parameters calculated for the experiment conducted with 10^{-2}M $NiSO_4$ solutions at different regimes of applied current. Evolution with time of (a) nickel removal rate, (b) cell voltage, (c) current efficiency of nickel and (d) specific energy consumption.

The results corresponding to mixtures of 10^{-2}M $NiSO_4$ and 10^{-3}M CrO_3 are shown in Fig. 4.112. In this case the nickel removal rate also increases with the applied current, which confirms the positive effect of electroconvection also in mixture solutions containing chromic acid. Moreover, there is a change in the trend of the X values, which increase moderately for the first hours of the experiments, and then (after the second hour) increase more notoriously, maybe due to the positive effect of coupled convection on the transport of Ni^{2+} ions. For the experiments carried out at a current of 75%·i_{lim}, the concentration at which the applied current coincides with the limiting one may also be reached, since a slight increase in the U_{cell} took place after the first two hours. The first increase in U_{cell} is also very slight in the test corresponding to 100%·i_{lim} and appears at the beginning of the experiment, whereas it is unnoticeable in the case of 125%·i_{lim}. Finally,

an additional increase in the U_{cell} values appears in each case at the time when the nickel removal rate reaches a value of 40% (at 5, 4 and 3 h of electrodialysis for 75, 100 and 125%·i_{lim}, respectively), as indicated in Fig. 4.112(a)-(b). The dilution in the central compartment may promote the final increment in U_{cell} because the resistance of the solution in the central compartment rises.

The current efficiency and specific energy consumption (Fig. 4.112(c)-(d)) show the same trend as that observed previously for single salt solutions. The current efficiency increases with time due to the emergence of electroconvection, which leads to decreasing values of E_s with time. The improvement in the transport of Ni^{2+} ions with the applied current density could be caused by the generation of electroconvective vortices of higher height, as already observed in the chronopotentiometric results presented in section 4.3 (see for example Fig. 4.90). However, in contrast to the results obtained in the absence of chromic acid, here the differences between the three curves are small, thus confirming the important role of the electrolyte composition on the magnitude of electroconvection. Electroconvection seems to be enhanced by ions with high hydrated size, such as Ni^{2+} ions, since their motion involves the mixing of large volumes of electrolyte and implies a more important distortion of the diffusion boundary layers. On the contrary, higher concentrations of CrO_3, which provides H^+ to the solution, reduce the increase in the current efficiency associated with the transition from under- to overlimiting regimes. In addition, as already deduced from the current-voltage curves obtained with different electrolyte compositions, the transition to overlimiting currents implies larger membrane voltage drops ($I_{plateau}$) with increasing concentrations of H^+ ions, thus causing the moderate differences registered in Fig. 4.112(d).

As discussed in the previous section (4.3), the different behavior of H^+ and Ni^{2+} ions can be explained by the different transport mechanism showed by protons, since protons are transported in the solution preferentially being exchanged between different water molecules (Grotthuss transport). This kind of transport allows for an increase in the current transfer through the membrane, but does not imply an additional mixing of the diffusion boundary layer. As a consequence, the increase in the current efficiency for the transport of Ni^{2+} ions decreases for lower $[Ni^{2+}]/[H^+]$ ratios, since the lowered predominance of nickel in the solution reduces its implication in the motion of important volumes of solution originated by electroconvective vortices. These results are in congruence with previous studies that proved that electroconvection is facilitated by the presence of ionic species with high Stokes radius, such as Ni^{2+} ions [61,78,102]. However,

high concentrations of H^+ ions force the salt counterions (in this case Ni^{2+}) out of the space-charge region, considerably weakening the electroconvection [78].

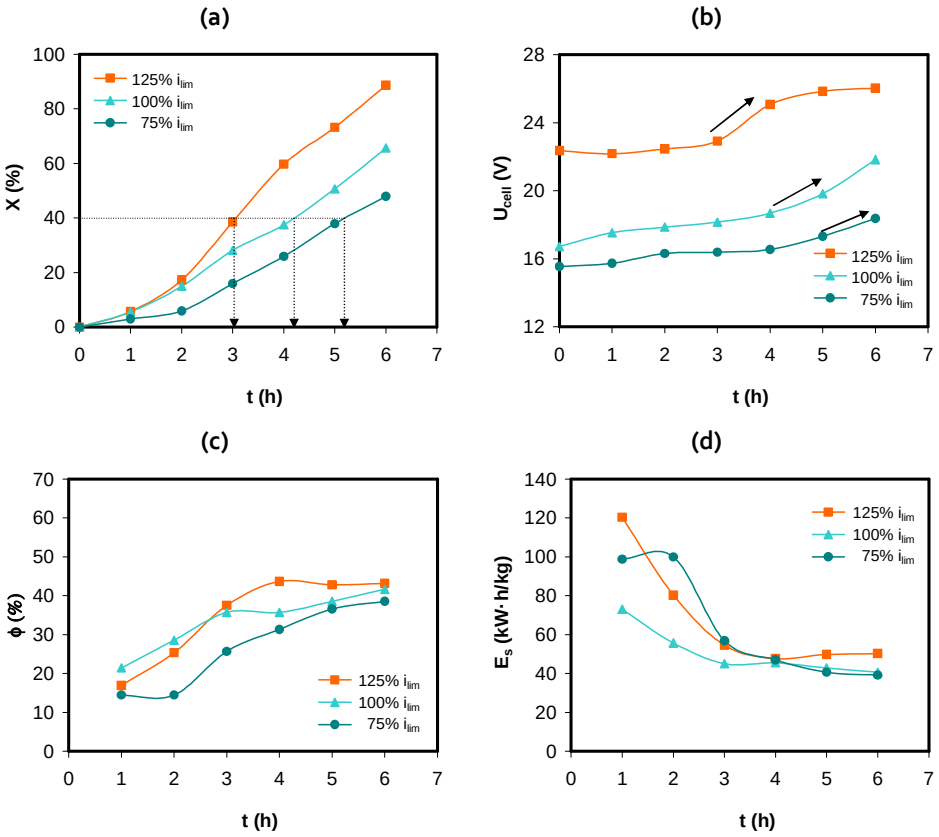

Figure 4.112. Parameters calculated for the experiment conducted with mixtures of 10^{-2}M $NiSO_4$ and 10^{-3}M CrO_3 at different regimes of applied current. Evolution with time of (a) nickel removal rate, (b) cell voltage, (c) current efficiency of nickel and (d) specific energy consumption.

The results obtained with the mixtures of 10^{-2}M $NiSO_4$ and 10^{-2}M CrO_3 are analogous to those shown previously, being consequently omitted for the sake of conciseness. The results obtained with 10^{-3}M $NiSO_4$ solutions are presented in Fig. 4.113. In this case, an improvement of the removal rate at overlimiting current regimes is also observed. In Fig. 4.113(b) the initial sharp increase in U_{cell} associated with the development of important concentration gradients is clearly observed in all the cases. A further increase of the cell voltage occurs immediately for the highest current, whereas in the experiment corresponding to 100%·i_{lim}, U_{cell} even decreases after the second hour of experiment and

only increases at the end of the experiment. For this reason, the difference between the voltage drops in the three experiments is quite significant. These differences result in high values of E_s for overlimiting currents, as shown in Fig. 4.113(d), even though the values of current efficiency are still better for these experiments than for that conducted at 75%·i_{lim} (represented in Fig. 4.113(c)).

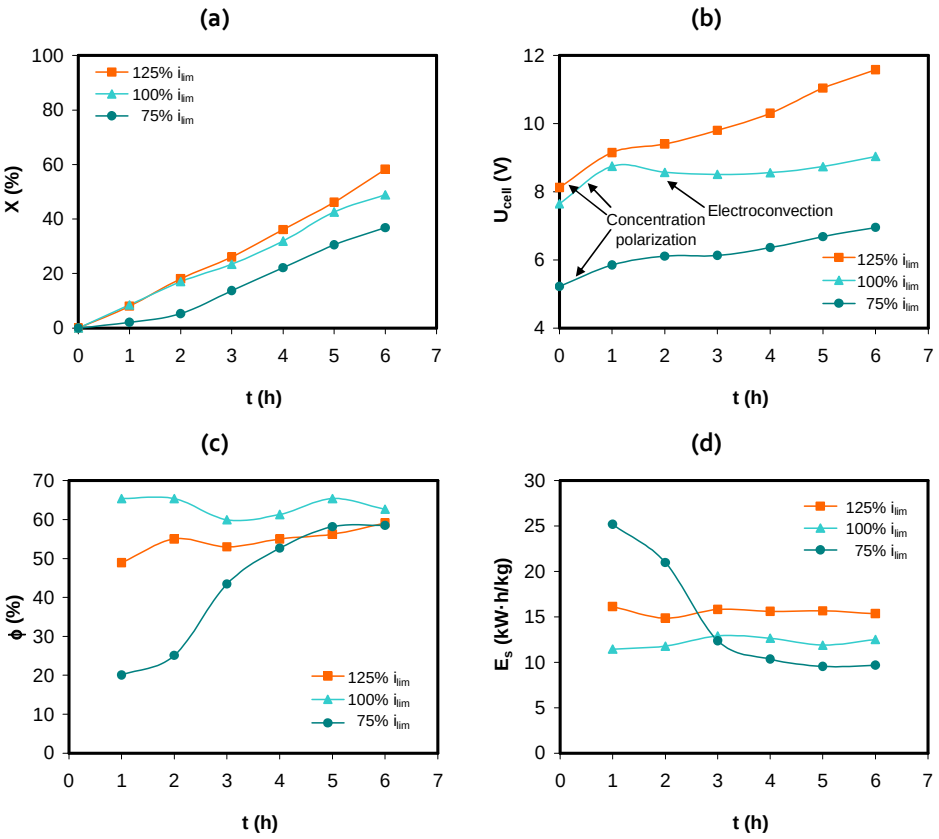

Figure 4.113. Parameters calculated for the experiment conducted with 10^{-3}M $NiSO_4$ solutions at different regimes of applied current. Evolution with time of (a) nickel removal rate, (b) cell voltage, (c) current efficiency of nickel and (d) specific energy consumption.

The experimental results obtained with mixtures of 10^{-3}M $NiSO_4$ and 10^{-3}M CrO_3 are presented in Fig. 4.114. The evolution of X and U_{cell} is similar to that discussed previously for other compositions. Moreover, the fact that currents above the i_{lim} lead to an increase in the transport of nickel across the membrane is verified by the similar values of current efficiency registered in all cases. However, the increase in U_{cell} is much more significant for overlimiting currents, due to the high values of applied current and also to the faster

depletion of ions occurred in the central compartment of the electrodialysis cell. As a consequence of the high voltage cells, the values of E_s obtained for the overlimiting currents were comparatively higher than the values obtained for the underlimiting current (see Fig. 4.114(d)). In addition, the increase in the E_s values with the applied current could be strongly related to the fact that having a major proportion of protons in relation to that of Ni^{2+} ions hampers electroconvection, and therefore the magnitude of the membrane voltage drop associated to the application of overlimiting currents is significantly higher than in the previous experiments where the $[Ni^{2+}]/[H^{+}]$ ratio was higher.

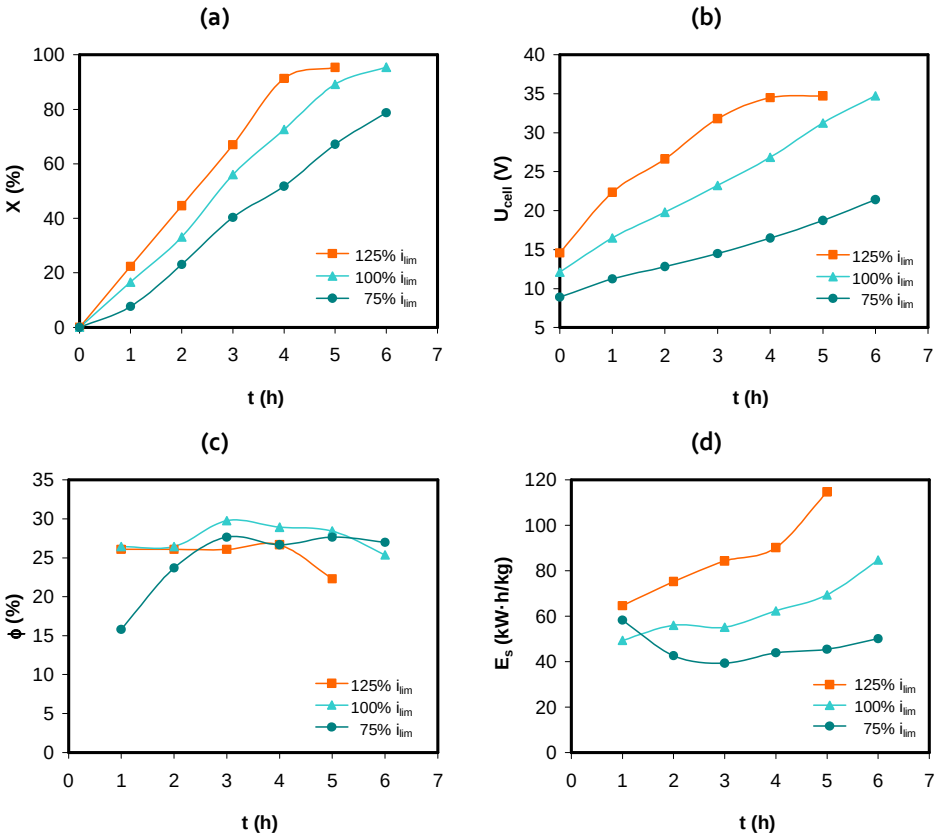

Figure 4.114. Parameters calculated for the experiment conducted with the mixtures of 10^{-3}M $NiSO_4$ and 10^{-3}M CrO_3 at different regimes of applied current. Evolution with time of (a) nickel removal rate, (b) cell voltage, (c) current efficiency of nickel and (d) specific energy consumption.

In general, it has to be pointed out that the fact of imposing currents higher than i_{lim} is not detrimental for the performance of the electrodialytic removal of Ni^{2+} ions for both $NiSO_4$ concentrations. Actually, the results show increased removal rates of Ni^{2+} at intensive currents with respect to those achieved at currents under the i_{lim}, with similar or even better values of current efficiency. The improvement achieved at overlimiting currents is comparatively greater in the case of single salt solutions without chromic acid, showing a general improvement in all the figures of merit. However, when the concentration of chromic acid is high, an increase in the specific energy consumption associated with the imposition of currents above the i_{lim} values makes the application of intensive current regimes less convenient in terms of the energy consumption. These results corroborate the conclusions of section 4.3, thus confirming the positive effect of overlimiting currents applied to solutions containing heavy metal ions. The height of the electroconvective vortices might increase at higher current densities in solutions containing heavy metals, hence implying a greater distortion of the diffusion boundary layers. On the contrary, higher concentrations of H^+ ions hamper electroconvection and imply an important increase in the membrane voltage drop as a result of applying overlimiting currents.

4.4.4 Assessment of the convenience of applying overlimiting currents

In this section, the figures of merit obtained in each galvanostatic experiment of 6 hour duration will be correlated with the current-voltage characteristics obtained in the previous chapters. This would allow us to obtain a general overview of the convenience of applying overlimiting currents and also to identify the trends in the performance of electrodialysis units associated with variations in the electrolyte composition.

In previous studies, the tendency of a specific membrane/electrolyte system to reach the overlimiting regime of currents has been evaluated by means of measuring the length of the plateau region of the current-voltage curves ($l_{plateau}$) [89,102]. Technically, the $l_{plateau}$ of a membrane/electrolyte system is an indicative of the necessary voltage drop that has to be surpassed to change the main transport mechanism in the solution layer near the membrane from diffusion and migration to electroconvection. Thus, short $l_{plateau}$ values have been typically associated with systems in which the onset of electroconvective vortices is enhanced and occurs for low membrane voltage drops. Moreover, large values of $l_{plateau}$, apart from implying high U_{cell} values, could also increase the potential of

generation of water splitting products, since higher electric fields have to be imposed between both sides of the ion-exchange membrane to reach the transition to overlimiting currents. In other words, the region of the current-voltage curves delimited by the i_{lim} and the $I_{plateau}$ (shown schematically in Fig. 4.115 as a shaded region) can be regarded as a measure of the energy dissipated in the membrane region, which is not properly used to increase the transport of electrolyte counterions through the membranes.

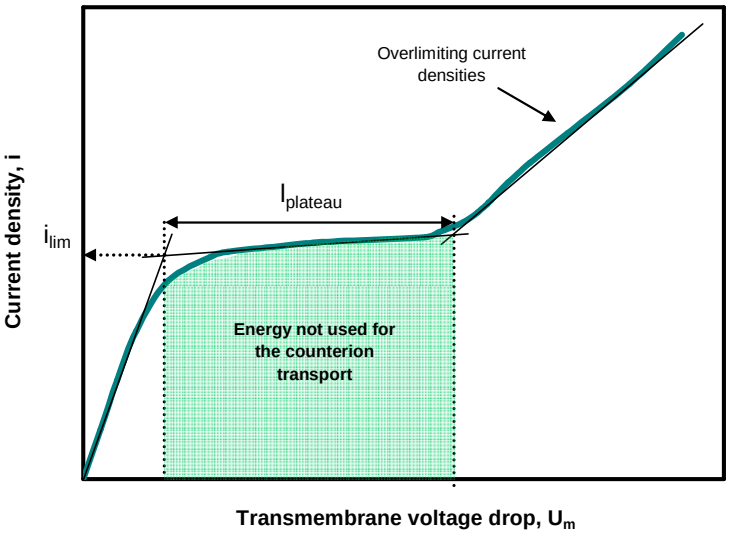

Figure 4.115. Area of the current-voltage curves representing the energy consumed in the membrane region which is not effectively used for the ion transport.

The values of $I_{plateau}$ summarized in Table 4.14 for the different electrolyte composition tested can be represented as a function of the time-weighted mean of current efficiency. The time-weighted mean of current efficiency gives an average value of the current efficiency representative of the behavior of the electrodialysis during the whole duration of the galvanostatic experiments. The time-weighted mean of current efficiency cell can be calculated by means of Eq. (4.80):

$$\overline{\phi} = \frac{\int_0^t \phi(t)dt}{t} \tag{4.80}$$

In the present case, the time considered for the calculations corresponds to the 6 h of duration of the experiments. The $\bar{\phi}$ values are represented as a function of the $I_{plateau}$ in Fig. 4.116. The points linked by vertical lines correspond to experiments carried out at different current regimes for each solution composition. As already deduced from Table 4.14, increasing concentrations of Ni^{2+} and decreasing of H^+ ions in the electrolyte induce a reduction in the $I_{plateau}$ values, which can be interpreted as a facilitated emergence of electroconvection. Moreover, the trends shown in Fig. 4.116 also indicate that the lowest values of current efficiency are those attained with solutions whose composition implied larger $I_{plateau}$ values in their respective current-voltage curves. Obviously, the values of current efficiency are implicitly affected by the composition of the electrolyte, since the $\bar{\phi}$ values may be higher for solutions implying large $[Ni^{2+}]/[H^+]$ values, where the transport of Ni^{2+} ions predominates over that of H^+ ions. However, there is also a strong dependence between the $I_{plateau}$ values and the current efficiency, since the highest efficiencies are obtained for the lowest $I_{plateau}$ values. Moreover, the difference between the $\bar{\phi}$ values obtained for a specific composition at under- and overlimiting currents is broader as the $I_{plateau}$ decreases. These results may be associated with the formation of vortices of greater height as more Ni^{2+} ions are involved in the emergence of electroconvection and, therefore, would indicate an improved supply of Ni^{2+} ions to the membrane surface occurring at overlimiting currents. On the contrary, for larger $I_{plateau}$ values the differences between the different current regimes are almost negligible. The dependence between the current efficiency for the removal of Ni^{2+} ions and the $I_{plateau}$ values calculated from the current-voltage curves with different electrolyte compositions is strongly connected to the results obtained by Pismenskaia et al. [78,109], in which intensive electroconvection was observed only in the case where low H^+ ions were involved in the process.

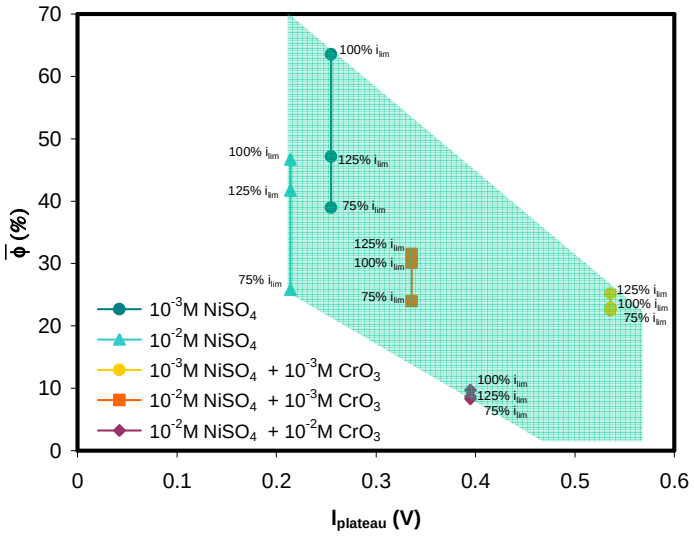

Figure 4.116. Relationship between the time-weighted mean of current efficiency ($\overline{\phi}$) obtained at different current regimes with the plateau length for different solution compositions.

In terms of energy consumption, if the values of $I_{plateau}$ are multiplied by the values of i_{lim} of their corresponding current-voltage curve and the effective membrane area (A_m), a parameter indicative of the energy cost related to surpassing the i_{lim} values is obtained. Then, the time-weighted mean of E_s ($\overline{E_s}$) could be also related to this parameter. The values of $\overline{E_s}$ were calculated with an analogous procedure to that used for the time-weighted mean of current efficiency:

$$\overline{E_s} = \frac{\int_0^t E_s(t)dt}{t} \tag{4.81}$$

Fig. 4.117 shows the relationship existing between the values of $\overline{E_s}$ and the parameter $I_{plateau} \cdot i_{lim} \cdot A_m$ for each solution composition. Due to the different range of i_{lim} values, the different results have been grouped by constant concentrations of $NiSO_4$ (10^{-3}M and 10^{-2}M). Within each group of compositions, the specific energy consumption increases with the parameter $I_{plateau} \cdot i_{lim} \cdot A_m$. These results indicate that there is a strong correlation between the energy consumption of the electrodialysis cell and the energy dissipated in the membrane region. Moreover, for a specific concentration (fixed value of $I_{plateau} \cdot i_{lim} \cdot A_m$),

the differences between the $\overline{E_s}$ values obtained at 75%·i_{lim} and 125%·i_{lim} are almost irrelevant for low $I_{plateau}·i_{lim}·A_m$ values. On the contrary, significant differences are observed for the highest values of $I_{plateau}·i_{lim}·A_m$, since the change from under- to overlimiting currents implies a notorious increase in the energy consumption. Therefore, from a point of view based on energetic considerations, when this parameter takes the highest values, the convenience of applying overlimiting current regimes is reduced. In this respect, several studies have been conducted in order to develop ion-exchange membranes with induced surface inhomogeneity, as this has been proven to imply reduced $I_{plateau}$ values and would consequently increase the advantages of applying intensive current regimes [62,87,111]. In the same way, the present work demonstrates the importance of the composition of the electrolyte in terms of the transport properties of the species present in the solutions and their relative predominance in the electrolyte, which determine to a certain extent the values of $I_{plateau}$ and the convenience of applying overlimiting currents. Accordingly, in order to achieve a good management of industrial waste effluents their composition and the ions involved in the concentration polarization mechanisms should deserve special attention.

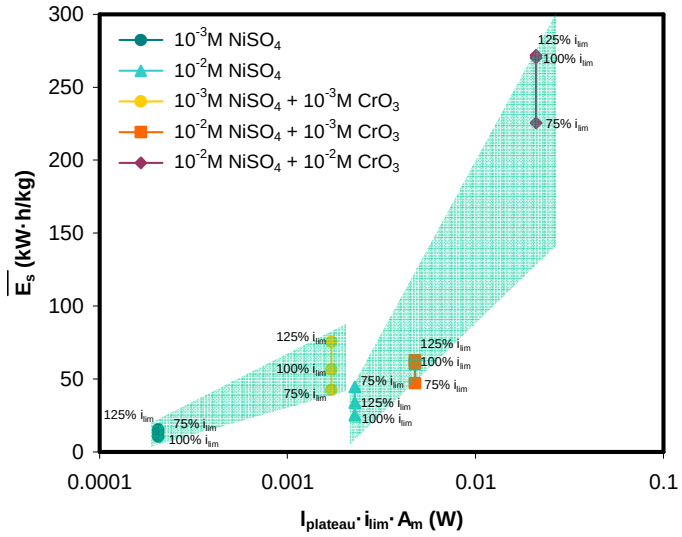

Figure 4.117. Relationship between the time-weighted mean of specific energy consumption ($\overline{E_S}$) obtained at different current regimes with the values of $I_{plateau}·i_{lim}·A_m$ for different solution compositions.

4.4.5 Conclusions

The experiments carried out in this section (4.4) have been useful to corroborate some of the conclusions already obtained from the previous ones (4.1, 4.2 and 4.3). Moreover, other effects related to long-term effects arising in an electrodialysis cell have been investigated. The main conclusions drawn from the galvanostatic experiments are:

- For a constant underlimiting current, the transport of Ni^{2+} ions through the cation-exchange membrane decreases with an increase in the concentration of CrO_3. The H^+ ions provided by chromic acid compete with the Ni^{2+} ions for the transport through the membrane, hence diminishing the values of current efficiency for the transport of Ni^{2+} ions. However, the higher conductivity of the mixtures of $NiSO_4$ and CrO_3 lead to lower U_{cell} values.

- The potential of the electrodialysis operations within the underlimiting range of currents is higher in the case of mixtures of $NiSO_4$ and CrO_3 with respect to single salt solutions of $NiSO_4$. This is caused by the significantly higher i_{lim} values obtained in the case of the mixture solutions. Nevertheless, the increased nickel removal rates with the mixture solutions are achieved at the cost of an increased specific energy consumption of the electrodialysis cell.

- The effect of the CrO_3 concentration on the transport of Ni^{2+} ions through the membrane is more significant in the case of 10^{-3}M $NiSO_4$ than in 10^{-2}M $NiSO_4$ solutions. These results reveal an important role of the $[Ni^{2+}]/[H^+]$ ratio on the current efficiency of the cells. When the concentration of $NiSO_4$ is higher, the evolution of ϕ with time is increasing, which could be a consequence of the decreasing concentration of SO_4^{2-} ions in the central compartment as they cross the anion-exchange membrane. The decreasing concentration of membrane coions allows for a higher selectivity of the membrane and could also imply the dissociation of the uncharged complex specie $NiSO_4$, thus increasing the supply of Ni^{2+} ions to the membrane.

- The galvanostatic operation at overlimiting current densities leads to a general increase of the nickel removal rates with respect to the results obtained at underlimiting currents. These results are achieved without implying a decline in the current efficiency, which is even increased in some cases. Therefore,

electroconvection may be the main mechanism of overlimiting conductance, which implies an increased supply of electrolyte counterions to the membrane surface. On the other hand, the role of the dissociation of water is less important. The increased transport of electrolyte counterions through the membrane can also imply a decrease in the specific energy consumption. Nevertheless, as the conductivity of the electrolyte in the central compartment decreases, the voltage cell can increase notoriously at longer times of the electrodialysis operations, hence attenuating the positive effect of the overlimiting currents on the energy consumption.

- The strong correlation between the $I_{plateau}$ and $\overline{\phi}$ and $\overline{E_s}$ values confirms the use of current-voltage curves of ion-exchange membranes as a simple and useful tool to evaluate the viability of applying overlimiting currents to electrodialysis systems. There is a strong relationship between the values of $I_{plateau}$, which indicate the energy dissipated in the membrane region when overlimiting currents are applied, and the E_s values, which indicate the energy consumed in the entire electrodialysis cell.

- In general, the convenience of applying overlimiting currents in terms of energy consumption is higher for systems with low $I_{plateau}$ values, namely, with solution compositions with high concentrations of Ni^{2+} and low concentrations of H^+ ions. Therefore, the galvanostatic experiments also confirm that electroconvection is the main mechanism of overlimiting mass transfer, as it was already deduced from the chronopotentiometric experiments and current-voltage characteristics.

4.5 References

[1] A. Gruger, A. Régis, T. Schmatko, P. Colomban, Nanostructure of Nafion® membranes at different states of hydration: An IR and Raman study, Vibrational Spectroscopy, 26 (2001) 215-225.

[2] I. Herraiz-Cardona, E. Ortega, V. Pérez-Herranz, Evaluation of the Zn^{2+} transport properties through a cation-exchange membrane by chronopotentiometry, Journal of Colloid and Interface Science, 341 (2010) 380-385.

[3] P. Sistat, G. Pourcelly, Chronopotentiometric response of an ion-exchange membrane in the underlimiting current-range. Transport phenomena within the diffusion layers, Journal of Membrane Science, 123 (1997) 121-131.

[4] S. Kotrlý, L. Sucha, Handbook of Chemical Equilibria in Analytical Chemistry, Ellis Horwood Ltd., Chinchester, 1985.

[5] D.R. Lide, CRC Handbook of Chemistry and Physics, CRC Press Inc., Boca Raton, 2009.

[6] P. Dlugolecki, B. Anet, S.J. Metz, K. Nijmeijer, M. Wessling, Transport limitations in ion exchange membranes at low salt concentrations, Journal of Membrane Science, 346 (2010) 163-171.

[7] J.S. Park, J.H. Choi, J.J. Woo, S.H. Moon, An electrical impedance spectroscopic (EIS) study on transport characteristics of ion-exchange membrane systems, Journal of Colloid and Interface Science, 300 (2006) 655-662.

[8] P. Dlugolecki, P. Ogonowski, S.J. Metz, M. Saakes, K. Nijmeijer, M. Wessling, On the resistances of membrane, diffusion boundary layer and double layer in ion exchange membrane transport, Journal of Membrane Science, 349 (2010) 369-379.

[9] F.G. Wilhelm, N.F.A. Van der Vegt, M. Wessling, H. Strathmann, Chronopotentiometry for the advanced current-voltage characterisation of bipolar membranes, Journal of Electroanalytical Chemistry, 502 (2001) 152-166.

[10] F.G. Wilhelm, N.F.A. Van der Vegt, H. Strathmann, M. Wessling, Comparison of bipolar membranes by means of chronopotentiometry, Journal of Membrane Science, 199 (2002) 177-190.

[11] M. García-Gabaldón, V. Pérez-Herranz, E. Ortega, Evaluation of two ion-exchange membranes for the transport of tin in the presence of hydrochloric acid, Journal of Membrane Science, 371 (2011) 65-74.

[12] L. Marder, E.M. Ortega Navarro, V. Pérez-Herranz, A.M. Bernardes, J.Z. Ferreira, Chronopotentiometric study on the effect of boric acid in the nickel transport properties through a cation-exchange membrane, Desalination, 249 (2009) 348-352.

[13] C. Korzenowski, M.A.S. Rodrigues, L. Bresciani, A.M. Bernardes, J.Z. Ferreira, Purification of spent chromium bath by membrane electrolysis, Journal of Hazardous Materials, 152 (2008) 960-967.

[14] R. Baker, Membrane technology and applications, John Wiley & Sons, Ltd., Menlo Park, California, 2004.

[15] R. Audinos, G. Pichelin, Characterization of electrodialysis membranes by chronopotentiometry, Desalination, 68 (1988) 251-263.

[16] L. Marder, E.M. Ortega Navarro, V. Pérez-Herranz, A.M. Bernardes, J.Z. Ferreira, Evaluation of transition metals transport properties through a cation-exchange membrane by chronopotentiometry, Journal of Membrane Science, 284 (2006) 267-275.

[17] A. Alcaraz, F.G. Wilhelm, M. Wessling, P. Ramírez, The role of the salt electrolyte on the electrical conductive properties of a polymeric bipolar membrane, Journal of Electroanalytical Chemistry, 513 (2001) 36-44.

[18] D.A. Cowan, J.H. Brown, Effect of turbulence on limiting current in electrodialysis cells, Industrial & Engineering Chemistry, 51 (1959) 1445-1448.

[19] N. Pismenskaya, V. Nikonenko, B. Auclair, G. Pourcelly, Transport of weak-electrolyte anions through anion exchange membranes: Current-voltage characteristics, Journal of Membrane Science, 189 (2001) 129-140.

[20] N.D. Pismenskaya, E.I. Belova, V.V. Nikonenko, C. Larchet, Electrical conductivity of cation- and anion-exchange membranes in ampholyte solutions, Russian Journal of Electrochemistry, 44 (2008) 1285-1291.

[21] N. Pismenskaya, E. Laktionov, V. Nikonenko, A. El Attar, B. Auclair, G. Pourcelly, Dependence of composition of anion-exchange membranes and their electrical conductivity on concentration of sodium salts of carbonic and phosphoric acids, Journal of Membrane Science, 181 (2001) 185-197.

[22] Membrane technology in the chemical industry, Wiley-VCH, 2001.

[23] T. Okada, Y. Ayato, M. Yuasa, I. Sekine, The effect of impurity cations on the transport characteristics of perfluorosulfonated ionomer membranes, Journal of Physical Chemistry B, 103 (1999) 3315-3322.

[24] X. Li, H. Zhang, Z. Mai, H. Zhang, I. Vankelecom, Ion exchange membranes for vanadium redox flow battery (VRB) applications, Energy & Environmental Science, 4 (2011) 1147-1160.

[25] M.E. Vallejo, F. Persin, C. Innocent, P. Sistat, G. Pourcelly, Electrotransport of Cr(VI) through an anion exchange membrane, Separation and Purification Technology, 21 (2000) 61-69.

[26] A. Agrawal, K.K. Sahu, An overview of the recovery of acid from spent acidic solutions from steel and electroplating industries, Journal of Hazardous Materials, 171 (2009) 61-75.

[27] J. Wisniewski and G. Wisniewska, Water and acid recovery from the rinse after metal etching operations, Hydrometallurgy, 53 (1999) 105-119.

[28] C. Vallois, P. Sistat, S. Roualdès, G. Pourcelly, Separation of H^+/Cu^{2+} cations by electrodialysis using modified proton conducting membranes, Journal of Membrane Science, 216 (2003) 13-25.

[29] G.l. Chamoulaud, D. Bélanger, Modification of ion-exchange membrane used for separation of protons and metallic cations and characterization of the membrane by current-voltage curves, Journal of Colloid and Interface Science, 281 (2005) 179-187.

[30] T. Benvenuti, R.S. Krapf, M.A.S. Rodrigues, A.M. Bernardes, J. Zoppas-Ferreira, Recovery of nickel and water from nickel electroplating wastewater by electrodialysis, Separation and Purification Technology, 129 (2014) 106-112.

[31] D.C. Buzzi, L.S. Viegas, M.A.S. Rodrigues, A.M. Bernardes, J.A.S. Tenório, Water recovery from acid mine drainage by electrodialysis, Minerals Engineering, 40 (2013) 82-89.

[32] P.G. Priya, C.A. Basha, V. Ramamurthi, S.N. Begum, Recovery and reuse of Ni(II) from rinsewater of electroplating industries, Journal of Hazardous Materials, 163 (2009) 899-909.

[33] K.P. Nickens, S.R. Patierno, S. Ceryak, Chromium genotoxicity: A double-edged sword, Chemico-Biological Interactions, 188 (2010) 276-288.

[34] Y. Lorrain, G. Pourcelly, C. Gavach, Influence of cations on the proton leakage through anion-exchange membranes, Journal of Membrane Science, 110 (1996) 181-190.

[35] H. Strathmann, Chapter 6: Ion-exchange membrane processes in water treatment, in: Sustainability science and engineering sustainable water for the future: water recycling versus desalination, pp. 141-199, Elsevier, 2010.

[36] H. Luo, G. Liu, R. Zhang, Y. Bai, S. Fu, Y. Hou, Heavy metal recovery combined with H_2 production from artificial acid mine drainage using the microbial electrolysis cell, Journal of Hazardous Materials, 270 (2014) 153-159.

[37] S.S. Chen, C.W. Li, H.D. Hsu, P.C. Lee, Y.M. Chang, C.H. Yang, Concentration and purification of chromate from electroplating wastewater by two-stage electrodialysis processes, Journal of Hazardous Materials, 161 (2009) 1075-1080.

[38] J. Khan, B.P. Tripathi, A. Saxena, V.K. Shahi, Electrochemical membrane reactor: In situ separation and recovery of chromic acid and metal ions, Electrochimica Acta, 52 (2007) 6719-6727.

[39] L. Hartinger, Handbook of effluent treatment and recycling for the metal finishing industry, ASM International, Finishing Publications Ltd., 1994.

[40] Reference document on best available techniques for the surface treatment of metals and plastics. IPPC Bureau, European Comission, 2014.

[41] Nickel and chromium plating, Butterworth-Heinemann, 1986.

[42] I. Frenzel, H. Holdik, D.F. Stamatialis, G. Pourcelly, M. Wessling, Chromic acid recovery by electro-electrodialysis: I. Evaluation of anion-exchange membrane, Journal of Membrane Science, 261 (2005) 49-57.

[43] I. Frenzel, H. Holdik, D.F. Stamatialis, G. Pourcelly, M. Wessling, Chromic acid recovery by electro-electrodialysis: II. Pilot scale process, development, and optimization, Separation and Purification Technology, 47 (2005) 27-35.

[44] G. Orhan, C. Arslan, H. Bombach, M. Stelter, Nickel recovery from the rinse waters of plating baths, Hydrometallurgy, 65 (2002) 1-8.

[45] J.J. Qin, M.H. Oo, M.N. Wai, C.M. Ang, F.S. Wong, H. Lee, A dual membrane UF/RO process for reclamation of spent rinses from a nickel-plating operation - a case study, Water Research, 37 (2003) 3269-3278.

[46] S. Logette, C. Eysseric, G. Pourcelly, A. Lindheimer, C. Gavach, Selective permeability of a perfluorosulphonic membrane to different valency cations. Ion-exchange isotherms and kinetic aspects, Journal of Membrane Science, 144 (1998) 259-274.

[47] E. Vallejo, G. Pourcelly, C. Gavach, R. Mercier, M. Pineri, Sulfonated polyimides as proton conductor exchange membranes. Physicochemical properties and separation H^+/M^{z+} by electrodialysis comparison with a perfluorosulfonic membrane, Journal of Membrane Science, 160 (1999) 127-137.

[48] P.V. Vyas, P. Ray, G.S. Trivedi, S.K. Adhikary, R. Rangarajan, Studies on exchange equilibria of cations between cation-exchange membranes and electrolytic solutions, Journal of Colloid and Interface Science, 246 (2002) 366-371.

[49] L.X. Tuan, C. Buess-Herman, H.D. Hurwitz, Absorption equilibrium and permselectivity of cation exchange membranes in sulfuric acid, sodium chloride and nickel sulfate media, Journal of Membrane Science, 323 (2008) 288-298.

[50] J. Kotas, Z. Stasicka, Chromium occurrence in the environment and methods of its speciation, Environmental Pollution, 107 (2000) 263-283.

[51] S. Sang, Q. Wu, K. Huang, A discussion on ion conductivity at cation exchange membrane/solution interface, Colloids and Surfaces A: Physicochemical and Engineering Aspects, 320 (2008) 43-48.

[52] P. Sobron, A. Sanz, T. Acosta, F. Rull, A Raman spectral study of stream waters and efflorescent salts in Rio Tinto, Spain, Spectrochimica Acta Part A: Molecular and Biomolecular Spectroscopy, 71 (2009) 1678-1682.

[53] J.M. Nieto, A.M. Sarmiento, M. Olías, C.R. Canovas, I. Riba, J. Kalman, T.A. Delvalls, Acid mine drainage pollution in the Tinto and Odiel rivers (Iberian Pyrite Belt, SW Spain) and bioavailability of the transported metals to the Huelva Estuary, Environment International, 33 (2007) 445-455.

[54] Treatment of acid mine drainage. London, House of Commons Library, 1999.

[55] K.L. Huang, T.M. Holsen, J.R. Selman, Impurity partitioning in Nafion and ceramic separators used for purification of spent chromium plating solutions, Journal of Membrane Science, 210 (2002) 137-145.

[56] P.N. Pintauro, R. Tandon, L. Chao, W. Xu, R. Evilia, Equilibrium partitioning of monovalent/divalent cation-salt mixtures in Nafion cation-exchange membranes, Journal of Physical Chemistry, 99 (1995) 12915-12924.

[57] M. Taky, G. Pourcelly, C. Gavach, A. Elmidaoui, Chronopotentiometric response of a cation exchange membrane in contact with chromium(III) solutions, Desalination, 105 (1996) 219-228.

[58] J.M. Casas, G. Crisóstomo, L. Cifuentes, Speciation of the Fe(II)-Fe(III)-H_2SO_4-H_2O system at 25 and 50 ºC, Hydrometallurgy, 80 (2005) 254-264.

[59] M. Wang, Y.X. Jia, T.T. Yao, K.K. Wang, The endowment of monovalent selectivity to cation exchange membrane by photo-induced covalent immobilization and self-crosslinking of chitosan, Journal of Membrane Science, 442 (2013) 39-47.

[60] T. Chakrabarty, B. Shah, N. Srivastava, V.K. Shahi, U. Chudasama, Zirconium tri-ethylene tetra-amine ligand-chelator complex based cross-linked membrane for selective recovery of Cu^{2+} by electrodialysis, Journal of Membrane Science, 428 (2013) 462-469.

[61] V.V. Nikonenko, N.D. Pismenskaya, E.I. Belova, P. Sistat, P. Huguet, G. Pourcelly, C. Larchet, Intensive current transfer in membrane systems: Modelling, mechanisms and application in electrodialysis, Advances in Colloid and Interface Science, 160 (2010) 101-123.

[62] J. Balster, M.H. Yildirim, D.F. Stamatialis, R. Ibanez, R.G.H. Lammertink, V. Jordan, M. Wessling, Morphology and microtopology of cation-exchange polymers and the origin of the overlimiting current, Journal of Physical Chemistry B, 111 (2007) 2152-2165.

[63] Y. Tanaka, Water dissociation in ion-exchange membrane electrodialysis, Journal of Membrane Science, 203 (2002) 227-244.

[64] Y. Tanaka, M. Seno, Concentration polarization and water dissociation in ion-exchange membrane electrodialysis. Mechanism of water dissociation, Journal of the Chemical Society, Faraday Transactions 1, 82 (1986) 2065-2077.

[65] N. Pismenskaia, P. Sistat, P. Huguet, V. Nikonenko, G. Pourcelly, Chronopotentiometry applied to the study of ion transfer through anion exchange membranes, Journal of Membrane Science, 228 (2004) 65-76.

[66] I. Rubinstein, B. Zaltzman, O. Kedem, Electric fields in and around ion-exchange membranes, Journal of Membrane Science, 125 (1997) 17-21.

[67] F. Maletzki, H.W. Rösler, E. Staude, Ion transfer across electrodialysis membranes in the overlimiting current range: stationary voltage current characteristics and current noise power spectra under different conditions of free convection, Journal of Membrane Science, 71 (1992) 105-116.

[68] R. Simons, Electric field effects on proton transfer between ionizable groups and water in ion exchange membranes, Electrochimica Acta, 29 (1984) 151-158.

[69] V.I. Zabolotsky, V.V. Nikonenko, N.D. Pismenskaya, E.V. Laktionov, M.K. Urtenov, H. Strathmann, M. Wessling, G.H. Koops, Coupled transport phenomena in overlimiting current electrodialysis, Separation and Purification Technology, 14 (1998) 255-267.

[70] I. Rubinstein, B. Zaltzman, Electro-osmotically induced convection at a permselective membrane, Physical Review E, 62 (2000) 2238-2251.

[71] J.H. Choi, S.H. Moon, Structural change of ion-exchange membrane surfaces under high electric fields and its effects on membrane properties, Journal of Colloid and Interface Science, 265 (2003) 93-100.

[72] R. Simons, Strong electric fields effects on proton transfer between membrane-bound amines and water, Nature, 280 (1979) 824-826.

[73] V.I. Zabolotskii, Dissociation of water molecules in systems with ion-exchange membranes, Russian Chemical Reviews, 57 (1988) 801.

[74] M.S. Kang, Y.J. Choi, H.J. Lee, S.H. Moon, Effects of inorganic substances on water splitting in ion-exchange membranes: I. Electrochemical characteristics of ion-exchange membranes coated with iron hydroxide/oxide and silica sol, Journal of Colloid and Interface Science, 273 (2004) 523-532.

[75] Y. Kharkats, Theory of the exaltation effect and the effect of correlation exaltation of migration current, Journal of Electroanalytical Chemistry and Interfacial Electrochemistry, 105 (1979) 97-114.

[76] Y. Kharkats, A.V. Sokirko, Theory of the effect of migration current exaltation taking into account dissociation-recombination reactions, Journal of Electroanalytical Chemistry and Interfacial Electrochemistry, 303 (1991) 27-44.

[77] V.I. Zabolotsky, V.V. Nikonenko, N.D. Pismenskaya, On the role of gravitational convection in the transfer enhancement of salt ions in the course of dilute solution electrodialysis, Journal of Membrane Science, 119 (1996) 171-181.

[78] N.D. Pismenskaya, V.V. Nikonenko, E.I. Belova, G.Y. Lopatkova, P. Sistat, G. Pourcelly, K. Larshe, Coupled convection of solution near the surface of ion-

exchange membranes in intensive current regimes, Russian Journal of Electrochemistry, 43 (2007) 307-327.

[79] N.D. Pismenskaya, V.V. Nikonenko, V.I. Zabolotsky, R. Sandoux, G. Pourcelly, A.A. Tskhay, Effects of the desalination chamber design on the mass-transfer characteristics of electrodialysis apparatuses at overlimiting current densities, Russian Journal of Electrochemistry, 44 (2008) 818-827.

[80] E.I. Belova, G.Y. Lopatkova, N.D. Pismenskaya, V.V. Nikonenko, C. Larchet, G. Pourcelly, Effect of anion-exchange membrane surface properties on mechanisms of overlimiting mass transfer, Journal of Physical Chemistry B, 110 (2006) 13458-13469.

[81] V.V. Nikonenko, A.V. Kovalenko, M.K. Urtenov, N.D. Pismenskaya, J. Han, P. Sistat, G. Pourcelly, Desalination at overlimiting currents: State-of-the-art and perspectives, Desalination, 342 (2014) 85-106.

[82] C. Larchet, S. Nouri, B. Auclair, L. Dammak, V. Nikonenko, Application of chronopotentiometry to determine the thickness of diffusion layer adjacent to an ion-exchange membrane under natural convection, Advances in Colloid and Interface Science, 139 (2008) 45-61.

[83] V.I. Zabolotskii, V.V. Nikonenko, M.K. Urtenov, K.A. Lebedev, V.V. Bugakov, Electroconvection in systems with heterogeneous ion-exchange membranes, Russian Journal of Electrochemistry, 48 (2012) 692-703.

[84] I. Rubinstein, L. Shtilman, Voltage against current curves of cation exchange membranes, Journal of the Chemical Society, Faraday Transactions 2, 75 (1979) 231-246.

[85] S.M. Rubinstein, G. Manukyan, A. Staicu, I. Rubinstein, B. Zaltzman, R.G.H. Lammertink, F. Mugele, M. Wessling, Direct observation of a nonequilibrium electro-osmotic instability, Physical Review Letters, 101 (2008) 236101.

[86] R. Kwak, G. Guan, W.K. Peng, J. Han, Microscale electrodialysis: Concentration profiling and vortex visualization, Desalination, 308 (2013) 138-146.

[87] R. Ibanez, D.F. Stamatialis, M. Wessling, Role of membrane surface in concentration polarization at cation exchange membranes, Journal of Membrane Science, 239 (2004) 119-128.

[88] E.D. Belashova, N.A. Melnik, N.D. Pismenskaya, K.A. Shevtsova, A.V. Nebavsky, K.A. Lebedev, V.V. Nikonenko, Overlimiting mass transfer through cation-exchange membranes modified by Nafion film and carbon nanotubes, Electrochimica Acta, 59 (2012) 412-423.

[89] M. Wessling, L.G. Morcillo, S. Abdu, Nanometer-thick lateral polyelectrolyte micropatterns induce macrosopic electro-osmotic chaotic fluid instabilities, Scientific Reports, 4 (2014).

[90] Y. Kim, D.F. Lawler, Overlimiting current by interactive ionic transport between space charge region and electric double layer near ion-exchange membranes, Desalination, 285 (2012) 245-252.

[91] N.D. Pismenskaya, V.V. Nikonenko, N.A. Melnik, G. Pourcelli, G. Larchet, Effect of the ion-exchange-membrane/solution interfacial characteristics on the mass transfer at severe current regimes, Russian Journal of Electrochemistry, 48 (2012) 610-628.

[92] V.V.R. Nandigana, N.R. Aluru, Understanding anomalous current-voltage characteristics in microchannel-nanochannel interconnect devices, Journal of Colloid and Interface Science, 384 (2012) 162-171.

[93] A. Yaroshchuk, What makes a nano-channel? A limiting-current criterion, Microfluid Nanofluid, 12 (2012) 615-624.

[94] T.A. Zangle, A. Mani, J.G. Santiago, Theory and experiments of concentration polarization and ion focusing at microchannel and nanochannel interfaces, Chemical Society Reviews, 39 (2010) 1014-1035.

[95] R. Simons, The origin and elimination of water splitting in ion exchange membranes during water demineralisation by electrodialysis, Desalination, 28 (1979) 41-42.

[96] Y. Tanaka, Water dissociation reaction generated in an ion exchange membrane, Journal of Membrane Science, 350 (2010) 347-360.

[97] S.S. Mel'nikov, O.V. Shapovalova, N.V. Shel'deshov, V.I. Zabolotskii, Effect of d-metal hydroxides on water dissociation in bipolar membranes, Petroleum Chemistry, 51 (2011) 577-584.

[98] S. Mafé, P. Ramírez, A. Alcaraz, Electric field-assisted proton transfer and water dissociation at the junction of a fixed-charge bipolar membrane, Chemical Physics Letters, 294 (1998) 406-412.

[99] M.S. Kang, Y.J. Choi, S.H. Moon, Effects of inorganic substances on water splitting in ion-exchange membranes: II. Optimal contents of inorganic substances in preparing bipolar membranes, Journal of Colloid and Interface Science, 273 (2004) 533-539.

[100] J. Pretz, E. Staude, Reverse electrodialysis (RED) with bipolar membranes, an energy storage system, Berichte der Bunsengesellschaft für physikalische Chemie, 102 (1998) 676-685.

[101] N.D. Pismenskaya, V.V. Nikonenko, N.A. Melnik, K.A. Shevtsova, E.I. Belova, G. Pourcelly, D. Cot, L. Dammak, C. Larchet, Evolution with time of hydrophobicity and microrelief of a cation-exchange membrane surface and its impact on overlimiting mass transfer, Journal of Physical Chemistry B, 116 (2011) 2145-2161.

[102] J.H. Choi, H.J. Lee, S.H. Moon, Effects of electrolytes on the transport phenomena in a cation-exchange membrane, Journal of Colloid and Interface Science, 238 (2001) 188-195.

[103] I. Rubinstein, F. Maletzki, Electroconvection at an electrically inhomogeneous permselective membrane surface, Journal of the Chemical Society, Faraday Transactions, 87 (1991) 2079-2087.

[104] J. Barthel, W. Kunz, P. Turq, O. Bernard, Electrolyte solutions, transport properties, in: Encyclopedia of Physical Science and Technology (Third Edition), pp. 243-259, Academic Press, New York, 2003.

[105] R. Tadmor, E. Hernández-Zapata, N. Chen, P. Pincus, J.N. Israelachvili, Debye length and double-layer forces in polyelectrolyte solutions, Macromolecules, 35 (2002) 2380-2388.

[106] V.M. Barragán, C. Bauzá, Current-voltage curves for ion-exchange membranes: A method for determining the limiting current density, Journal of Colloid and Interface Science, 205 (1998) 365-373.

[107] J.J. Krol, M. Wessling, H. Strathmann, Concentration polarization with monopolar ion exchange membranes: current-voltage curves and water dissociation, Journal of Membrane Science, 162 (1999) 145-154.

[108] N. Agmon, The Grotthuss mechanism, Chemical Physics Letters, 244 (1995) 456-462.

[109] E. Belova, G. Lopatkova, N. Pismenskaya, V. Nikonenko, C. Larchet, Role of water splitting in development of electroconvection in ion-exchange membrane systems, Desalination, 199 (2006) 59-61.

[110] V.K. Shahi, S.K. Thampy, R. Rangarajan, Studies on transport properties of surfactant immobilized anion-exchange membrane, Journal of Membrane Science, 158 (1999) 77-83.

[111] E. Volodina, N. Pismenskaya, V. Nikonenko, C. Larchet, G. Pourcelly, Ion transfer across ion-exchange membranes with homogeneous and heterogeneous surfaces, Journal of Colloid and Interface Science, 285 (2005) 247-258.

Chapter 5
CONCLUSIONS

5.1 Conclusions

The improvement and development of sustainable electromembrane processes could imply an important progress in the treatment of metal containing effluents. However, the systems composed of ion-exchange membranes and solutions with multivalent metals are complex. Therefore, a deep understanding of the mass transfer processes involved in electrodialysis cells is required in order to introduce them in industrial processes. The research conducted in the present Thesis aims to contribute to increase the knowledge on these mass transfer processes. The general conclusions of this Doctoral Thesis are presented in different sections, according to the main subjects addressed in Chapter 4:

5.1.1 Transport of single salt solutions

The transport of metals of different valence through the Nafion 117 cation-exchange has been investigated in systems of single salt solutions (section 4.1). The main conclusions regarding this study are:

- In general all the membrane fixed charges are equilibrated with the solution counterions. In the case of Na_2SO_4 and $NiSO_4$ solutions; Na^+ and Ni^{2+} ions, respectively, balance the membrane fixed charges. However, in the case of $Cr_2(SO_4)_3$ and $Fe_2(SO_4)_3$, apart from the free metal ions (Cr^{3+} and Fe^{3+}), also complex ions can be bound to the membrane fixed charges.

- The chronopotentiometric response obtained for Na_2SO_4 solutions is the typical one observed in the literature, and the curves show a sharp increase in U_m associated with the depletion of Na^+ ions at the membrane surface in the diluting compartment. On the contrary, the chronopotentiograms registered for multivalent metals show several increases in U_m, which denote that apart from the depletion of free cations (Ni^{2+}, Cr^{3+} and Fe^{3+}), other complex ions positively charged cross the membrane. In the case of $NiSO_4$ solutions, the dissociation of $NiSO_4$ and the generation of hydroxilated species could occur at high current densities. On the contrary, with $Cr_2(SO_4)_3$ and $Fe_2(SO_4)_3$ solutions, the complex ions $CrSO_4^+$ and $FeSO_4^+$ are present from the beginning of the experiments.

- The formation of $Ni(OH)_2$ and $Fe(OH)_3$ precipitates at the anodic side of the membrane occurred during the chronopotentiometric experiments as a consequence of the application of overlimiting currents. This phenomenon occurs when the pH of the electrolyte near the membrane region (pH_{eq}) increases and reaches the pH at which the solubility of the metallic hydroxides decreases.

- In general, the current-voltage curves obtained show three characteristic regions, the quasi-ohmic region, the plateau region and the region of overlimiting currents. However, in those cases where the formation of precipitates at the membrane surface takes place (concentrated solutions of $NiSO_4$ and $Fe_2(SO_4)_3$), very long plateaus are formed. With the $NiSO_4$ solutions the extended plateaus lead to a sharp increase of current with U_m due to the enhanced dissociation of water occurring at the membrane/precipitate interface. On the contrary, with the $Fe_2(SO_4)_3$ solutions, the precipitates formed obstruct the membrane pores and the current-voltage curves do not present overlimiting region. In the case of diluted solutions of $Cr_2(SO_4)_3$ two plateaus associated with the depletion of different ionic species are clearly identified in the curves.

- In general the electrical resistance of the membrane systems corresponding to the quasi-ohmic region, R_1, decreases as the electrolyte concentration increases. The i_{lim} values increase with the electrolyte concentration with an approximately linear dependence for the systems of Na_2SO_4, $NiSO_4$ and $Fe_2(SO_4)_3$, as predicted by the Peers' equation. This trend is not accomplished with the $Cr_2(SO_4)_3$ solutions because several i_{lim} values were obtained for the most diluted concentrations.

5.1.2 Transport of multicomponent mixtures

The competitive ion transport has been investigated by considering two different multicomponent mixtures (section 4.2). Solutions of $NiSO_4$ and CrO_3 (which forms chromic acid, H_2CrO_4) have been used to study the transport competition between Ni^{2+} and H^+ ions through cation-exchange membranes. These solutions resemble the composition of rinse waters generated in the metal finishing industry. The main conclusions reached with this system are:

- When immersed in mixtures of $NiSO_4$ and CrO_3, the membrane fixed charges are preferentially balanced with multicharged Ni^{2+} ions. At low concentrations of $NiSO_4$, the addition of CrO_3 alters more significantly the ion uptake of the membranes, and the amount of fixed charges equilibrated with H^+ ions increases.

- In general, the chronopotentiometric and the current-voltage curves obtained for the mixtures of $NiSO_4$ and CrO_3 have an analogous shape to that obtained with single salt solutions of $NiSO_4$. However, the presence of CrO_3 increases the magnitude of current values at which each feature is registered in the chronopotentiograms. This indicates that the H^+ ions compete with the Ni^{2+} ions for the transport through the membrane, thus shifting the depletion of the Ni^{2+} ions from the membrane surface to higher values of current density. Moreover, the presence of CrO_3 reduces the initial pH to values around 2-3, which makes more difficult the formation of $Ni(OH)_2$ precipitates at the membrane surface.

- The transport number of Ni^{2+} through the membrane (T_{Ni}^{2+}) is significantly high in single salt solutions of $NiSO_4$, reaching values around 0.9. In the mixture solutions, the T_{Ni}^{2+} decreases for decreasing $[Ni^{2+}]/[H^+]$ ratios.

Mixtures of $Fe_2(SO_4)_3$ and Na_2SO_4 having concentrations that resemble the composition of acid mine drainage solutions have been considered to study the competitive ion transport between ions of different valence. The main conclusions of this study are:

- The membrane fixed charges show a higher affinity for Fe(III) with respect to that for Na^+ ions. These results are due to the stronger electrostatic interactions existing between the sulfonate groups of the membranes and multivalent ions. The speciation of Fe(III) inside the membrane is altered with the increase in the concentration of Na_2SO_4 in the equilibrating solution, since the formation of $FeSO_4^+$ ions is favored and the proportion of these ions in the membrane phase increases while that of Fe^{3+} ions decreases.

- The chronopotentiometric and current-voltage results obtained for 0.02M $Fe_2(SO_4)_3$ solutions show two different membrane behaviors in the underlimiting range of currents. At low underlimiting currents the concentration of $FeSO_4^+$ ions is predominant in the electrolyte and these are the main cationic species crossing the cation-exchange membrane. However, as the polarization of the membrane is intensified, $FeSO_4^+$ ions dissociate into Fe^{3+} and SO_4^{2-} ions. This phenomenon promotes the transport of Fe^{3+} ions through the membrane, and implies a reduction of the electrical resistance of the membrane system. The reduced electrical resistance is consequence of the higher mobility and conductivity of Fe^{3+} ions.

- The chronopotentiometric curves obtained for the mixtures of $Fe_2(SO_4)_3$ and Na_2SO_4 show an inflexion point at low current densities, which is related to a first limiting current density, i_{lim1}, and its corresponding plateau in the current-voltage curves. These features are attributed to the depletion of Na^+ ions from the membrane surface in the diluting compartment. Therefore, the transport of Na^+ ions seems to be favored at low current densities; whereas at current densities higher than i_{lim1}, the transport of Fe^{3+} through the membrane is more significant. A second limiting current density, i_{lim2}, is reached when the formation of $Fe(OH)_3$ precipitates occurs at the anodic side of the membrane.

- The resistance of the membrane system strongly depends on the counterions that are equilibrating the membrane fixed charges. For a constant $Fe_2(SO_4)_3$ concentration of 0.02M, the values of R_1 increase with respect to the single salt solutions with a concentration of Na_2SO_4 of 0.01M, whereas it decreases again

when the concentration of Na_2SO_4 is increased to 0.02M. The first increase in R_1 seems to be caused by the replacement of Fe^{3+} ions inside the membrane phase with Na^+ ions, which reduces the conductivity of the membrane. However, the decrease in R_1 obtained for higher Na_2SO_4 concentrations is mainly due to the positive effect of the Na^+ ions on the conductivity of the diffusion boundary layers, which compensates the decrease in conductivity of the membrane phase.

5.1.3 Mechanisms of overlimiting currents

The effect of the electrolyte composition on the mechanisms of overlimiting currents has been also investigated (section 4.3). The main conclusions of these results are summarized as follows:

- The dissociation of water is the main mechanism originating the overlimiting currents when the formation of metallic hydroxides takes place at the anodic membrane surface (concentrated solutions of $NiSO_4$ and $Fe_2(SO_4)_3$). This has been corroborated by the acute pH changes occurred once the layer of precipitates was formed. The dissociation of water is very important in systems with precipitates of $Ni(OH)_2$. On the contrary, the dissociation of water is less important in systems with precipitates of $Fe(OH)_3$ due to the blockage of the membrane pores by the precipitates.

- Electroconvection is the main mechanism of overlimiting mass transfer in diluted solutions of all the metals tested: Na_2SO_4, $NiSO_4$, $Cr_2(SO_4)_3$ and $Fe_2(SO_4)_3$. The electroconvective vortices induce the distortion of the diffusion boundary layer and are manifested in the chronopotentiograms as oscillations in U_m. The magnitude of the oscillations in U_m increases with the applied current density, which indicates that the height of the electroconvective vortices becomes higher at high overlimiting currents, thus increasing the supply of counterions to the membrane depleting surface.

- The role of gravitational convection on the overlimiting currents is important in concentrated solutions of $Cr_2(SO_4)_3$ and $NiSO_4$. The magnitude of gravitational convection increases with the electrolyte concentration and, at higher currents, gravitational convection and electroconvection have a synergic effect on the reduction of the electrical resistance of the membrane system.

- The length of the plateau region of the current-voltage curves, $l_{plateau}$, has been used as an indicator for comparing the tendency to initiate the overlimiting currents of different membrane/electrolyte systems. Systems with short plateaus imply an inducement of the overlimiting currents for shorter membrane voltage drops. The $l_{plateau}$ values decrease for higher concentrations of multivalent metals. This is caused by the large size of multivalent ions, which promote the motion of large volumes of fluid when the phenomena of coupled convection are initiated. On the contrary, higher concentrations of H^+ ions are associated with large $l_{plateau}$ values. Protons hamper electroconvection because they displace the multivalent ions from the space charge region. Moreover, H^+ ions are transported via the Grotthuss mechanism without involving the motion of large volumes of fluid.

5.1.4 Galvanostatic electrodialysis experiments

Finally, galvanostatic experiments were conducted (section 4.4) in order to corroborate the results obtained in the previous sections. The effect of the electrolyte composition on the membrane selectivity and on the development of overlimiting currents was evaluated using mixtures of $NiSO_4$ and CrO_3. The main conclusions obtained from the galvanostatic experiments are summarized as follows:

- In the range of underlimiting current densities, for a constant concentration of $NiSO_4$, the selectivity of the cation-exchange membrane for Ni^{2+} ions decreases with an increase of the concentration of CrO_3. This is caused by the increasing participation of H^+ ions in the current transfer through the membranes, which reduces the current efficiency for the transport of Ni^{2+}. These results are in agreement with the T_{Ni}^{2+} values previously calculated.

- The values of i_{lim} increase with the concentration of CrO_3 for the multicomponent mixtures. Therefore, the mass transfer rates of Ni^{2+} ions can be improved within the underlimiting range of currents in the case of the mixtures of $NiSO_4$ and CrO_3. However, this improvement is attained at the expense of higher specific energy consumptions.

- Overlimiting current densities lead to higher nickel transport rates. In terms of energy consumption, this increased transfer of Ni^{2+} ions through the membranes is beneficial for the process when the concentration of Ni^{2+} is relatively higher

than that of H^+ ions. On the contrary, for high concentrations of CrO_3, the increased Ni^{2+} transfer rates achieved at overlimiting currents imply an important increase in the specific energy consumption, E_s. These results corroborate the good correlation between the $I_{plateau}$ values, the electrolyte composition, and the convenience of applying overlimiting currents. The U_{cell} values achieved at overlimiting currents in systems with large $I_{plateau}$ values confirm the important contribution of the membrane voltage drop to the total cell voltage. Moreover, the E_s values increase considerably with time as a consequence of the depletion of ions occurring in the central compartment.